**Title**
Biomechanical implications of muscle cell-ECM communication

**Permalink**
https://escholarship.org/uc/item/8qf1428m

**Author**
Meyer, Gretchen Ann

**Publication Date**
2011

Peer reviewed|Thesis/dissertation

UNIVERSITY OF CALIFORNIA, SAN DIEGO

**Biomechanical Implications of Muscle Cell-ECM Communication**

A dissertation submitted in partial satisfaction of the
requirements for the degree
Doctor of Philosophy

in

Bioengineering

by

Gretchen Ann Meyer


Committee in charge:

      Professor Richard L. Lieber, Chair
      Professor Andrew D. McCulloch, Co-Chair
      Professor Anne Hoger
      Professor Geert Schmid-Schonbein
      Professor Samuel R. Ward


2011

The dissertation of Gretchen Ann Meyer is approved, and it is acceptable in quality and form for publication on microfilm and electronically:

_____

_____

_____

_____
Co-Chair

_____
Chair

University of California, San Diego

2011

DEDICATION

This work is dedicated to my parents whose constant
and unconditional support has always made me feel invincible.
And to my colleagues and friends whose light has guided me
through this mysterious world of science.

# EPIGRAPH

*Muscle is a metaphor for life;*
*sometimes we could all use a good stretch.*

## TABLE OF CONTENTS

## LIST OF FIGURES

LIST OF TABLES

xiii

# ACKNOWLEDGEMENTS

I wish to thank first and foremost my doctoral adviser and mentor, Dr. Richard Lieber, for years of patient input and guidance. I could always rely on him to push me when I needed a push but to allow me to pursue my own ideas, even when they seemed ill-conceived. I could not have gotten past square one without him. I am indebted to him as a leader, a mentor and a friend. I gratefully acknowledge funding support secured by Dr. Lieber on my behalf including grants from the Veterans Administration and the National Institute of Health.

I benefitted in innumerable ways from generous help and encouragement provided by colleagues in the Skeletal Muscle Physiology Lab. In particular, I would like to acknowledge the feedback and guidance of Dr. Sam Ward and Dr. Simon Schenk whose unique perspectives and ideas consistently broadened and enhanced my work. I would also like to acknowledge the constant help and support of Lucas Smith who was my sounding board and right-hand man throughout my graduate work and Shannon Bremner who could make anything happen and could fix everything. Others, including many inside and outside our lab group, provided input and assistance as co-authors on the publications listed below.

Chapter 2, in full, is a reprint of the published article "Theoretical Predictions of the Effects of Force Transmission by Desmin on Intersarcomere Dynamics." Meyer G.A., Kiss B., Morgan D.L., Kellermayer M.S., and Lieber R.L. *Biophysical Journal*, 20;98(2):258-266, 2010. The dissertation author was the primary investigator and author of this paper.

Chapter 3, in full, is a reprint of the published article "Elucidation of Extracellular Matrix Mechanics from Muscle FIbers and Fiber Bundles." Meyer G.A., and Lieber R.L., *Journal of Biomechanics.* 44(4): 771-773, 2011. The dissertation author was the primary investigator and author of this paper.

Chapter 4, in full, has been submitted for publication of the material as it may appear in *Journal of Biomechanical Engineering.* "A Nonlinear Model of Passive Muscle Viscosity." Meyer G.A., McCulloch A.D., and Lieber R.L. The dissertation author was the primary investigator and author of this paper.

Chapter 5 in full, has been submitted for publication of the material as it

may appear in *Journal of Physiology, London.* "Skeletal Muscle Fibrosis Develops in Response to Compliant Fibers." Meyer G.A., and Lieber R.L. The dissertation author was the primary investigator and author of this paper.

Chapter 6 contains the dissertation author's contributions to a manuscript submitted for publication of the material as it may appear in *WILEY Interdisciplinary Reviews: Systems Biology and Medicine* "Systems Analysis of Genes Related to Skeletal Muscle Function." Smith, L.R., Meyer G.A., and Lieber R.L.

Chapter 7 in part is currently being prepared for submission for publication of the material "Transcriptional Alterations in Aging and Injured Skeletal Muscle due to Desmin Deletion." Meyer G.A., and Lieber R.L. The dissertation author was the primary investigator and author of this material.

# VITA

| | |
|---|---|
| 2004 | B. S. in Mechanical Engineering *magna cum laude*, Washington University, St. Louis, Missouri |
| 2004 | M. S. in Mechanical Engineering with an emphasis in Applied Mechanics, Washington University, St. Louis, Missouri |
| 2004-2006 | Structural Dynamics Engineer, The Boeing Company, St. Louis, Missouri |
| 2006-2011 | Graduate Research Assistant, University of California, San Diego |
| 2007-2008 | Graduate Teaching Assistant, University of California, San Diego |
| 2009 | M. S. in Bioengineering, University of California, San Diego |
| 2011 | Ph. D. in Bioeningeering, University of California, San Diego |

Meyer, G.A., and Lieber R.L., "Skeletal Muscle Fibrosis Develops in Response to Compliant Fibers", *Journal of Physiology, London (in review).*

Meyer, G.A., McCulloch, A.D. and Lieber R.L., "A Nonlinear Model of Passive Muscle Viscosity", *Journal of Biomechanical Engineering (in review).*

Palmisano, M.G., Bremner, S.N., Hornberger, T.A., Meyer, G.A., Shah, S.B., Kellermayer, M., Ryan, A.F. and Lieber, R.L., "Muscle Intermediate Filaments Form a Stress-Transmitting and Stress-Signaling Network", *Proceedings of the National Academy of Sciences (in final preparation).*

Smith L.R., Meyer, G.A., and Lieber R.L., "Systems Analysis of Genes Related to Skeletal Muscle Function", *Wyley Interdisciplinary Reviews Systems Biology and Medicine (in review).*

Philip, A., Chen, A., Lan, D., Meyer, G.A., Murphy, A.N., Knapp, A., Macrotte, G.R., Olfert, I.M., Carr, J.A., Hogan, M.C., Lieber, R.L., Barr, K. and Schenk, S., "Sirtuin 1 (SIRT1) Deacetylase Activity is not Required for Mitochondrial Biogenesis or Peroxisome Proliferator Activated Receptor-Gamma Coactivator-1 Alpha (PGC-1Alpha) Deacetylation Following Endurance Exercise", *Journal of Biological Chemistry (in press).*

Meyer, G.A. and Lieber, R.L., "Elucidation of Extracellular Matrix Mechanics from Muscle Fibers and Fiber Bundles", *Journal of Biomechanics* 44(4):771-773, 2011.

Meyer G.A., Kiss B., Ward S.R., Morgan D.L., Kellermayer M. and Lieber R.L., Theoretical Predictions of the Effects of Force Transmission by Desmin on Intersarcomere Dynamics" *Biophysical Journal* 98(2):258-266, 2010.

Lange S., Ouyang K., Meyer G., Cui L., Cheng H., Lieber R.L. and Chen J., "Obscurin Determines the Architecture of the Longitudinal Sarcoplasmic Reticulum" *Journal of Cell Science* 1;122(Pt 15):2640-2650, 2009.

ABSTRACT OF THE DISSERTATION

**Biomechanical Implications of Muscle Cell-ECM Communication**

by

Gretchen Ann Meyer

Doctor of Philosophy in Bioengineering

University of California, San Diego, 2011

Professor Richard L. Lieber, Chair
Professor Andrew D. McCulloch, Co-Chair

Proper regulation of the composition and structure of muscle is vital to both its load bearing and force producing capabilities. At every scale of muscular organization, from the individual protein to the whole organ, components communicate with each other to develop and maintain a complex and dynamic equilibrium. The mechanisms and major players involved in this communication are poorly understood. Desmin is an intermediate filament protein integral to the muscle fiber cytoskeleton. It is thought to be involved in stabilizing the contractile apparatus and providing a mechanical link between the cytoskeleton and the extracellular environment. The purpose of this work was to investigate the effects of communication loss caused by desmin deletion on muscle physiology. An approach combining experiments and computational modeling was implemented to show that cytoskeletal alterations in muscle can have wide ranging functional consequences, from gene expression changes in the nucleus to extracellular matrix remodeling.

# Chapter 1

# Introduction

Skeletal muscle is a complex and highly dynamic system of specialized proteins that interact in coordinated networks to meet the mechanical demands of the body. Structure and function are intimately linked in this interaction, from actin-myosin overlap which enables force production to the extracellular matrix (ECM) which provides a scaffold for cellular support. Though many players have been identified in the maintenance of streamlined physiology, the mechanisms and pathways through which it occurs remain largely unknown. One thing is clear however: intercellular and intracellular communication is essential to proper muscle function.

## 1.1 Structure and function in skeletal muscle

The skeletal muscle system has two primary functions in movement: force production and joint stability. Each of these functions is intimately linked to the physical arrangement of the muscle components, from the micro to the macro scale. Thus, any discussion of function must be built on a foundation of composite structure.
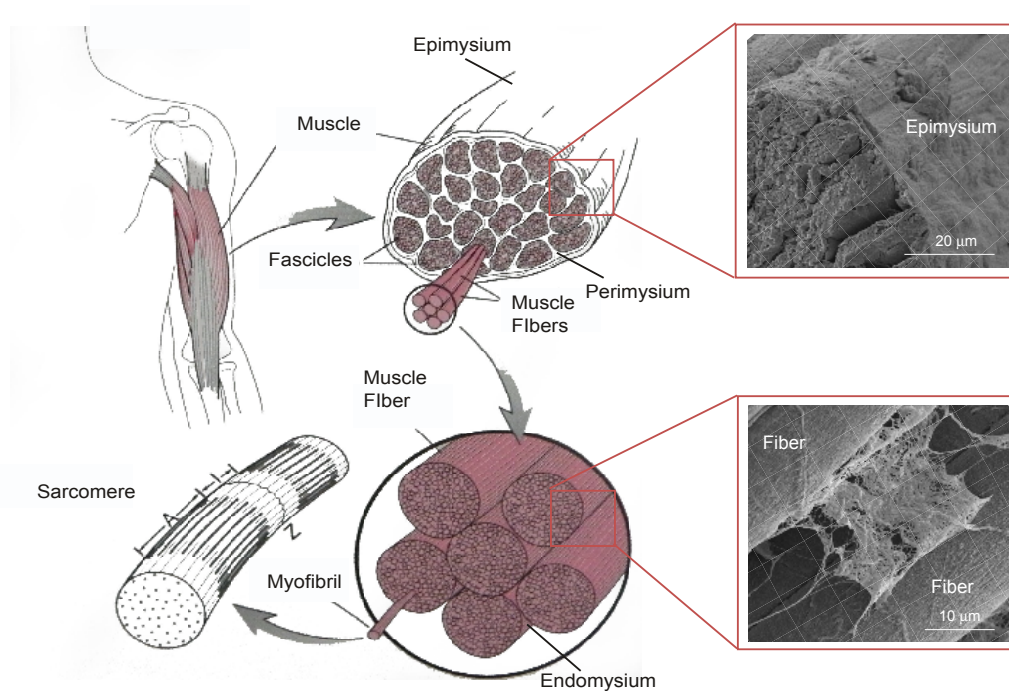
Figure 1.1: diagram of muscle macroanatomy. Muscle is ensheathed by a connective tissue matrix, the epimysium (inset), which integrates with the tendon at the myotendinous junction. Inside the epimysium, muscle can be subdivided into fascicles which are bundles of fibers surrounded by the perimysium. Each fiber is embedded in extracellular matrix. the endomysium (inset), and composed of radially packed myofibrils. Myofibrils consist of serially arranged sarcomeres (the force producing unit of muscle). Schematic from [1], SEM images from [2].

## 1.1.1 Extracellular structure

At the most basic level, a muscle is composed of individual force-producing cells (fibers) embedded in a connective tissue matrix. This extracellular matrix has a hierarchical structure: it ensheathes the muscle (epimysium), surrounds bundles of fibers (perimysium) and provides inter-fiber connections (endomysium) (Fig. 1.1). It not only provides fiber support at each structural level, but also affords the muscle access to the external world by transmitting forces and supporting nerves and blood vessels. The role of the ECM in muscle function has been largely neglected in favor of contractile studies, but new evidence is emerging suggesting that the ECM plays a large role in muscle physiology.

Although ECM comprises less than 20% of healthy muscle by volume, biomechanical studies indicate that it bears a significant portion of passive load, suggesting it plays a large role in joint range of motion and stiffness [3]. Evidence has also suggested that the basal lamina, a component of the ECM, is vital for the maintenance of the satellite cell niche, the basis for muscle repair and adaptation [4]. Moreover, alterations to the ECM are a hallmark of nearly every case of myopathy or altered muscle use, from diabetes and muscular dystrophies to exercise and aging, highlighting its significance to proper muscle function [5–7]. There appears to be significant communication between muscle fibers and the matrix that surrounds them, but how fiber dysfunction translates to ECM adaptation remains unknown.

## 1.1.2   Intracellular structure

Skeletal muscle is able to generate forces due to highly coordinated interactions between myofilaments (actin thin filaments and myosin thick filaments). These filaments are organized in a repeating array, the fundamental unit of which is called the sarcomere. Sarcomeres are arranged serially to form myofibrils, which are then packed radially into a muscle fiber (Fig. 1.1). Myofibrils are interconnected by a specialized intermediate filament system. The main component of this system is desmin, which forms a mesh-like network around Z-disk structures providing mechanical coupling of sarcomeres. Desmin also binds to nuclei, mitochondria and to costameres at the sarcolemma (Fig. 1.2). In this way, it provides a cytoskeletal support system, stabilizing the contractile apparatus and localizing organelles.

The ability of a sarcomere to generate force is regulated by many factors including nervous excitation, intracellular calcium concentration, availability of metabolic fuel, sarcomere length and contraction velocity. The properties that relate sarcomere kinematics with active force production have been well defined in the length-tension [9, 10] and force-velocity [11, 12] relationships.

The length-tension relationship has a profound impact on muscle function, but has its mechanistic origins in structure. The amount of force a sarcomere
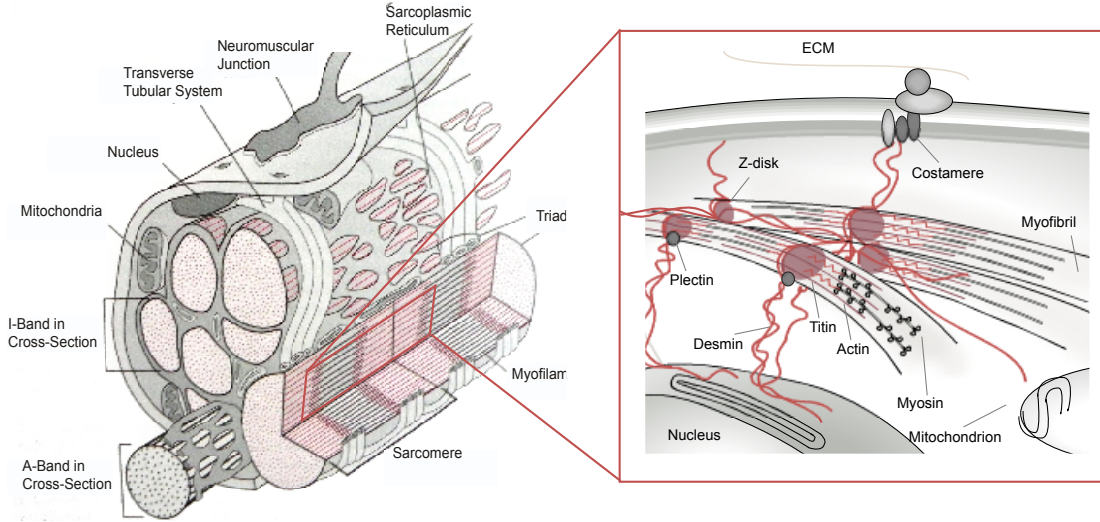
Figure 1.2: Diagram of muscle microanatomy. A muscle fiber is composed of a repeating array of myofibrils which are in turn a repeating array of sarcomeres. Overlap between myofilaments (actin and myosin) allow for force production in the sarcomere. Myofibrils are stabilized at the Z-disk by a desmin filament network which also links to the extracellular matrix at the costamere and to cellular organelles such as mitochondria and nuclei. Schematic from [1] and [8].

can generate is proportional to the number of myosin heads that can bind to the actin thin filament, which is in turn a function of actin-myosin filament overlap. When overlap is optimized, force production is maximized (Fig. 1.3A, area 2). As sarcomere length increases, filament overlap decreases resulting in force reduction (Fig. 1.3A, area 3). Similarly, as sarcomere length decreases, actin filaments interfere with each other and overlap also decreases (Fig. 1.3A, area 1). This theoretical relationship was shown to hold experimentally in frog fibers [9] and mouse fibers [13] stimulated at constant length.

It is impossible, however, to determine the force of a shortening muscle simply using the length tension curve because contractile force is also a function of velocity. The force-velocity relationship was developed based on cross-bridge kinetic theory and was determined by allowing a muscle to shorten against a constant load. The result is a relationship stating that the faster a muscle contracts, the less force it can generate (Fig. 1.3B, area 1). On the other hand, if a muscle is lengthened during contraction, it produces forces in excess of those it can pro-
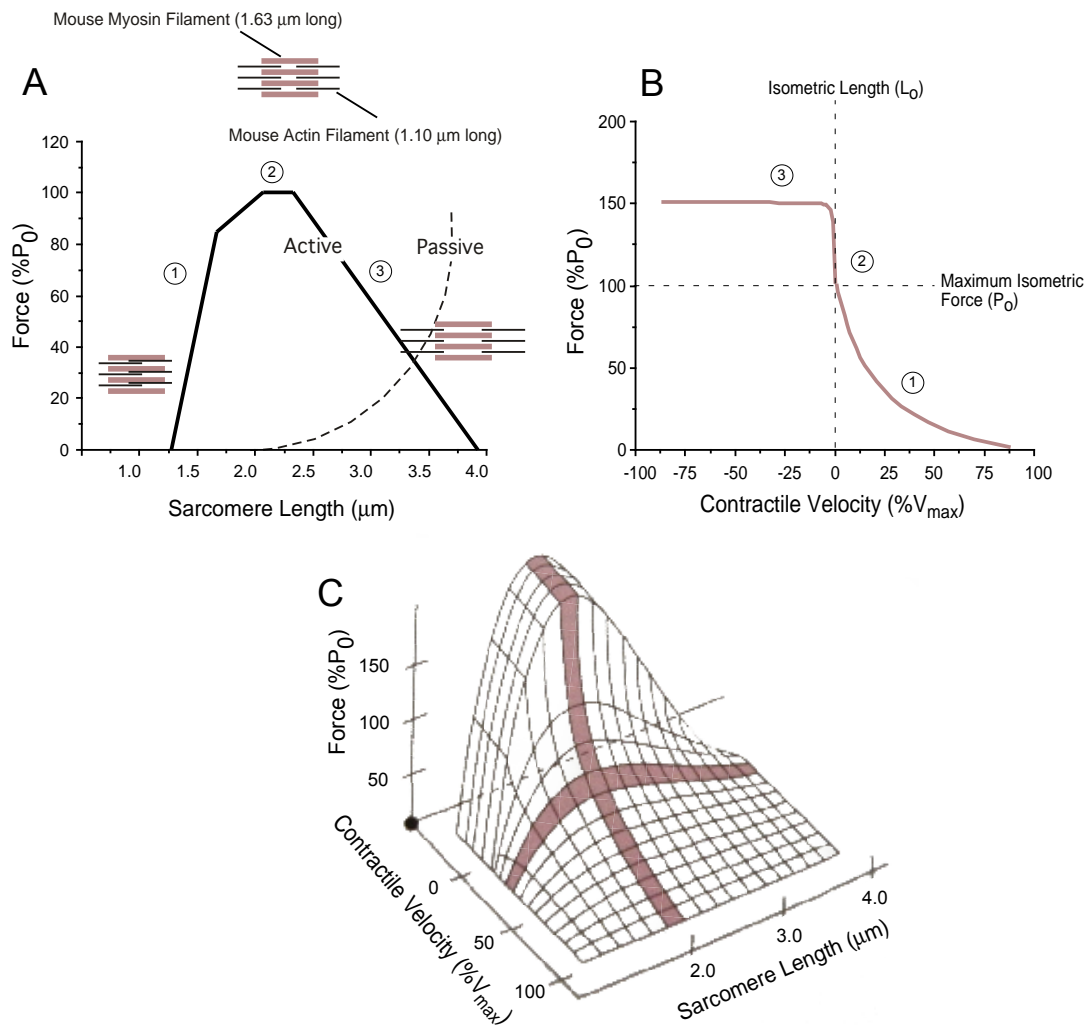
Figure 1.3: The length-tension and force-velocity relationships in muscle. A) The amount of force a muscle can produce is proportional to the amount of actin-myosin overlap in the sarocmere. On the plateu region (1), overlap is maximized, but as sarcomere length increases or decreases, overlap decreases as does force production (2) and (3). B) The amount of force a muscle can produce is also a function of shortening velocity. As velocity increases, force production decreases as it becomes more difficult for cross-bridges to bind. Force production increases over the isometric value in conditions of lengthening. C) Physiologically, muscles operate in situations that call for a combination of the length-tension and force-velocity curves, visualized in a three-dimensional surface. Schematic from [1].

duce isometrically (Fig. 1.3B, area 3). Physiologically, muscle is rarely at constant length or velocity and thus both relationships must be used in combination, as force production will be a more complex function of sarcomere length and velocity (Fig. 1.3C).

Muscle doesnt simply produce force, however, it can also provide resistance to stretch in the absence of activation. This resistance is frequently referred to as passive tension or passive stiffness. Within the muscle fiber, the primary source of passive tension is the giant protein titin [14, 15], though other intermediate filaments may play a role as well. Titin spans from the Z-disk to the middle of the myosin thick filament and thus provides longitudinal connection through the sarcomere such that when the sarcomere is lengthened, titin is lengthened.

## 1.2 Desmin in muscle physiology

Desmin is a 52 kDa muscle-specific intermediate filament protein first discovered in 1976 by Lazarides et al. [16], though a filamentous network in muscle cells had been recognized previously. They described desmin as a cytoskeletal network localized to the Z-disk periphery and cell-cell junctures that mechanically integrates the contractile apparatus (Fig. 1.4A). In addition to forming a network around Z-disks laterally, some desmin filaments also run longitudinally along the length of the myofibril from Z-disk to Z-disk (Fig. 1.4B). In this configuration, desmin filaments can resist sarcomere lengthening, in a mechanism similar to titin. However, there are few longitudinal desmin filaments compared to the dense network that exists laterally and thus the desmin cytoskeleton will primarily act to resist radial strain and inter-myofibrillar shear. Specifically, if one sarcomere were inclined to move independently from its lateral neighbor, desmin would act to prevent this deviant behavior by providing a lateral link between the neighbors Z-disks (Fig. 1-5A). Finally, desmin has also been shown to bind to mitochondria [17] and nuclei [16] and thus could play a role in muscle metabolism and gene expression.

Elucidating the function of desmin beyond speculation based on its localization, has been greatly aided by the development of the desmin knockout ($des^{-/-}$)
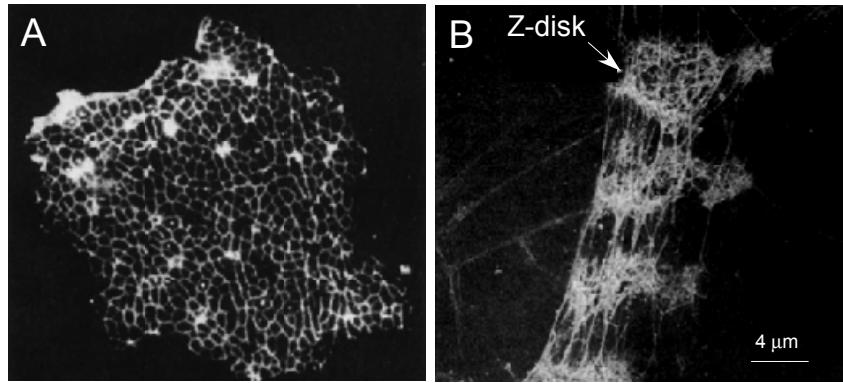
Figure 1.4: Desmin filaments visualized by immunofluorescence and light microscopy. A) A transverse cross-section of a muscle fiber showing the desmin network surrounding myofibrillar Z-disks. B) A longitudinal view of the desmin network illustrating concentrations at Z-disks and a few longitudinal filaments. Image A from [16], Image B from [18].

mouse [17, 19]. ( $Des^{-/-}$) mice are fertile and by gross appearance are indistinguishable from their wildtype ($wt$) counterparts, however they do exhibit myopathies of skeletal, smooth and cardiac muscle and have shortened lifespans due to cardiac and respiratory complications [17]. One of the first observations in the ( $des^{-/-}$) mouse was abnormalities in muscle architecture including sarcomere disruption, Z-disk streaming and Z-disk misalignment [19, 20] (Fig. 1.5B). These observations led to examinations of $des^{-/-}$ muscle function. Initial studies found that $des^{-/-}$ muscles produced less stress than their wt counterparts and fatigued more quickly [19, 21]. Additionally, $des^{-/-}$ muscles were found to experience a lower isometric stress decline following eccentric contraction induced injury [21].

The role of desmin in injury is especially interesting in light of the observation that, immediately following eccentric contraction induced injury, muscle fibers have been shown to lose immunostaining for desmin [22]. Days later, the concentration of desmin in the muscle has increased beyond its pre-injury levels [23]. It is tempting to speculate that this effect is causally related to the observation that muscle is protected for weeks from a repeat bout of eccentric contraction induced injury and show little to no resultant stress decline [24]. Especially since eccentric contraction induced injury is thought to involve highly non-uniform sarcomere
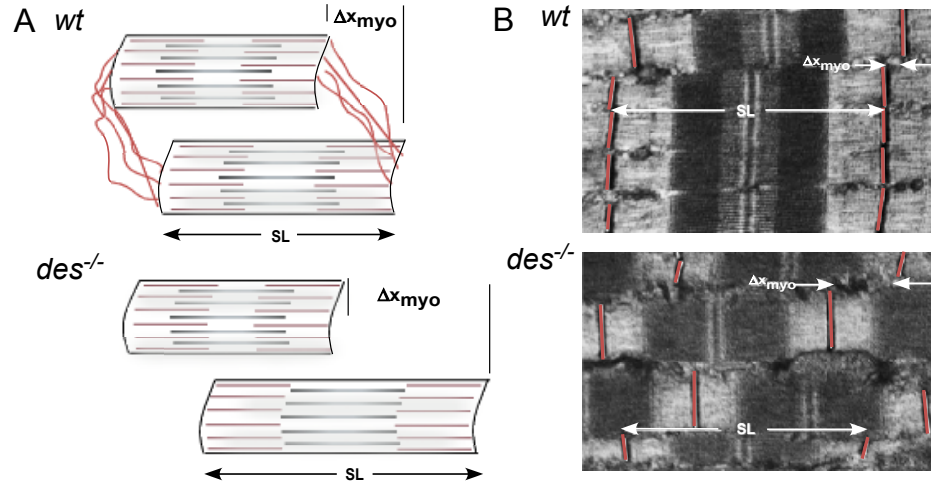
Figure 1.5: Z-disk misalignment in $des^{-/-}$ muscle. A) Schematic drawing depicting how in $wt$ fibers, desmin restricts relative sarcomere extension and intermyofibrillar shear. In $des^{-/-}$ fibers, without desmin to link adjacent sarcomeres, the lower sarcomere is allowed to extend independently of the upper. Note, in this depiction it has extended beyond filament overlap. B) Longitudinal micrographs of $wt$ and $des^{-/-}$ muscle. $Des^{-/-}$ muscle shows a much greater degree of Z-disk misalignment ($\Delta x_{myo}$) Micrographs from [20].

lengths and sarcomere overextension, which desmin may act to prevent (Fig. 1.5). This response could suggest a role for desmin in protecting muscle from injury, but the literature investigating injury in $des^{-/-}$ muscle is mixed, with some studies citing evidence for lower injury [21], some citing increased injury [19] and some citing no difference [25, 26]. These discrepancies could be explained by differences in measurement techniques or definitions of injury, but the role of desmin in muscle injury is by no means clear.

## 1.3 Clinical relevance

It is clear that components of skeletal muscle interact and communicate to maintain a physiologically efficient composite. Examples abound of the detrimental consequences that result from interrupting this delicate balance, from congenital myopathies to sports injuries. Still, many therapeutic interventions for muscle are aimed at altering these lines of communications, such as Botox in-
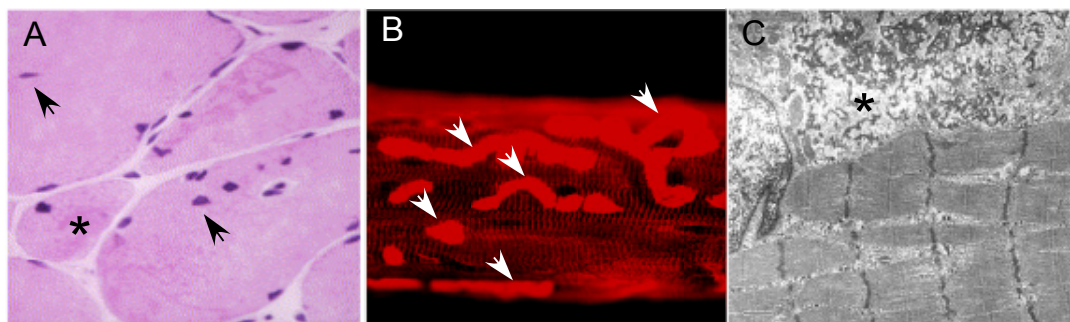
Figure 1.6: Biopsies from desmin-related myopathy (DRM) patients. A) A hematoxylin and eosin (H&E) stained section from a patient suffering from DRM. Section shows centrally localized nuclei (arrows) and undersized fibers (asterisk) hallmarks of muscle regeneration. B) A single fiber isolated from a DRM patient and immunolabeled for desmin. Patients typically exhibit subsarcolemmal dense accumulations of intermediate filaments (arrows). These are also visible on electron micrographs (asterisk in C) where myofibrillar disarray is also seen. A from [27], B from [28], C from [29].

jections which block neuromuscular communication and anti-fibrotic treatments which break down or block elements of the ECM [30, 31]. Without a concrete understanding of how these target components interact with the rest of muscle, these therapies could have any number of unintended consequences.

Desmin-related myopathies (DRM) in human patients are typically due to inherited muataions in the desmin or $\alpha\beta$-crystallin gene. These disorders typically manifest as progressive muscle weakness eventually involving respiratory muscles. Severe cases eventually involve resipiratory and/or cardiac failure and early mortality [8, 32]. Though the incidence of DRM is low, it is likely highly underdiagnosed due to its heterogeneous symptoms [8]. Most patients display typical ultrastructural alterations such as centrally nucleated fibers, myofibril disarray and filament aggregation (Fig. 1.6). Development of interventional therapies for desmin-related myopathies is underway in isolated cell populations [33, 34]. And yet, not only is the specific function of desmin not well defined in intact muscle, the broad consequences of desmin loss or mutation are just beginning to be revealed.

## 1.4   Summary

The overarching objective of this dissertation was to investigate the mechanisms of intra- and extra-cellular communication by desmin in skeletal muscle. Chapter 2 of this dissertation describes insights into the effect of desmin on intersarcomere dynamics with a finite element model. It describes how desmin can theoretically evenly distribute strain imposed on a fiber such that variations in sarcomere lengths and sarcomere overextension are minimized. In Chapter 3, a novel method for determining the mechanical properties of the ECM is described, so that it's contribution to passive muscle mechanics can be isolated from the fiber contribution. In Chapter 4, a novel method for determining the viscoelastic properties of muscle fibers is described incorporating the development of a computational model. Chapter 5 describes the development of fibrosis in $des^{-/-}$ muscle including evidence pointing to injury due to increased fiber compliance as a mechanism for adaptation of the ECM. Chapter 6 reviews gene expression pathways relevant to skeletal muscle physiology and their relationship to function. Finally, Chapter 7 describes differential gene expression changes in response to injury in $wt$ and $des^{-/-}$ muscle to further elucidate the role of desmin in injury prevention.

## 1.5   References

[1] Lieber, R.L., 2002. Skeletal muscle structure, function & plasticity.

[2] Gillies, A. Structure and function of the skeletal muscle extracellular matrix. *Muscle & nerve.*

[3] Purslow, P.P., 2002. The structure and functional significance of variations in the connective tissue within muscle. *Comparative biochemistry and physiology Part A, Molecular & integrative physiology*, 133:947–966.

[4] Kuang, S., Gillespie, M.A., and Rudnicki, M.A., 2008. Niche regulation of muscle satellite cell self-renewal and differentiation. *Cell stem cell*, 2:22–31.

[5] Kang, L., Ayala, J.E., Lee-Young, R.S., Zhang, Z., James, F.D., Neufer, P.D., Pozzi, A., Zutter, M.M., and Wasserman, D.H., 2011. Diet-induced

muscle insulin resistance is associated with extracellular matrix remodeling and interaction with integrin alpha2beta1 in mice. *Diabetes*, 60:416–426.

[6] Foidart, M., Foidart, J.M., and Engel, W.K., 1981. Collagen localization in normal and fibrotic human skeletal muscle. *Archives of neurology*, 38:152–157.

[7] Gao, Y., Kostrominova, T.Y., Faulkner, J.A., and Wineman, A.S., 2008. Age-related changes in the mechanical properties of the epimysium in skeletal muscles of rats. *Journal of biomechanics*, 41:465–469.

[8] Goldfarb, L.G. and Dalakas, M.C., 2009. Tragedy in a heartbeat: malfunctioning desmin causes skeletal and cardiac muscle disease. *The Journal of clinical investigation*, 119:1806–1813.

[9] Gordon, A.M., Huxley, A.F., and Julian, F.J., 1966. The variation in isometric tension with sarcomere length in vertebrate muscle fibres. *The Journal of physiology*, 184:170–192.

[10] Edman, K.A., 1966. The relation between sarcomere length and active tension in isolated semitendinosus fibres of the frog. *The Journal of physiology*, 183:407–417.

[11] Hill, A., 1938. The heat of shortening and the dynamic constants of muscle. In Proceedings of the Royal Society of London Series B.

[12] Katz, B., 1939. The relation between force and speed in muscular contraction. *The Journal of physiology*, 96:45–64.

[13] Edman, K.A.P., 2005. Contractile properties of mouse single muscle fibers, a comparison with amphibian muscle fibers. *The Journal of experimental biology*, 208:1905–1913.

[14] Magid, A. and Law, D.J., 1985. Myofibrils bear most of the resting tension in frog skeletal muscle. *Science (New York, NY)*, 230:1280–1282.

[15] Horowits, R., Kempner, E.S., Bisher, M.E., and Podolsky, R.J., 1986. A physiological role for titin and nebulin in skeletal muscle. *Nature*, 323:160–164.

[16] Lazarides, E., 1980. Intermediate filaments as mechanical integrators of cellular space. *Nature*, 283:249–256.

[17] Milner, D.J., Weitzer, G., Tran, D., Bradley, A., and Capetanaki, Y., 1996. Disruption of muscle architecture and myocardial degeneration in mice lacking desmin. *The Journal of cell biology*, 134:1255–1270.

[18] Wang, K. and Ramirez-Mitchell, R., 1983. A network of transverse and longitudinal intermediate filaments is associated with sarcomeres of adult vertebrate skeletal muscle. *The Journal of cell biology*, 96:562–570.

[19] Li, Z., Mericskay, M., Agbulut, O., Butler-Browne, G., Carlsson, L., Thornell, L.E., Babinet, C., and Paulin, D., 1997. Desmin is essential for the tensile strength and integrity of myofibrils but not for myogenic commitment, differentiation, and fusion of skeletal muscle. *The Journal of cell biology*, 139:129–144.

[20] Shah, S.B., Su, F.C., Jordan, K., Milner, D.J., Fridén, J., Capetanaki, Y., and Lieber, R.L., 2002. Evidence for increased myofibrillar mobility in desmin-null mouse skeletal muscle. *The Journal of experimental biology*, 205:321–325.

[21] Sam, M., Shah, S., Fridén, J., Milner, D.J., Capetanaki, Y., and Lieber, R.L., 2000. Desmin knockout muscles generate lower stress and are less vulnerable to injury compared with wild-type muscles. *American journal of physiology Cell physiology*, 279:C1116–22.

[22] Peters, D., Barash, I.A., Burdi, M., Yuan, P.S., Mathew, L., Fridén, J., and Lieber, R.L., 2003. Asynchronous functional, cellular and transcriptional changes after a bout of eccentric exercise in the rat. *The Journal of physiology*, 553:947–957.

[23] Barash, I.A., Peters, D., Fridén, J., Lutz, G.J., and Lieber, R.L., 2002. Desmin cytoskeletal modifications after a bout of eccentric exercise in the rat. *American journal of physiology Regulatory, integrative and comparative physiology*, 283:R958–63.

[24] Newham, D.J., Jones, D.A., and Clarkson, P.M., 1987. Repeated high-force eccentric exercise: effects on muscle pain and damage. *Journal of applied physiology (Bethesda, Md : 1985)*, 63:1381–1386.

[25] Lovering, R.M., O'Neill, A., Muriel, J.M., Prosser, B.L., Strong, J., and Bloch, R.J., 2011. Physiology, structure, and susceptibility to injury of skeletal muscle in mice lacking keratin 19-based and desmin-based intermediate filaments. *American journal of physiology Cell physiology*, 300:C803–13.

[26] Camargo, F.D., Green, R., Capetanaki, Y., Jackson, K.A., Goodell, M.A., and Capetenaki, Y., 2003. Single hematopoietic stem cells generate skeletal muscle through myeloid intermediates. *Nature medicine*, 9:1520–1527.

[27] Schröder, R., Goudeau, B., Simon, M.C., Fischer, D., Eggermann, T., Clemen, C.S., Li, Z., Reimann, J., Xue, Z., Rudnik-Schöneborn, S., Zerres, K., van der Ven, P.F.M., Fürst, D.O., Kunz, W.S., and Vicart, P., 2003. On noxious desmin: functional effects of a novel heterozygous desmin insertion mutation

on the extrasarcomeric desmin cytoskeleton and mitochondria. *Human molecular genetics*, 12:657–669.

[28] Olivé, M., Goldfarb, L., Moreno, D., Laforet, E., Dagvadorj, A., Sambuughin, N., Martínez-Matos, J.A., Martínez, F., Alió, J., Farrero, E., Vicart, P., and Ferrer, I., 2004. Desmin-related myopathy: clinical, electrophysiological, radiological, neuropathological and genetic studies. *Journal of the neurological sciences*, 219:125–137.

[29] Muñoz-Mármol, A.M., Strasser, G., Isamat, M., Coulombe, P.A., Yang, Y., Roca, X., Vela, E., Mate, J.L., Coll, J., Fernández-Figueras, M.T., Navas-Palacios, J.J., Ariza, A., and Fuchs, E., 1998. A dysfunctional desmin mutation in a patient with severe generalized myopathy. *Proceedings of the National Academy of Sciences of the United States of America*, 95:11312–11317.

[30] Koman, L.A., Mooney, J.F., Smith, B., Goodman, A., and Mulvaney, T., 1993. Management of cerebral palsy with botulinum-A toxin: preliminary investigation. *Journal of pediatric orthopedics*, 13:489–495.

[31] Fukushima, K., Badlani, N., Usas, A., Riano, F., Fu, F., and Huard, J., 2001. The use of an antifibrosis agent to improve muscle recovery after laceration. *The American journal of sports medicine*, 29:394–402.

[32] van Spaendonck-Zwarts, K., van Hessem, L., Jongbloed, J.D.H., de Walle, H.E.K., Capetanaki, Y., van der Kooi, A.J., van Langen, I.M., van den Berg, M.P., and van Tintelen, J.P., 2010. Desmin-related myopathy: a review and meta-analysis. *Clinical genetics*.

[33] Nédellec, P., Edling, Y., Perret, E., Fardeau, M., and Vicart, P., 2002. Glucocorticoid treatment induces expression of small heat shock proteins in human satellite cell populations: consequences for a desmin-related myopathy involving the R120G alpha B-crystallin mutation. *Neuromuscular disorders : NMD*, 12:457–465.

[34] Ito, H., Kamei, K., Iwamoto, I., Inaguma, Y., Tsuzuki, M., Kishikawa, M., Shimada, A., Hosokawa, M., and Kato, K., 2003. Hsp27 suppresses the formation of inclusion bodies induced by expression of R120G alpha B-crystallin, a cause of desmin-related myopathy. *Cellular and molecular life sciences : CMLS*, 60:1217–1223.

# Chapter 2

# Theoretical Predictions of the Effects of Force Transmission by Desmin on Intersarcomere Dynamics

## Abstract

Desmin is an intermediate filament protein in skeletal muscle that forms a meshlike network around Z-disks. A model of a muscle fiber was developed to investigate the mechanical role of desmin. A two-dimensional mesh of viscoelastic sarcomere elements was connected laterally by elastic elements representing desmin. The equations of motion for each sarcomere boundary were evaluated at quasiequilibrium to determine sarcomere stresses and strains. Simulations of passive stretch and fixed-end contractions yielded values for sarcomere misalignment and stress in wildtype ($wt$) and desmin knockout ($des^{-/-}$) fibers. Passive sarcomere misalignment increased nonlinearly with fiber strain in both $wt$ and $des^{-/-}$ simulations and was significantly larger without desmin. During fixed-end contraction, $des^{-/-}$ simulations also demonstrated greater sarcomere misalignment and reduced stress production compared with $wt$. In simulations with only a

fraction of *wt* desmin present, fixed-end stress increased as a function of desmin concentration and this relationship was influenced by the cellular location of the desmin filaments. This model suggests that desmin stabilizes Z-disks and enables greater stress production by providing a mechanical tether between adjacent myofibrils and to the extracellular matrix and that the significance of the tether is a function of its location within the cell.

## 2.1   Introduction

A skeletal muscle fiber is a three-dimensional meshwork of sarcomeres interconnected longitudinally and laterally by a network of cytoskeletal proteins. These proteins, including titin, $\alpha$-actinin, dystrophin-associated proteins, and intermediate filaments, are fundamental to sustaining active and passive sarcomere loads. One fundamental component of the cytoskeleton is the intermediate filament protein desmin, which forms a network around the periphery of adjacent Z-disks, anchoring myofibrils to nuclei, mitochondria, and extracellular matrix (ECM) at the sarcolemma [1–3]. The localization of desmin suggests that it may play an important role in muscle fiber force transmission. Specifically, it is proposed that desmin acts as a lateral mechanical link between Z-disks, providing stability to the fiber by maintaining sarcomere homogeneity and transmitting force radially [3, 4]. Desmin-related myopathies in humans have debilitating effects, highlighting the vital role desmin plays in the proper functioning of muscle.

Recent experiments involving the desmin knockout ($des^{-/-}$) mouse have further defined the detrimental effects of desmin loss in skeletal muscle. $Des^{-/-}$ muscle fibers have decreased sarcomere connectivity, as measured by the stagger of radially adjacent myofibrillar Z-disks in electron micrographs of stretched extensor digitorum longus muscles [5]. This result was later confirmed using immunofluorescence in stretched single fibers [6]. In addition to these passive disparities, $des^{-/-}$ muscles develop lower fixed-end stress compared to wildtype (*wt*) muscles on the descending limb of the length-tension curve [7]. It was surprising to find, however, that these muscles show less stress decline (injury) after eccentric con-

tractions, even when correction is made for their smaller muscle size and initial stress production [7]. Building on this study, $des^{-/-}$l fibers were transfected with a green- fluorescent-protein (GFP)-desmin fusion protein and functionally evaluated [8]. Increasing GFP-desmin content was shown to attenuate Z-disk misalignment, increase fixed-end stress production, and increase injury as a logarithmic function of GFP-desmin content [8].

Although these studies have defined the functional consequences of desmin loss in muscle, the causative mechanism has yet to be described. High-resolution, real-time sarcomere array studies in intact muscle are currently not technically feasible, and thus, determining the role of desmin is an ideal problem to investigate using modeling.

Finite-element-type models of muscle fiber mechanics have already been developed [9, 10] and have been used successfully to simulate experimental fiber behavior. Two models explicitly incorporate the intermediate filament lattice, but they are of small scale and include no connection to the ECM [11, 12]. Thus, the purpose of this study was to develop a two-dimensional finite-element model of a muscle fiber incorporating desmin as a linear elastic spring element connecting Z-disks laterally. This model was then used to simulate passive stretch and fixed-end contraction of $des^{-/-}$ and $wt$ fibers and to predict the mechanical effect of desmin on sarcomere connectivity and fixed-end stress production.

## 2.2  Methods

### 2.2.1  The sarcomere finite element

A finite-element model of a muscle fiber is constructed here as a repeating connection of sarcomere elements, similar to previous approaches [9, 10]. The mechanical equivalent of a sarcomere is represented as a viscoelastic structure similar to the three-element muscle model proposed by Hill [26]. The contractile element (CE) represents the active force generated by myosin cross-bridges and is contiguous with an elastic element (SE) that represents their compliance (tendon is modeled explicitly here). A Maxwell viscoelastic unit (PVE) is connected in

Table 2.1: Model sensitivity analysis. The 17 model parameters were based on experimental data taken from the reference(s) shown. Confidence in each parameter was estimated subjectively on a scale from 1-4. based on support for that value in the literature. Low confidence and high sensitivity values are in italic print.

| Parameter | Reference | Value | Confidence | Sensitivity |
| --- | --- | --- | --- | --- |
| Myofibril spacing | [13] | 19 nm | 3 | 0.0 |
| Myofibril diameter | [6, 14] | 0.6 $\mu m$ | 4 | *8.1* |
| Maximum contractile stress (of a sarcomere) | [15, 16] | 368 kPa | 4 | *8.1* |
| Sarcomere length range (end to center) | [9, 17] | 0.2 $\mu m$ | 3 | 0.3 |
| Number of sarcomeres in series | [15, 18] | 200 | 2 | 0.6 |
| Number of myofibrils in parallel | [6, 15] | 10 | 2 | *7.7* |
| Passive tension exponential constant (m) | [6, 9] | 5.5 $\mu m$ | 2 | 0.3 |
| Passive tension exponential constant ($\lambda$) | [6, 9] | 0.5 | 2 | 0.2 |
| Length-tension curve (base width) | [15] | 1.27-3.9 $\mu m$ | 4 | *4.3* |
| Length-tension curve (peak width) | [15] | 2.1-2.45 $\mu m$ | 4 | 0.0 |
| Desmin elastic modulus | | 3.7 MPa | 2 | 0.2 |
| Passive viscosity coefficient | [19] | 0.8 kN-s/m$^2$ | 2 | 1.0 |
| Hill coefficients ($\frac{a}{P_0}, \frac{b}{V_{\max}}$) | [15] | 0.2 | 3 | 0.9 |
| Maximum velocity in shortening | [15, 20] | 4 L/s | 3 | 1.0 |
| ECM passive stress at $SL_{max}$ | [21–23] | 743 kPa | 1 | 1.9 |
| Endomysium thickness | [21, 23] | 0.1 $\mu m$ | 3 | 1.9 |
| Tendon elastic modulus | [24, 25] | 500 MPa | 3 | 0.0 |

parallel with the CE and SE to model the passive tension and damping of titin and other proteins that extend longitudinally between Z-disks. The forces in the CE and PVE are nonlinear functions of sarcomere length (SL) and sarcomere shortening velocity and are determined from scaled literature values for muscle fiber behavior (Table 2.1). The tension sustained by the SE is a linear function of extension ($E$).

The fiber is modeled as a two-dimensional array of sarcomere elements rigidly connected longitudinally to form myofibrils. Myofibrils are coupled laterally via desmin elastic elements (Fig. 2.1A). Viscoelastic elements representing the ECM, including the sarcolemma, and the tendon are included in the model with properties estimated from the literature (Table 2.1). The ECM forms the lateral bounds of the array and the tendon caps at either end. The coupled, noninertial equations of motion are solved simultaneously at each nodal point.

## 2.2.2 Equations of motion

A free body diagram of the forces sustained by the sarcomere shows the active (*red*), elastic (*blue*), and damping (*green*) contributions to the nodal equations of motion (Fig. 2.1B). The direction of the force in each element is indicated by arrows and the associated force (*upper case*) or element constant (*lower case*) is labeled. Calculating the sum of these forces at each node and setting the result equal to zero yields the nodal equations of motion in the longitudinal plane. Motion in the lateral plane is assumed to be negligible. Inertial forces are neglected in these equations due to the exceedingly small sarcomere mass. (Note that for inertial forces to be on the order of magnitude of viscous and elastic forces, the acceleration of a node would have to exceed $10^{12}$ $\mu$m/s$^2$, which is physiologically unreasonable [10].

The contribution of the elastic force of a desmin filament to forces in the longitudinal plane is not a linear function of its extension even if the filament is linearly elastic, since the force acts obliquely to the plane. The relationship between the component of the filament extension ($f(x)$) and the net nodal displacement ($x$)
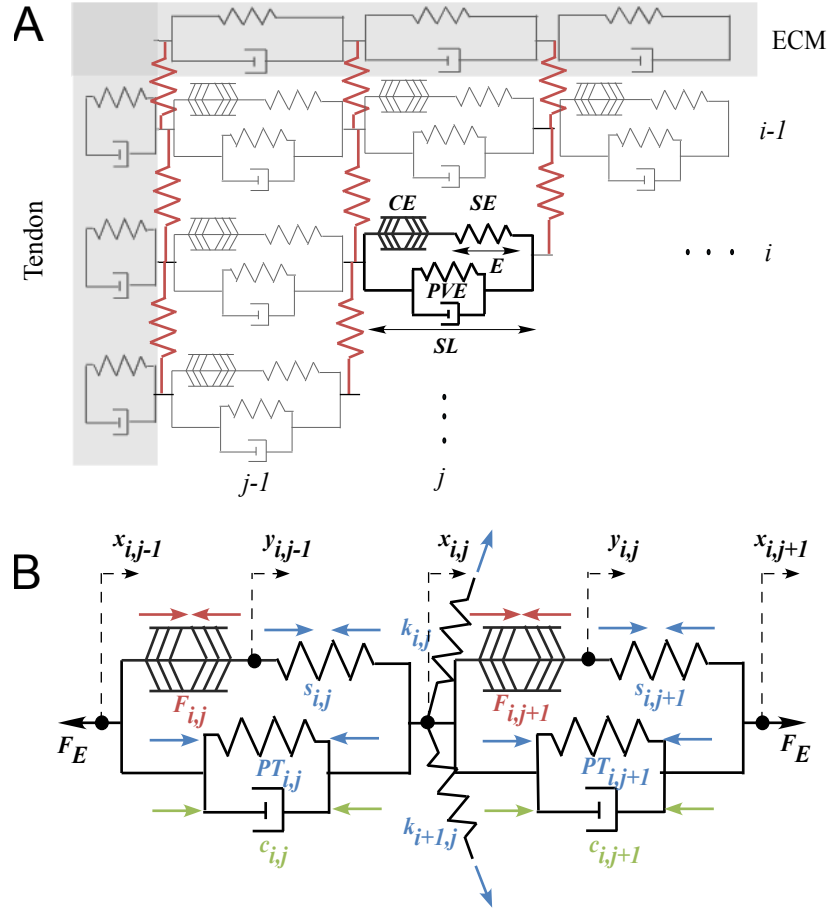
Figure 2.1: (A) Graphical representation of the finite- element muscle fiber array. (B) Free body diagram of two sarcomeres linked at a Z-disk. Viscoelastic sarcomere elements are linked longitudinally at Z-disk nodes to form myofibrils and laterally by desmin elastic filaments (*red*) to form a two-dimensional fiber. ECM elements form the upper and lower bounds of the array, whereas tendon elements define each end. The location of each element is indexed by its row ($i$) and column ($j$). The contractile element (CE), the series elastic element (SE), the parallel viscoelastic element (PVE), the sarcomere length (SL), and the series spring extension (E) are labeled in the bold sarcomere. Forces involved in the calculation of the nodal equations of motion are illustrated by color-coded arrows (*red*, active; *blue*, elastic; and *green*, viscous). Variables $x_{i,j}$ and $y_{i,j}$ are the displacements at the $x$ and $y$ nodes, respectively. $F_E$ are the forces external to the sarcomeres pictured and $F_{i,j}$ is the contractile force in the CE of sarcomere *(i, j)*. $PT_{i,j}$ is the passive tension developed in the PVE and $c_{i,j}$ is the damping constant of the PVE of the same sarcomere. Constant $s_{i,j}$ is the stiffness of the SE and $k_{i,j}$ is the stiffness of desmin.

in the longitudinal direction is given by

$$f(x) = x \left( 1 - \frac{L}{\sqrt{L^2 + x^2}} \right) \tag{2.1}$$

where $L$ is the unstretched filament length, which is exactly at rest, neither stretched nor slackened. When this function is incorporated into the desmin elastic terms, the equation of motion at node $x_{i,j}$ is given by

$$F_{i,j+1} - s_{i,j}(x_{i,j} - y_{i,j-1}) = PT_{i,j} - PT_{i,j+1}+ \tag{2.2}$$
$$c_{i,j}(\dot{x}_{i,j} - \dot{x}_{i,j-1}) - c_{i,j+1}(\dot{x}_{i-1,j} - \dot{x}_{i,j}) - k_{i,j}(x_{i-1,j} - x_{i,j}) - k_{i+1,j}(x_{i+1,j} - x_{i,j})$$

where variables are as defined in (Fig. 2.1B). $k_{i,j}$ are the elastic spring constants of the desmin elements and $c_{i,j}$ are the passive sarcomere viscosity coefficients, both of which are constants. Location indices $i$ and $j$ are included simply to specify nodal position. The passive tension of the PVE elements is given by $PT_{i,j}$ where $m$, $\lambda$, and $p_{i,j}$ are constants.

$$PT_{i,j} = p_{i,j} \exp \left( \frac{x_{i,j} - x_{i,j-1} - m}{\lambda} \right) \tag{2.3}$$

The equation of motion at node $y_{i,j-1}$ is

$$F_{i,j} = s_{i,j}(x_{i,j} - y_{i,j-1}) \tag{2.4}$$

Note that this equation indicates that terms involving tension sustained by the SE in any equation (i.e., the lefthand side of Eq. 2.2) can be replaced by the force of the CE (i.e., the lefthand side of Eq. 2.4). Thus, the equations of motion are only evaluated at the $x_{i,j}$ nodes (Z-disks) and are of the form

$$F_{i,j+1} - F_{i,j} = PT_{i,j} - PT_{i,j+1}+ \tag{2.5}$$
$$c_{i,j}(\dot{x}_{i,j} - \dot{x}_{i,j-1}) - c_{i,j+1}(\dot{x}_{i-1,j} - \dot{x}_{i,j}) - k_{i,j}(x_{i-1,j} - x_{i,j}) - k_{i+1,j}(x_{i+1,j} - x_{i,j})$$

The nodal equations of motion can be expressed in the general matrix form

$$A\dot{x} + B\exp\left(\frac{(x-a)}{\lambda}\right) + Cf(x) = d \tag{2.6}$$

where $x$ and $\dot{x}$ are the displacement and velocity, respectively, of each node (Z-disk). Matrix $A$ is the damping matrix and contains only the constants $c_{i,j}$. Matrices $B$ and $C$ contain the constants for PVE and desmin elasticity, respectively, whereas the vector $d$ contains the forces of the contractile elements.

The complexity of this system of nonlinear differential equations is simplified by computing nodal velocities first, and then determining displacements from these velocities at discrete time steps, typically on the order of 0.01 ms. In this method, the $x$ and $f(x)$ terms become constants that can be lumped into the contractile force term. Thus, the system is simplified to

$$Ax = b \tag{2.7}$$

where the variable of interest, $x$, is now velocity and $b$ is a nonlinear function of nodal displacement.

### 2.2.3  Model parameters

The parameters used in the model equations were derived from 17 empirical measurements obtained from the literature, primarily from mouse muscle fibers (Table 2.1). Each parameter was assigned a subjective confidence level from 1 to 4 based on the number of corroborating studies, with 4 representing our opinion of an excellent assumption and 1 representing a questionable assumption. Then, a sensitivity analysis was performed for each model parameter to determine the relative change in force production resulting from a 10% parameter change. Sensitive parameters whose confidence is low represent more severe model limitations (however, all parameters in this model with sensitivities $> 4\%$ had confidence levels of at least 2). These parameters were then incorporated into the relationships governing the behavior of the CE and PVE as discussed below.
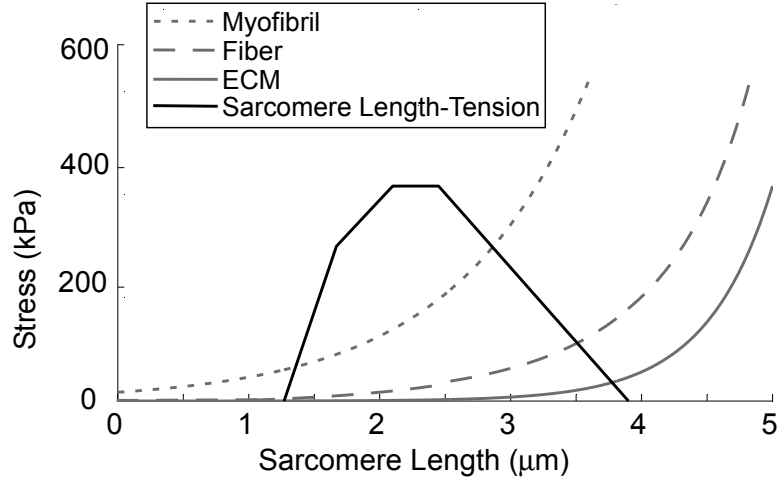
Figure 2.2: Myofibril passive stress, ECM passive stress, and the sarcomere length-tension relationship as estimated from work by others [6, 15, 21–23, 26]. The fiber average passive stress is calculated for a simulated fiber with 10 myofibrils laterally by summing the force contribution of each myofibril and the two ECM elements and dividing by the total cross-sectional area.

## 2.2.4 The contractile element

The ability of a model sarcomere to generate contractile force was dependent on the degree of actin-myosin overlap in the manner originally described for single fibers by Gordon et al. [27]. The model described here makes no attempt to model individual cross-bridge interactions, but instead uses the length-tension relationship measured by Edman et al. from mouse flexor digitorum brevis single fibers during fixed-end tetani [15]. The piecewise linear curve fit has zero force at sarcomere lengths <1.27 $\mu$m, 0.72 times the maximum force at 1.68 $\mu$m, maximum force between 2.1 and 2.45 $\mu$m, and zero force above a sarcomere length of 3.9 $\mu$m (Fig. 2.2).

The force-generating capacity of a shortening sarcomere as a function of velocity was modeled using the classic Hill equation [26], whose constants were determined to be $b/V_{max} = a/P_0 = 0.2$ for mouse fast fibers [15]. For lengthening sarcomeres, the force-velocity curve was assumed to have a slope equal to six times the shortening slope at very small velocities and a maximum force production of

1.8 $P_0$ [28] at maximum velocity, $V_{max}$. For simplicity, $V_{max}$ is assumed to be constant in this model, although some variation with sarcomere length has been reported [29].

### 2.2.5   The parallel viscoelastic element

The passive-tension exponential constants used in this model were determined by fitting Eq. 2.3 to skinned mouse single fiber stress-strain data [6] (Fig. 2.2). The viscosity coefficient of the sarcomere PVE was 0.8 kN-s/m$^2$, as given by the mouse fast fiber data of Mutungi and Ranatunga [19].

### 2.2.6   Variation in sarcomere properties

Sarcomere elements in the model have identical properties except for their initial lengths (exponential variation) and passive tension (random variation) relationships, and each sarcomere is assumed to be symmetric. The initial sarcomere length distribution for a half-myofibril is defined by the equation

$$SL_i = \mu_{SL} - \delta_{SL} \exp(-40i/N) \qquad (2.8)$$

yielding end sarcomere lengths that are shorter than average and a sarcomere length distribution that is smooth along the length of the myofibril [17, 30] (Fig. 2.3). The constants $\mu_{SL}$ and $\delta_{SL}$ are the mean sarcomere length and the sarcomere length range, respectively, of the distribution, $i$ is the index of the current sarcomere, and $N$ is the number of sarcomeres in a half-myofibril. This distribution is then mirrored at the center to create the myofibril distribution with shorter sarcomeres at each end.

Superimposed on this distribution is a 5% uniform random variation in the passive tension constant, $\lambda$ (Fig. 2.3). This random component is intended to reflect the biological variation in passive load-bearing structures such as titin that contribute to sarcomere stiffness variation. This is one possible explanation for the variability in sarcomere lengths across the length of fibers and myofibrils observed experimentally [31, 32].
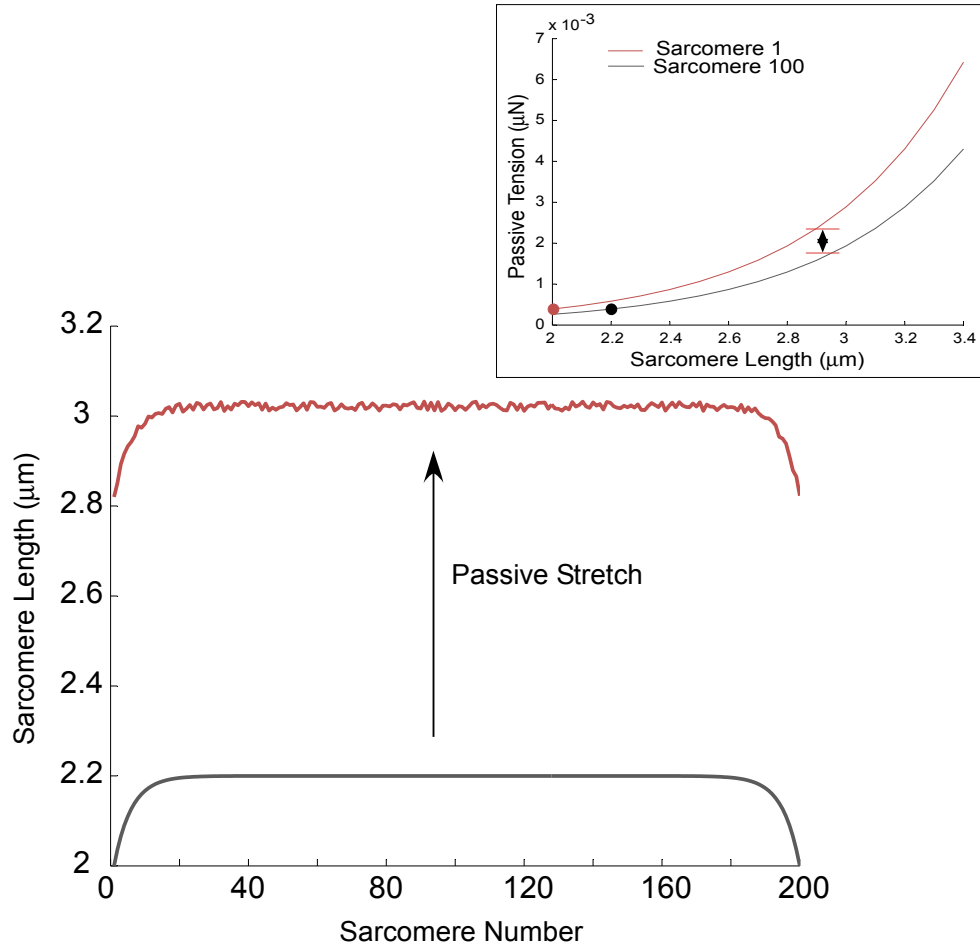
Figure 2.3: Sarcomere length distributions across the fiber length and depiction of initial passive tension (*inset*). The gray trace is the sarcomere length distribution generated by Eq. 2.8, with a mean sarcomere length of 2.2 $\mu$m and a length range of 0.2 $\mu$m. The red trace shows what happens to the distribution after passive stretch to a mean sarcomere length of 3 $\mu$m. The variation in sarcomere length is a result of the random variation in the passive tension coefficient, $\lambda$. (*Inset*) Passive tension curves for sarcomeres 1 and 100, where the curve for sarcomere 1 has been multiplied by a larger coefficient so that the passive tensions are equal for the two sarcomeres at their initial lengths (*dots* on *inset*).

### 2.2.7 Properties of the ECM and tendon

ECM and tendon elements are constructed of parallel viscoelastic and series elastic elements only and have no active element. In addition, the parameters of these elements are unique for the ECM and tendon compared to the sarcomeres. Initially, each ECM row is given an element length distribution identical to the initial sarcomere length distribution defined by Eq. 2.8 so that desmin elements initially are oriented laterally and have no longitudinal loading. Each myofibril is connected to two tendon elements, one on each end, and tendon elements do not interact with their lateral neighbors. Neither ECM nor tendon elements have random property variations.

### 2.2.8 Desmin stiffness

Desmin stiffness was calculated using atomic force microscopy measurements of isolated desmin filaments and fitting data to the wormlike chain model. The details of the desmin preparation and stiffness estimation can be found in Appendix A.

### 2.2.9 Simulations

All simulations used model fibers with 10 laterally connected myofibrils with 200 sarcomeres longitudinally. These dimensions were chosen for computational tractability. The computational routine determines the initial exponential sarcomere length distribution from a user-defined mean sarcomere length. This distribution is then used to calculate the passive tension relationship for each sarcomere by adjusting the constant $p_{i,j}$ from Eq. 2.3 such that all sarcomeres begin at the same initial passive tension and the fiber rests in static equilibrium. This adjustment is illustrated in the inset of Fig. 2.3, where the curve for sarcomere 1 is adjusted by increasing its $p_{i,j}$ compared to sarcomere 100 so that the two sarcomeres at different initial lengths have the same passive tension. The isometric force producing capacity ($P_0$) of each contractile element is calculated using the sarcomere length-tension curve (Fig. 2.2). An activation ramp is then imposed on

the fiber using

$$P = \left( \frac{t}{0.005 + t} \right) P_0 \qquad (2.9)$$

where $P$ is the amount of force the sarcomere can generate at time $t$, to ensure that sarcomeres dont switch from passive to active instantaneously. The contractile element force and velocity are then computed from the equations of motion and the force-velocity curve. The sarcomere length distribution is updated by multiplying contraction velocity by a discrete time step, and the computation is then repeated under the new conditions. Thus, the routine computes the strain map and force production of the fiber over time. Stress production is calculated by dividing the force by the average cross-sectional area of a mouse EDL myofibril multiplied by the number of myofibrils in parallel.

Passive stretch was performed on ten simulated fibers, each with a unique variation in sarcomere properties (length and passive tension), by constraining fiber ends to move with a constant velocity of 0.085 mm/s and allowing stretch from a mean sarcomere length of 2.2 $\mu$m to 5 $\mu$m (strain = 1.27). Data are presented as the mean and standard deviations of these 10 fibers. Z-disk stagger was determined by computing the absolute difference between the positions of laterally adjacent nodes over the length of the fiber and averaging these values at each Z-disk (column). Mean Z-disk stagger was determined every 5% strain by averaging Z-disk stagger over the length of the fiber.

Fixed-end contraction was also simulated with 10 fibers. Immediately before activation, sarcomeres are simulated to stretch from a mean sarcomere length of 2.2 $\mu$m to 3 $\mu$m as described above. This was intended to provide a variation in sarcomere lengths at 3 $\mu$m and does not qualitatively affect the simulation results. Sarcomeres were then activated for 2.5 s. Measurements of Z-disk stagger were made, as described above, in increments of 100 ms, and fixed-end stress production was computed as the maximum stress achieved during the simulation. All simulations were written and executed in MATLAB (The MathWorks, Natick, MA).

## 2.3 Results

### 2.3.1 Passive stretch

To investigate the effect of strain on sarcomere alignment, passive stretch of 10 $wt$ and 10 $des^{-/-}$ fibers was simulated, differing only in the random component of their initial passive tension parameter. $Des^{-/-}$ fibers had significantly greater mean Z-disk stagger than wildtype at sarcomere lengths $> 3$ $\mu$m (Fig. 2.4A). Both the magnitude and the discrepancy in mean Z-disk stagger between $des^{-/-}$ and $wt$ fibers increased nonlinearly as a function of strain. To find any localization of high Z-disk misalignment, the stagger of each Z-disk along the fiber length was measured. Z-disk stagger was significantly higher for $des^{-/-}$ fibers along the length of the fiber, with the exception of the fiber ends, which were constrained by the tendon to have near-zero stagger (Fig. 2.4B). The midsection of the fiber is predicted to have the highest Z-disk misalignment.

### 2.3.2 Fixed end contraction

Fixed-end contractions of 10 $wt$ and 10 $des^{-/-}$ fibers were simulated with the same parameters used for the passive stretch simulations. Intersarcomere dynamics, similar to those observed using the model of Morgan et al. [9], demonstrated that end sarcomeres rapidly shortened, whereas center sarcomeres lengthened during contraction (Fig. 2.5). Similar to passive stretch simulations, mean Z-disk stagger measurements showed significantly greater misalignment for $des^{-/-}$ fibers over the contraction, and this discrepancy increased as a function of time (Fig. 2.6A). In addition, the stagger at the majority of Z-disks along the fiber was significantly higher for $des^{-/-}$ than for $wt$ fibers (Fig. 2.6B). Again, the largest misalignment occurred in the fiber midsection.

Stress production was also examined during fixed-end contractions. Fixed-end stress production was reduced by 20% in the simulated $des^{-/-}$ fiber compared with $wt$ (Fig. 2.7). To investigate the role desmin localization plays in fixed-end stress development, desmin links were applied to 1, 5, 10, 25, 50, and 90% of the possible Z-disk connections, using one of three spatial arrangements: 1), randomly
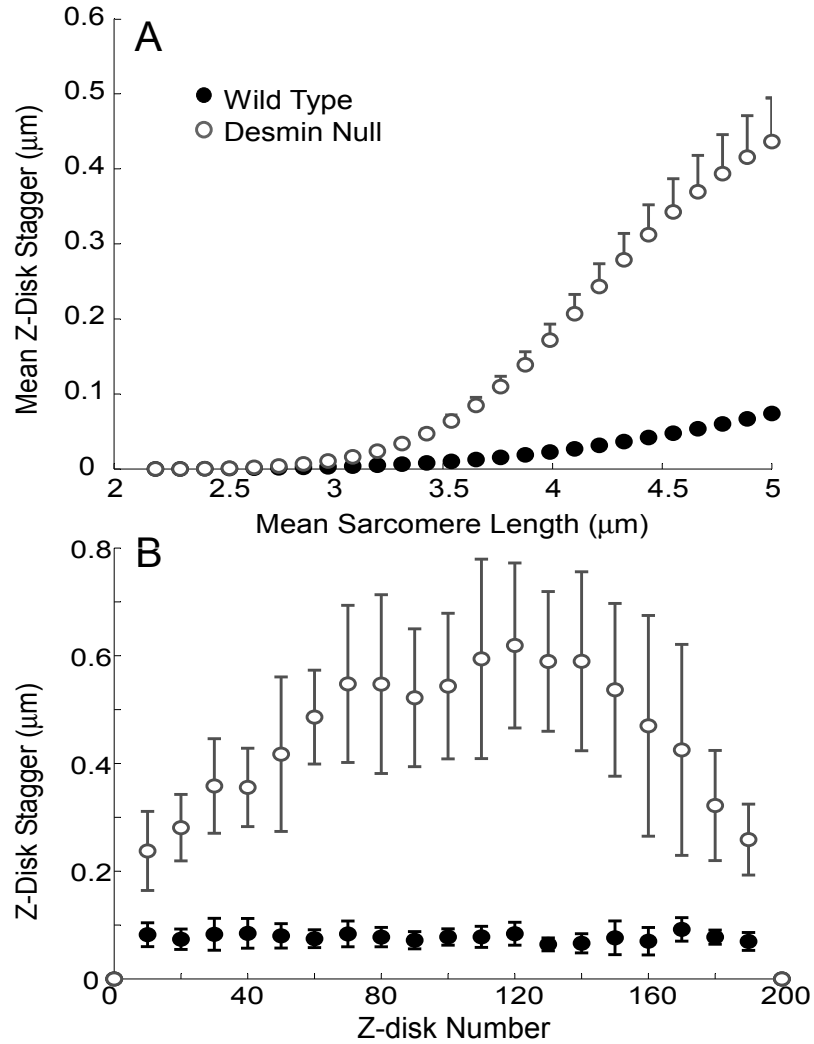
Figure 2.4: (A) Mean Z-disk stagger as a function of sarcomere length over the course of a passive stretch. (B) Measurements of stagger at every 10th Z-disk over the length of the fiber at a sarcomere length of 5 $\mu$m. Data points are the mean value from 10 runs in each group, with a different random variation in the passive tension constant used for each run, and error bars are the standard deviations. $Des^{-/-}$ fibers have a significantly higher mean Z-disk stagger than $wt$ at all sarcomere lengths ¿3 $\mu$m and at all Z-disks except for the fiber ends, which are constrained. Some error bars are small and are obscured by the data marker.
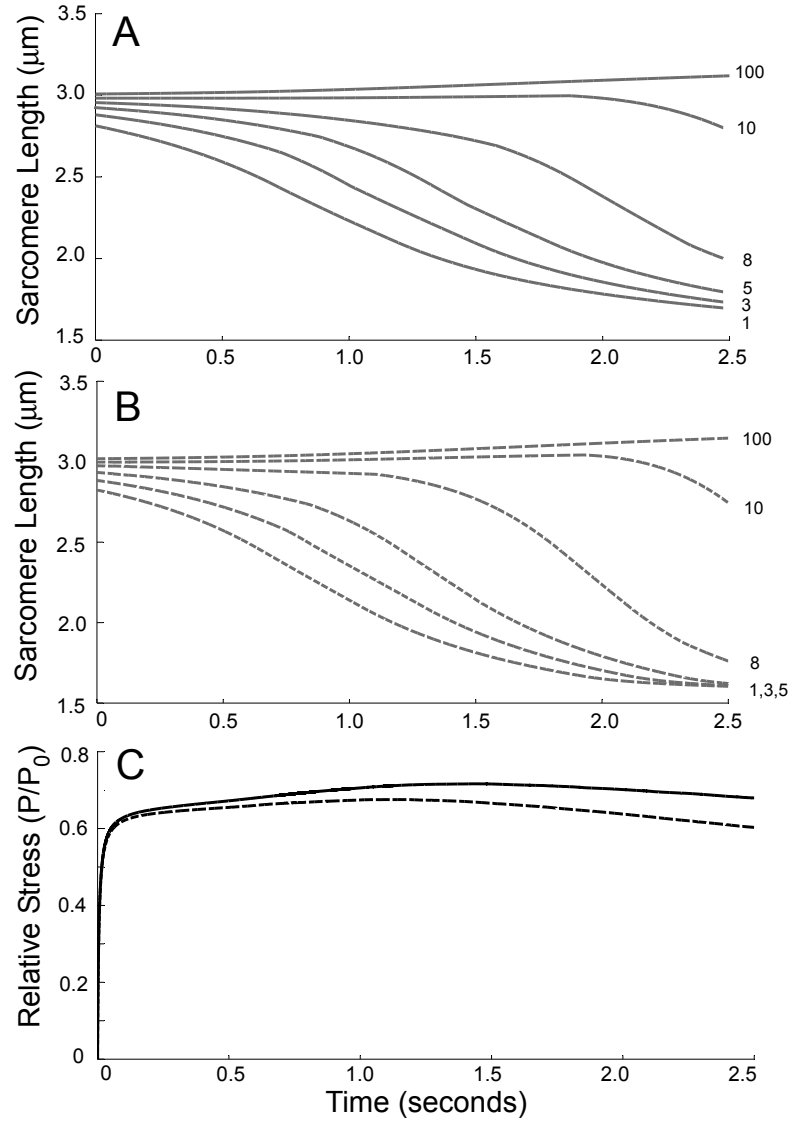
Figure 2.5: Length traces over time of a representative run for selected sarcomeres from (A) *wt* and (B) *des*$^{-/-}$ fibers and the overall normalized force traces (C) during simulated fiber fixed-end contraction. Solid lines correspond to *wt* simulations and dotted lines to *des*$^{-/-}$. Sarcomere numbers (labeled right side of A and B) are increasing along the length of the fiber. End sarcomeres shorten significantly over the contraction period, whereas center sarcomeres lengthen more slowly and continuously. Note that end sarcomeres in the *des*$^{-/-}$ traces (B) are shorter than in the *wt* (A), and their corresponding force is lower (C). Compare with simulations reported previously (Figs. 4A and 5 in Morgan et al. [9]).
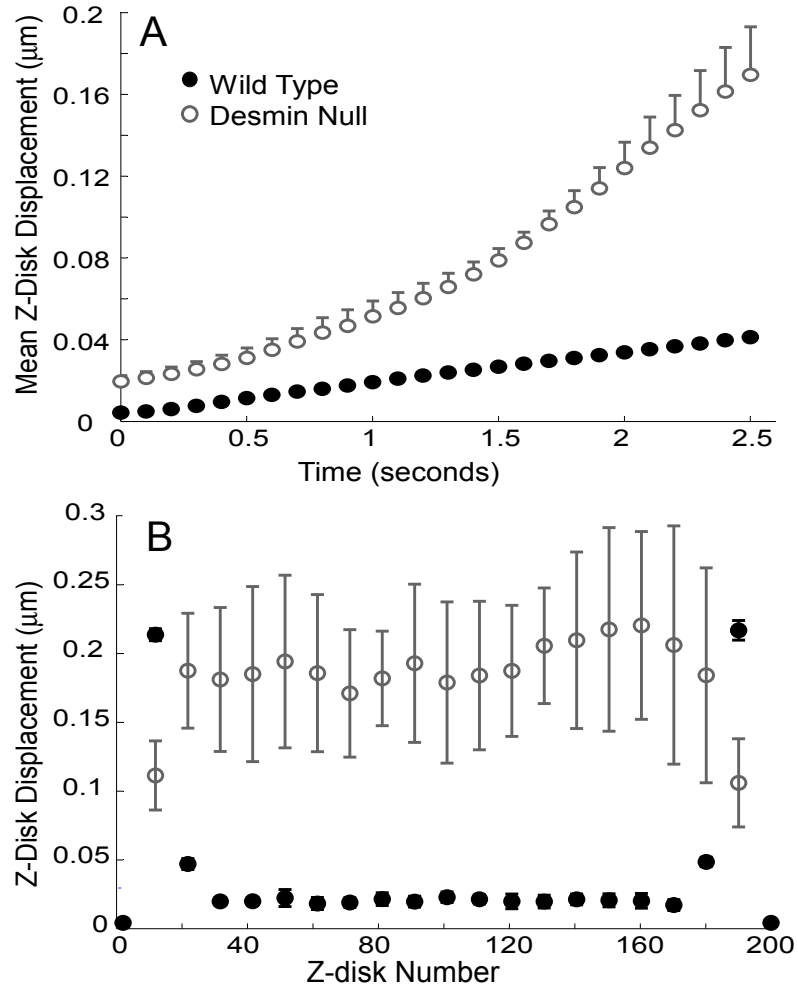
Figure 2.6: (A) Z-disk stagger as a function of the time course of simulated fixed-end contraction. (B) Measurements of stagger at every $10^{th}$ Z-disk over the length of the fiber at 2.5 s. Mean Z-disk stagger is significantly higher for $des^{-/-}$ fibers than for $wt$ at all time points and increases nonlinearly as a function of time. Z-disk stagger and hence differences in stagger between $wt$ and $des^{-/-}$ fibers are small at the fiber ends due to the abrupt force drop modeled in the contractile element, with shortening beyond 1.68 $\mu$m sarcomere length and the limited opportunity for sarcomere length variations to compound due to the proximity to the tendon. Z-disk staggers are on the same order as those seen during passive stretch.
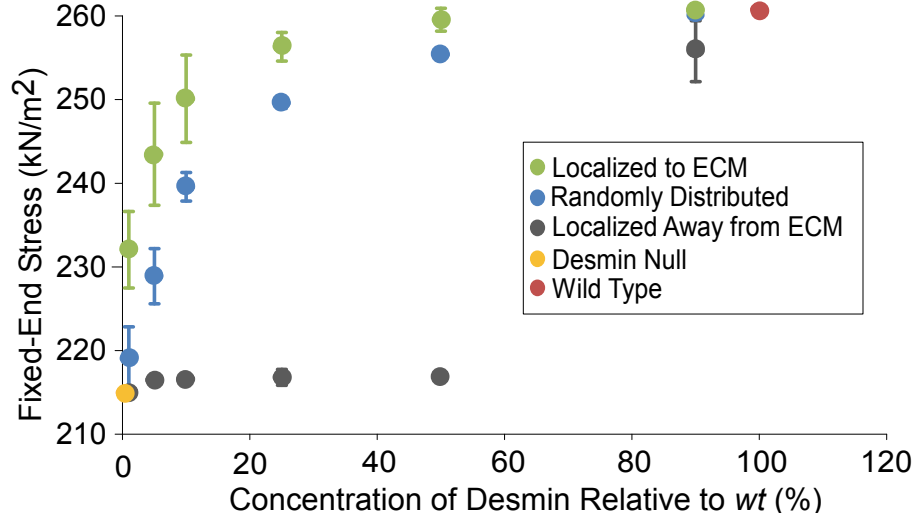
Figure 2.7: Plot of the maxiumum stress production during simulated fixed-end contraction of fibers with varying concentrations and localizations of desmin. Stress production is greater when desmin is preferentially localized to the fiber membrane (*green*) than when it is distributed randomly (*blue*) or preferentially localized away from the fiber membrane (*gray*). Each data point represents the mean of 10 simulations under its color-coded condition, and error bars are standard deviations.

across the fiber; 2), preferentially to the ECM; or 3), preferentially away from the ECM. To select preferential arrangement, each desmin link was assigned a number based on its position in the fiber array. The numbers were then arranged into a vector of length 11 myofibrils X 199 sarcomeres, with either the peripheral or central numbers in the center. Then, an algorithm was used which drew pseudorandom numbers from a normal distribution with a mean at the center of the vector and a standard deviation of 200. This number was used to index the vector, selecting a specific desmin link. The relationship between desmin content and fixed-end stress production showed a different degree of nonlinearity for each case considered.

Restoring 1% of the desmin content in the $des^{-/-}$ fiber at the ECM attenuated 40% of the fixed-end stress-producing deficit. Restoring 1% of the desmin randomly attenuated the deficit by 10%, whereas away from the ECM, 1% desmin did not significantly change the fixed-end stress. When 50% of the desmin content was restored either near the ECM or randomly, the stress-producing deficit was reduced by 97% or 88%, respectively; however, when desmin was localized away

from the ECM, this degree of stress restoration is not seen until the desmin concentration is at 90%. When 90% of the desmin was restored either to the ECM or randomly, the stress production was not significantly different from that seen in the *wt* fiber (Fig. 2.7).

## 2.4   Discussion

This model was developed to isolate the mechanical contributions of desmin to sarcomere movement during passive stretch and fixed-end contraction. We based our assumptions on relationships that have been demonstrated in single fibers, then scaled to the sarcomere level, an approach validated by previous investigators [9, 10]. The novel aspect of this model is that it explicitly incorporates desmin intermediate filament elements into the finite-element mesh at locations, and in orientations, that they appear to occupy based on structural data [3, 4]. In addition, we measured material properties of isolated desmin filaments and incorporated them into the model, thus increasing the models predictive potential.

The novel predictions of the model are that 1), desmin modulates intersarcomere dynamics during passive stretch and fixed-end contraction; 2), by anchoring to the ECM, and thus restricting sarcomere shortening, desmin enables the fiber to produce more active stress; and 3), the magnitude of this effect is dependent on the localization of desmin, with desmin near the ECM having the most influence on stress production. Results suggest that the experimentally observed increase in sarcomere misalignment during passive stretch [5, 6], decrease in fixed-end stress production [7], and, as discussed later, relationship between desmin concentration and injury [8] may be explained, at least in part, by the loss of desmin between Z-disks and the ECM.

$Des^{-/-}$ simulated fibers were shown to have significantly higher Z-disk misalignment in comparison with *wt* fibers during passive stretch at nearly all strains and across the majority of the fiber length (Fig. 2.4). These results are consistent with previous demonstrations of increased "Z-disk displacement" (our "stagger") observed in electron micrographs [5] and increased Z-disk variance using confocal

microscopy [6]. The magnitude of "Z-disk displacement" measured was in the range of 0-0.5 $\mu$m, which is consistent with model predictions. The results also agree with the observation that the difference between $wt$ and $des^{-/-}$ "displacements", as well as the magnitudes of each in passive muscle, increase with increasing strain [5, 6].

Agreement between predictions of misalignment during passive stretch and experimental observations supports the idea that desmin acts to mechanically couple sarcomeres, thereby restricting longitudinal shear, the movement of a myofibril past its neighbor. The predicted attenuation of shear is primarily a function of the sarcomeric variation in the passive tension parameter at long length and the elastic modulus of desmin. An overestimate of either parameter would result in an overprediction of the increase in $des^{-/-}$ sarcomere misalignment over that of $wt$. The estimated random variation in the passive tension parameter resulted in a 1% predicted variation in sarcomere length after passive stretch from a mean sarcomere length of 2.2 $\mu$m to 5 $\mu$m. Based on experimental data that cite the variation in sarcomere length along a fiber to be between 2 and 11%, the modeled passive tension parameter variation is likely conservative [27, 32, 33].

The elastic modulus used for desmin was determined using the wormlike chain model. It is possible that if the filaments are stretched longitudinally with relatively large forces, deviations will occur from the theoretically predicted entropic chain behavior. Recent studies by Kreplak et al. [34] in which the center of an isolated desmin filament was stretched perpendicular to the long axis revealed a desmin modulus between 10 and 15 MPa, which is considerably larger than the value computed here. Their experiment is subject to its own assumptions and limitations, but it is reasonable to assume that the modulus value used in this model is conservative. In addition, it is possible that each lateral connection is composed of more than just the one filament modeled here. In the model, incorporating more filaments would be equivalent to increasing the stiffness of the desmin spring. The one-filament link is used here to be a limiting conservative case, as an increase in the stiffness of desmin increases its effect on sarcomere alignment and stress production.

No experimental data are available that compare Z-disk alignment between

*wt* and *des*$^{-/-}$ fibers during fixed-end contraction, but we predict from these simulations that Z-disk misalignment would be higher in *des*$^{-/-}$ compared with *wt* fibers (Fig. 2.6).

By coupling sarcomeres laterally and anchoring them to the ECM, desmin serves as a mechanism to prevent large length discrepancies between laterally adjacent sarcomeres. If a sarcomere were to attempt to shorten faster than its neighbors, desmin filaments would transmit a portion of this force to adjacent sarcomeres or to the ECM, preventing shortening of the original sarcomere until its neighbors could catch up. Thus, the desmin intermediate filament network behaves as an intersarcomere stiffness, preventing sharp divisions in length between sarcomere populations. In fact, comparison of a simulation run by Morgan et al. [9, 30] that lacked intersarcomere stiffness to one including intersarcomere stiffness show differences similar to those seen in comparing Fig. 2.5A and Fig. 2.5B, in this article. The initial stress rise is similar, but the peak is somewhat lower and the decline after the peak is faster. This model suggests, then, a possible mechanism for intersarcomere stiffness that warrants a more in-depth exploration.

Stress production during fixed-end contraction was predicted by the model to be on average 20% lower for *des*$^{-/-}$ fibers compared to *wt* fibers (Fig. 2.7). This result is consistent with experimental data indicating that on the descending limb of the length-tension curve, *des*$^{-/-}$ muscles produce 10-20% lower fixed-end stress compared to *wt* muscles (7). The mechanistic basis for this prediction is that desmin behaves as a tether, limiting the longitudinal variation in sarcomere length. In the absence of this tether, end sarcomeres, which begin on the descending limb of the length-tension curve, are allowed to shorten more freely and cross the plateau onto the ascending limb.

The predicted decrease in fixed-end stress production in *des*$^{-/-}$ fibers is a function of the modulus of desmin, the properties of the ECM elements, the initial sarcomere lengths, and the dimensions of the sarcomere array. An overestimate of the modulus of desmin would result in a tighter link to adjacent myofibrils and to the ECM, which would increase the simulated difference in fixed-end stress between *des*$^{-/-}$ and *wt* fibers. However, as discussed previously, we believe our value to be

conservative. An overestimate of the ECM element modulus would also result in an overprediction of the mechanical contribution of desmin to stress production. The modulus used here for the sarcolemma and ECM composite is below values found in the literature [21–23], so we believe this value to be conservative as well.

All simulations presented here were activated at a mean sarcomere length of $3\,\mu$m, which is on the descending limb of the length-tension curve. At these lengths, intersarcomere dynamics play a large role in stress generation, as demonstrated by the rapid shortening of end sarcomeres and the gradual lengthening of central sarcomeres [9]. The predicted drop in fixed-end stress production for $des^{-/-}$ fibers is a direct consequence of this phenomenon, as end-sarcomere velocity is unrestrained and sarcomeres cross onto the ascending limb of the length-tension curve. Simulations run with mean sarcomere lengths beginning on the plateau or ascending limb show little to no difference in stress production between $wt$ and $des^{-/-}$ models. This is consistent with published results by other groups, who have reported no significant stress difference between $wt$ and $des^{-/-}$ muscles at optimal length [35, 36].

The dimensions of the sarcomere array were chosen based on computational tractability and are only about one-tenth the size of a mouse fiber in the lateral and longitudinal directions. In addition, the model only includes sarcomeres in two dimensions, whereas myofibrils in a real fiber are arranged in a three-dimensional hexagonal close-packing arrangement. Increasing the model dimensions laterally increases the distance between the central sarcomeres and the stiffer ECM, decreasing the desmin-mediated influence it has over them. However, explorative model runs at half and twice the current dimensions have shown only changes in the quantitative effects of desmin and have the same qualitative effect. We believe that further increasing the model to realistic dimensions would have the same result: increased stagger and decreased stress production for the $des^{-/-}$ over the $wt$ case, with the same dependence on desmin location. In addition, although central sarcomeres will be further removed from the ECM in a three-dimensional model of correct dimensions, they will also be connected to more neighboring myofibrils, which will in turn interconnect with even more neighbors, eventually binding the

ECM > 300 times per Z-line. Thus, expanding the scale to three dimensions would serve to dramatically increase the desmin-mediated influence of the ECM, making our two-dimensional model a conservative case.

In *wt* model fibers, end sarcomere shortening is restrained by the ECM only because desmin transmits force between it and adjacent Z-disks. In the fiber center, desmin acts to restrain relative stagger between laterally adjacent sarcomeres, but does not provide the same anchoring effect as it does at the ECM. As expected, the model then predicts that if desmin links are restored preferentially at the ECM, fixed-end stress production is increased compared to the case where they are restored in the interior of the fiber. As more elements are restored to the ECM, stress increases dramatically until all are present ( 20% desmin concentration in this model); then stress production begins to level off as desmin concentration increases to 100%. This is an interesting result in light of recent findings by Palmisano et al. [8] that injury to desmin transfected fibers increases with desmin content in a similar logarithmic fashion. This data may indicate that transfected desmin localizes preferentially to the membrane to maximize the stability it can provide to the fiber.

If a larger sarcomere array was used in these simulations, the ratio of ECM desmin links to central fiber links would decrease, making it less likely that an ECM link would be chosen at random. This would then cause the randomly distributed desmin prediction (Fig. 2.7, *blue curve*) to more closely resemble the prediction where desmin is selected away from the ECM (Fig. 2.7, *gray curve*), strengthening the case for preferential desmin localization. Future experimental studies are required to investigate whether desmin localization plays a role in stress generation during fixed-end contractions.

# Acknowledgements

Chapter 2, in full, is a reprint of the published article "Theoretical Predictions of the Effects of Force Transmission by Desmin on Intersarcomere Dynamics." Meyer G.A., Kiss B., Morgan D.L., Kellermayer M.S., and Lieber R.L. *Biophysical Journal*, 20;98(2):258-266, 2010. The dissertation author was the primary investigator and author of this paper.

## 2.5 References

[1] Granger, B.L. and Lazarides, E., 1979. Desmin and vimentin coexist at the periphery of the myofibril Z disc. *Cell*, 18:1053–1063.

[2] Paulin, D. and Li, Z., 2004. Desmin: a major intermediate filament protein essential for the structural integrity and function of muscle. *Experimental cell research*, 301:1–7.

[3] Wang, K. and Ramirez-Mitchell, R., 1983. A network of transverse and longitudinal intermediate filaments is associated with sarcomeres of adult vertebrate skeletal muscle. *The Journal of cell biology*, 96:562–570.

[4] Lazarides, E., 1980. Intermediate filaments as mechanical integrators of cellular space. *Nature*, 283:249–256.

[5] Shah, S.B., Su, F.C., Jordan, K., Milner, D.J., Fridén, J., Capetanaki, Y., and Lieber, R.L., 2002. Evidence for increased myofibrillar mobility in desmin-null mouse skeletal muscle. *The Journal of experimental biology*, 205:321–325.

[6] Shah, S.B., Davis, J., Weisleder, N., Kostavassili, I., McCulloch, A.D., Ralston, E., Capetanaki, Y., and Lieber, R.L., 2004. Structural and functional roles of desmin in mouse skeletal muscle during passive deformation. *Biophysical journal*, 86:2993–3008.

[7] Sam, M., Shah, S., Fridén, J., Milner, D.J., Capetanaki, Y., and Lieber, R.L., 2000. Desmin knockout muscles generate lower stress and are less vulnerable to injury compared with wild-type muscles. *American journal of physiology Cell physiology*, 279:C1116–22.

[8] Palmisano, M., Bremner, S., Shah, S., Ryan, A., and Lieber, R.L., 2007. Rescue of mechanical function in desmin knockout muscles by plasmid transfection. In Annual Meeting of the Orthopaedic Research Society. San Diego, CA.

[9] Morgan, D.L., Mochon, S., and Julian, F.J., 1982. A quantitative model of intersarcomere dynamics during fixed-end contractions of single frog muscle fibers. *Biophysical journal*, 39:189–196.

[10] Denoth, J., Stüssi, E., Csucs, G., and Danuser, G., 2002. Single muscle fiber contraction is dictated by inter-sarcomere dynamics. *Journal of theoretical biology*, 216:101–122.

[11] Anderson, J., Li, Z., and Goubel, F., 2002. Models of skeletal muscle to explain the increase in passive stiffness in desmin knockout muscle. *Journal of biomechanics*, 35:1315–1324.

[12] Telley, I.A., Denoth, J., and Ranatunga, K.W., 2003. Inter-sarcomere dynamics in muscle fibres. A neglected subject? *Advances in experimental medicine and biology*, 538:481–500; discussion 500.

[13] Goldspink, G., 1971. Changes in striated muscle fibres during contraction and growth with particular reference to myofibril splitting. *Journal of cell science*, 9:123–137.

[14] Goldspink, G., 1970. The proliferation of myofibrils during muscle fibre growth. *Journal of cell science*, 6:593–603.

[15] Edman, K.A.P., 2005. Contractile properties of mouse single muscle fibers, a comparison with amphibian muscle fibers. *The Journal of experimental biology*, 208:1905–1913.

[16] González, E., Messi, M.L., and Delbono, O., 2000. The specific force of single intact extensor digitorum longus and soleus mouse muscle fibers declines with aging. *The Journal of membrane biology*, 178:175–183.

[17] Huxley, A.F. and PEACHEY, L.D., 1961. The maximum length for contraction in vertebrate straiated muscle. *The Journal of physiology*, 156:150–165.

[18] Felder, A., Ward, S.R., and Lieber, R.L., 2005. Sarcomere length measurement permits high resolution normalization of muscle fiber length in architectural studies. *The Journal of experimental biology*, 208:3275–3279.

[19] Mutungi, G. and Ranatunga, K.W., 1996. The viscous, viscoelastic and elastic characteristics of resting fast and slow mammalian (rat) muscle fibres. *The Journal of physiology*, 496 ( Pt 3):827–836.

[20] Barclay, C.J. and Lichtwark, G.A., 2007. The mechanics of mouse skeletal muscle when shortening during relaxation. *Journal of biomechanics*, 40:3121–3129.

[21] Rapoport, S.I., 1972. Mechanical properties of the sarcolemma and myoplasm in frog muscle as a function of sarcomere length. *The Journal of general physiology*, 59:559–585.

[22] Fields, R.W. and Faber, J.J., 1970. Biophysical analysis of the mechanical properties of the sarcolemma. *Canadian journal of physiology and pharmacology*, 48:394–404.

[23] Tidball, J.G., 1986. Energy stored and dissipated in skeletal muscle basement membranes during sinusoidal oscillations. *Biophysical journal*, 50:1127–1138.

[24] Wu, J.J., 2006. Quantitative constitutive behaviour and viscoelastic properties of fresh flexor tendons. *The International journal of artificial organs*, 29:852–857.

[25] Bensamoun, S.F., Tsubone, T., Subramaniam, M., Hawse, J.R., Boumediene, E., Spelsberg, T.C., An, K.N., and Amadio, P.C., 2006. Age-dependent changes in the mechanical properties of tail tendons in TGF-beta inducible early gene-1 knockout mice. *Journal of applied physiology (Bethesda, Md : 1985)*, 101:1419–1424.

[26] Hill, A., 1938. The heat of shortening and the dynamic constants of muscle. In Proceedings of the Royal Society of London Series B.

[27] Gordon, A.M., Huxley, A.F., and Julian, F.J., 1966. The variation in isometric tension with sarcomere length in vertebrate muscle fibres. *The Journal of physiology*, 184:170–192.

[28] Katz, B., 1939. The relation between force and speed in muscular contraction. *The Journal of physiology*, 96:45–64.

[29] Edman, K.A., 1979. The velocity of unloaded shortening and its relation to sarcomere length and isometric force in vertebrate muscle fibres. *The Journal of physiology*, 291:143–159.

[30] Morgan, D.L., 1990. New insights into the behavior of muscle during active lengthening. *Biophysical journal*, 57:209–221.

[31] Edman, K.A. and Flitney, F.W., 1982. Laser diffraction studies of sarcomere dynamics during 'isometric' relaxation in isolated muscle fibres of the frog. *The Journal of physiology*, 329:1–20.

[32] Telley, I.A., Denoth, J., Stüssi, E., Pfitzer, G., and Stehle, R., 2006. Half-sarcomere dynamics in myofibrils during activation and relaxation studied by tracking fluorescent markers. *Biophysical journal*, 90:514–530.

[33] Burton, K., Zagotta, W.N., and Baskin, R.J., 1989. Sarcomere length behaviour along single frog muscle fibres at different lengths during isometric tetani. *Journal of muscle research and cell motility*, 10:67–84.

[34] Kreplak, L., Herrmann, H., and Aebi, U., 2008. Tensile properties of single desmin intermediate filaments. *Biophysical journal*, 94:2790–2799.

[35] Balogh, J., Li, Z., Paulin, D., and Arner, A., 2003. Lower active force generation and improved fatigue resistance in skeletal muscle from desmin deficient mice. *Journal of muscle research and cell motility*, 24:453–459.

[36] Wieneke, S., Stehle, R., Li, Z., and Jockusch, H., 2000. Generation of tension by skinned fibers and intact skeletal muscles from desmin-deficient mice. *Biochemical and biophysical research communications*, 278:419–425.

# Chapter 3

# Elucidation of Extracellular Matrix Mechanics from Muscle Fibers and Fiber Bundles

## Abstract

The importance of the extracellular matrix (ECM) in muscle is widely recognized, since ECM plays a central role in proper muscle development [1], tissue structural support [2], and transmission of mechanical signals between fibers and tendon [3]. Since substrate biomechanical properties have been shown to be critical in the biology of tissue development and remodeling [4, 5], it is likely that mechanics are critical for ECM to perform its function. Unfortunately, there are almost no data available regarding skeletal muscle ECM viscoelastic properties. This is primarily due to the impossibility of isolating and testing muscle ECM. Therefore, this note presents a new method to quantify viscoelastic ECM modulus by combining tests of single muscle fibers and fiber bundles. Our results demonstrate that ECM is a highly nonlinearly elastic material, while muscle fibers are linearly elastic.

## 3.1   Introduction

Extracellular matrix (ECM) is essential for the development, maintenance and regeneration of skeletal muscle [1] and [2]. ECM is involved in the macrostructure of muscle, arranging fibers into bundles, bundles into fascicles and integrating muscle structure with aponeurosis and tendon. Additionally, ECM is thought to play a vital role in mechanotransduction and transmitting force laterally from the fiber to the tendon and *vice versa* [3, 6–8]. The mechanical strength and elasticity of the ECM are critical to its functional performanceit must be strong enough to sustain the loads of contraction yet elastic enough to prevent tearing under externally applied strains [2]. These properties change both with age and disease, where chronic alterations to the ECM appear to impair muscle function [9, 10]. Unfortunately, there are almost no data available regarding skeletal muscle ECM viscoelastic properties. This is primarily due to the impossibility of isolating and testing muscle ECM.

Attempts to remove muscle cells chemically from the ECM to test its properties directly have all met with some degradation or compromised mechanical properties [11, 12]. Additionally, the geometry of the ECM structure is modified when part of its composite structure (the fiber) is removed, which likely affects the orientation of collagen fibers and thus the modulus of elasticity. This report describes a new technique for indirectly determining the mechanical properties of the ECM without digestion, by combining tests from single muscle fibers and fiber bundles and using the analytical approach of composite theory.

## 3.2   Methods

Experiments were performed on single muscle fibers and muscle fiber bundles from the $5^{th}$ toe of the extensor digitorum longus (EDL) muscle in mice (129/Sv 79 weeks old; Taconic Farms, Germantown, NY, USA). Details of the dissection procedure and the solutions used have been described previously [13]. All procedures were performed in accordance with the NIH Guide for the Use and Care of Laboratory Animals and were approved by the University of California

and Department of Veterans Affairs Committees on the Use of Animal Subjects in Research.

Briefly, muscles were skinned overnight in a glycerinated relaxation solution and single fibers and bundles (composed of 10-20 muscle fibers) were dissected in chilled relaxation solution composed of (mM): EGTA (7.5), potassium propionate (170), magnesium acetate (2), imidazole (5), creatine phosphate (10), ATP (4), leupeptin (17 $\mu$g/ml) and E64 (4 $\mu$g/ml) to prevent protein degradation. One end of the specimen (either fiber, fiber group or fiber bundle) was attached via 10-0 suture to a motor arm (Newport MT-RS; Irvine, CA, USA) that controlled specimen length and the other to a force transducer (Aurora Scientific 405 A; Aurora, Ontario, Canada) that recorded force. The experimental paradigm (Fig. 3.1) illustrates the three types of specimens tested: (1) single fibers, (2) bundles of 10-20 fibers or (3) 10-20 single fibers dissected individually that were then secured together to approximate the size of a bundle, but these fiber groups contained no interfibrillar ECM. Sarcomere lengths provided objective assessments of muscle strain and myofibrillar array quality control and were measured by transilluminating the specimen with a low power laser diode.

Elastic properties were derived from an incremental stress relaxation protocol. Specimens were stretched in 10% strain increments at 2000%/s to impose a 0.25 $\mu$m sarcomere length change per stretch. Length was then maintained for 3 min, while the specimen was allowed to stress-relax. Elastic properties were determined from quadratic fits to fully stress-relaxed data. Elastic properties of the ECM were derived using the rule of mixtures for composites:

$$E_m = \frac{E_c - E_f(1 - A_m)}{A_m} \tag{3.1}$$

where $E_m$ is the modulus of the ECM, $E_f$ is the fiber modulus, $E_c$ is the composite or bundle modulus and $A_m$ is the cross-sectional area fraction occupied by ECM.

Data were compared across sample type by one-way ANOVA and considered significant ($\alpha$) at p<0.05. Statistical power (1 - $\beta$) was calculated for differences that were not significant. Individual experimental groups were compared using Tukeys multiple comparison test. Data are presented as mean±SEM.
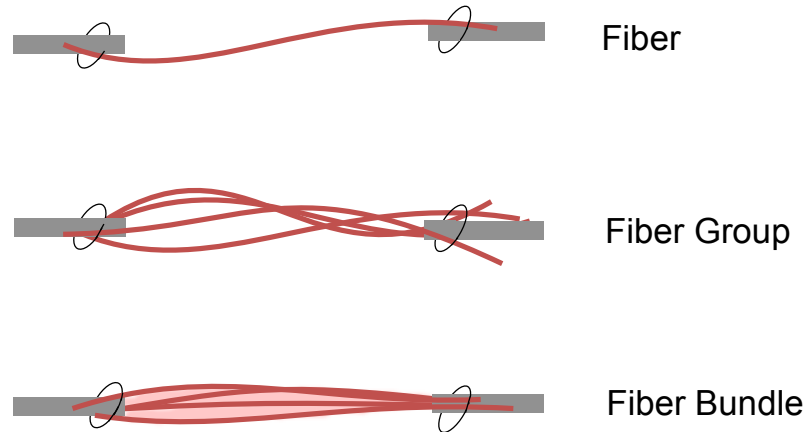
Figure 3.1: Schematic illustration of the arrangement of the three specimen types. Single fibers (curved red lines) were isolated from the muscle and either tested individually or secured in groups. Bundles of a similar number of fibers embedded in ECM (pink) were isolated and similarly secured.

## 3.3 Results

The relaxed quadratic modulus, representing the amount of nonlinearity present in the stress-sarcomere length relationship of the three experimental groups revealed that fiber bundle modulus was six fold greater than the modulus of individual fibers, where elasticity is essentially linear (Fig. 3.2). This indicates that a source of nonlinearity present in the fiber bundles is not present in isolated fibers.

Because fiber bundles are composites of fibers and ECM, nonlinearity could arise from natural variations in the passive tension of fibers or from an intrinsic nonlinearly elastic ECM. This concept is illustrated graphically (Fig. 3.3), where the relaxed stress-sarcomere length relation is plotted for 10 experimentally tested fibers for two different theoretical cases. In the first case, fibers all develop passive tension at approximately the same sarcomere length and the fiber composite stress-strain relationship is linear (Fig. 3.3A). If this was the case for fibers in the bundle, the observed nonlinearity would have to arise from the ECM surrounding the fibers. In the second case, fiber stress-strain curves are artificially shifted such that each fiber develops passive tension at slightly different sarcomere lengths (Fig. 3.3B). This results in a nonlinear fiber composite stress-sarcomere length relationship
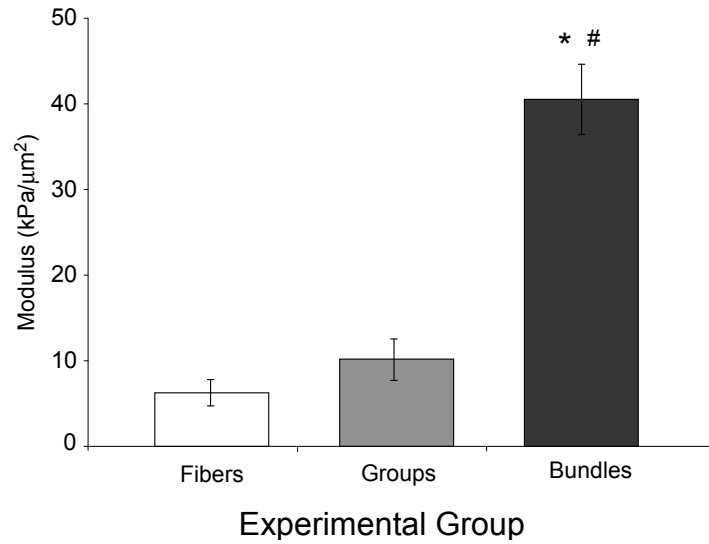
Figure 3.2: Quadratic moduli for fibers, fiber groups and fiber bundles. Fiber bundles have a significantly higher modulus than either individual fibers or fiber groups. Fiber and fiber group moduli were not significantly different from each other (p>0.1). Fibers: n=17, fiber groups: n=6, fiber bundles: n=10. ∗ and # indicate p<0.05 compared to Fibers and Groups respectively.

even though the single fibers are linearly elastic. Thus, if fibers in a bundle were at different sarcomere lengths at a given bundle length, bundle stress-strain behavior could appear to be nonlinear whereas each of its components was actually linear. In this case, the contribution of the ECM to the nonlinearity of bundle elasticity could not be determined by subtraction from the contribution of fiber variability and composite theory could not be used to determine ECM elasticity.

To differentiate between these possibilities, we combined and biomechanically tested individual isolated fibers into groups without the lateral connection of ECM. In this case, the contribution of fiber-to-fiber variability to the nonlinearity of the stress-strain relationship was isolated. Our results demonstrated that fiber groups have a quadratic modulus that is significantly lower than fiber bundles indicating that interfibrillar variability is not the primary contributing factor to fiber bundle nonlinearity (Fig. 3.2). In fact, fiber group modulus was not significantly different from single fiber modulus suggesting that a group of fibers behaves like an individual fiber (p>0.1, 1-$\beta$=0.9). Based on these data, we can calculate bundle
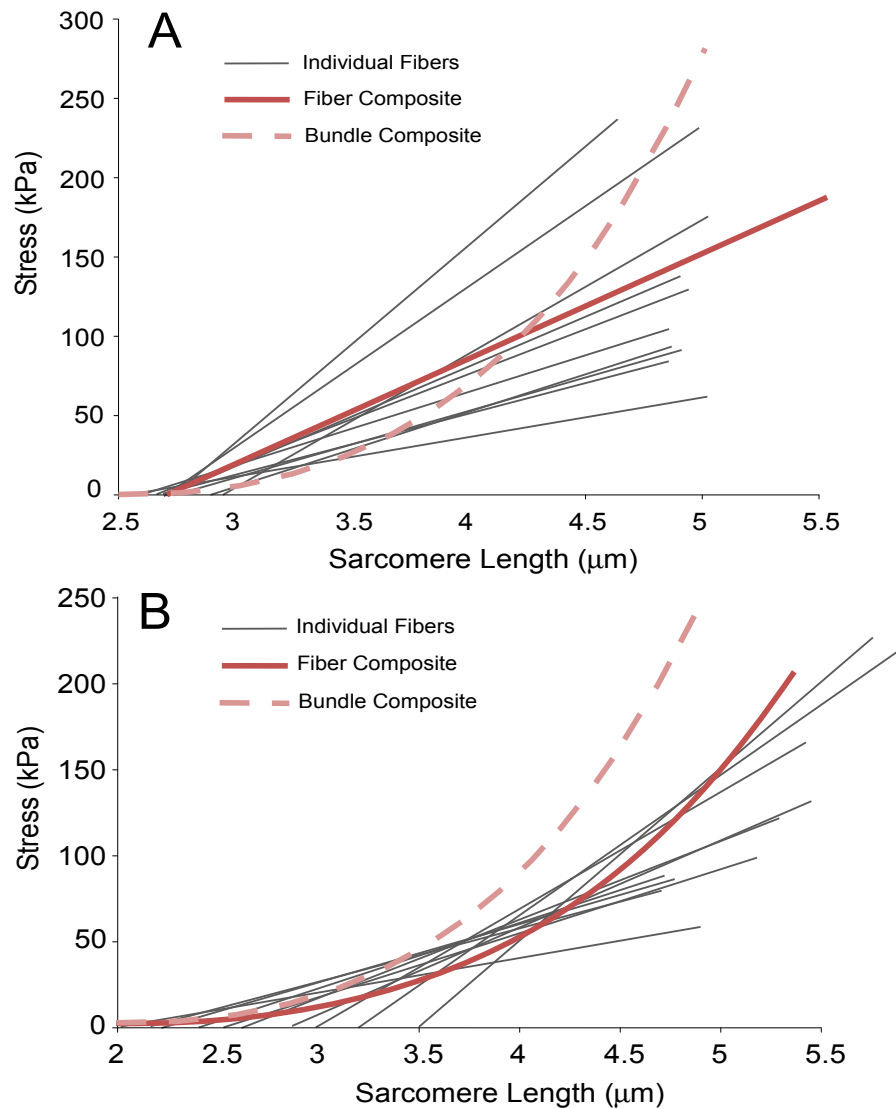
Figure 3.3: Illustration of the potential sources of nonlinearity in fiber bundles. (A) Experimental data from 10 fibers is plotted in gray (each thin line represents an individual fiber) with composite fiber behavior shown in thick red line. In this case, all fibers develop tension at the same sarcomere length and the composite behavior is linear. Since nonlinear bundle behavior is observed, ECM elasticity must be nonlinear (dashed line). (B) Same experimental data as in (A) are plotted but now each fiber has been shifted to develop tension at different sarcomere lengths, which yields a nonlinear composite behavior (dashed line). In this case, nonlinear bundle elasticity could be obtained with a linearly or nonlinearly elastic ECM.

ECM modulus using Eq. 3.1 , knowing only fiber and bundle mechanics and fiber area fraction.

Assuming that 5% of the bundle cross sectional area is made up of ECM [9], and using experimentally-derived modulus values (Fig. 3.2) the quadratic modulus of ECM in fiber bundles from the mouse $5^th$ toe EDL muscle is $692\ \mathrm{kPa}/\mu\mathrm{m}^2$. This indicates that the elasticity of ECM in muscle is highly nonlinear.

## 3.4    Discussion

Here we describe a new method to quantify passive mechanical properties of the muscle ECM without tissue digestion. Previous studies used methods of subtraction, where the ECM was preferentially digested from muscle and its properties inferred from subtracting the digested state from the undigested state (see review by [6] and [14]). However, this method includes the uncertainty of incomplete or non-specific digestion. Additionally, it has not been rigorously demonstrated that the differences observed were due to only the removal of ECM. The current study provides a control by using groups of fibers, which differ from bundles only in that they contain no ECM that could interconnect muscle fibers. Such interconnections have been shown to be significant in defining the mechanical properties of tendon [15]. The modulus of the fiber groups was not significantly different from the modulus of individual fibers indicating that the observed difference between the elasticity of fibers and bundles is likely due to ECM.

It is possible that our fiber isolation had some effect on mechanical properties. Fibers were dissected from intact muscles after chemical skinning and the shear stress applied during isolation or the skinning procedure itself could cause fibers to behave differently in isolation than in their unperturbed state. For instance, the sarcolemma and associated proteins could be disrupted or collagen fibrils could remain attached during isolation, affecting the elasticity of the fiber although this possibility seems unlikely, as hydroxyproline assays were unable to detect the presence of collagen in samples composed only of isolated fibers (unpublished data). Further studies will be needed to determine the extent to which

these factors affect our conclusions.

Bundle quadratic modulus was almost four fold larger than that of fiber groups. The magnitude of this effect supports the conclusion that the primary contributor to bundle stiffness is the ECM. Small perturbations to proteins on the fiber surface would likely contribute minimally to elasticity, as would the occasional remaining collagen fiber. Although this method was evaluated on bundles of only 10-20 fibers it could be extended to larger scales using fascicles and whole muscles for a more complete picture of the material properties of the ECM.

## Acknowledgments

Chapter 3, in full, is a reprint of the published article "Elucidation of extracellular matrix mechanics from muscle fibers and fiber bundles " Meyer G.A. and Lieber, R.L. *Journal of Biomechanics.* 44(4):771-773, 2011. The dissertation author was the primary investigator and author of this paper.

## 3.5    References

[1] Buck, C.A. and Horwitz, A.F., 1987. Cell surface receptors for extracellular matrix molecules. *Annual review of cell biology*, 3:179–205.

[2] Purslow, P.P., 2002. The structure and functional significance of variations in the connective tissue within muscle. *Comparative biochemistry and physiology Part A, Molecular & integrative physiology*, 133:947–966.

[3] Huijing, P.A., 1999. Muscle as a collagen fiber reinforced composite: a review of force transmission in muscle and whole limb. *Journal of biomechanics*, 32:329–345.

[4] Engler, A.J., Sen, S., Sweeney, H.L., and Discher, D.E., 2006. Matrix elasticity directs stem cell lineage specification. *Cell*, 126:677–689.

[5] Gilbert, P.M., Havenstrite, K.L., Magnusson, K.E.G., Sacco, A., Leonardi, N.A., Kraft, P., Nguyen, N.K., Thrun, S., Lutolf, M.P., and Blau, H.M., 2010. Substrate elasticity regulates skeletal muscle stem cell self-renewal in culture. *Science (New York, NY)*, 329:1078–1081.

[6] Fomovsky, G.M., Thomopoulos, S., and Holmes, J.W., 2010. Contribution of extracellular matrix to the mechanical properties of the heart. *Journal of molecular and cellular cardiology*, 48:490–496.

[7] Purslow, P.P. and Trotter, J.A., 1994. The morphology and mechanical properties of endomysium in series-fibred muscles: variations with muscle length. *Journal of muscle research and cell motility*, 15:299–308.

[8] Street, S.F., 1983. Lateral transmission of tension in frog myofibers: a myofibrillar network and transverse cytoskeletal connections are possible transmitters. *Journal of cellular physiology*, 114:346–364.

[9] Lieber, R.L., Runesson, E., Einarsson, F., and Fridén, J., 2003. Inferior mechanical properties of spastic muscle bundles due to hypertrophic but compromised extracellular matrix material. *Muscle & nerve*, 28:464–471.

[10] Zhou, L. and Lu, H., 2010. Targeting fibrosis in Duchenne muscular dystrophy. *Journal of neuropathology and experimental neurology*, 69:771–776.

[11] Borschel, G.H., Dennis, R.G., and Kuzon, W.M., 2004. Contractile skeletal muscle tissue-engineered on an acellular scaffold. *Plastic and reconstructive surgery*, 113:595–602; discussion 603–4.

[12] Qing, Q. and Qin, T., 2009. [Optimal method for rat skeletal muscle decellularization]. *Zhongguo xiu fu chong jian wai ke za zhi = Zhongguo xiufu chongjian waike zazhi = Chinese journal of reparative and reconstructive surgery*, 23:836–839.

[13] Shah, S.B., Davis, J., Weisleder, N., Kostavassili, I., McCulloch, A.D., Ralston, E., Capetanaki, Y., and Lieber, R.L., 2004. Structural and functional roles of desmin in mouse skeletal muscle during passive deformation. *Biophysical journal*, 86:2993–3008.

[14] Granzier, H.L. and Irving, T.C., 1995. Passive tension in cardiac muscle: contribution of collagen, titin, microtubules, and intermediate filaments. *Biophysical journal*, 68:1027–1044.

[15] Haraldsson, B.T., Aagaard, P., Qvortrup, K., Bojsen-Moller, J., Krogsgaard, M., Koskinen, S., Kjaer, M., and Magnusson, S.P., 2008. Lateral force transmission between human tendon fascicles. *Matrix biology : journal of the International Society for Matrix Biology*, 27:86–95.

# Chapter 4

# A Nonlinear Model of Passive Muscle Viscosity

## Abstract

The material properties of passive skeletal muscle are critical to proper function and are frequently a target for therapeutic and interventional strategies. Investigations into the passive viscoelasticity of muscle have primarily focused on characterizing the elastic behavior, largely neglecting the viscous component. However, viscosity is a sizeable contributor to muscle stress and extensibility during passive stretch and thus there is a need for characterization of the viscous as well as the elastic components of muscle viscoelasticity. Single mouse muscle fibers were subjected to incremental stress relaxation tests to characterize the dependence of passive muscle stress on time, strain and strain rate. A model was then developed to describe fiber viscoelasticity incorporating the observed nonlinearities. The results of this model were compared with two commonly used linear viscoelastic models in their ability to represent fiber stress relaxation and strain rate sensitivity. The viscous component of mouse muscle fiber stress was not linear as is typically assumed, but rather a more complex function of time, strain and strain rate. The model developed here, which incorporates these nonlinearities, was better able to represent the stress relaxation behavior of fibers under the conditions tested than

commonly used models with linear viscosity. It presents a new tool to investigate the changes in muscle viscous stresses with age, injury and disuse.

## 4.1 Introduction

Skeletal muscle is a composite tissue composed of interconnected contractile and structural proteins, membranes and extracellular matrix that enable both load bearing and force production. Understanding the mechanism of force production in muscle has been a primary research focus for the past century as it is unequivocally essential for human mobility, stability and vitality. In contrast, much less is known about the load bearing properties of muscle in the absence of activation even though passive muscle properties are equally vital to proper function. This is easily appreciated when passive mechanical properties change due to disuse, disease, or injury, leaving patients debilitated [1–3]. Thus, maintaining or improving passive extensibility of muscle is a primary goal of therapeutic strategies to improve surgical outcomes or increase stability and performance [4]. Understanding the material properties of load bearing structures in muscle is important to developing these strategies, especially in terms of passive stretching applied in physical therapies and diagnostic situations. Additionally, if the efficacy of such treatments is to be defined, consistent and comprehensive metrics of passive extensibility must be available. Thus, our goal is to develop a comprehensive description of the passive mechanical properties of skeletal muscle.

Passive skeletal muscle, like most biological tissues, has long been recognized to exhibit time- and strain-dependent responses to tensile loads [5–7]. Early attempts to model passive muscle viscoelastic behavior mathematically assumed linear elastic and viscous responses [5, 6]. Since then, many researchers have shown the elastic component of muscle tension is nonlinear and most current models include either a polynomial or exponential elastic response [7–9]. Nonlinear viscosity has been characterized in other soft tissues such as ligament [10, 11], but characterization of viscous muscle properties has been largely neglected and muscle viscosity is typically modeled as linear although there is evidence to suggest sig-

nificant nonlinearity [12–14].

Current approaches to passive viscoelastic modeling of skeletal muscle fall into three general categories: (1) structural spring-dashpot models [15, 16], (2) quasi-linear viscoelastic (QLV) models [9, 17], and (3) hyperelastic models [18, 19]. The primary difference among models in these categories lies in the characterization of the elastic response with some models using as many as 12 independent parameters to describe elastic nonlinearities [20]. In contrast, the vast majority of these models use only one or two parameters to describe a simple viscous response that has no dependence on strain or strain rate (i.e. is linear). Physiologically, skeletal muscle is subjected to a large range of strains and strain rates and frequently functions at different degrees of stress-relaxation. Thus, viscous properties likely play as large a role as elastic in determining passive muscle stress. It is not sufficient to characterize the passive properties of such a dynamic system by defining its elasticity in a fully relaxed state, or by defining its viscosity at one super-physiological strain rate as is frequently done [9, 16, 21].

Our hypothesis is that muscle fibers have a complex viscosity that is strain and strain rate dependent and that this behavior can be explained and described with a model of pseudoplasticity. In this study, stress relaxation tests were performed on skinned single fibers from the mouse to define the dependence of fiber viscosity on time, strain and strain rate. These data were then used to develop a pseudoplastic model incorporating the observed viscous nonlinearities. The capabilities of this pseudoplastic model were compared with two commonly used models: the $3^{rd}$ order Hill model and the QLV model, in their ability to represent fiber stress relaxation and strain rate dependence.

## 4.2 Methods

Experiments were performed on single fibers from the $5^{th}$ toe of the mouse extensor digitorum longus (EDL) muscle (129/Sv, average body mass: $23.3 \pm 1.4$ g; Taconic Farms, Germantown, NY). All procedures were performed in accordance with the NIH Guide for the Use and Care of Laboratory Animals and were approved

by the University of California and Department of Veterans Affairs Committees on the Use of Animal Subjects in Research. Animals were anesthetized with 2% isoflurane at 2 L/min and then euthanized by cervical dislocation. Hindlimbs were transected proximal to the knee and fibers were isolated as described previously [22].

Briefly, the $5^{th}$ toe of the EDL muscle was dissected and stored in a glycerinated relaxing solution overnight at $-20\,^{\circ}$C. Prior to mechanical testing, muscles were removed from storage solution and transferred to a relaxing solution at pCa 8.0. Single fiber segments (2-3 mm in length) were carefully dissected and mounted in a custom chamber (n=5). They were secured on one end to a force transducer (Aurora Scientific 405A; Aurora, Ontario, Canada) and on the other end to a titanium wire rigidly attached to a rotational bearing (Newport MT-RS; Irvine, CA) using 10-0 monofilament nylon suture. Sarcomere length provided an objective assessment of internal strain and was measured by transilluminating the specimen using a low power diode. Segments displaying obvious abnormalities were not used.

## 4.2.1   Stress relaxation testing

The fiber was brought to slack length, which was determined by the knot-to-knot length at which passive tension was just measurable above the noise level of the force transducer ($\sim$1mN, signal to noise ratio $> 5$). The fiber was then loaded to a specified strain at a specified strain rate and allowed to stress-relax at the final strain for 3 minutes, where stress decay was determined to be minimal. Strains were imposed over a range of 10-50% fiber length (FL), which was determined in preliminary studies to be the maximum strain range where plastic deformation or damage of the fiber did not occur. Fibers were tested at rates from 0.2-200 FL/sec, which were chosen as a range from physiological [23] to maximum motor speed. Following stress-relaxation, fibers were either further stretched incrementally or returned to slack length to rest for 3 minutes before being subjected to another stretch. Two fibers were subjected to incremental (10% FL) stretches at three rates (Fiber 1: 0.2, 2 and 20 FL/sec, Fiber 2: 2, 20 and 200 FL/sec). Two fibers were subjected to stretches at 20 FL/sec at different increments (10%, 20%, 30%,

40% and 50% FL). An additional fiber was subjected to stretches at 40% FL at rates of 50, 100 and 200 FL/sec. Stretches were performed in random order to ensure there was no order effect over the strain and strain rates considered. At the conclusion of testing, the first stretch was performed again and compared to the initial value to ensure no plastic deformation had occurred in the sample. Data from fibers showing a decrease in passive tension following the testing protocol were excluded from analysis.

During the first 0.15 seconds of the stretch, data were acquired at a rate of 30,000 Hz to ensure that rapid force transients were captured. For the remainder of the 3-minute hold, data were acquired at a rate of 30 Hz, which was determined to be sufficient to characterize the slow force transients during this period. Fiber Cauchy stress was determined by diving the tension measurement by a predicted current fiber cross-sectional area. This prediction was based on the measured fiber diameter at slack length, the current fiber length and the assumption that the fiber was cylindrical and isovolumic [24]. Fiber strain was calculated at each stretch by dividing the change in fiber length by the initial slack length.

## 4.2.2    Pseudoplastic model formulation

A pseudoplastic model incorporating nonlinear viscosity requires a viscous term that is time, strain and strain rate dependent. This complex viscosity can be incorporated into a single nonlinear element in the 3-element Hill model of passive muscle [6] with a viscous parameter given by $\eta(t, \varepsilon, \dot{\varepsilon})$ (Fig. 4.1A). This approach is similar to the modified superposition method used by Lakes et al. [25] to describe nonlinearities in ligament behavior, where the relaxation modulus is modified to include a strain dependence. In the pseudoplastic model it is further modified to also include strain rate dependence.

This model contains linear elastic elements due to the essentially linear stress-strain behavior of mouse EDL fibers [26]. The mathematical form of the strain rate dependence of viscosity can be derived from an equation frequently used in rheology to describe pseudoplastic material behavior (Eq. 4.1) [27]. A pseudo-plastic material exhibits decreasing viscosity with increasing shear-rate (Fig. 4.1B-
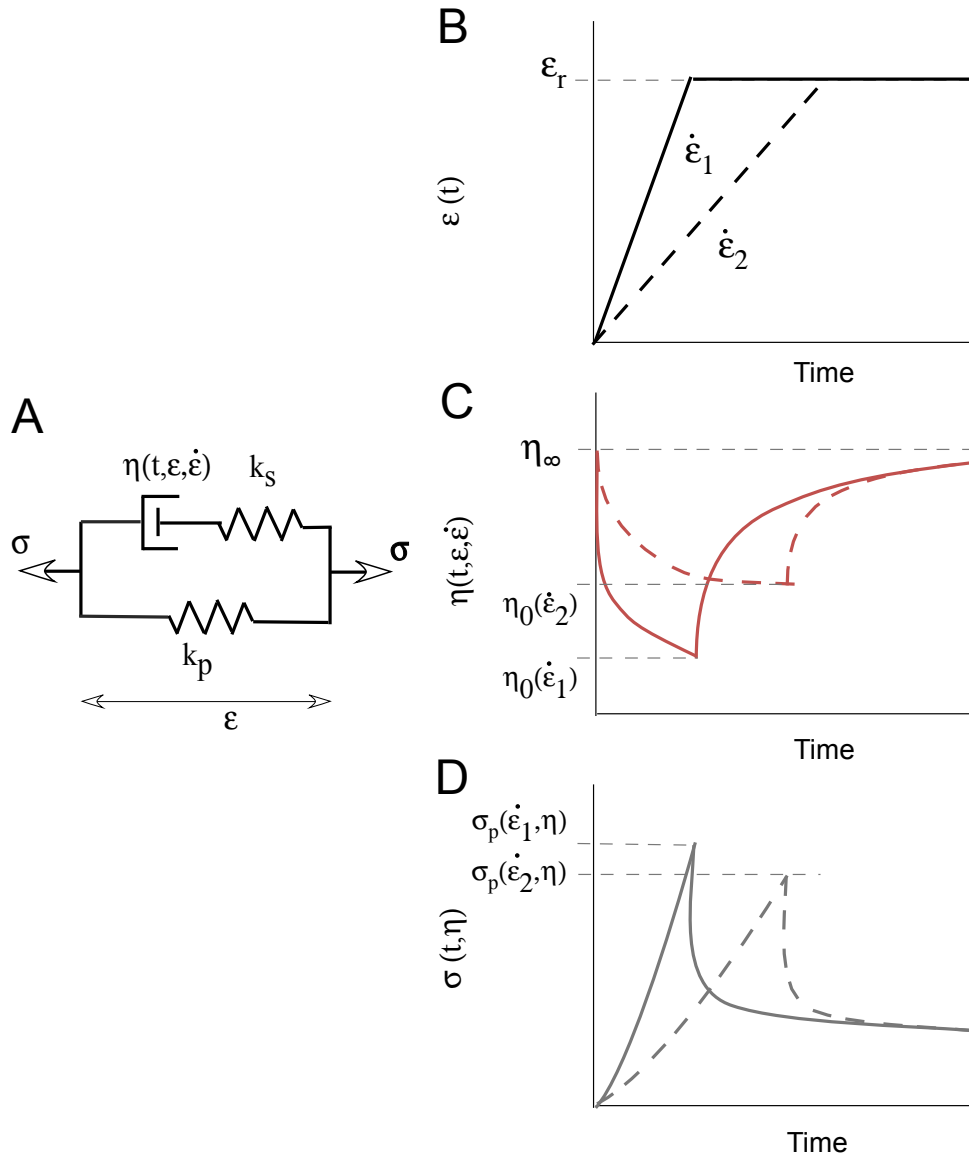
Figure 4.1: Schematic representation of a pseudoplastic model of passive muscle mechanics. (A) Modified version of the Hill 3-element model [6]. Spring elements are linear due to the linear stress-strain behavior of mouse muscle fibers and the dashpot is a nonlinear element whose behavior is a function of time, strain and strain rate. (B) Schematic of two step strain inputs for a stress relaxation test, one at high strain rate ($\dot{\varepsilon}_1$) and one a low strain rate ($\dot{\varepsilon}_2$). Viscosity in this model is a function of time, strain and strain rate ($\eta(t, \varepsilon, \dot{\varepsilon})$) illustrated graphically in (C). The shape of the resulting stress relaxation curves are shown in (D) where the stretch at the higher strain rate results in the higher peak stress ($\sigma_p(\dot{\varepsilon}_1, \eta)$).

C). In this formulation, viscosity ($\eta$) is inversely proportional to strain rate ($\dot{\varepsilon}$), and the initial and minimal viscosities are defined by $m$ and $\eta_0$ respectively.

$$\eta_{shear} = \eta_0 + \frac{m - \eta_0}{(1 + \dot{\varepsilon})} \tag{4.1}$$

The dependence of viscosity on time during the period of stress relaxation can be explained by pseudoplastic theory. When the shear stress is removed (the material is held at a constant strain) the viscosity returns to the initial, larger value, $\eta_\infty$, (Fig. 4.1B-C). This buildup is represented by Eq. 4.2.

$$\eta_{rest} = \frac{\tau^2}{\tau - t\dot{\tau}} \tag{4.2}$$

Where the function $\tau$ is given by Eq. 4.3.

$$\tau = \frac{\eta_\infty \eta_0 (t^2 + (1 + 2\alpha)t + \alpha)}{\eta_0 t^2 + (\eta_0 + 2\alpha\eta_\infty)t + \alpha\eta_\infty} \tag{4.3}$$

In this formulation, the increase in viscosity under zero shear load is hyperbolic beginning at a minimal value of $\eta_0$ and increasing to a final value of $\eta_\infty$. The constant $\alpha$ controls the hyperbolic curvature, or the rate at which viscosity increases. Finally, the dependence of the viscous parameters $\eta_0$ and $\alpha$ on resting strain can be described by Eq. 4.4 where $\varepsilon_r$ is resting strain and $a$ and $b$ are constants.

$$\begin{aligned} \eta_0 &= a\varepsilon_r \\ \alpha &= b\varepsilon_r \end{aligned} \tag{4.4}$$

With the dependence of viscosity on time, strain and strain rate thus defined, the response of mouse muscle fibers to a stress relaxation test of any rate can be determined by solving the constitutive equation of the 3-element Hill model as piecewise continuous under conditions of shear and rest (Eq. 4.5).

$$\dot{\sigma} + \frac{k_s}{\eta(t, \varepsilon_r, \dot{\varepsilon})}\sigma = \frac{k_s k_p}{\eta(t, \varepsilon_r, \dot{\varepsilon})}\varepsilon + (k_s + k_p)\dot{\varepsilon}, \text{ where} \tag{4.5}$$

$$\eta(t, \varepsilon_r, \dot{\varepsilon}) = \eta_{shear}(\dot{\varepsilon}) \quad \text{for } \dot{\varepsilon} > 0$$
$$\eta(t, \varepsilon_r, \dot{\varepsilon}) = \eta_{rest}(t, \varepsilon_r) \quad \text{for } \dot{\varepsilon} = 0$$

As an example, a commonly used material test for muscle is to perform a single stress relaxation test at a high rate that approximates an instantaneous change in strain. In this approximation, $\eta$ changes instantaneously to $\eta_0$ under shear and (Eq. 4.5) can be solved for the rest case only (Eq. 4.6).

$$\sigma = k_s \exp\left(\frac{-k_s t(at^2 + (a + 2\alpha b)t + b)}{ab\varepsilon_r(t^2 + (1 + 2\alpha)t + \alpha)}\right) + k_p \tag{4.6}$$

### 4.2.3 Model fitting

All analysis was performed using Matlab. Solutions to models with instantaneous step strain profiles were exact while solutions to models with ramp strain profiles were solved numerically using a nonstiff initial value ordinary differential equation solver. These solution methods were combined with a nonlinear least-squares parameter-fitting algorithm to optimize the solutions. Initial parameter guesses within a 100-fold range of the solution were shown to result in the same solution, indicating high model robustness.

## 4.3 Results

The most commonly performed test to evaluate the viscoelastic properties of skeletal muscle is a ramp-and-hold stress relaxation test (depicted in Fig. 4.1B) [9, 12, 16, 21, 28]. In this test, strain is increased at a fixed rate to a final value at which the muscle is allowed to relax until stress reaches a steady state. Frequently these tests are performed at very high strain rates to approximate instantaneous changes in strain [9, 15, 16, 29]. This infinite-rate assumption simplifies the model fitting process, as an exact solution is available for both structural and QLV models. These models can be fit to either a single stress relaxation (a locally linear model) or to stress relaxations over a range of strains. For simplicity, locally linear models will be considered first.
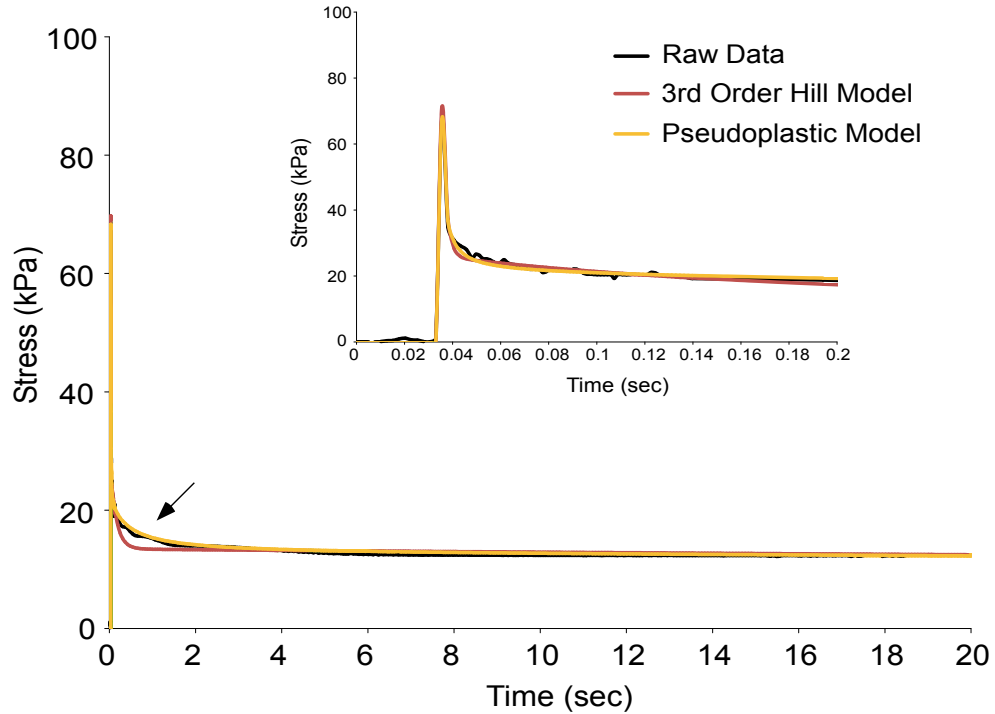
Figure 4.2: The pseudoplastic model better represents stress relaxation data from a mouse compared to the $3^{rd}$ order Hill structural model. The fiber was stretched to 30% FL at 20 FL/sec to approximate an instantaneous length change. The pseudoplastic model (gold) is a better fit to the raw data (black) than the $3^{rd}$ order Hill model (red) during the phase of fast relaxation. Inset shows the data magnified over the first 0.2 seconds of stress relaxation.

### 4.3.1 Locally linear models

Figure 4.2 presents data from a stress relaxation test on a mouse EDL fiber at a super-physiological strain rate (20 FL/sec) to approximate an instantaneous change in strain. These data were then fit with a $3^{rd}$ order Hill structural model (Appendix B) using the infinite rate assumption. This structural model uses three viscous elements to describe the relaxation process, which results in distinctive error during the fast phase of relaxation as the model attempts to represent a continuous process with discrete structural elements (arrow). The pseudoplastic model described here assumes a continuous spectrum of relaxation similar to that frequently used in conjunction with QLV models [9, 30] where a single viscous element is allowed to change its viscosity over time.
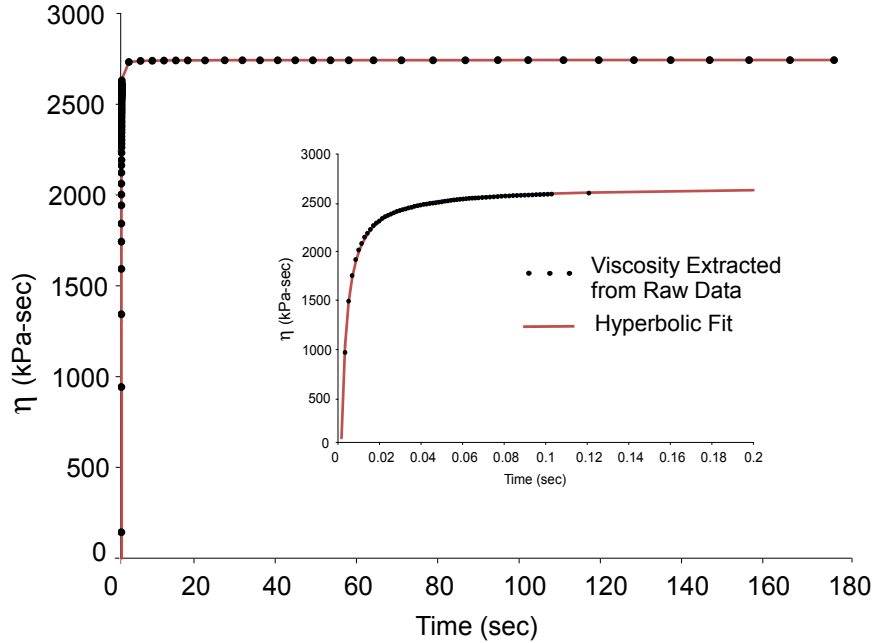
Figure 4.3: Change in viscosity over time during fiber stress relaxation. Individual data points were derived from 1st order Hill fits to the stress relaxation of a fiber at discrete time points. Eq. 4.3 provided a good fit to the data ($r^2 = 0.998$).

To evaluate how the viscosity of the fiber changes over time during the process of stress relaxation, data from a fiber was fit with individual $1^{st}$ order Hill models at discrete time points during relaxation. The viscosities of these models were then plotted as a function of time during the course of stress relaxation (Fig. 4.3). The model viscosity increases as a function of time and was best fit by a hyperbolic relationship (Eq. 4.3, $r^2$=0.998)). Incorporating this relationship into the pseudoplastic model solution for an infinite-rate stress relaxation test Eq. 4.6, gives an analytical solution that can be fit to stress relaxation data. Figure 4.2 illustrates this fit compared to the $3^{rd}$ order Hill model fit where superior representation of the data can be seen with the pseudoplastic model (arrow) especially during the fast phase of stress-relaxation ($r^2$= 0.949 ($3^{rd}$ order Hill), $r^2 = 0.987$ (pseudoplastic) during 0-2 sec). Though both models could be said to yield good fits to the data, the $3^{rd}$ order Hill model requires 7 independent parameters while the pseudoplastic model requires only 5, optimizing the number of parameters to the goodness of fit.

Table 4.1: : Comparison of the locally linear fits of three models to mouse fiber stress relaxation. Data were taken from 40 total stretches of 5 fibers over the strains and strain rates discussed. Goodness of fit was calculated over the first 2 seconds of stress relaxation. The pseudoplastic model provides a superior goodness of fit to both the $3^{rd}$ order Hill model and the QLV model (using exponential integral reduced relaxation).

|  | # Parameters | Average $r^2$ |
| --- | --- | --- |
| $3^r d$ Order Hill Model | 7 | $0.918 \pm 0.035$ |
| QLV (Exponential Int) | 4 | $0.785 \pm 0.334$ |
| Pseudoplastic Model | 5 | $0.958 \pm 0.018$ |

QLV models frequently also incorporate a continuous spectrum of relaxation defined by exponential integrals (Appendix B) and such models require only 4 independent parameters. However, the exponential integral stress relaxation poorly characterizes mouse fiber data at low strains and thus this model did not represent the experimental data described here as well as either the $3^{rd}$ order Hill model or the pseudoplastic model (Table 4.1).

## 4.3.2   Strain rate sensitivity

The peak stress experienced by a passively ramp-stretched muscle is known to be a function of the rate at which it is strained. Structural models such as the $3^{rd}$ order Hill model inherently predict high strain rate sensitivity. This is due to the fact that the fastest decay constant (associated with the dashpot with lowest viscosity) will cause significant stress decay during the finite time stress ramp. The magnitude of this decay will increase as strain rate decreases and the amount of time spent in the strain ramp increases. The QLV model predicts the same high strain rate sensitivity since viscosity is only a function of time and thus the $3^{rd}$ Order Hill model is representative of both responses.

At the strains and strain rates considered here, the mouse muscle fibers were found to be significantly less strain rate sensitive than the $3^{rd}$ order Hill model predicted. $3^{rd}$ order Hill model fits to high strain rate data were found to underestimate peak stresses at lower rates by as much as 50%. Figure 4.4 shows
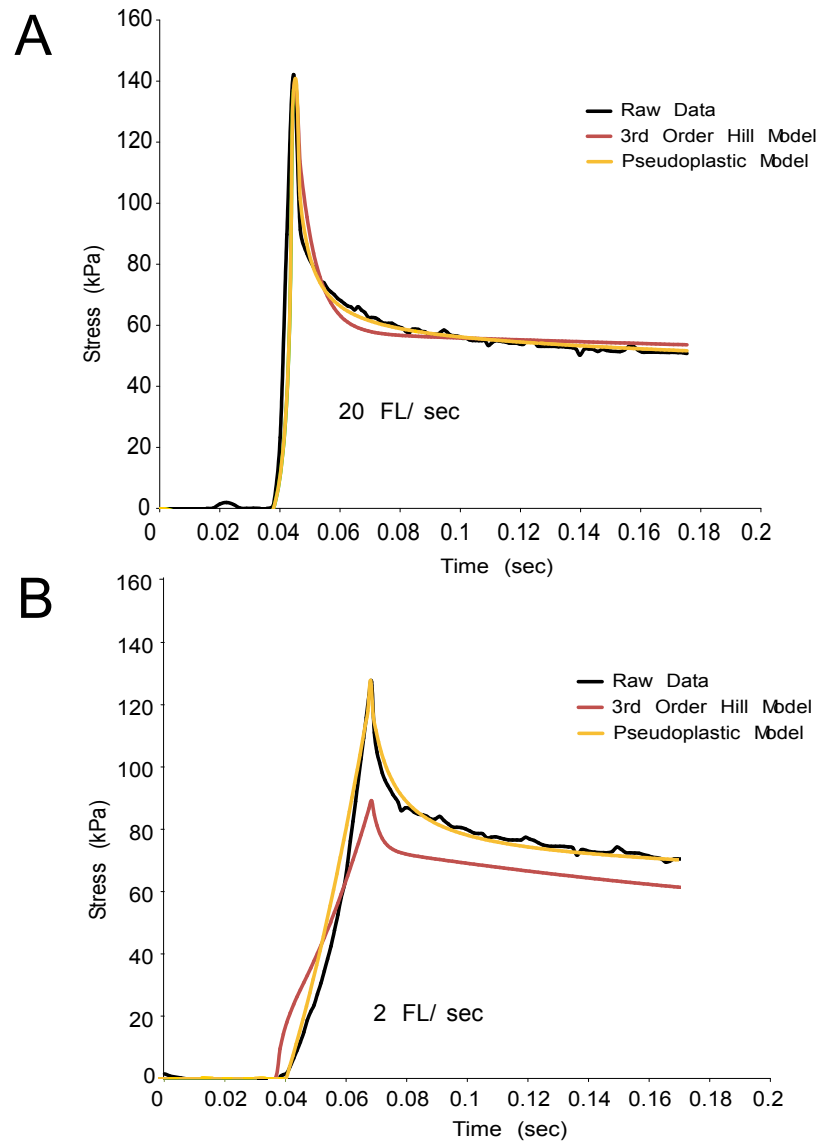
Figure 4.4: The pseudoplastic model better represents the strain rate sensitivity of a mouse muscle fiber than the $3^{rd}$ order Hill structural model. A single mouse muscle fiber was strained to 50% FL at 20 FL/sec (A) and at 2 FL/sec (B). The $3^{rd}$ order Hill model (red) and the pseudoplastic model (gold) were fit to raw data (black) at 20 FL/sec and then used to predict behavior during a 2 FL/sec stretch. The $3^{rd}$ order Hill model underestimates stress at 2 FL/sec, while the pseudoplastic model accurately represents peak stress.

raw data from a single mouse muscle fiber strained to 50% FL at two strain rates. The $3^{rd}$ order Hill model was fit to 20 FL/sec data and then used to predict 2 FL/sec data (red traces). The model is unable to explain the fiber behavior at 2 FL/sec, underestimating peak stress by 30%. The difference in strain rate sensitivities between the $3^{rd}$ order Hill model and mouse muscle fibers was seen at all strains between 10 and 50% FL (data not shown).

Pseudoplastic theory offers an explanation for this disparity by introducing nonlinearity to the viscosity. The viscosity of a pseudoplastic material decreases inversely proportionally with strain rate during the time the material is subjected to stress. Thus, during the ramp stretch, the material would experience less stress decay, as it would have begun at a high viscosity and only reached the lowest viscosity at the end of the ramp. The pseudoplastic model considered here is able to provide good fits to fiber data at both strain rates with a single set of parameters and an appropriate dependence of viscosity on strain rate (Fig. 4.4, gold traces). Similarly, the pseudoplastic model fit to slow strain rate data is able to well represent faster strain rate data whereas the $3^{rd}$ order Hill model overpredicts peak stress at the faster rate with parameters based on the slower rate (data not shown).

Evidence from mouse muscle fibers suggests that they behave like a pseudoplastic material. It is difficult to measure viscosity in a fiber during shear, but the initial rate of stress relaxation following strain can be used as an indication of the minimum viscosity reached, $\eta_0$ [31]. Three stretches of the same fiber are shown, each at a different strain rate ranging from 50 FL/sec (Fig. 4.5A, gold) to 200 FL/sec (Fig. 4.5A, red). The stress is normalized on a scale from zero to one to enable a direct comparison of stress decay rates in different stretches. The stress clearly decays fastest at the highest strain rate indicating the fiber reaches the lowest viscosity under this condition. This behavior is typical of a pseudoplastic material where viscosity decreases with increasing strain rate.

The three stretches depicted reached the same final resting strain (40% FL), but the initial strain for each was selected such that the fiber spent the same time under shear load for each case. This was done deliberately to separate pseudoplas-
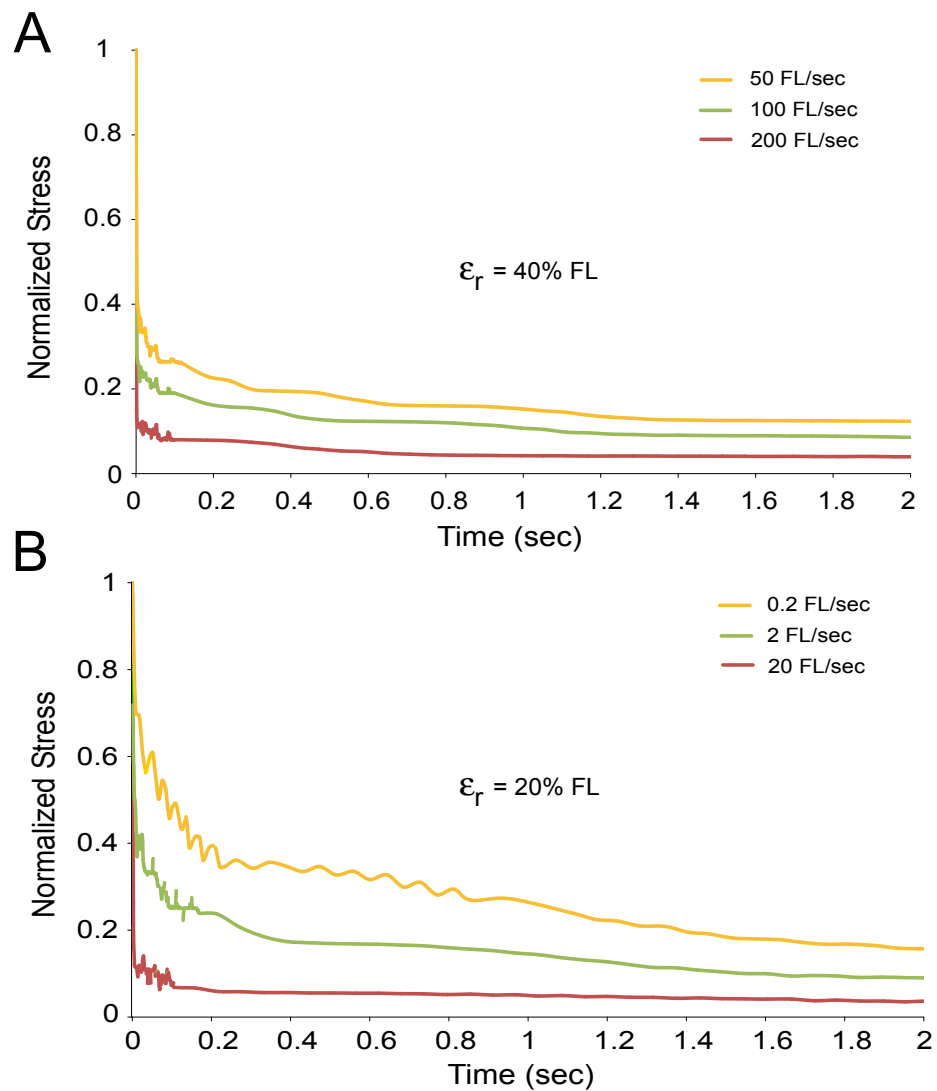
Figure 4.5: Mouse muscle fibers exhibit pseudoplasticity. (A) A single fiber was strained to 40% FL at three different rates. The fastest rate stretch resulted in the fastest stress decay (red) indicating the lowest viscosity. All strain ramps had the same time interval and the same peak stress. (B) A single fiber was strained from slack length to 20%FL at three different rates. Again, the fastest stretch had the fastest stress decay, indicative of pseudoplastic behavior. Noise on the traces represents less than 1mV noise at these low stresses.

tic (viscosity as a function of strain rate) effects from thixotropic (viscosity as a function of shear time) effects. Additionally, peak stresses for the three stretches were within 10% of each other, eliminating stress as a compounding factor. The length change to which the fiber was subjected was still variable in this test, however. Three stretches of the same fiber were again performed at three different strain rates ranging from 0.2 FL/sec to 20 FL/sec but this time all strains were from slack length to 20%FL (Fig. 4.5B). Again, the stretch at the highest rate had the fastest relaxation indicating that it reached the lowest viscosity and suggesting pseudoplastic behavior. Time spent under shear load for each stretch is variable in this data, but the stretch with the longest time (0.2 FL/sec) had the slowest relaxation rate and thus the highest viscosity - the opposite of a thixotropic effect.

### 4.3.3   Superposition

Stress relaxation tests are usually performed on muscle either from a predefined slack length [9, 28] or incrementally at set step increments [14, 21, 29]. Linear models, which are most commonly used, obey the principle of superposition, meaning that that the stress response to reach a given strain is necessarily equal to the net stress responses of any number of intermediate steps to that strain. The QLV model also obeys superposition, and results in similar predictions of peak forces as linear models.

However, experimental data indicate that mouse muscle fibers do not obey the principle of superposition. In fact, the peak stress experienced by fibers seems to be nearly completely a function of the final strain reached regardless of the magnitude of the strain step, an observation also noted by Quaia et al. in passive extraocular muscles [32]. Peak stress (Fig. 4.6A, filled circles) and relaxed stress (Fig. 4.6A, open circles) data are shown from a mouse muscle fiber subjected to a variety of stress relaxation tests. In the first test (red circles), the fiber is strained in 10% FL increments to 40% FL. The peak and relaxed stresses are then respectively summed to yield the superposition prediction of the peak and relaxed stress for a strain from slack length to 40% FL (red asterisk). In the second test, the same fiber was strained in increments of 20% FL (green circles) and the

Figure 4.6: Mouse muscle fibers do not obey superposition. (A) Peak (closed circles) and relaxed (open circles) stresses from a single fiber strained incrementally at 10% FL increments (red) and 20% FL increments (green). These data were used to predict stresses from a stretch from slack to 40% FL based on the principle of superposition (asterisks). Predictions match experimental data for the relaxed stress (open gold circle), but overestimate the peak stress by as much as 95% (closed gold circle). (B) Raw stress relaxation data from a fiber stretched in 10% FL increments (black). The $3^{rd}$ order Hill model is fit to stretches of the same fiber from slack but provides a poor prediction of incremental stress (red). The pseudoplastic model overcomes the limitations of superposition by adding strain dependent viscous parameters and provides a much better fit (gold). Relaxation plots are truncated at 0.3 seconds to show the initial fast phase of relaxation. Both models converge with the raw data at the fully relaxed stress.

superposition prediction was made in the same way (green asterisk). Finally, the fiber was stretched from slack length to 40% FL (gold circles). The superposition predictions of relaxed stress are close to the fiber measurement, but the peak superposition predictions overestimate the fiber measurement by 40% and 95% respectively. Thus, superposition is only a reasonable assumption for the relaxed stress measurement. It does not reflect peak stress or stress relaxation behavior.

Because a linear model by definition obeys the principle of superposition, a fit to stress relaxation data from slack length would be unable to describe incremental stress relaxation data and vice versa. This is true of the $3^{rd}$ order Hill model and the QLV model, though only the $3^{rd}$ order Hill fit is shown. Figure 4.6B shows raw incremental stress relaxation data for three consecutive stretches of a mouse muscle fiber (black traces) at 10% FL. The $3^{rd}$ order Hill model was fit to stress relaxation data from slack length and then used to predict incremental stress relaxation values (red traces). The model underestimates the raw data by increasing margins with succeeding increments (30% at 20% FL and 50% at 30% FL). Nonlinearities introduced into the dashpot elements of this model may be able to explain some of the muscle fiber's deviation from superposition. If, for instance, the viscosity of the dashpot element increased with increasing resting strain, a stretch from 30% to 40% FL could develop as much stress as a stretch from slack length to 40% FL simply due to its higher initial viscosity.

Experimental data indicate that the viscosity of mouse muscle fibers increases with increasing resting strain, as revealed by normalized stress relaxation data from a fiber subjected to a series of incremental stretches from slack length to 50% FL (Fig. 4.7A). Normalized stress decays from the same maximum to the same minimum more slowly as the strain is increased from 0 to 50% FL. If the pseudoplastic model is locally fit to each stretch, the parameters $\eta_0$ and $\alpha$ both increase as a function of resting strain ($\varepsilon_r$). Analysis of the three viscous parameters of the pseudoplastic model as a function of resting strain for incremental stretches of six fibers to 100%FL (Fig. 4.7B), revealed that the parameters $\eta_0$ and $\alpha$ increase linearly with resting strain ($\mathrm{r}^2 = 0.97$ and 0.95 respectively) while $\eta_\infty$ remains essentially constant. With stain dependent viscous parameters (Eq. 4.4),
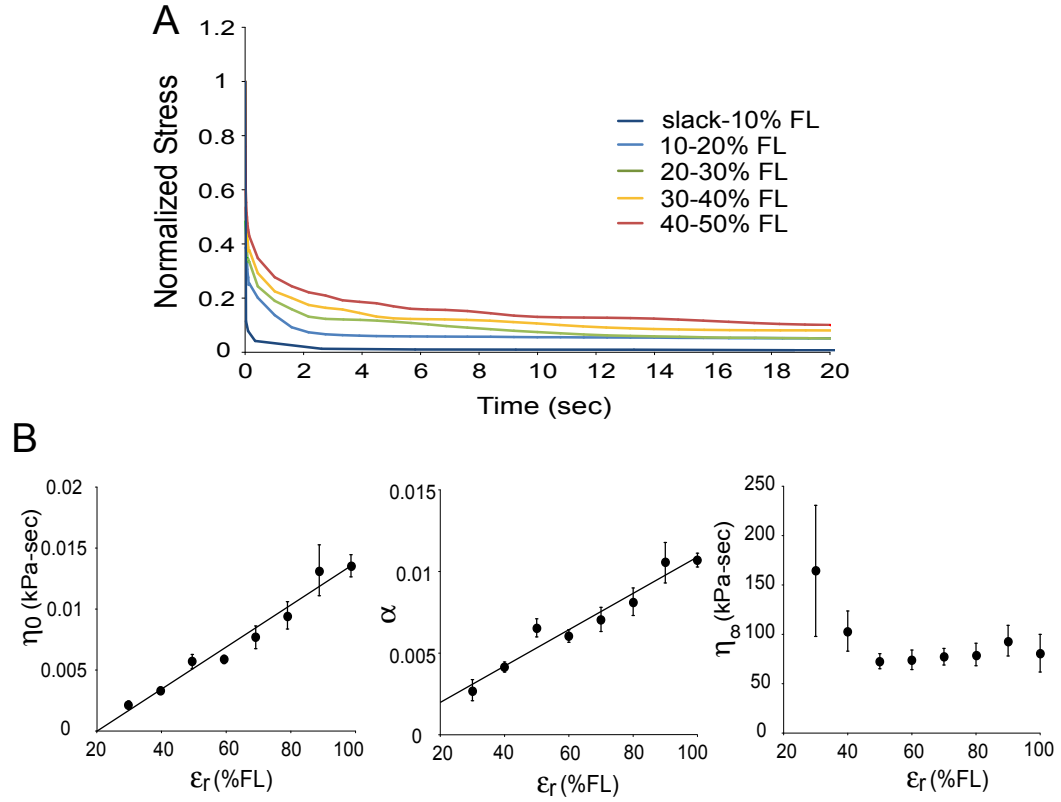
Figure 4.7: Viscosity is a function of strain in mouse muscle fibers. (A) Normalized stress relaxation data from a single fiber subjected to an incremental stress relaxation test from slack length to 50% FL at 20 FL/sec. Stress is decay is slower with increasing strain, indicating fiber viscosity is increasing as a function of resting strain. (B) The pseudoplastic model was used to locally fit incremental stress relaxation data from six fibers from slack length to 100% FL at 20 FL/sec. Parameters $\eta_0$ and $\alpha$ both increase linearly as a function of resting strain, but $\eta_\infty$ remains relatively constant.

the pseudoplastic model can characterize the fibers deviation from superposition (Fig. 4.6B, gold traces).

## 4.4   Discussion

The purpose of this study was to define the passive mechanical behavior of single fibers from the mouse $5^{th}$ toe EDL muscle under a variety of strains and strain rates to evaluate the applicability of a linearly viscous model. The data acquired demonstrate that the viscosity of mouse muscle fibers is not linear as is typically assumed, but rather a more complex function of time, strain and strain rate. A new pseudoplastic model was developed to describe these nonlinearities and was shown to provide an excellent fit to stress relaxation data and to account for the strain rate sensitivity and deviation from superposition observed in the fibers.

The pseudoplastic model was compared with two models frequently used to describe stress relaxation in muscle, the $3^{rd}$ order Hill model and the QLV model. The pseudoplastic model is an adaptation of the $1^{st}$ order Hill model to include nonlinearities in viscosity and thus the comparison between this model and the $3^{rd}$ order Hill model reduces to a comparison between nonlinear and linear viscosity. The $3^{rd}$ order Hill model is frequently only used locally to obtain parameters from a single high strain rate stress relaxation test in a comparative study where the conditions are the same between groups. Under these conditions, viscosity would be only a function of time and this dependence can be reasonably well approximated by combining linear viscous elements. The more viscous elements combined in parallel, the better fit the Hill model provides. However, the ideal model would describe the maximum amount of data with the minimum number of parameters. Continuing to add viscous elements to the Hill models increases the model complexity. Thus, for the purposes of comparison, the $3^{rd}$ order Hill model was chosen to balance complexity with goodness of fit. The pseudoplastic model provided a much better fit to the data described here than the $3^{rd}$ order Hill model with fewer parameters because it allowed the viscosity to change at every

time point rather than limiting it to three discrete values.

The QLV model also allows viscosity to be a function of time by mathematically incorporating a continuous spectrum of relaxation into the model. However, a primary tenet of this model is that the relaxation response is separable, i.e., that the relaxation response is not a function of strain. It has been shown in the data presented here and elsewhere [13, 32] that this is not the case for muscle. Nekouzadeh et al. developed an extension of the QLV model, which allows relaxation to adapt to strain history and eliminates the requirement for separability [33]. However, both this adaptive QLV model and the original QLV model still obey superposition and thus cannot describe the response of the muscle to incremental stretches [32]. The pseudoplastic model allows the stress relaxation process to be a function of strain and allows fiber viscosity to decrease during stretch, which enables it to explain fiber behavior over all of the strains and strain rates considered here.

Hyperelastic models are also frequently used to model skeletal muscle mechanics especially as they are applied to finite element models. However, these have either neglected the contribution of viscosity or modeled it as linear [18–20] and typically require a large number of parameters. Thus, these models were not used to fit the data described here but could theoretically be modified to include viscous nonlinearities.

Other nonlinear model formulations have been developed and implemented to describe the material behavior of other soft tissues such as ligament with good success [10, 11, 25]. These models have employed similar strategies to the pseudoplastic model described here where the viscous parameters of a linear model are modified to include nonlinearities. The pseudoplastic model takes the description further, however, allowing the viscous parameters to be continuous and to be functions of strain rate. Also, in addition to describing these dependencies mathematically, it offers a physical explanation for the deviation of fiber behavior from separability and superposition. If muscle is indeed a pseudoplastic material, its viscosity would be continuously changing as intermolecular bonds are continuously formed and broken and it is likely that these interactions change with geometry.

### 4.4.1 Muscle as a non-Newtonian material

Muscle has long been considered to be non-Newtonian in nature, i.e. it exhibits a viscosity that is not constant. Sinusoidal studies on passive muscles and single fibers show a short range stiffness where the sample is initially very stiff but then becomes more compliant as the strain profile continues [34–36]. This observation was attributed to the muscle being thixotropic, or having a viscosity that decreases with time spent under shear load. However, the observation that muscle viscosity decreases under load could also be explained by pseudoplasticity, where the viscosity decreases inversely proportionally to the increase in strain rate. The data presented here suggest that mouse single fibers are pseudoplastic rather than thixotropic, but it is possible that the decrease in viscosity under shear load is a more complex function of both strain rate and time. Quaia et al. created a passive muscle model that incorporates thixotropy, but they noted as well that during relaxation, the stress drops faster following faster elongations, an indication of pseudoplastic behavior [32].

The mechanism behind this non-Newtonian behavior is not well understood, but the applied stress is supposed to induce reversible microstructural breakdown, possibly through bond or network disruption, thus reducing viscosity. After the removal of the stress, the bonds or networks are reformed spontaneously leading to a rebuilding of viscosity. In this study, the data suggest that components of the breakdown and rebuilding phases in muscle fibers are functions of strain. It is possible that, as cytoskeletal elements are lengthened and interstitial space is reduced in the fibers, that the kinetics of these phases are altered. For example, as strain increases, it could become more difficult to break the molecular interactions, leading to a smaller decrease in viscosity for a given strain rate (i.e. an increase in $\eta_0$ with strain). The parameter $\alpha$ is also increased with strain, which reflects slower rebuilding, but eventually all interactions are reformed and the fiber is back to a relatively strain insensitive viscosity ($\eta_\infty$). Another mechanism proposed in the ligament literature is that increased strains result in increased fluid loss, causing the tissue to become more elastic in nature [11], which is certainly a possibility in these skinned fibers where fluid is allowed to flow freely into and out of the cell.

### 4.4.2   Sources of passive viscosity

Many components of muscle have been proposed to contribute to viscosity including the myoplasm, weakly attached cross-bridges, collagen fibrils, titin and other cytoskeletal proteins [37]. Only muscle fiber viscosity is considered here eliminating any contribution of the extracellular matrix (ECM), but it will be interesting to compare the properties measured here in fibers to bundles and whole muscle. Although fiber elasticity is essentially linear (Fig. 4.6A), the inclusion of ECM at the bundle and whole muscle scale imparts significant nonlinearity [26].

It is likely that, like elasticity, the dependence of viscosity on time, strain and strain rate could change dramatically with scale, aging or disease. Chronic alterations in viscosity may well have a large effect on muscle function and thus sources of viscosity should be considered as potential therapeutic targets. This new pseudoplastic model is a tool to evaluate these changes and their effect on function.

## Acknowledgements

Chapter 4, in full, has been submitted for publication of the material as it may appear in *Journal of Biomechanical Engineering.* "A Nonlinear Model of Passive Muscle Viscosity." Meyer G.M., McCulloch A.D., and Lieber R.L. The dissertation author was the primary investigator and author of this paper.

## 4.5   References

[1] Foidart, M., Foidart, J.M., and Engel, W.K., 1981. Collagen localization in normal and fibrotic human skeletal muscle. *Archives of neurology*, 38:152–157.

[2] Gao, Y., Kostrominova, T.Y., Faulkner, J.A., and Wineman, A.S., 2008. Age-related changes in the mechanical properties of the epimysium in skeletal muscles of rats. *Journal of biomechanics*, 41:465–469.

[3] Smith, L.R., Lee, K.S., Ward, S.R., Chambers, H.G., and Lieber, R.L., 2011. Hamstring contractures in children with spastic cerebral palsy result from a stiffer extracellular matrix and increased in vivo sarcomere length. *The Journal of physiology*, 589:2625–2639.

[4] Gajdosik, R.L., 2001. Passive extensibility of skeletal muscle: review of the literature with clinical implications. *Clinical biomechanics (Bristol, Avon)*, 16:87–101.

[5] Levin, A., 1927. The viscous elastic properties of muscle. In Proceedings of the Royal Society of London Series B.

[6] Hill, A., 1938. The heat of shortening and the dynamic constants of muscle. In Proceedings of the Royal Society of London Series B.

[7] Buchthal, F., 1951. The rheology of the cross striated muscle fibre: with particular reference to isotonic conditions.

[8] Glantz, S.A., 1977. A three-element description for muscle with viscoelastic passive elements. *Journal of biomechanics*, 10:5–20.

[9] Best, T.M., McElhaney, J., Garrett, W.E., and Myers, B.S., 1994. Characterization of the passive responses of live skeletal muscle using the quasi-linear theory of viscoelasticity. *Journal of biomechanics*, 27:413–419.

[10] Thornton, G.M., Oliynyk, A., Frank, C.B., and Shrive, N.G., 1997. Ligament creep cannot be predicted from stress relaxation at low stress: a biomechanical study of the rabbit medial collateral ligament. *Journal of orthopaedic research : official publication of the Orthopaedic Research Society*, 15:652–656.

[11] Provenzano, P.P., Lakes, R.S., Corr, D.T., and Vanderby, R., 2002. Application of nonlinear viscoelastic models to describe ligament behavior. *Biomechanics and modeling in mechanobiology*, 1:45–57.

[12] Bagni, M.A., Cecchi, G., Colombini, B., and Colomo, F., 1999. Mechanical properties of frog muscle fibres at rest and during twitch contraction. *Journal of electromyography and kinesiology : official journal of the International Society of Electrophysiological Kinesiology*, 9:77–86.

[13] Van Loocke, M., Lyons, C.G., and Simms, C.K., 2008. Viscoelastic properties of passive skeletal muscle in compression: stress-relaxation behaviour and constitutive modelling. *Journal of biomechanics*, 41:1555–1566.

[14] Quaia, C., Ying, H.S., and Optican, L.M., 2009. The viscoelastic properties of passive eye muscle in primates. II: testing the quasi-linear theory. *PloS one*, 4:e6480.

[15] Anderson, J., Li, Z., and Goubel, F., 2002. Models of skeletal muscle to explain the increase in passive stiffness in desmin knockout muscle. *Journal of biomechanics*, 35:1315–1324.

[16] Wolff, A.V., Niday, A.K., Voelker, K.A., Call, J.A., Evans, N.P., Granata, K.P., and Grange, R.W., 2006. Passive mechanical properties of maturing extensor digitorum longus are not affected by lack of dystrophin. *Muscle & nerve*, 34:304–312.

[17] Navajas, D., Mijailovich, S., Glass, G.M., Stamenović, D., and Fredberg, J.J., 1992. Dynamic response of the isolated passive rat diaphragm strip. *Journal of applied physiology (Bethesda, Md : 1985)*, 73:2681–2692.

[18] Blemker, S.S. and Delp, S.L., 2005. Three-dimensional representation of complex muscle architectures and geometries. *Annals of biomedical engineering*, 33:661–673.

[19] Odegard, G.M., Donahue, T.L.H., Morrow, D.A., and Kaufman, K.R., 2008. Constitutive modeling of skeletal muscle tissue with an explicit strain-energy function. *Journal of biomechanical engineering*, 130:061017.

[20] Lu, Y.T., Zhu, H.X., Richmond, S., and Middleton, J., 2010. A visco-hyperelastic model for skeletal muscle tissue under high strain rates. *Journal of biomechanics*, 43:2629–2632.

[21] Shah, S.B., Davis, J., Weisleder, N., Kostavassili, I., McCulloch, A.D., Ralston, E., Capetanaki, Y., and Lieber, R.L., 2004. Structural and functional roles of desmin in mouse skeletal muscle during passive deformation. *Biophysical journal*, 86:2993–3008.

[22] Shah, S.B. and Lieber, R.L., 2003. Simultaneous imaging and functional assessment of cytoskeletal protein connections in passively loaded single muscle cells. *The journal of histochemistry and cytochemistry : official journal of the Histochemistry Society*, 51:19–29.

[23] James, R.S., Altringham, J.D., and Goldspink, D.F., 1995. The mechanical properties of fast and slow skeletal muscles of the mouse in relation to their locomotory function. *The Journal of experimental biology*, 198:491–502.

[24] Smith, L.R., Gerace-Fowler, L., and Lieber, R.L., 2011. Muscle extracellular matrix applies a transverse stress on fibers with axial strain. *Journal of biomechanics*, 44:1618–1620.

[25] Lakes, R.S. and Vanderby, R., 1999. Interrelation of creep and relaxation: a modeling approach for ligaments. *Journal of biomechanical engineering*, 121:612–615.

[26] Meyer, G.A. and Lieber, R.L., 2011. Elucidation of extracellular matrix mechanics from muscle fibers and fiber bundles. *Journal of biomechanics*, 44:771–773.

[27] Sisko, A., 1958. The flow of lubricating greases. *Industrial & Engineering Chemistry*.

[28] Ranatunga, K.W., 2001. Sarcomeric visco-elasticity of chemically skinned skeletal muscle fibres of the rabbit at rest. *Journal of muscle research and cell motility*, 22:399–414.

[29] Bensamoun, S., Stevens, L., Fleury, M.J., Bellon, G., Goubel, F., and Ho Ba Tho, M.C., 2006. Macroscopic-microscopic characterization of the passive mechanical properties in rat soleus muscle. *Journal of biomechanics*, 39:568–578.

[30] Fung, Y.c., 1993. Biomechanics. mechanical properties of living tissues. Springer.

[31] Doehring, T.C., Carew, E.O., and Vesely, I., 2004. The effect of strain rate on the viscoelastic response of aortic valve tissue: a direct-fit approach. *Annals of biomedical engineering*, 32:223–232.

[32] Quaia, C., Ying, H.S., and Optican, L.M., 2010. The viscoelastic properties of passive eye muscle in primates. III: force elicited by natural elongations. *PloS one*, 5:e9595.

[33] Nekouzadeh, A., Pryse, K.M., Elson, E.L., and Genin, G.M., 2007. A simplified approach to quasi-linear viscoelastic modeling. *Journal of biomechanics*, 40:3070–3078.

[34] Hill, D.K., 1968. Tension due to interaction between the sliding filaments in resting striated muscle. The effect of stimulation. *The Journal of physiology*, 199:637–684.

[35] Lakie, M. and Robson, L.G., 1988. Thixotropy: the effect of stretch size in relaxed frog muscle. *Quarterly journal of experimental physiology (Cambridge, England)*, 73:127–129.

[36] Wiegner, A.W., 1987. Mechanism of thixotropic behavior at relaxed joints in the rat. *Journal of applied physiology (Bethesda, Md : 1985)*, 62:1615–1621.

[37] Moss, R.L. and Halpern, W., 1977. Elastic and viscous properties of resting frog skeletal muscle. *Biophysical journal*, 17:213–228.

# Chapter 5

# Skeletal Muscle Fibrosis Develops in Response to Compliant Fibers

## Abstract

Skeletal muscle is dynamic composite of proteins that responds to both internal and external cues to facilitate muscle adaptation. In cases of disease or altered use, these messages can be distorted resulting in myopathic conditions such as fibrosis. The mechanisms and pathways by which fibrosis occurs remain largely unknown, but this study suggests that mechanotransduction between the cytoskeleton and the extracellular matrix (ECM) plays a role in maintaining proper muscle-ECM homeostasis. Muscle lacking the intermediate filament desmin becomes increasingly fibrotic with age as indicated by increased stiffness, collagen accumulation and elevated ECM related gene expression. Although fiber bundle stiffness was increased in the absence of desmin, individual fibers were more compliant suggesting fibrosis may develop as a compensatory stiffening response to the mechanically compromised fibers. In the absence of desmin, muscle is in an increased state of inflammation and regeneration as indicated by increased centrally nucleated fibers, elevated inflammation and regeneration related gene expression, and increased numbers of inflammatory cells as determined by flow cytometry. Together, this data suggest that desmin acts to protect muscle from injury, possibly

by restraining sarcomere overextension, and in its absence muscle becomes fibrotic in an attempt to compensate for this lack of mechanical support.

## 5.1   Introduction

Skeletal muscle is a composite tissue composed of multinucleated muscle cells embedded in a connective tissue matrix. The interaction between active muscle force generating components and passive extracellular matrix (ECM) force transmitting components provides skeletal muscle with its characteristic biomechanical properties, which enable it to produce work and resist extension. The amount of ECM is surprisingly consistent across individuals and across muscles, presumably due to the physiological balance between the passive and active mechanical properties of a muscle. However, in cases of disease (e.g. muscular dystrophies, diabetes) or altered use (e.g. immobilization, aging, exercise, denervation) the amount of ECM can increase dramatically relative to muscle fibers, resulting in a condition known as fibrosis [1–5]. Tissue fibrosis represents a tremendous clinical problem, not only in muscles where it restricts range of motion and may be related to the process of contracture formation, but also other tissues such as liver, kidney, lung and heart [6]. Thus, it is important to examine the factors that regulate the relative amount of ECM in an organ in order to create effective antifibrotic therapies and, in that context, skeletal muscle provides a unique system in which to study such factors.

Skeletal muscle cells are very mechanosensitive, as are the other cells that reside in the matrix [7, 8]. In addition to multinucleated post-mitotic muscle cells, muscle tissue contains mononucleated endothelial cells, fibroblasts, mesenchymal stem cells, satellite cells, and the so-called fibroadipogenic progenitor cells, all of which have the ability to differentiate and produce ECM components [9–11]. Since it is known that cells are extremely sensitive to their mechanical environment, the possibility exists that some of the communication that occurs amongst these cells types is mechanical in nature. Again, skeletal muscle represents a tissue with well-defined mechanical properties that can be exploited to try to understand the

nature of this communication.

While numerous experimental models of muscle fibrosis exist, including muscle laceration, cardiotoxin-induced degeneration, and strain injury, most of these models create a dramatic and heterogeneous response by the skeletal muscle [9, 12]. Additionally, they are acutely imposed on healthy muscle, which is dissimilar to the progressively developing pathology that occurs in cases of disease and altered use. As a result, it may be difficult, using these models, to identify the mechanical and biological factors that result in fibrosis that is associated with pathology. In this report, we exploit the fact that desmin intermediate filament knockout in skeletal muscle results in increased muscle cell compliance, and a compensatory response by the muscle ECM. Desmin filaments form a mesh-like network around Z-disks, stabilizing the contractile apparatus and linking it to the surrounding environment via the ECM [13, 14]. It is thought to be involved in both intracellular and extracellular mechanotransduction and thus the desmin knockout provides an ideal system in which to study the effects of mechanical communication on ECM regulation. We use this system to identify a possible causal relationship between increased cellular compliance and the proliferative response of the extracellular matrix cellular constituents.

## 5.2 Methods

### 5.2.1 Ethical approval

All procedures were performed in accordance with the National Institutes of Health Guide for the Use and Care of Laboratory Animals and were approved by the University of California and Department of Veterans Affairs Committees on the Use of Animal Subjects in Research.

### 5.2.2 Experimental design

Experiments were performed on muscles from wildtype ($wt$) 129/Sv (Taconic Farms, Germantown, NY) and desmin knockout ($des^{-/-}$) 129/Sv [15] mice. Mice

were age matched in three age groups: Neonatal (10-20 days), Adult (7-9 weeks) and Aged (12-14 months). Animals were anesthetized with 2% isoflurane at 2 L/min and then euthanized by cervical dislocation. Hindlimbs were transected proximal to the knee and placed in a mammalian Ringers solution composed of (mM): NaCl (137), KCl (5), $NaH_2PO_4$ (1), Na $HCO_3$ (24), $CaCl_2$ (2), $MgSO_4$ (1), and glucose (11) with 10 mg/L curare for dissection.

### 5.2.3  Muscle mechanical testing

Passive mechanical testing was performed on single fibers and fiber bundles from the $5^{th}$ toe of the extensor digitorum longus (EDL) muscle. Samples were isolated from $\geq 5$ muscles per group (2 genotypes x 3 ages) with approximately 3 fibers and 3 bundles per muscle subjected to testing (n=97 total fibers, n=84 total bundles). After dissection, muscles were stored in a glycerinated storage solution overnight composed of (mM): KPropionate (170), $K_3EGTA$ (5), $MgCl_2$ (5.3), imidazole (10), $Na_2ATP$ (21.2), $NaN_3$ (1), glutathione (2.5), 50 $\mu$M leupeptin, and 50% (v/v) glycerol. Prior to mechanical testing, muscles were removed from storage solution and transferred to a relaxing solution at pCa 8.0 and pH 7.1 consisting of (mM): imidazole (59.4), $KCH_4O_3S$ (86), $Ca(KCH_4O_3S)_2$ (0.13), $Mg(KCH_4O_3S)_2$ (10.8), $K_3EGTA$ (5.5), $KH_2PO_4$ (1), $Na_2ATP$ (5.1), and 50.0 $\mu$M of the protease inhibitor leupeptin.

Single fiber or fiber bundle segments (2-3 mm in length) were carefully dissected and mounted in a custom chamber. They were secured using 10-0 monofilament nylon suture on one end to a force transducer (Aurora Scientific 405A; Aurora, Ontario, Canada) and on the other end to a titanium wire rigidly attached to a rotational bearing (Newport MT-RS; Irvine, CA). Sarcomere length provided an objective assessment of internal specimen strain and was measured by transilluminating the specimen with a low power laser diode. Segments displaying obvious abnormalities were not used.

Single fibers were brought to slack length ($L_0$), which was determined by the knot-to-knot length at which passive tension was just measurable above the noise level of the force transducer ($\sim$1mN). Sample length and diameter were measured

with a cross-hair reticule mounted on a dissecting microscope and micromanipulators on an x-y mobile stage. The fiber was deformed incrementally in 10% $L_0$ steps at a strain rate of 20 FL/sec and then allowed to stress-relax for 3 minutes. Fibers were strained either to failure or to 100% $L_0$, whichever was reached first. Fiber Cauchy stress was determined by dividing the tension by the fiber cross-sectional area at the end of each stretch. Fiber cross-sectional area was calculated based on the measured initial fiber diameter and the assumption that the fiber was cylindrical and isovolumic [16]. Fiber bundles were tested in the same manner as single fibers and consisted of 10-20 fibers and their constitutive extracellular matrix.

Passive mechanical data were acquired via customized LabView software throughout the 3-minute stress-relaxation and analyzed in Matlab. Stress was plotted against sarcomere length at each stretch and fit with quadratic regression ($r^2 > 0.98$ for all samples). Tangent modulus was computed as the slope of the regression line at a sarcomere length of 3.9 $\mu$m (the end of the predicted length-tension curve for mouse muscle).

ECM material properties were determined using the theory of composites, which states that the elastic modulus of a composite material is the sum of the elastic modulus of each component multiplied by its volume fraction [17]. This relationship is given mathematically by the rule of mixtures, stated below, and has been used previously to define the contribution of the ECM to muscle passive mechanics [18].

$$E_c = E_m V_m + E_f V_f \tag{5.1}$$

The composite elastic modulus is given by $E_c$, where $E_m$ and $E_f$ are the matrix and fiber elastic moduli and $V_m$ and $V_f$ are the matrix and fiber volume fractions, respectively.

### 5.2.4   Microarray processing

To gain insights into the biological processes associated with fibrosis, microarray analysis was performed on the tibialis anterior (TA) muscle from *wt* and

$des^{-/-}$ mice. RNA was extracted from whole muscles ($\sim$30 mg tissue) using a combination of standard Trizol (Invitrogen Carlsbad, CA) and RNeasy (Qiagen, Valencia, CA) protocols. Muscles were homogenized for 60 seconds in a rotor-stator homogenizer on ice in 0.5 ml Trizol, 0.1 ml of chloroform was then added and the sample was vigorously vortexed for 15 seconds followed by centrifugation. The supernatant was removed and combined with an equal volume of 70% ethanol and the mixture was filtered through the RNeasy spin column. The column was then washed, incubated with RNAse-free DNAse (Qiagen), washed again and eluted as described in the manufacturers protocol. RNA concentration was determined by the absorbance at 260nm and the 260 nm to 280 nm absorbance ratio was calculated to define RNA purity.

Individual Affymetrix microarrays ("GeneChip" Mouse Genome 430A 2.0 Array; Affymetrix, Santa Clara, CA) were used for each muscle. A total of 19 chips were used with 4-5 chips per group (2 genotypes x 2 ages). RNA processing for the GeneChip, including stringent quality control measures, was performed by the Gene Chip Core at the Department of Veterans Affairs San Diego Health Care System (San Diego, CA).

Genespring software (SiliconGenetics, Redwood City, CA) was used to identify genes that were differentially expressed as a function of genotype ($wt$ or $des^{-/-}$) at two ages (adult and aged). Three independent probe set algorithms were used for background subtraction and normalization (MAS5, RMA and GCRMA) and each feature was normalized per chip and per gene as previously described [19]. Normalized expressions of identified genes, excluding putative genes and expressed sequence tags, were subjected to two-way ANOVA with a significance level ($\alpha$) set to 0.05 and a Benjamini and Hochberg False Discovery Rate multiple testing correction for present features.

To investigate the biological context of transcriptional changes, the role of significant genes in various muscle pathways was investigated. Gene ontology (GO) analyses were performed using a Web-based Gene Set Analysis Toolkit (WebGestalt; bioinfo.vanderbilt.edu/webgestalt/). In this analysis, a p-value is generated for each pathway based on hypergeometric comparison of the number of

genes present in that list to the number of genes expected to be present based on the size of the list.

### 5.2.5  Quantitative real-time PCR

In addition to microarray processing, isolated RNA samples were subjected to quantitative real-time PCR (QPCR) to provide validation of GeneChip expression values. After RNA was extracted from the muscle (as described for microarray processing) and diluted 1:5 with DNase/RNase free water, 1 $\mu$L of each sample was reverse transcribed using standard protocols (Superscript III; Invitrogen). cDNA was amplified with the eppendorf MasterCycler GradientS (Hamburg, Germany) with primers specific to the genes of interest. All primers were tested for cross-reactivity with other transcripts using nBLAST and Oligo (version 6.6; Molecular Biology Insights, Cascade, CO). All samples were run at least in triplicate on a 96 well plate. Each well contained 10 $\mu$L volume made up of the KAPA SYBR FAST Master Mix (2x) Universal (KAPA Biosystems), and forward and reverse primers (Table D.1).

Amplification conditions were as follows: An initial hold at 95 °C for 2 min was followed by 40 cycles of denaturing at 95 °C for 15 s, followed by annealing/extension at 68 °C for 40 s. The success of each reaction was deduced based on the observation of a single reaction product on an agarose gel and a single peak on the DNA melting temperature curve determined at the end of the reaction. To express QPCR results, the standard curve method was used with the cycles to threshold value representing the PCR cycle number at which the SYBRgreen signal was increased above the threshold. Expression of each gene was normalized to its mean value.

### 5.2.6  Hydroxyproline assay for collagen content

Total collagen content was determined in the TA muscle using a colorimetric assay for hydroxyproline content [20]. Samples were taken from $\geq$ 5 muscles per group (n=45 total muscles). TA muscles were dissected from the hindlimb and

immediately flash-frozen in liquid nitrogen cooled isopentane. Portions of the muscle that contained no internal tendon were isolated and hydrolyzed in 6N HCl at 110 °C for 18 hours. After hydrolysis, samples were neutralized and treated with a chloramine T solution for 20 minutes at room temperature followed by a solution of p-diaminobenzaldehyde for 30 minutes at 60 °C. Sample absorbance was read from three aliquots of each sample at 550 nm. Hydroxyproline content was converted to collagen content using the extinction coefficient for hydroxyproline and dividing by the number of hydroxyproline residues in a molecule of collagen.

### 5.2.7   Immunohistochemistry

Cross-sections (10 $\mu$m thick) from flash frozen muscle were cut from the midbelly of the TA muscle on a cryostat at -20 °C (Microm HM500, Waldorf, Germany). Serial sections were stained with hematoxylin and eosin (H&E) to view overall fiber appearance (n=16 muscles). Centrally nucleated fibers were identified and manually counted as a fraction of all fibers in the cross-section by an observer blinded to experimental identity. To visualize ECM components in the muscle, serial sections were immuono-labeled with primary antibodies to laminin (rabbit polyclonal, Sigma, St. Louis, MO) and type I collagen (rabbit polyclonal, Rockland, Gilbertsville, PA). Muscle sections were treated with bovine serum albumin as a blocking agent and incubated with antibodies overnight. An AlexaFluor 594 goat anti-rabbit immunoglobulin G (Invitrogen, Carlsbad, CA) secondary antibody was used for visualization.

Determination of fiber size was performed on laminin stained sections (n=16 muscles) as previously described using a custom macro in ImageJ (NIH, Bethesda, MD) [21]. Filtering criteria required that fibers have an area above 50 $\mu$m$^2$ but below 5600 $\mu$m$^2$ to eliminate neurovascular structures and optically fused fibers and fibers touching the edge of the field were excluded. Additionally, circularity was required to be between 0.3 and 1.0 to prevent inclusion of obliquely sectioned fibers. Area fraction of ECM was also determined from laminin stained sections (n=20 total muscles). A background subtraction algorithm was applied to each image to normalize intensity values and remove any effects of background noise.

Fiber centers, considered image background, were set to a value of 0 in the RGB channel and image intensity was rescaled from 0 to 255. A threshold was then applied to each image and the relative number of white (stained) pixels vs. black (unstained) pixels was computed using ImageJ. Before analysis, each image was inspected, and areas with sectioning artifacts, large blood vessels or poor staining quality were omitted from quantification.

### 5.2.8   Flow cytometry

Tibialis anterior, gastrocnemius and quadriceps muscle groups were dissected from both hindlimbs of *wt* and *des$^{-/-}$* mice. Muscles were incubated in a digestive solution consisting of: collagenase type I (2.67 g/L), dispase II (75 g/L), penicillin (50 units/mL), and streptomycin (50 units/mL) in Dulbeccos Modified Eagle Medium. Cells were then strained through a 70 $\mu$m nylon filter, centrifuged and resuspended in a buffer solution consisting of: EDTA (1 mM) and normal goat serum (2.5%) in sterile PBS. Cell preparations were incubated with primary antibodies on ice for 20 minutes (antibodies listed in Table C.2). Compensation beads (BD CompBead Plus) were used as compensation controls for the fluorophores and fluorescence-minus-one (FMO) controls were generated by combining cells from each sample population with appropriate antibodies. After incubation, samples and controls were centrifuged, the supernatant removed, and the pellet resuspended in buffer solution. Two of the antibodies used (ER-TR7 and $\alpha$SMA) were specific for intracellular structures and thus cells used for this gating were fixed and permeabilized to allow the antibodies access to the cell interior. Cells were fixed by suspending them in a 70% ethanol solution on ice for 20 minutes and permeabilized by re-suspending them for an additional 10 minutes in a blocking solution consisting of: BSA (2%), FBS (5%), Triton X-100 (0.2%) and sodium azide (0.1%).

Analysis was performed on a Special Order LSRFortessa (BD Biosciences, San Jose) with four lasers (405 nm, 50 mW; 488 nm, 50 mW; 561 nm, 100 mW; 640nm 50 mW). Fluors were detected at the following wavelengths: FITC, 497-523 nm; PE, 575-589 nm; Alexa Fluor 700, 710-750 nm; eFluor 450, 425-475

nm ; PerCP, 675-715 nm; APC, 663-677 nm. Cytometer performance and laser delay settings were verified daily with the Cytometer Setup and Tracking (CST) system (BD Biosciences, San Jose) according to the manufacturers directions. Data was collected using FacsDiVa (BD Biosciences, San Jose) software version 6.2 and analyzed with FlowJo 9.3.1. All gating was performed on FMO controls with a 1% error rate. Detailed gating information is provided in Appendix C.

### 5.2.9  Data processing and statistical analysis

For comparisons across genotype and age, two-way ANOVA was used with a significance level ($\alpha$) set to 0.05 and with a Tukey multiple corrections post-hoc test where appropriate. Results in the text and in tables are presented as mean $\pm$ standard error.

## 5.3  Results

### 5.3.1  Altered fiber and bundle material properties

Cauchy stress of isolated single fibers computed at the end of stress relaxation was fit with quadratic regression as a function of sarcomere length. Average fits of $des^{-/-}$ fibers resulted in significantly higher stresses than $wt$ at long sarcomere lengths (Fig. 5.1A, Fig. C.1). At the neonatal time point, when desmin levels first reach their mature level, $wt$ and $des^{-/-}$ fiber stresses and moduli were not significantly different (p>0.1; Fig. 5.1B, Fig. C.1). However, as the muscle matured, $des^{-/-}$ fibers failed to develop normal biomechanical properties and were significantly more compliant compared to $wt$ (p<0.05; Fig. 5.1B, Adult). As the muscle continued to age, $des^{-/-}$ fibers maintained their modulus, while $wt$ fibers became significantly more compliant (Fig. 5.1B, Aged).

In contrast to the finding that adult and aged $des^{-/-}$ fibers were more compliant or equally compliant as $wt$, adult and aged $des^{-/-}$ bundles had higher stresses (Fig. 5.2A, Fig. C.2) and were stiffer compared to $wt$ bundles (p<0.05; Fig. 5.2B). This difference in biomechanical properties occurred in spite of the fact
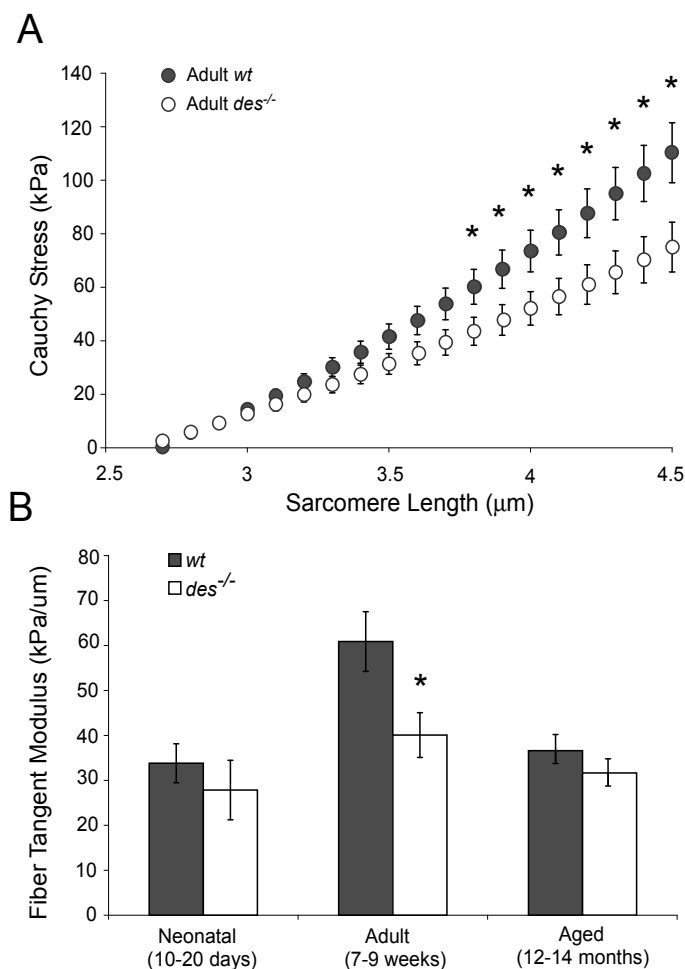
Figure 5.1: $Des^{-/-}$ fibers from adult muscle were more compliant compared to *wt*. (A) Passive Cauchy stress-sarcomere length quadratic curve-fits for adult *wt* (n=17) and $des^{-/-}$ (n=14) fibers. Although raw data was fit with quadratic regression, fiber stress-sarcomere length curves were nearly linear. $Des^{-/-}$ fibers had significantly lower stress compared to *wt* at sarcomere lengths greater than 3.7 $\mu$m as determined by ANOVA with repeated measures. (B) Tangent moduli calculated from curve-fits at a sarcomere length of 3.9 $\mu$m for $des^{-/-}$ and *wt* fibers in three age groups. Adult $des^{-/-}$ fibers were significantly more compliant compared to *wt*. However there was no difference between neonatal or aged fiber stiffness values with genotype. Asterisks indicate p<0.05.
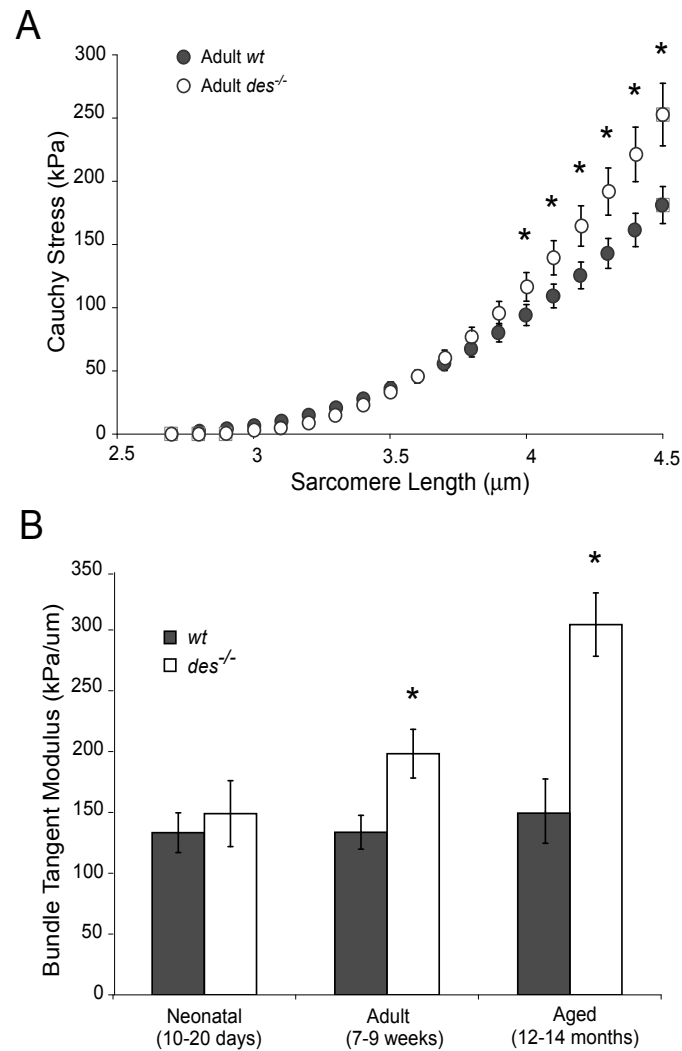
Figure 5.2: $Des^{-/-}$ bundles from adult and aged muscle were stiffer compared to *wt*. (A) Passive Cauchy stress-sarcomere length quadratic curve-fits for adult *wt* (n=10) and $des^{-/-}$ (n=12) bundles. Bundle curves were more nonlinear than fiber curves (compare with Fig. 5.1A) with increased nonlinearity in the adult $des^{-/-}$ curve relative to adult *wt*. $Des^{-/-}$ bundles had significantly higher stress than *wt* at sarcomere lengths greater than 4.1 $\mu$m as determined by ANOVA with repeated measures. (B) Tangent moduli for $des^{-/-}$ and *wt* bundles in three age groups. Adult and aged $des^{-/-}$ bundles were significantly stiffer compared *wt*, however there is no difference in neonatal bundle stiffness with genotype. Additionally, there was a significant genotype-age interaction as determined by 2-way ANOVA due to continually increasing bundle stiffness with age in $des^{-/-}$ bundles that was absent in *wt* bundles. Asterisks indicate p<0.05.

that bundles showed no significant genotype differences at the neonatal time point (p>0.5; Fig. 5.2B, Fig. C.2). Additionally, $des^{-/-}$ bundles exhibited increasing modulus with age, a trend that was absent in $wt$ bundles. Two-way ANOVA revealed a significant effect of genotype (p<0.01), age (p<0.01) and a significant interaction (p<0.01), explicitly demonstrating an age-dependent effect of genotype on modulus. In other words, the $des^{-/-}$ muscle became disproportionately stiffer with age.

In light of a recent report demonstrating that differences in the material properties of single fibers and fiber bundles are due to the contribution of the ECM [22], bundle modulus data suggest that $des^{-/-}$ muscle is chronically altering its ECM. There is support for this hypothesis based on the shapes of the stress-sarcomere length curves as well. Fibers have nearly linear stress-sarcomere length relationships (Fig. 5.1A), whereas the curves for bundles are significantly more nonlinear (Fig. 5.2A). This nonlinearity is likely due to the contribution of the ECM which is known to have distinctly nonlinear material properties [18]. In addition to the fact that the adult $des^{-/-}$ bundles sustain higher passive stress at longer sarcomere lengths, an increase in the nonlinearity of the stress-sarcomere length relationship is also evident (Fig. 5.2A, $des^{-/-}$).

No significant differences were detected in either degree or rate of stress relaxation between genotype and age in either fibers or bundles. Thus, the observed relationships between fully relaxed stress and sarcomere length are representative of the entire spectrum of stress relaxation. Additionally, no significant differences were observed in slack sarcomere length and fiber and bundle mechanical properties were qualitatively the same as a function of sarcomere length or specimen strain (data not shown).

## 5.3.2   Increased expression of ECM constituients

To investigate the basis for altered ECM properties in $des^{-/-}$ muscle, gene expression in the TA from adult and aged mice was investigated. Of the 9,161 identified genes on the mouse chip, 1,018 (11%) genes in the adult muscle and 3,172 (35%) genes in the aged muscle were differentially expressed with genotype. Only
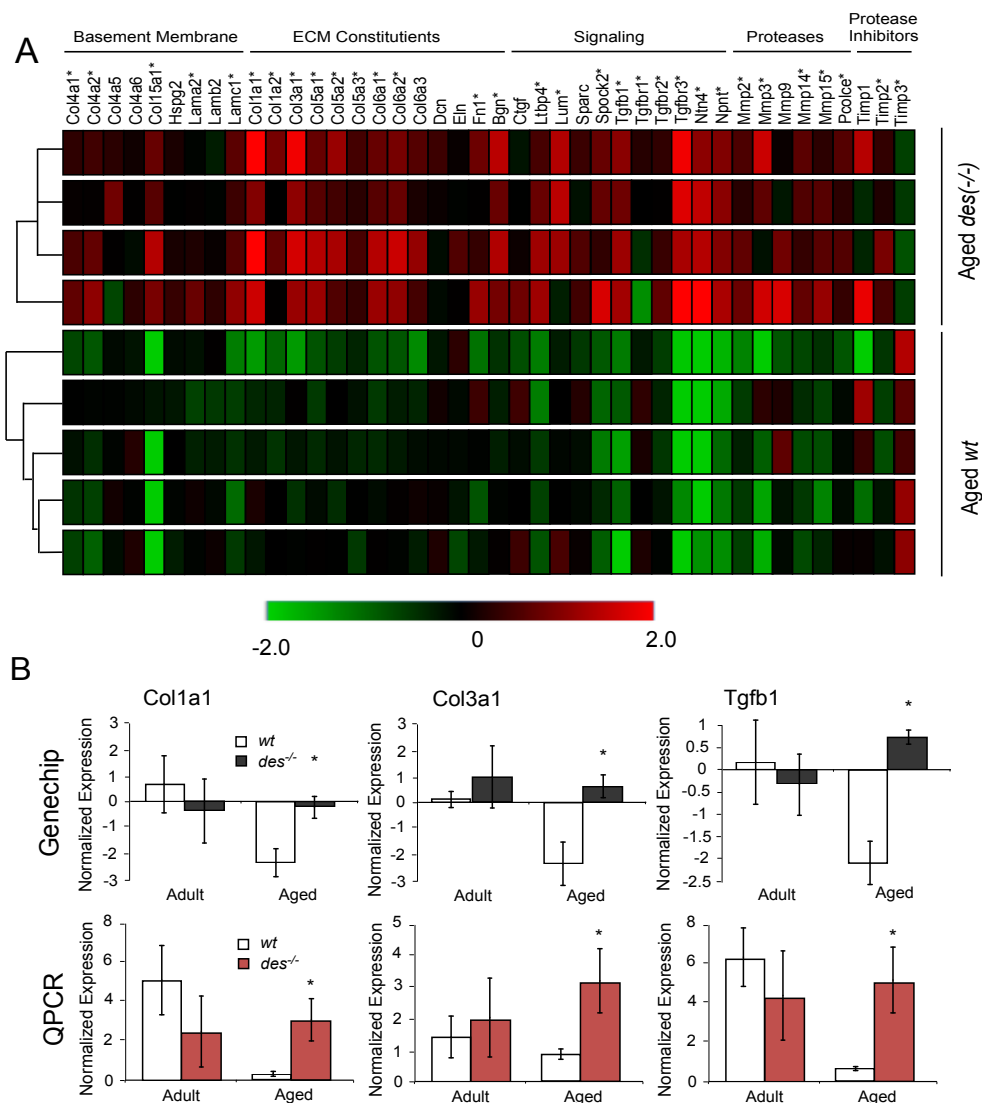
Figure 5.3: Aged $des^{-/-}$ muscle showed increased ECM specific gene expression. (A) Normalized gene expression for 42 genes involved in ECM structure. Hierarchical clustering is represented by connecting lines to the left of the grid with lines closest to the grid denoting the most similar samples. The aged $des^{-/-}$ samples show higher expression of the majority of the listed genes. Those with significantly higher expression values, as determined by 2-way ANOVA, are indicated with an asterisk. (B) Normalized expression as determined by GeneChip and QPCR for three important ECM genes: Col1a1 (type I collagen), Col3a1 (type III collagen) and Tgfb1 (transforming growth factor $\beta$). Asterisks indicate p < 0.05.

452 of these genes were shared by both ages indicating that, not only was there a larger genotype effect in the aged muscle (over twice the number of significant genes) but the effect was different between adult and aged muscles.

The primary genes involved in ECM structure, organization and remodeling in muscle were identified based on published pathways and literature searches [19, 23, 24]. A hierarchical gene clustering condition tree generated based on these genes did not cluster adult $des^{-/-}$ separately from adult $wt$, but did result in the aged $des^{-/-}$ samples being clustered separately from the aged $wt$, indicating that the ECM was differentially regulated in these samples (Fig. 5.3A). The condition tree clusters samples with similar expression patterns of genes of interest, which can be visualized by plotting gene expression by color with red indicating high expression and green indicating low expression. The four aged $des^{-/-}$ samples were clearly differentiated by their red color scheme indicating most of the genes involved in muscle ECM had higher normalized expression in aged $des^{-/-}$ muscle (Fig. 5.3A). Indeed, 29 out of the 42 genes were significantly upregulated in the aged $des^{-/-}$ compared to the aged $wt$ ($p<0.01$), while only 5 were significantly upregulated in the adult $des^{-/-}$, compared to the adult $wt$ ($p<0.01$).

The expression of three genes in the ECM list was confirmed by QPCR for adult and aged muscle (Fig. 5.3B). Consistent with GeneChip data, QPCR indicated that the expression of collagen type I (Col1a1), collagen type III (Col3a1) and transforming growth factor $\beta$ (Tgfb1) were significantly elevated in the aged $des^{-/-}$ muscle compared with $wt$ muscle.

Although the genes presented in Figure 5.3 are thought to be the primary contributors to ECM structure and maintenance, the list is by no means exhaustive. The gene ontology (GO) pathway for extracellular matrix provides a more extensive list and a means to determine whether the pathway itself is overrepresented in aged $des^{-/-}$ muscle. Consistent with the expression results (Fig. 5.3A), the extracellular matrix cellular component pathway (GO:0031012) was significantly overrepresented in aged $des^{-/-}$ muscle compared to aged $wt$ ($p<0.05$), but not in the adult $des^{-/-}$ ($p>0.1$).

To confirm that gene expression changes result in an accumulation of protein
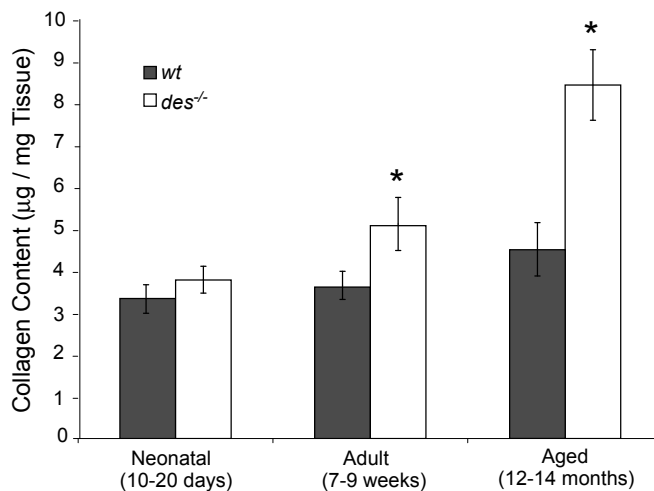
Figure 5.4: Adult and aged $des^{-/-}$ muscle had increased collagen content compared to *wt*. There was an increase in collagen content in the $des^{-/-}$ muscle with age that mirrored the increase in stiffness seen in the bundle data (compare with Fig. 5.2B). Collagen content nearly doubles in the aged $des^{-/-}$ compared with the aged *wt* as does bundle tangent modulus. There is a significant genotype-age interaction determined by 2-way ANOVA. Asterisks indicate $p < 0.05$.

in the ECM, intramuscular collagen content was measured. Collagen content was similar between genotypes in neonatal muscle, but was significantly increased in adult and aged $des^{-/-}$ muscle (p<0.05; Fig. 5.4). Additionally, collagen content increased with age in $des^{-/-}$ muscle, a trend absent from *wt* muscle but similar to the increasing $des^{-/-}$ bundle stiffness (Fig. 5.2). Two-way ANOVA revealed a significant effect of genotype (p<0.05) and age (p<0.05) as well as a significant interaction (p<0.05), indicating that collagen content varied between genotypes in an age-dependent manner. This provides a biochemical explanation for the differential functional response of $des^{-/-}$ muscle to age.

Although higher collagen content and gene expression were detected in $des^{-/-}$ muscle, flow cytometry data indicate no significant increase in the number of reticular (collagen producing) fibroblasts present in the muscle and no switch to a myofibroblastic phenotype (Fig. C.3), suggesting that fibroblasts increased their production of collagen in $des^{-/-}$ muscles rather than proliferating.

### 5.3.3 Altered ECM quantity and quality

Although fiber bundle mechanics combined with gene and protein expression data demonstrated changes to the ECM in $des^{-/-}$ muscle with age, it is unclear whether there is simply excessive ECM accumulation or whether the properties of existing ECM are being altered (collagen arrangement, cross-linking, swelling, etc.). It is possible to calculate the material properties of the ECM from fiber and bundle data using the theory of composites, but first the volume fraction of ECM relative to muscle fibers must be defined. Since fiber bundles were manually dissected from the midbelly of the muscle away from either tendon, there is likely little variation in collagen content with length. Additionally, since all bundles were similar lengths, it is reasonable to assume that the volume fraction of ECM will scale with area fraction, or in other words, that the changes in ECM volume fraction will all occur laterally in the spaces between fibers. Thus, ECM area fraction can be determined histologically and substituted for volume fraction into Equation 5.1 since both values are unitless.

On H&E stained cross-sections, a small increase in inter-fiber spacing can be seen in the $des^{-/-}$ muscle compared to the $wt$ muscle (Fig. 5.5A, a & d). Presumably this increased spacing is due to accumulation of ECM, but to ensure that it was not a sectioning artifact, sections were immunostained for two important components of the ECM: laminin and type I collagen. In immunostained sections, a small increase in staining apparent in $des^{-/-}$ compared to $wt$ muscle demonstrated that the increased inter-fiber spacing was indeed ECM (Fig. 5.5A, b, c, d & e). The area fraction of laminin staining was slightly, but significantly greater in the $des^{-/-}$ compared to $wt$ muscle, from approximately 10% to 15% in both adult and aged sections, suggesting an accumulation of ECM in $des^{-/-}$ muscle (p<0.05; Fig. 5B). Laminin staining was chosen for quantification so as not to exclude the basement membrane from the ECM definition, but area fraction measures on H&E and type I collagen stained sections yielded similar results (data not shown).

Using the ECM area fraction calculated from the laminin images (Fig. 5.5B), $des^{-/-}$ and $wt$ fiber moduli (Fig. 5.1B) and $des^{-/-}$ and $wt$ bundle moduli (Fig. 5.2B), a modulus value for $des^{-/-}$ and $wt$ ECM was calculated using composite theory.
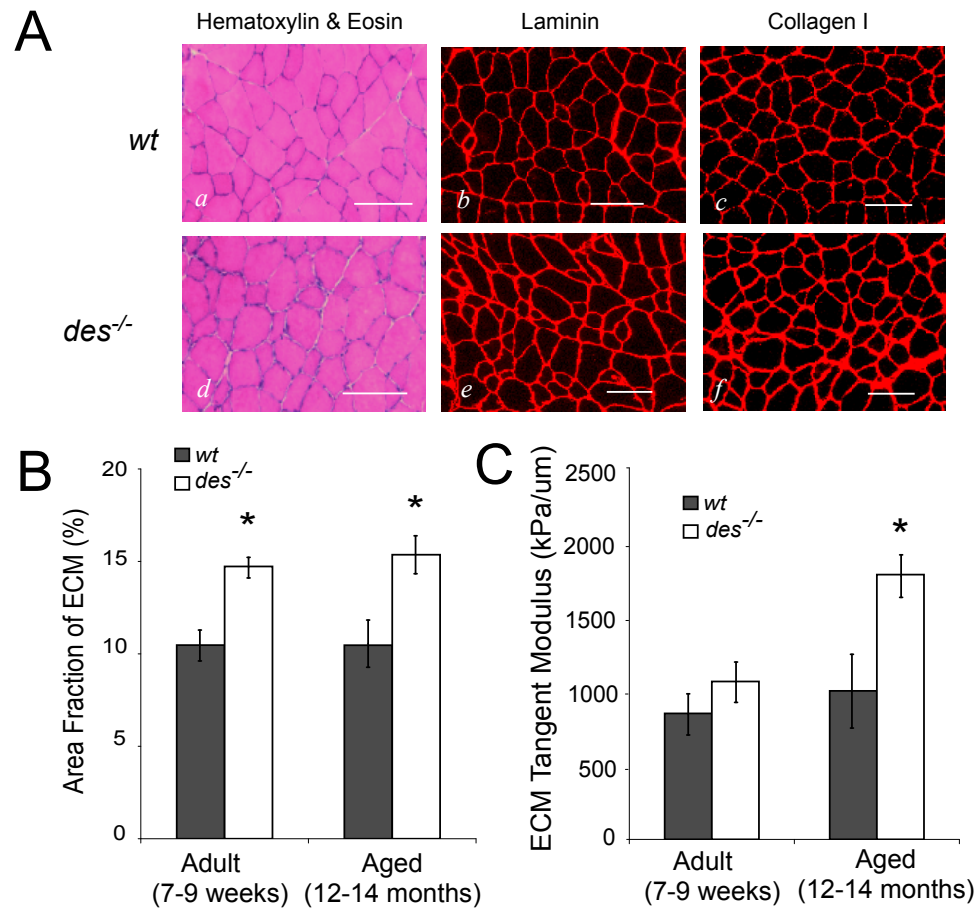
Figure 5.5: $Des^{-/-}$ muscle contained a higher fraction of ECM compared to $wt$. (A) Representative images from $wt$ and $des^{-/-}$ muscle stained for hematoxylin and eosin (H&E) (a&d), laminin (b&e), and collagen type I (c&f). H&E staining revealed a slight but notable increase in inter-fiber spacing in $des^{-/-}$ sections, which correlated with thicker and brighter staining for laminin and collagen I, suggesting an increase in ECM area. Scale bars are 100 $\mu$m. (B) The area fraction of ECM quantified from laminin stained sections. There was a small, but significant, increase in the area fraction of the ECM in both adult and aged $des^{-/-}$ muscle. (C) Although there was an increase in the area fraction of the ECM in both adult and aged $des^{-/-}$ muscle, it was not enough to account for the measured changes in aged bundle stiffness, and calculated ECM tangent modulus was significantly higher in aged $des^{-/-}$ muscle. Asterisks indicate p < 0.05.

Although there was a significant increase in the area fraction of ECM in both adult and aged $des^{-/-}$ muscle, it did not quantitatively account for the altered aged fiber bundle properties. Since ECM modulus was significantly higher in aged $des^{-/-}$ muscle (p<0.01; Fig. 5.5C), but not in adult, these data suggest that the ECM in $des^{-/-}$ muscle first proliferated and then altered its mechanical properties with age.

### 5.3.4   Signs of inflammation and regeneration

While these results indicate a progressive change in $des^{-/-}$ ECM with age, the mechanism for this alteration is unknown. Frequently, muscle fibrosis is preceded by inflammation, potentially caused by injury and cycles of regeneration [24, 25]. Injury studies in $des^{-/-}$ muscle have yielded conflicting results with some noting an increased susceptibility to injury, some noting a decreased susceptibility and some noting no difference [14, 26, 27]. To investigate the potential role of inflammation and regeneration in $des^{-/-}$ muscle fibrosis, gene expression profiles in these categories were investigated. A gene list composing 18 genes involved in inflammation and 11 genes involved in muscle regeneration was generated based on previously published physiological pathways and literature results [19, 28, 29]. A condition tree of expression data generated based on these genes clustered adult $des^{-/-}$ separately from adult wt (p<0.05; Fig. 5.6), but did not cluster the aged $des^{-/-}$ samples separately from the aged wt (p>0.1). This result suggests that inflammation and regeneration could play a significant role in adult $des^{-/-}$ muscle ECM remodeling. Six of the 18 genes identified as being involved in inflammation (33%) were significantly upregulated in adult $des^{-/-}$ samples over $wt$ compared with only 3 in aged $des^{-/-}$. Expression of three genes involved in inflammation and regeneration was again confirmed by QPCR (Fig. 5.6B). Consistent with GeneChip data, QPCR expression of interleukin-6 (Il6) was significantly higher in the adult $des^{-/-}$ compared with $wt$ and expression of muscle LIM protein (Csrp3) and insulin-link growth factor (Igf1) were both increased (though not significantly) in the aged $des^{-/-}$ compared with $wt$.

Consistent with these results, GO pathways involved in inflammation and
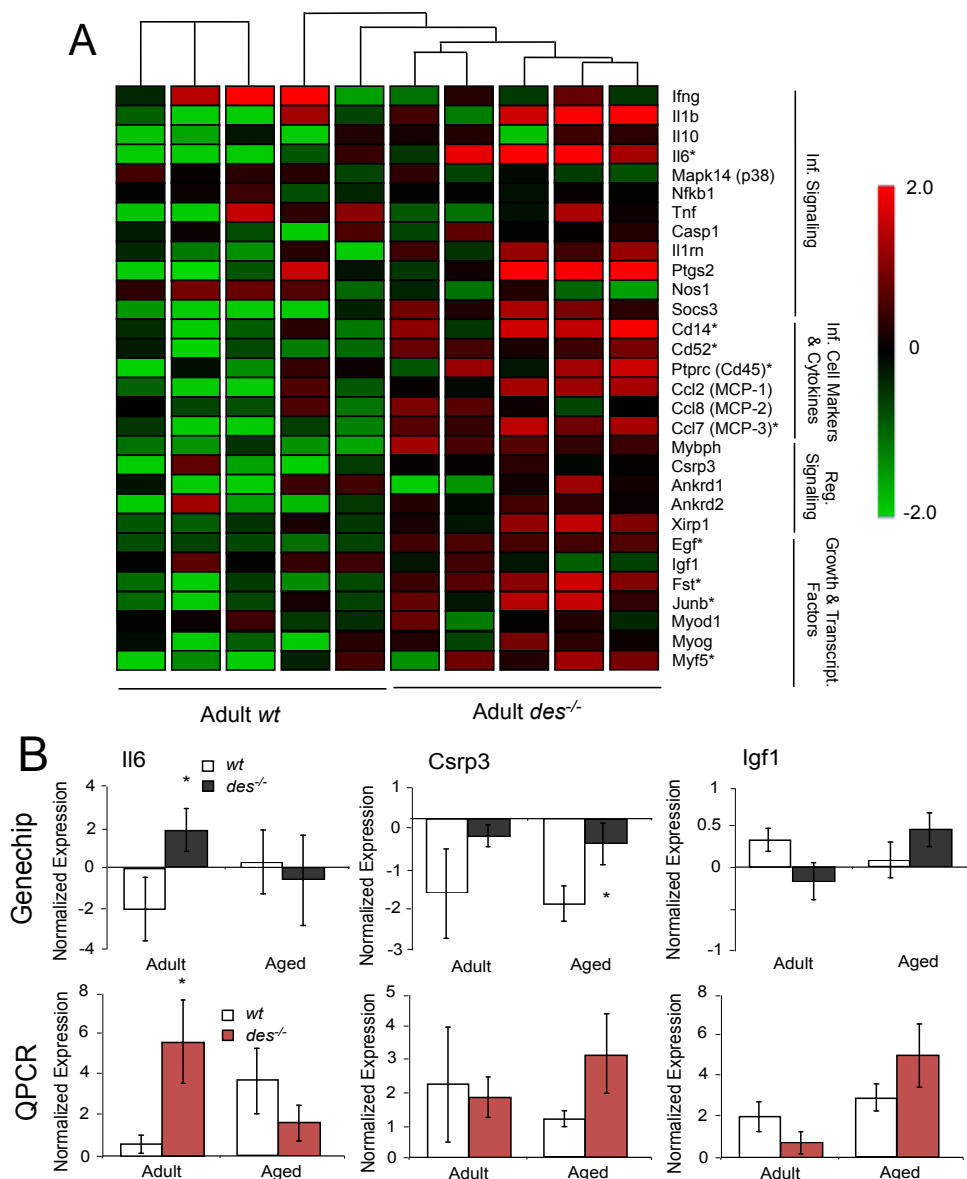
Figure 5.6: Adult $des^{-/-}$ muscle showed increased inflammation and regeneration specific gene expression. (A) Normalized gene expression for 18 genes involved in inflammation and 11 genes involved in regeneration. Hierarchical clustering is represented by connecting lines at the top of the grid with lines closest to the grid noting the most similar samples. The adult $des^{-/-}$ samples showed higher expression of the majority of the listed genes. Those with significantly higher expression values, as determined by 2-way ANOVA, are indicated with an asterisk. (B) Normalized expression as determined by GeneChip and QPCR for three important inflammation/regeneration genes: Il6 (interleukin 6), Csrp3 (muscle LIM protein) and Igf1 (insulin like growth factor). Asterisks indicate $p < 0.05$.

response to stress were overrepresented in the adult $des^{-/-}$ compared with the adult $wt$ including response to wounding (GO: 0009611, p<0.05), inflammatory response (GO:0006954, p<0.005) and regulation of tumor necrosis factor (GO:0032680, p<0.05), none of which were significantly different in the aged muscle groups.

Two hallmarks of regenerating fibers in muscle are small cross-sectional areas and centrally located nuclei. Centrally nucleated fibers were identified in $des^{-/-}$ and $wt$ muscle using H&E stained sections (Fig. 5.7A). Quantification of the number of centrally nucleated fibers as a fraction of total fibers in the cross section showed a significant increase in adult $des^{-/-}$ muscle compared with $wt$ (2.23±0.06% and 0.37±0.10% respectively, p<0.001; Fig. 5.7B). Interestingly, the number of centralized nuclei continued to increase in the $des^{-/-}$ muscle with age, but remained the same in $wt$ (5.85±0.49% and 0.42±0.05% respectively, Fig. 5.7B). Consistent with this result, a histogram of fiber sizes in both adult and aged $des^{-/-}$ cross-sections shows a leftward shift toward smaller fiber diameters, with over twice the number of fibers with areas less than 100 $\mu$m2 in the $des^{-/-}$ sections compared to $wt$ (Fig. 5.7C).

Flow cytometry data support an increased state of injury and inflammation as well. Muscle-resident stem cells can be classified in two primary populations, muscle progenitor (MP) cells and fibroadipogenic progenitor (FAP) cells, whose dynamics have been shown to change with injury. Specifically, in response to injury, the MP population decreases while the FAP population increases [10]. Stem cell populations in $des^{-/-}$ muscle show a similar shift in population dynamics. Cell populations identified by the MP marker $\alpha$7-integrin were significantly decreased in $des^{-/-}$ muscle compared to $wt$ while cell populations identified by the FAP marker Sca-1 were elevated in $des^{-/-}$ muscle compared to $wt$ though not significantly (Fig. 5.8A). Additionally, cell populations identified by the macrophage markers CD11b and F4/80 were significantly elevated in $des^{-/-}$ muscle compared to $wt$ indicating increased macrophage infiltration (Fig. 5.8B). The macrophage population can be further subdivided into classically activated macrophages (M1), which are inflammatory and initially recruited to the injury site, and alternatively activated macrophages (M2), which are fibrotic and appear at a later stage [30].
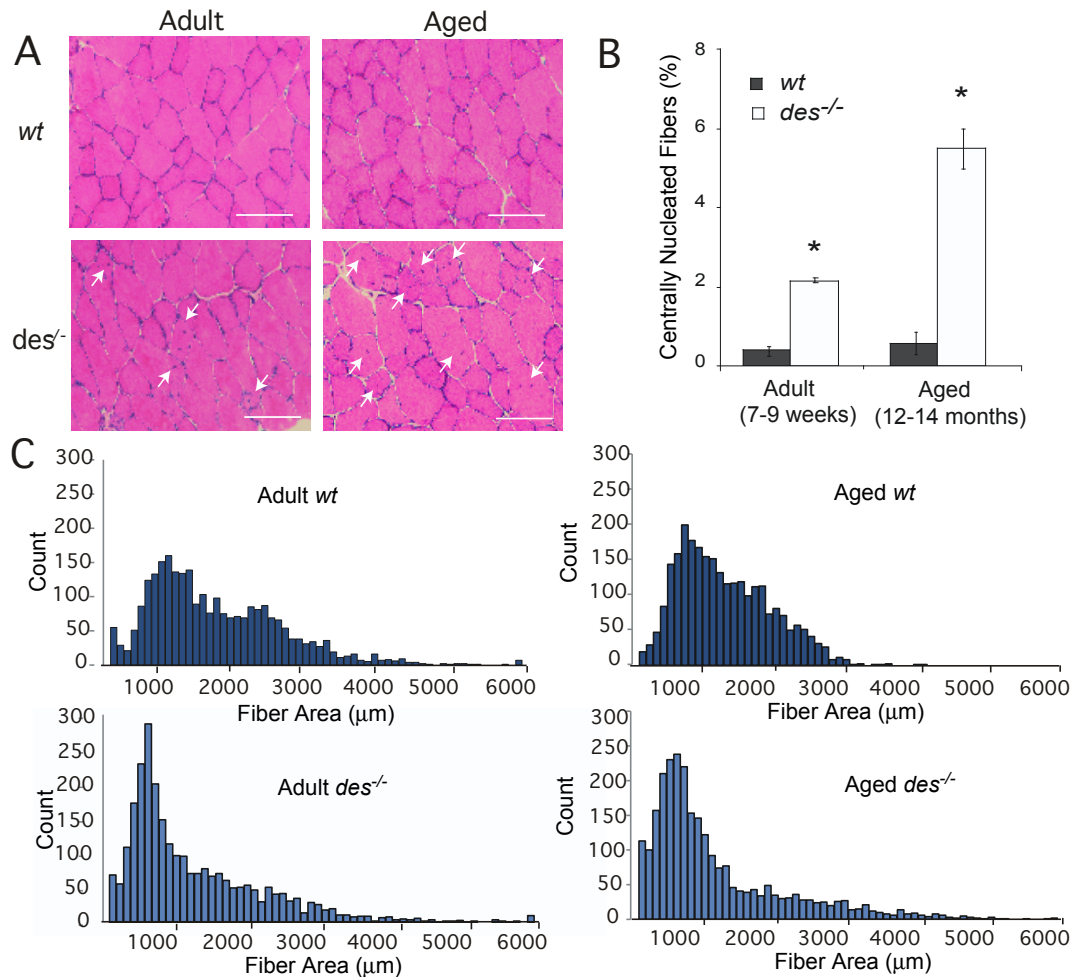
Figure 5.7: $Des^{-/-}$ muscle showed increased signs of regeneration. (A) Sections from the TA midbelly of adult and aged $des^{-/-}$ muscle stained with H&E showed an increased number of centrally nucleated fibers (arrows) compared to *wt*, a hallmark of muscle regeneration. Scale bars are 100 $\mu$m. (B) Quantification of H&E stained sections showed a significant increase in the number of centrally nucleated fibers in both adult and aged $des^{-/-}$ sections compared to *wt*. Additionally, the number of centrally nucleated fibers increased in the $des^{-/-}$ muscle with age but did not in the *wt*. Two-way ANOVA yielded a significant effect of genotype and a significant genotype-age interaction. (C) Histograms of adult and aged $des^{-/-}$ fiber sizes quantified from laminin stained sections revealed a leftward shift toward smaller fiber sizes compared with *wt*. Asterisks indicate p < 0.05.
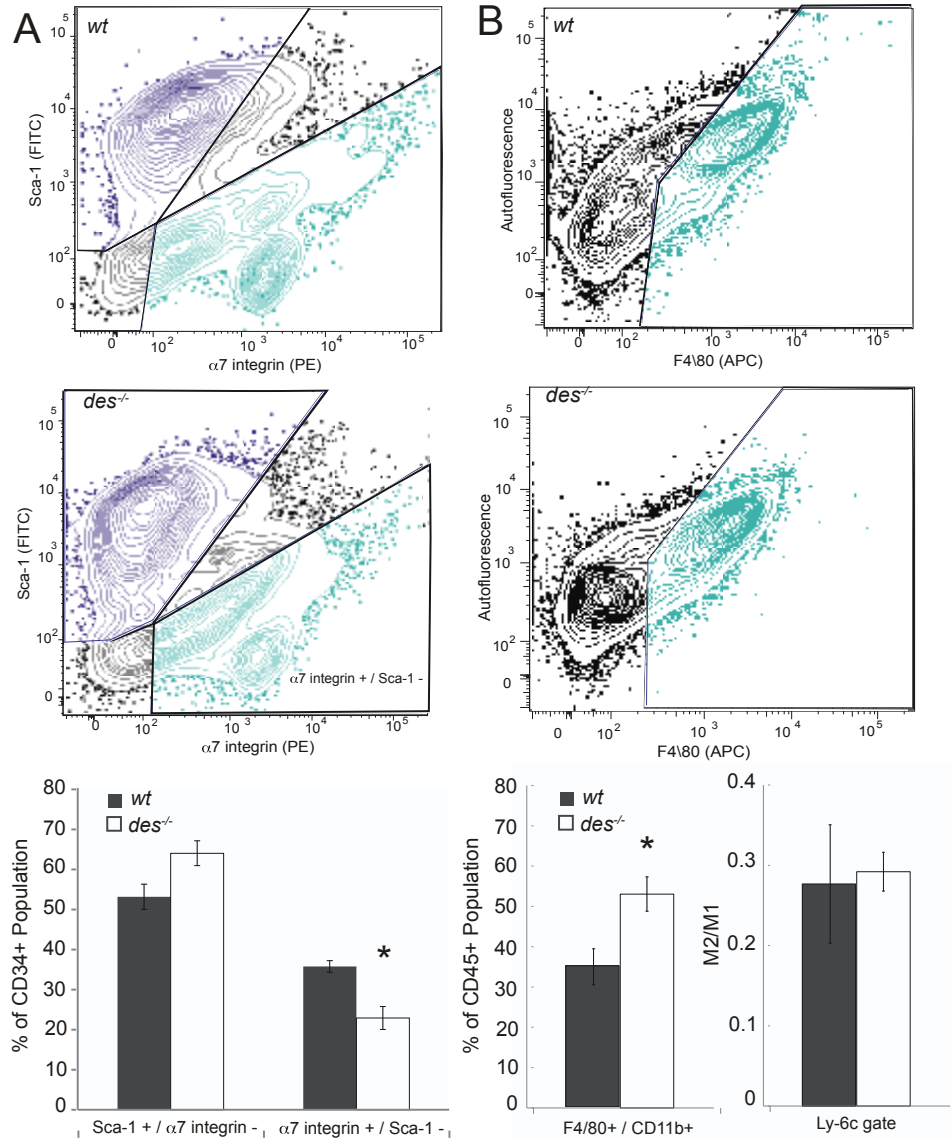
Figure 5.8: Flow cytometery indicated signs of increased injury in the $des^{-/-}$ muscle. (A) Cell populations positive for the MP marker, $\alpha$7-integrin, and negative for the FAP marker, Sca-1, are significantly reduced in $des^{-/-}$ muscle. Cell populations positive for Sca-1 but negative for $\alpha$7-integrin are elevated in $des^{-/-}$ muscle, though not significantly so. (B) Populations positive for the immune cell marker, CD11b, and positive for the macrophage marker, F4/80, are significantly elevated in $des^{-/-}$ muscle. However, the fraction of this population that is negative for Ly-6c (M2), a marker of classically activated macrophages, relative to those that are positive (M1) remains unchanged. See Fig. C.4 and Fig. C.5 for gating information.

Although both populations were elevated in the $des^{-/-}$ muscle, the relative contribution of each population remained the same as in $wt$ (Fig. 5.8B). Together, these data indicate an increased state of inflammation and regeneration in $des^{-/-}$ muscle that resembles an injury response.

## 5.4    Discussion

The main result of this study is that while $des^{-/-}$ and $wt$ muscles are "born" with identical fiber and ECM material properties, these properties diverge becoming quite different with age. Specifically, $des^{-/-}$ fibers become more compliant compared to $wt$ fibers (Fig. 5.1) while $des^{-/-}$ bundles become progressively stiffer with age compared to $wt$ bundles (Fig. 5.2). This result suggests that $des^{-/-}$ muscles are chronically altering their ECM and likely increasing the fraction of the load that is born by the ECM rather than the muscle fibers themselves. Evidence supporting this hypothesis was consistently observed using a number of measurement methods including direct measurement of fiber and bundle biomechanical properties, biochemical assay of collagen content, morphological measurement of ECM area fraction, gene expression patterns and flow cytometry.

It is tempting to speculate that decreased fiber compliance and increased ECM stiffness are causally related. In other words, perhaps the normal stiffening of muscle fibers that occurs with maturation does not occur in $des^{-/-}$ muscle and the $des^{-/-}$ ECM responds by increasing the amount and stiffness of the ECM itself. It is also interesting that $wt$ fibers became more compliant with age while $des^{-/-}$ fibers maintained their properties. The mechanism for this difference is unknown, but GeneChip data indicate a significant decrease in desmin expression in the aged $wt$ samples compared with adult (data not shown), so the $wt$ fiber cytoskeleton may be becoming compromised with age. More studies are required to investigate this hypothesis. The general notion that muscle fibers and their ECM properties are somehow complimentary is already deeply rooted in the muscle physiology literature. For example, it has been established in animal models and human experiments that the compliance of muscle connective tissue is extremely

consistent and has a specific relation to the properties of the contractile tissue within the muscle. Usually, this relationship is interpreted functionally in terms of the amount of sarcomere shortening that would be allowed by the extension of the tendon during muscle force generation which leads to muscle-tendon units that have different functional designs [31]. Connective tissue compliance is also interpreted in terms of functional differences, as variations between sprinters and endurance runners has been documented in terms of locomotion efficiency [32] or body acceleration [33]. In all cases, it is not known whether such different connective tissue properties "develop" or are "born" into the system. The results of the current study suggest that either process is possible.

The mechanism by which ECM adapts to altered muscle fiber properties is not known. While there is tremendous evidence for mechanotransduction in cells, whereby cells alter their gene expression patterns based on the biomechanical properties of the substrate [34, 35], the precise mechanism for this mechanotransduction is not known. Several systems have been identified that accomplish this task including members of the G-protein family that transduce membrane shear stress [36], integrin receptors that sense cell surface tension through ligand binding [37] and strain activated ion channels that alter conductance when deformed [8]. Additionally, it has been proposed that the cellular cytoskeleton provides a network through which the mechanical state may be transduced by microfilaments, microtubules and/or intermediate filaments to induce protein conformational change and nuclear deformation that can alter biological activity [38–40]. It is interesting that, in the absence of the muscle specific intermediate filament desmin, altered fiber mechanical properties lead to whole muscle adaptation. Our gene expression data provide some insight into a potential mechanism of muscle adaptation in this particular system. We noted that in adult $des^{-/-}$ muscle, genes involved in the inflammatory pathway were upregulated (Fig. 5.6). We speculate that the loss of desmin results in a loss of inter-myofibrillar mechanotransduction, which leads to muscle injury during development, as the muscle is less equipped to distribute strains imposed by everyday activity. In response to this injury, the muscle then experiences an inflammatory response that eventually results in regeneration.

However, since the regenerated fibers still lack desmin, they will still be susceptible to further injury. Since the inflammatory pathway is already known to be fibrosis-inducing [9, 24], we speculate that the mechanism of stiffening of the ECM is mediated through these inflammatory pathways. Importantly, this type of response would provide a negative feedback loop in that, after stiffening, the ECM would prevent excessive fiber strain, which is believed to be related to muscle fiber injury [41–43] which would then relieve the inflammatory stimulus and stabilize the ECM system. Of course, this suggested mechanism is speculative at this point but can be experimentally tested.

Although there is some existing evidence for increased stiffness [44] and regeneration [14, 27] in desmin knockout muscle, this paper provides a potential mechanistic link between these findings. Additionally, The current data have implications for interpreting our previous results on $des^{-/-}$ muscle injury with age. Previously, we reported that $des^{-/-}$ muscles generated lower isometric stress were less susceptible to injury compared to their $wt$ counterparts [26]. These results were interpreted exclusively in terms of the mechanical effects of desmin on the cytoskeletal lattice. This finding was then followed by reports demonstrating increased myofibrillar compliance [45] and by a theoretical model that provided the same results [46]. We used these approaches to suggest that $des^{-/-}$ muscles generate lower stress because of less efficient force transmission across the myofibrillar lattice and experience less injury because of lower shear stresses across the fiber. In light of the current results, it is possible that the lower stress generated by $des^{-/-}$ muscles is a result of the inflammatory process that has compromised either the excitation-contraction coupling system, the force transmitting system, or the force generating system. Previous demonstrations of the deleterious effects of inflammation on muscle force generation are consistent with this idea. Further, it is possible that the "lower" injury to $des^{-/-}$ muscles simply results from the fact that they are already in a state of inflammation and regeneration from everyday activity. The fact that such divergent mechanisms can be invoked to explain the current experimental results highlights, in part, the complex nature of the skeletal muscle tissue force-generating system.

Skeletal muscle fibrosis is a highly sensitive but nonspecific adaptation to a multitude of altered use paradigms. Nearly all primary myopathies have fibrosis as a defining parameter which is obvious to the practicing pathologist and diagnostic for disease. However, the development of therapies for prevention and reversal of fibrosis are still in their infancy. There is an increased focus on the development of antifibrotic therapies [9, 47], however, most of these are accomplished indirectly by suppression of the muscle inflammatory response. In light of the current studies, we suggest that inhibition of fibrosis might ultimately be detrimental to the muscle since no structure would be present that could prevent the excessive sarcomere strain that leads to muscle fiber injury. More "physiological" therapies might be envisioned that mechanically stabilize the muscle tissue without preventing the excessive fibrosis that can lead to contracture or tissue dysfunction. Future studies are required in this area that take into account both the biological biomechanical complexity of skeletal muscle tissue.

## 5.5    Acknowledgements

Chapter 5 in full, has been submitted for publication of the material as it may appear in *Journal of Physiology, London.* "Skeletal Muscle Fibrosis Develops in Response to Compliant Fibers." Meyer G.M., and Lieber R.L. The dissertation author was the primary investigator and author of this paper.

# 5.6 References

[1] Foidart, M., Foidart, J.M., and Engel, W.K., 1981. Collagen localization in normal and fibrotic human skeletal muscle. *Archives of neurology*, 38:152–157.

[2] Savolainen, J., Myllylä, V., Myllylä, R., Vihko, V., Väänänen, K., and Takala, T.E., 1988. Effects of denervation and immobilization on collagen synthesis in rat skeletal muscle and tendon. *The American journal of physiology*, 254:R897–902.

[3] Ferreira, R., Neuparth, M.J., Ascensão, A., Magalhães, J., Vitorino, R., Duarte, J.A., and Amado, F., 2006. Skeletal muscle atrophy increases cell proliferation in mice gastrocnemius during the first week of hindlimb suspension. *European journal of applied physiology*, 97:340–346.

[4] Gao, Y., Kostrominova, T.Y., Faulkner, J.A., and Wineman, A.S., 2008. Age-related changes in the mechanical properties of the epimysium in skeletal muscles of rats. *Journal of biomechanics*, 41:465–469.

[5] Kang, L., Ayala, J.E., Lee-Young, R.S., Zhang, Z., James, F.D., Neufer, P.D., Pozzi, A., Zutter, M.M., and Wasserman, D.H., 2011. Diet-induced muscle insulin resistance is associated with extracellular matrix remodeling and interaction with integrin alpha2beta1 in mice. *Diabetes*, 60:416–426.

[6] Leask, A. and Abraham, D.J., 2004. TGF-beta signaling and the fibrotic response. *The FASEB journal : official publication of the Federation of American Societies for Experimental Biology*, 18:816–827.

[7] Chiquet, M., Gelman, L., Lutz, R., and Maier, S., 2009. From mechanotransduction to extracellular matrix gene expression in fibroblasts. *Biochimica et biophysica acta*, 1793:911–920.

[8] Frey, J.W., Farley, E.E., O'Neil, T.K., Burkholder, T.J., and Hornberger, T.A., 2009. Evidence that mechanosensors with distinct biomechanical properties allow for specificity in mechanotransduction. *Biophysical journal*, 97:347–356.

[9] Li, Y., Foster, W., Deasy, B.M., Chan, Y., Prisk, V., Tang, Y., Cummins, J., and Huard, J., 2004. Transforming growth factor-beta1 induces the differentiation of myogenic cells into fibrotic cells in injured skeletal muscle: a key event in muscle fibrogenesis. *The American journal of pathology*, 164:1007–1019.

[10] Joe, A.W.B., Yi, L., Natarajan, A., Le Grand, F., So, L., Wang, J., Rudnicki, M.A., and Rossi, F.M.V., 2010. Muscle injury activates resident fibro/adipogenic progenitors that facilitate myogenesis. *Nature cell biology*, 12:153–163.

[11] Trensz, F., Haroun, S., Cloutier, A., Richter, M.V., and Grenier, G., 2010. A muscle resident cell population promotes fibrosis in hindlimb skeletal muscles of mdx mice through the Wnt canonical pathway. *American journal of physiology Cell physiology*, 299:C939–47.

[12] Clarkson, P.M., 1992. Exercise-induced muscle damage–animal and human models. *Medicine and science in sports and exercise*, 24:510–511.

[13] Lazarides, E., 1980. Intermediate filaments as mechanical integrators of cellular space. *Nature*, 283:249–256.

[14] Li, Z., Mericskay, M., Agbulut, O., Butler-Browne, G., Carlsson, L., Thornell, L.E., Babinet, C., and Paulin, D., 1997. Desmin is essential for the tensile strength and integrity of myofibrils but not for myogenic commitment, differentiation, and fusion of skeletal muscle. *The Journal of cell biology*, 139:129–144.

[15] Milner, D.J., Weitzer, G., Tran, D., Bradley, A., and Capetanaki, Y., 1996. Disruption of muscle architecture and myocardial degeneration in mice lacking desmin. *The Journal of cell biology*, 134:1255–1270.

[16] Smith, L.R., Gerace-Fowler, L., and Lieber, R.L., 2011. Muscle extracellular matrix applies a transverse stress on fibers with axial strain. *Journal of biomechanics*, 44:1618–1620.

[17] Jones, R.M., 1999. Mechanics of composite materials. Hemisphere Pub.

[18] Purslow, P.P. and Trotter, J.A., 1994. The morphology and mechanical properties of endomysium in series-fibred muscles: variations with muscle length. *Journal of muscle research and cell motility*, 15:299–308.

[19] Smith, L.R., Pontén, E., Hedström, Y., Ward, S.R., Chambers, H.G., Subramaniam, S., and Lieber, R.L., 2009. Novel transcriptional profile in wrist muscles from cerebral palsy patients. *BMC medical genomics*, 2:44.

[20] GRANT, R.A., 1964. ESTIMATION OF HYDROXYPROLINE BY THE AUTOANALYSER. *Journal of clinical pathology*, 17:685–686.

[21] Minamoto, V.B., Hulst, J.B., Lim, M., Peace, W.J., Bremner, S.N., Ward, S.R., and Lieber, R.L., 2007. Increased efficacy and decreased systemic-effects of botulinum toxin A injection after active or passive muscle manipulation. *Developmental medicine and child neurology*, 49:907–914.

[22] Meyer, G.A. and Lieber, R.L., 2011. Elucidation of extracellular matrix mechanics from muscle fibers and fiber bundles. *Journal of biomechanics*, 44:771–773.

[23] Carmeli, E., Moas, M., Reznick, A.Z., and Coleman, R., 2004. Matrix metalloproteinases and skeletal muscle: a brief review. *Muscle & nerve*, 29:191–197.

[24] Serrano, A.L. and Muñoz-Cánoves, P., 2010. Regulation and dysregulation of fibrosis in skeletal muscle. *Experimental cell research*, 316:3050–3058.

[25] Porter, J.D., Khanna, S., Kaminski, H.J., Rao, J.S., Merriam, A.P., Richmonds, C.R., Leahy, P., Li, J., Guo, W., and Andrade, F.H., 2002. A chronic inflammatory response dominates the skeletal muscle molecular signature in dystrophin-deficient mdx mice. *Human molecular genetics*, 11:263–272.

[26] Sam, M., Shah, S., Fridén, J., Milner, D.J., Capetanaki, Y., and Lieber, R.L., 2000. Desmin knockout muscles generate lower stress and are less vulnerable to injury compared with wild-type muscles. *American journal of physiology Cell physiology*, 279:C1116–22.

[27] Lovering, R.M., O'Neill, A., Muriel, J.M., Prosser, B.L., Strong, J., and Bloch, R.J., 2011. Physiology, structure, and susceptibility to injury of skeletal muscle in mice lacking keratin 19-based and desmin-based intermediate filaments. *American journal of physiology Cell physiology*, 300:C803–13.

[28] Cannon, J.G. and St Pierre, B.A., 1998. Cytokines in exertion-induced skeletal muscle injury. *Molecular and cellular biochemistry*, 179:159–167.

[29] Barash, I.A., Mathew, L., Ryan, A.F., Chen, J., and Lieber, R.L., 2004. Rapid muscle-specific gene expression changes after a single bout of eccentric contractions in the mouse. *American journal of physiology Cell physiology*, 286:C355–64.

[30] Arnold, L., Henry, A., Poron, F., Baba-Amer, Y., van Rooijen, N., Plonquet, A., Gherardi, R.K., and Chazaud, B., 2007. Inflammatory monocytes recruited after skeletal muscle injury switch into antiinflammatory macrophages to support myogenesis. *The Journal of experimental medicine*, 204:1057–1069.

[31] Zajac, F.E., 1989. Muscle and tendon: properties, models, scaling, and application to biomechanics and motor control. *Critical reviews in biomedical engineering*, 17:359–411.

[32] Kubo, K., Kanehisa, H., Kawakami, Y., and Fukunaga, T., 2000. Elastic properties of muscle-tendon complex in long-distance runners. *European journal of applied physiology*, 81:181–187.

[33] Biewener, A.A., Farley, C.T., Roberts, T.J., and Temaner, M., 2004. Muscle mechanical advantage of human walking and running: implications for energy cost. *Journal of applied physiology (Bethesda, Md : 1985)*, 97:2266–2274.

[34] Engler, A.J., Sen, S., Sweeney, H.L., and Discher, D.E., 2006. Matrix elasticity directs stem cell lineage specification. *Cell*, 126:677–689.

[35] Discher, D.E., Janmey, P., and Wang, Y.L., 2005. Tissue cells feel and respond to the stiffness of their substrate. *Science (New York, NY)*, 310:1139–1143.

[36] Gudi, S.R., Clark, C.B., and Frangos, J.A., 1996. Fluid flow rapidly activates G proteins in human endothelial cells. Involvement of G proteins in mechanochemical signal transduction. *Circulation research*, 79:834–839.

[37] Tzima, E., Irani-Tehrani, M., Kiosses, W.B., Dejana, E., Schultz, D.A., Engelhardt, B., Cao, G., DeLisser, H., and Schwartz, M.A., 2005. A mechanosensory complex that mediates the endothelial cell response to fluid shear stress. *Nature*, 437:426–431.

[38] Lin, E.C. and Cantiello, H.F., 1993. A novel method to study the electrodynamic behavior of actin filaments. Evidence for cable-like properties of actin. *Biophysical journal*, 65:1371–1378.

[39] Maniotis, A.J., Chen, C.S., and Ingber, D.E., 1997. Demonstration of mechanical connections between integrins, cytoskeletal filaments, and nucleoplasm that stabilize nuclear structure. *Proceedings of the National Academy of Sciences of the United States of America*, 94:849–854.

[40] Janmey, P.A., 1998. The cytoskeleton and cell signaling: component localization and mechanical coupling. *Physiological reviews*, 78:763–781.

[41] Armstrong, R.B., Ogilvie, R.W., and Schwane, J.A., 1983. Eccentric exercise-induced injury to rat skeletal muscle. *Journal of applied physiology (Bethesda, Md : 1985)*, 54:80–93.

[42] Morgan, D.L., 1990. New insights into the behavior of muscle during active lengthening. *Biophysical journal*, 57:209–221.

[43] Patel, T.J., Das, R., Fridén, J., Lutz, G.J., and Lieber, R.L., 2004. Sarcomere strain and heterogeneity correlate with injury to frog skeletal muscle fiber bundles. *Journal of applied physiology (Bethesda, Md : 1985)*, 97:1803–1813.

[44] Anderson, J., Joumaa, V., Stevens, L., Neagoe, C., Li, Z., Mounier, Y., Linke, W.A., and Goubel, F., 2002. Passive stiffness changes in soleus muscles from desmin knockout mice are not due to titin modifications. *Pflügers Archiv : European journal of physiology*, 444:771–776.

[45] Shah, S.B., Davis, J., Weisleder, N., Kostavassili, I., McCulloch, A.D., Ralston, E., Capetanaki, Y., and Lieber, R.L., 2004. Structural and functional roles of desmin in mouse skeletal muscle during passive deformation. *Biophysical journal*, 86:2993–3008.

[46] Meyer, G.A., Kiss, B., Ward, S.R., Morgan, D.L., Kellermayer, M.S.Z., and Lieber, R.L., 2010. Theoretical predictions of the effects of force transmission by desmin on intersarcomere dynamics. *Biophysical journal*, 98:258–266.

[47] Bedair, H.S., Karthikeyan, T., Quintero, A., Li, Y., and Huard, J., 2008. Angiotensin II receptor blockade administered after injury improves muscle regeneration and decreases fibrosis in normal skeletal muscle. *The American journal of sports medicine*, 36:1548–1554.

# Chapter 6

# Systems Analysis of Genes Related to Skeletal Muscle Function

## 6.1 Abstract

Current microarray technologies allow researchers to probe expression across the genome to investigate tissue biology. Skeletal muscle is dependent on a specialized subset of genes to produce force efficiently. We have defined 9 gene networks whose coordination is critical to muscle function in order to facilitate objective analysis of muscle systems. We begin with genes involved in the neuromuscular junction and the creation of an action potential. That action potential is transmitted through the transverse-tubule and sarcoplasmic reticulum membrane systems to proteins involved in excitation contraction coupling and $Ca^{2+}$ handling. Released $Ca^{2+}$ interacts with contractile proteins involved in actin and myosin crossbridge cycling. The force generated in the sarcomere is transmitted through cytoskeletal proteins to the sarcolemma and out to the extracellular matrix of skeletal muscle. Contraction is fueled through many genes that regulate energy metabolism within muscle. Muscle is a highly dynamic system and gene pathways involved in inflammation and the regulate muscle size through atrophy or

hypertrophy are involved in the muscular adaptation to altered use. Additionally, muscles are known to specialize and adapt to energy demands by modulating fiber type ratios. Each of these systems and responses involves a specialized and coordinated set of genes. The pathways discussed in this review are not comprehensive, but represent important genes and interactions that have been established in skeletal muscle specifically through a review of the literature focusing on reviews themselves. Combining high throughput systems analysis with advanced networking software allows researchers to use these networks to objectively study skeletal muscle systems.

## 6.2   Introduction

The primary function of skeletal muscle is to generate force and produce movement. This requires coordination among many physiological pathways and their associated genes. Functional deficits in skeletal muscle myopathies result from a variety of biological factors and result in compex alterations in transcriptional pathways. Thus, understanding genes that regulate muscle function is a prerequisite to understanding the mechanisms of muscle pathology.

Proper muscle function requires the coordination of many integrated gene networks. Muscle contraction is initiated at the specialized neuromuscular junction (NMJ) where acetylcholine is released from the nerve ending, diffuses to muscle receptors and initiates an action potential. The action potential propagates along the sarcolemma, down the transverse tubules and, in a process known as excitation contraction-coupling (ECC) calcium is released from the sarcoplasmic reticulum. Calcium binding to the regulatory units of the thin filament trigger the myosin cross-bridge cycle that creates muscle contraction (MC). The force of muscle contraction is transmitted through specialized networks of proteins within the cell, the cytokeleton (CSK), to the costameres and out to the extracellular matrix (ECM). Myosin cross bridge cycling requires ATP, and thus skeletal muscle function also requires metabolism (MET) and storage of carbohydrates and fatty acids. When a muscle incurs damage, particularly in eccentric contractions, there is an inflamma-

tory (INF) system response that occurs within the muscle. As a very plastic tissue, muscle responds to injury by increasing muscle size dependent upon resident muscle progenitors, satellite cells. With altered use, muscle adapts by coordinating a change in muscle mass via synchronized muscle hypertrophy or atrophy (HA). Many aspects of muscle function require distinct protein isoforms specific to various fiber types. Muscles with predominantly slow fiber types are subjected to chronic use and high metabolic demand while muscles with predominately fast fiber types are designed more for rapid force production that requires tight calcium handling. Thus, it is not surprising that the control of fiber type is tightly regulated by a specialized gene network.

Understanding muscle diseases requires knowledge of the protein and gene systems used for force production. Duchenne Muscular Dystrophy (DMD) is the most frequently studied muscle disease and, although it results from the loss of a single gene product, dystrophin, many muscle functions are compromised [1]. Dystrophin is part of the costamere complex that links MC to the ECM and, when disrupted, allows mechanically-induced membrane damage [2]. This allows calcium influx that contributes ECC alterations and muscle degradation and damage [3] and is associated with a large INF response [4, 5] as well as cycles of regeneration [6]. As the HA pathway is exhausted, the muscle undergoes an increase in ECM fibrosis [7]. This illustrates the interconnectivity of these muscle functions and demonstrates how understanding a single proteins role is critical to understanding muscle pathology. This work will provide a framework for those investigating muscle disease and adaptation to efficiently inspect muscle function as a system of related proteins, especially to take advantage of the high-throughput technologies currently available.

This review highlights the genes that are most critical to muscle function and places them in a context of muscle physiology as a whole using current reviews in muscle physiology and muscle gene onotology [8]. We do not provide an exhaustive list of genes that regulate muscle function, but rather explore how various pathways are distorted in a variety of muscle pathologies and the downstream consequences of altered gene expression. The networks created here will provide

Table 6.1: Protein Complexes. Some complexes are interacting proteins, however, others are multiple isoforms of a portein that have the same function.

| Complex | Entrez IDs | Entrez Symbols |
|---|---|---|
| Neuromuscular Junction | | |
| CHRN | 1134;1140;1144;1145 | CHRNA1;CHRNB1;CHRND;CHRNE |
| COL4 | 1285;11286;1287;1288 | COL4A3;COL4A4;COL4A5;COL4A6 |
| GABP | 2551;2553 | GABPA;GABPB1 |
| ERBB | 2064;2066 | ERBB2;ERBB4 |
| Excitation Contraction Coupling | | |
| CACN | 779;781;782;786 | CACNA1S;CACNA2D1;CACNB1;CACNG1 |
| CASQ | 844;845 | CASQ1;CASQ2 |
| ATP2A1 | 487;488;489 | ATP2A1;ATP2A2;ATP2A3 |
| CAMK2 | 815;816;817;818 | CAMK2A;CAMK2B;CAMK2D;CAMK2G |
| CAPN | 823;824;825 | CANP1;CAPN2;CAPN3 |
| TRPC | 7220;7725 | TRPC1;TRPC6 |
| Muscle Contraction | | |
| MYH | 4619;4620;4626 | MYH1;MYH2;MYH7 |
| MYL | 4632;4633;4634 | MYL1;MYL2;MYL3 |
| MYBPC | 4605;4606 | MYBPC1;MYBPC2 |
| MYOM | 8736;8737 | MYOM1;MYOM2 |
| ACTA | 58;59;70 | ACTA1;ACTA2;ACTC1 |
| ACTN | 88;89 | ACTN2;ACTN3 |
| CAPZ | 829;830;832 | CAPZA1;CAPZA2;CAPZB |
| TMOD | 7111;29765 | TMOD1;TMOD4 |
| TNNT | 7138;7140 | TNNT1;TNNT3 |
| TNNI | 7135;7136 | TNNI1;TNNI2 |
| TNNC | 7134;7135 | TNNC1;TNNC2 |
| TPM | 7168;7169;7170 | TPM1;TPM2;TPM3 |
| Cytoskeleton | | |
| SGC | 6442;6443;6444;6445 | SGCA;SGCB;SGCD;SGCG |
| SNT | 6640;6641;6645;54212 | SNTA1;SNTB1;SNTB2;SNTG1 |
| DTN | 1837;1838 | DNTA;DNTB |
| SPT | 6708;6710 | SPTA1;SPTB |
| ANK | 286;287 | ANK1;ANK2 |

Table 6.1, Protein complexes, Continued. Some complexes are interacting proteins, however, others are multiple isoforms of a portein that have the same function.

| Complex | Entrez IDs | Entrez Symbols |
|---|---|---|
| Extracellular Matrix | | |
| COL1 | 1277;1278 | COL1A1;COL1A2 |
| COL4 | 1282;1284 | COL4A1;COL4A2 |
| COL6 | 1291;1292;1293 | COL6A1;COL6A2;COL6A3 |
| LAM | 3908;3912;3913;3915 | LAMA2;LAMB1;LAMB2;LAMC1 |
| P4H | 5033;5034 | P4HA1;P4HB |
| SDC | 6383;6385 | SDC2;SDC4 |
| Energy Metabolism | | |
| NDUF | 4694;4695;4696;4697 | NDUFA1;NDUFA2;NDUFA3;NDUFA4 |
| | 4698;4700;4701;4702 | NDUFA5;NDUFA6;NDUFA7;NDUFA8 |
| | 4704;4707;4708;4709 | NDUFA9;NDUFB1;NDUFB2;NDUFB3 |
| | 4711;4712;4713;4717 | NDUFB5;DNUFB6;NDUFB7;NDUFC1 |
| | 4718;4719;4720;4722 | NDUFC2;NDUFS1;NDUFS2;NDUFS3 |
| | 4724;4725;4726 | NDUFS4;NDUFS5;NDUFS6 |
| | 4728;4723;4729 | NDUFS8;NDUFV1;NDUFV2 |
| SDH | 6389;6390;6391;6392; | SDHA;SDHB;SDHC;SDHD |
| CYC | 1537;7386;7384;7385 | CYC1;UQCRFS1;UQCRC1;UQCRC2 |
| | 7388;7381;27089 | UQCRH;UQCRB;UQCRQ |
| COX | 1352;9377;1329;1339 | COX10;COX5A;COX5B COX6A2 |
| | 1340;1346;1349;1350 | COX6B1;COX7A1;COX7B;COX7C |
| | 1351;1353;1355;10063 | COX8A;COX11;COX15;COX17 |
| ATP5 | 498;506;509;513 | ATP5A1;ATP5B;ATP5C1;ATP5D |
| | 515;518;10476;521;522 | ATP5F1;ATP5G3;ATP5H;ATP5I;ATP5J |
| | 9551;10632;539;27109 | ATP5J2;ATP5L;ATP5O;ATP5S |
| AMPK | 5563;5565;53632 | PRKAA2;PRKAB2;PRKAG3 |
| TFB | 51106;64216 | TFB1M;TFB2M |
| MEF2 | 4205;4208;4209 | MEF2A;MEF2C;MEF2D |
| CAMK2 | 815;816;817 | CAMK2A;CAMK2B;CAMK2D |
| PDH | 5160;5162 | PDHA1;PDHB |
| Muscle Hypertrophy and Atrophy | | |
| MAPK1/3 | 5594;5595 | MAPK1;MAPK3 |
| FOXO | 2308;2309 | FOXO1;FOXO3 |
| MAP2K | 5604;5605 | MAP2K1;MAP2K2 |
| MEF2 | 4205;4208;4209 | MEF2A;MEF2C;MEF2D |
| HDAC | 9759;10019;51564 | HDAC4;HDAC5;HDAC7 |
| PIK3R | 5295;5296;8503 | PIK3R1;PIK3R2;PIK3R3 |

a foundation from which to build more detailed and specific networks. The networks have been created in Cytoscape (Cytoscape Consotrium) [9] for use in the interpretation of current high throughput and system level technologies such as microarrays [10] and protein arrays [11]. This work will also be useful to provide a general reference for studying the interaction between genes and muscle physiology.

## 6.3    Neuromuscular junction

The NMJ requires specific proteins to be expressed at the junction (Fig. 6.1). The action is initiated by acetylcholine (ACh) release from the motor neuron, which crosses the synaptic basal lamina to bind to the nicotinic acetylcholine receptor (CHRN), which consists of 5 subunits [12]. The gamma subunit (CHRNG) is expressed in immature muscle and replaced by the epsilon subunit upon maturity [13]. CHRN is a ligand gated channel that allows sodium influx upon binding to create an endplate potential. This potential activates the voltage gated sodium channels in muscle SCN4A to transform the end plate potential into an action potential which is propagated throughout the muscle and initiates ECC[14].

To maintain proper clustering in the postsynaptic muscle, motor neurons also release agrin (AGRN). AGRN binds to a receptor on the muscle transmembrane receptor MUSK along with its extracellular co-receptor LRP4 [12]. MUSK binding eventually results in the activation of RAPSN, which acts as an intracellular scaffold for CHRN. MUSK also interacts with 14-3-3$\gamma$ (YWHAG), a signal transduction protein involved in synaptic gene expression. Synaptic gene expression is also mediated through neuregulin (NRG1) a glycoprotein, which binds to a family epidermal growth factor receptor (ERBB). ERBB bind to NRG1 results in activation of GABP transcription factors for synaptic genes [13].

The synaptic basal lamina plays an important role in organizing the NMJ and includes a unique subset of genes that are expressed preferentially in the region. It is primarily made up of COL4 with the $\alpha$3-6 subunits, instead of the $\alpha$1-2 subunits found around the rest of muscle, and laminin subunits LAMA5 and LAMB2 [12]. The collagen and laminin networks are linked by glycoprotein NID1.
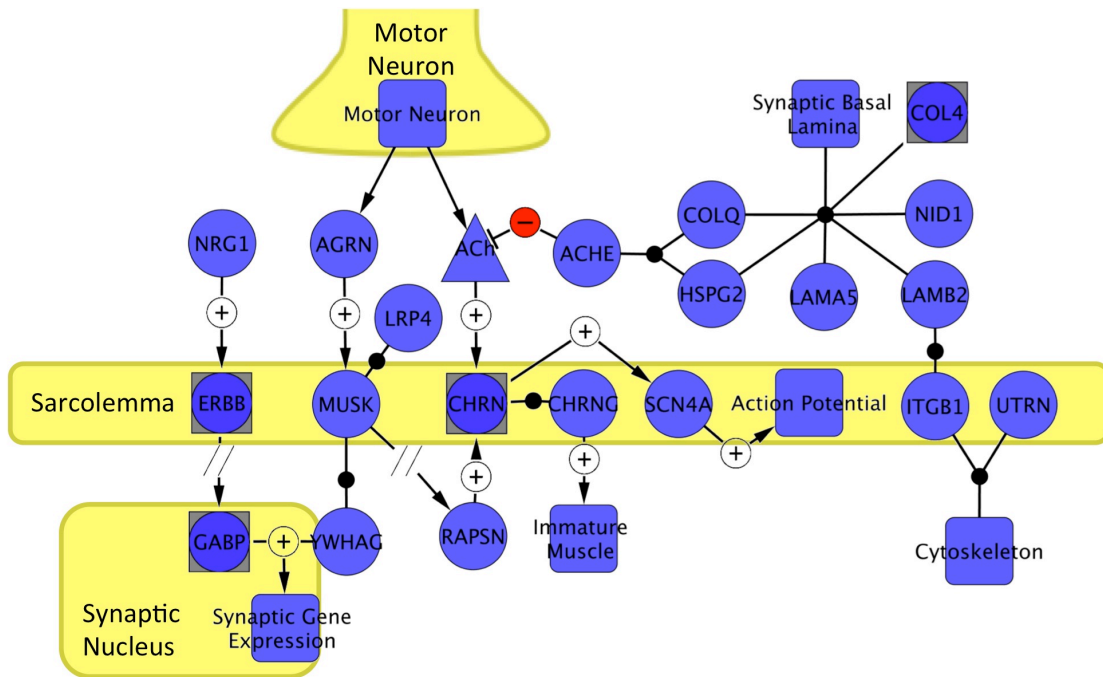
Figure 6.1: Neuromuscular junction. Motor neurons release the neurotransmitter acetylcholine, which trigger an action potential in the muscle. NMJ formation is also induced by motor neuron factors that signal muscle proteins. For all figures there are the following nodes: (○) entrez gene symbols, (⊡) complexes, (△) non-protein molecules, (□) modules or functions. There are the following interactions: (⊕) positive, (⊖) negative, (●) binding (//) intermediate and (?) unknown. There are the following lines (−) basic, (→) A proceeds to B, (⊣) A does not proceed to B, and (⤳) translocation of A. The genes within complexes are listed in Table 6.1.

Perlecan (HSPG2) is the major proteoglycan present. The synaptic basal lamina also includes COLQ, which along with HSPG2 binds and anchors acetylcholine esterase (ACHE) to the neuromuscular junction. The function of ACHE is to hydrolyze acetylcholine which inactivates it and terminates activation [14].

## 6.4 Excitation contraction coupling

The action potential generated at the neuromuscular junction travels throughout the muscle and to the interior of the muscle via the transverse-tubule (T-tubules) system (Fig. 6.2). The action potential activates the voltage gated $Ca^{2+}$ channel DHPR, which consists of 5 subunits. The close proximity of DHPR and the ryanodine receptor RYR1 on the sarcoplasmic reticulum (SR) ensures that $Ca^{2+}$ entering the cell triggers opening of RYR1 to release $Ca^{2+}$ from the SR store [15, 16]. A unique ryanodine receptor (RYR3) is expressed in immature muscle and is replaced by RYR1 during development [17]. $Ca^{2+}$ serves as the intracellular trigger for muscle contraction. RYR1 requires multiple proteins to modulate the open probability for $Ca^{2+}$ release. FKBP1A is an SR gene that directly interacts with RYR1 and is required for full conductance [16]; S100A1 also binds to RYR1 to increase open probability [18], and SYLP2 acts from the T-tubules to increase open probability without increasing current amplitude [17].

For muscle relaxation to occur, $Ca^{2+}$ is pumped back into the SR via the ATP dependent SERCA pumps (ATP2A), which have different isoforms for fast and slow muscle (Fig. 6.9) [17]. PVALB can act as an intracellular $Ca^{2+}$ store by binding free$Ca^{2+}$ [19]. Conversely SR proteins SLN and PLN, when dephosphorylated, slow relaxation by inhibiting ATP2A reuptake of $Ca^{2+}$ [17, 20]. Maintaining the high concentration of $Ca^{2+}$ within the SR requires $Ca^{2+}$ binding to CASQ, which also has different isoforms in fast and slow muscle (Fig. 6.9). CASQ is held within the SR and near RYR1 by luminal proteins triadin (TRDN) and junctin (ASPH). The SR is held in close approximation to the T-tubule system physically by the linking protein junctophilin (JPH1) [21].
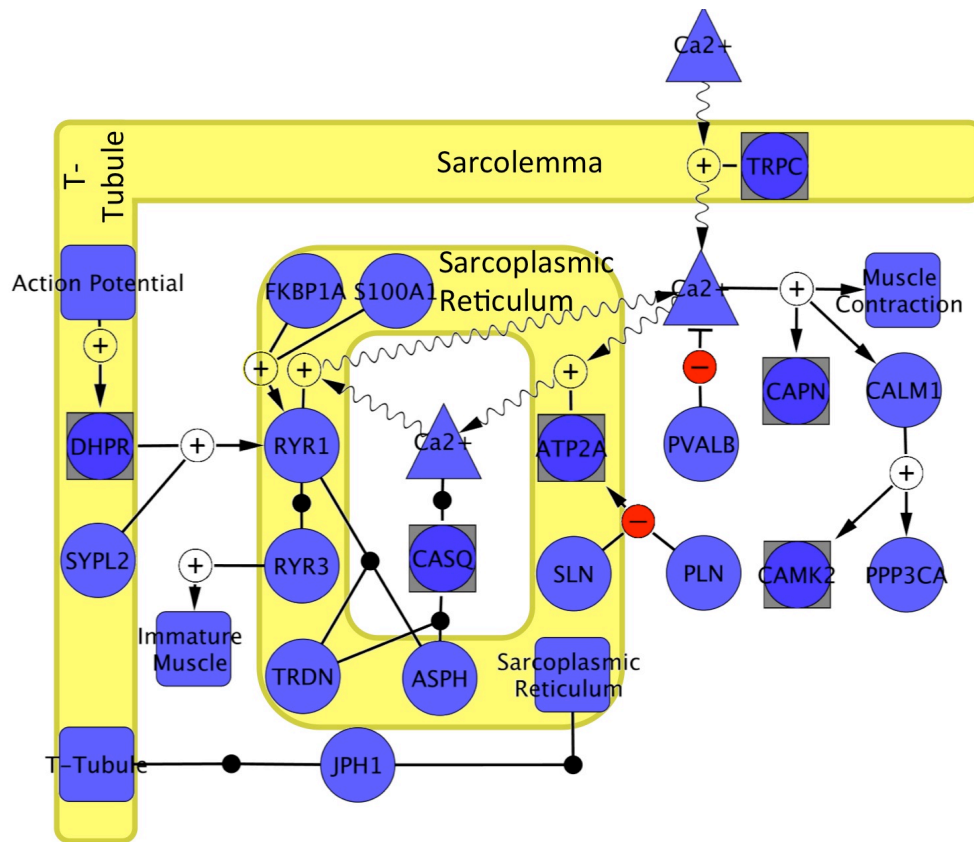
Figure 6.2: Excitation contraction coupling. Action potentials travel through the T-tubule system and induce $Ca^{2+}$ release from the SR through the ryanodine receptor. Intracellular $Ca^{2+}$ triggers muscle contraction and is then pumped back into the SR. $Ca^{2+}$ plays a role in many intracellular signalling pathways.

## 6.5  Sarcomere contraction

Sarcomere contraction is based on the sliding of interacting thick and thin filaments within the sarcomere [22, 23] (Fig. 6.3). The thick filament is made up primarily of type 2 myosin, which contains two myosin heavy chain (MYH) and four myosin light chain (MYL) subunits [24]. The myosin head interacts with the thin filament by binding to actin (ACTA) in a force generating mechanism is termed the cross-bridge cycle. TPM wraps around the thin filament and obscures the MYH binding pocket of ACTA filaments. TPM is regulated by the troponin (TN) complex, which consists of three subunits, each with different isoforms according to muscle type [25]. Regulation is mediated by $Ca^{2+}$ binding to TNNC, which removes the inhibitory subunit TNNI from its position with TPM and both subunits are anchored to the thin filament by the third TNNT [26]. MYH is an ATPase that requires ATP for the release phase of the cross-bridge cycle. ATP levels are maintained in skeletal muscle by CKM, which uses phospho-creatine to transfer a phosphate group to ATP [27]. Myosin binding proteins (MYBPC) are important for thick filament formation and maintenance. MYH is the major determinant of fiber type and both MYL and MYBPC have different isoforms corresponding to fiber type. MYH and MYL also have particular isoforms (MYH3, MYH8) and (MYL4, MYL5) respectively that is expressed in immature muscle [24].

The sarcomere structure is maintained by a variety of proteins. The largest protein in the body is TTN, which spans a half sarcomere from myosin in the middle of the sarcomere near the m-line and interacts with myomesin (MYOM) at the Z disc end of the sarcomere. The Z disc is made up primarily of ACTN with many interacting proteins. One of those is TCAP, which localizes titin to the Z disc. It also interacts with CAPZ, which caps the barbed end of the actin thin filament. The large protein NEB, which extends the full length of the thin filament and contains many repeated actin binding sites, maintains the thin filament structure [24]. On the pointed end, NEB interacts with the actin capping protein TMOD, which has different isoforms corresponding to muscle type [24]. NEB is anchored to the Z disc by MYPN and MYOT also plays a role in thin filament stability [24].
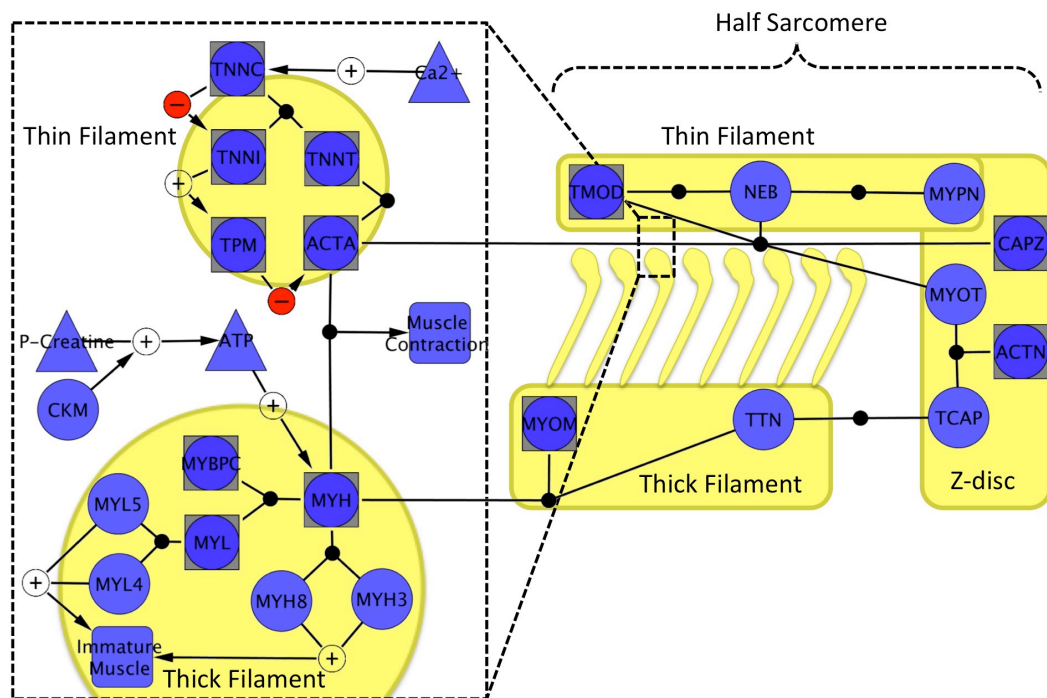
Figure 6.3: Sarcomere contraction. Myosin binds to actin and undergoes a cross-bridge cycling in order to produce contractile force. Myosin (thick) and actin (thin) filaments slide past each other during contraction. Sarcomeres are separated by Z-discs.

## 6.6 Cytoskeleton

The force generated within the sarcomere is transmitted throughout the cell to the surrounding tissue through various cytoskeletal proteins (Fig. 6.4). The most studied in skeletal muscle is dystrophin (DMD), which mechanically links the cytoskeleton to the ECM [28]. Utrophin (UTRN) provides a similar role as DMD, but functions in the NMJ and may be able to partially compensate in absence of DMD. DMD is associated with many proteins that interact to form the dystrophin-associated glycoprotein (DAG) complex. Dystroglycan (DAG1) serves as a link from the DAG to the ECM through its laminin binding properties. DAG1 is glycosolated by membrane proteins LARGE and FCMD. Also associated with the DMD are sarcoglycans (SGC), transmembrane proteins that help stabilize the sarcolemma and also link to the cytoskeleton through interactions with filamen $\gamma$ (FLNC). FLNC binds SGC at the sarcolemma and also filamen associated protein myozenin (MYOZ2) in the Z-disc [24]. Membrane stability is also maintained by dysferlin (DYSF) with its function in membrane fusion [29]. Dystrobrevins (DTN, two isoforms) bind DMD and syntrophins (SNT), which localize nitric oxide synthase 1 (NOS1) near the sarcolemma. DTN also connects the DAG complex to intermediate filaments syncoilin (SYNC) and synemin (SYNM).

These intermediate filaments connect to desmin (DES) the primary intermediate filament in skeletal muscle. However, VIM expression predominates during muscle development, but is then lost at maturity. DES links to both mitochondria and the nucleus within the cell. The nuclear membrane anchorage to the cytoskeleton is mediated by emerin (EMD), which also binds nuclear lamin (LMNA) with its role in nuclear stability and gene expression. DES binds these organelles to the muscle structure at the Z-disc. The Z-disc also contains ACTN binding protein cypher (LDB3), for the linkage of filamens through MYOZ2, and muscle LIM protein (CSRP3) which links to the ankryn (ANK) and spectrin (SPT) network within the muscle. ANK and SPT interact with actin and support membrane stability. They also interact with OBSCN, which plays a role in localizing the SR through interactions with both the SR and TTN in the sarcomere [24].

Integrins also provide a physical link between the cell and the ECM. In-
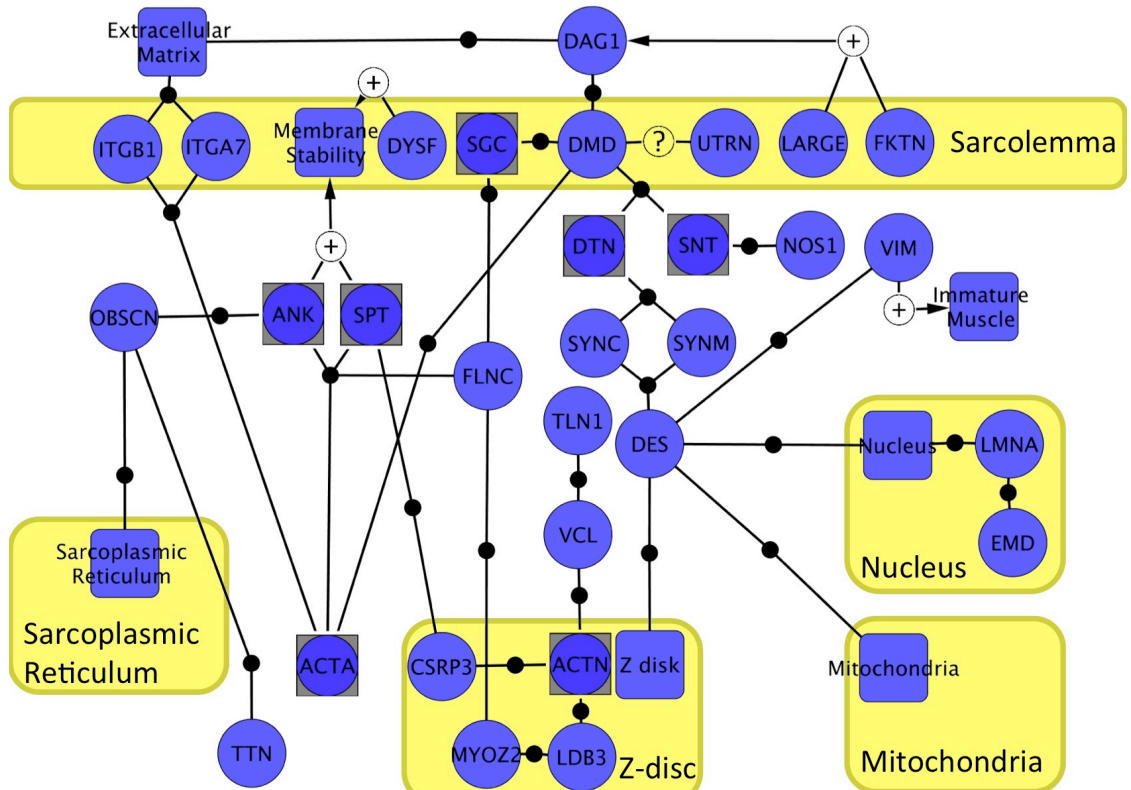
Figure 6.4: Cytoskeleton. Muscle force generated in the sarcomere is transmitted to the sarcolemma through the dystroglycan complex or integrins. Loads are transmitted to intracellular organelles through the intermediate filament network.

tegrins bind the actin cytoskeleton and also directly to laminins in the ECM. Integrins are dimers formed by $\alpha$ and $\beta$ subunits, of which ITGA7 and ITGB1 are the most common forms in muscle [24].

*Desmin in Skeletal Muscle: Desmin represents the muscle specific interme-diate filament protein that interconnects sarcomeres at their Z-disks and permits efficient force transmission throughout the sarcomere. Interestingly, mice lacking desmin generate lower stress due to this "impaired" mechanical force transmission, but also show less overt signs of injury. Recent studies have shown that the loss of desmin also results in a chronic inflammatory effect that appears to ultimately lead to skeletal muscle fibrosis of the extracellular matrix. Since the desmin knockout muscle fibers are more compliant compared to wildtype, but the ECM of knockouts is stiffer compared to wildtype, this suggests that the knockout is able to mount a compensatory response to the loss of desmin and increased fiber compliance. The precise mechanism for this compensation is not known.*

## 6.7  Extracellular matrix

The cytoskeleton provides a network to transmit force out to the ECM (Fig. 6.5). This is initially transmitted to the basal lamina, a mesh like network consisting primarily of COL4 (COL4A1 and COL4A2) and laminin (LAM; most commonly LAMA2; LAMB1/LAMB2, LAMC1 in muscle) [30]. HSPG2 is a proteo-glycan in the basal lamina that binds both COL4 and LAM. Other basal laminar proteoglycans include syndecans (SDC), which play an important role in satellite cell differentiation and biglycan (BGN) an important binding partner [28, 31]. The glycoprotein fibronectin (FN1) is a multimeric protein that serves as a link to many proteins within the basal lamina [32].

As opposed to the basal lamina, the fibrillar ECM has strong load bear-ing capabilities and is made up primarily of collagen I (COL1) and collagen III (COL3A1). Collagen VI (COL6) serves as an important link between the fibri-lar and laminar ECM [30]. Decorin (DCN) is the major fibrillar proteoglycan in muscle [31]. FN1 also plays an important role in fibrillar ECM. It binds to glyco-

Figure 6.5: Extracellular matrix. Provides network for intracellular loads to be transmitted extracellularly. The basal lamina is a mesh like network, while the fibrillar ECM is made up of larger collagen fibrils and associated proteins. Important growth factors are involved in ECM formation.

protein tenascin C (TNC) and provides strength and elasticity to the ECM and is highly expressed in regenerating fibers [32]. ECM strength is also determined by the amount of collagen crosslinking and lysyl oxidase (LOX) is a copper enzyme primarily responsible for crosslinking [33].

The ECM also has a program for degradation through zinc dependent matrix metalloproteinases (MMPs). MMP2 and MMP9 are abundant in muscle and breakdown COL4 found in the basal lamina. MMP2 is activated by membrane type MMP14 at the sarcolemma. MMP1 functions as a protease in the fibrillar ECM breaking down both COL1 and COL3A1. MMP activity is controlled by tissue inhibitors of metalloproteinases (TIMPs) and are represented by TIMP1 and TIMP2 and skeletal muscle [34].

Production of ECM proteins is controlled by specific growth factors. The

most well studied inducer of ECM in skeletal muscle for its role in fibrosis is transforming growth factor, beta 1 (TGFB1) [35]. TGFB1 binds BGN in skeletal muscle and its activity is also inhibited through binding to LTBP4 [36, 37]. Connective tissue growth factor (CTGF) is another critical component in ECM signalling that leads to expression of collagen genes and fibrosis [35]. Following expression, collagen must be processed before becoming functional. Prolyl 4-hydroxylase (P4) catalyzes the formation of hydroxyproline and PLOD3 catalyzes posttranslational modification and both proteins reflect the rate of collagen biosynthesis [33].

## 6.8 Energy metabolism

Muscle is a very energetically active tissue, requiring ATP to power the crossbridge cycle and also for calcium transport in relaxation (Fig. 6.6). Glucose is a primary substrate for energy metabolism and is transported across the sarcolemma by GLUT4 (SLC2A4). SLC2A4 translocation to the sarcolemma is controlled by AMPK. AMPK is an energy sensing enzyme that becomes activated in response to low energy levels [38]. Intracellular glucose can be stored in the form of glycogen via the enzyme glycogen synthase 1 (GYS1), which can then be broken down back into glucose via the enzyme glycogen phosphorylase (PYGM) when necessitated [39]. Glucose is broken down further into pyruvate through glycolysis, which nets ATP. Glucose is prepared for glycolysis by the phosphorylating enzyme hexokinase (HK1), glycolysis is maintained by lactate dehydrogenase A (LDHA), and the rate-limiting step of glycolysis is controlled by the enzyme phosphofructokinase (PFKM) [40].

Pyruvate conversation to Acetyl-CoA by pyruvate dehydrogenase (PDH) allows for progression through the TCA cycle and subsequent oxidative phosphorylation [40]. Acetyl-CoA can also be produced from fatty acids in skeletal muscle. Fatty acid uptake into the cell is also through an AMPK mediated transporter CD36 [38]. Shuttling proteins fatty acid binding protein 3 (FABP) and lipoprotein lipase (LPL) also mediate fatty acid transport [41]. Intracellular fatty acids may be stored as triglycerides for which the enzyme GPAM catalyzes the initial and
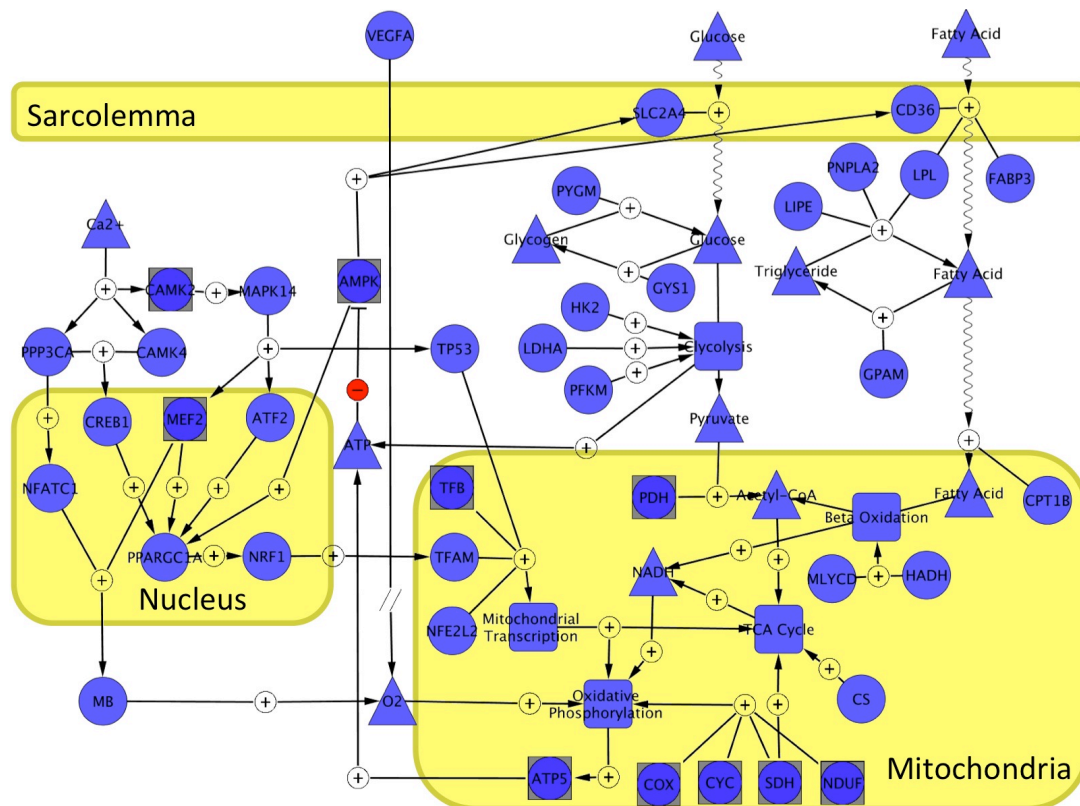
Figure 6.6: Energy metabolism. Muscles use ATP as the energy source for contraction. ATP is generated both glycolytically and oxidatively in the muscle from glucose or fatty acids. Muscle has energy sensing mechanisms to adapt transcriptionally to demand changes.

committing step [38]. Hormone sensitive lipase (LIPE) is responsible for triglyceride breakdown to free fatty acids in muscle along with ATGL (PNPLA2) for the initial step and also assisted by LPL for triglyceride hydrolysis [41]. To be used in energy metabolism fatty acids must be transported into the mitochondria via CPT1B [40]. Here fatty acids can undergo beta-oxidation to produce Acetyl-CoA and NADH, which is catalysed by enzymes MYLCD and HADH [41]. Acetyl-CoA enters the TCA cycle to produce NADH. Citrate synthase (CS) catalyses the rate limiting step within the TCA cycle, which also requires the enzyme succinate dehydrogenase (SDH) [42]. NADH is then used as an electron carrier in oxidative phosphorylation that also uses oxygen as an oxidising agent [43]. Oxygen is provided to the muscle through the vasculature, which is stimulated by VEGF, and transported within the muscle by MB [44, 45]. Oxidative phosphorylation is catalysed by a set of 4 complexes in series (NDUF, SDH, CYC, COX). The energy from the electron gradient produced is then converted to ATP by ATP synthase (ATP5) [43].

The production of metabolic transcripts is largely controlled by PGC-1$\alpha$ (PPARGC1) within skeletal muscle in conjunction with many other transcription factors [46]. AMPK activates PPARGC1A when energy levels are low [38]. Ca$^{2+}$ also plays a role through the activation of PPP3CA, CAMK4, and CAMK2. PPP3CA activates the transcription factor NFATC1 that acts to produce muscle metabolic genes including myoblogin (MB) [47] . PPP3CA and CAMK4 both activate CREB1, a transcription factor that is integral to PPARGC1A mediated expression [42]. CAMK2 activates p38 (MAPK14) that activates transcription factors MEF2 and ATF2, which participate in metabolic transcription through PPARGC1A [42, 43]. NRF1 together with PPARGC1A plays a large role in mitochondrial expression through transcription factor A, mitocontrial (TFAM). TFAM works in concert with transcription factor B1 and B2, mitochondrial (TFB) and nuclear respiratory factor 2 (NFE2L2) in the mitochondrial transcription complex which is also maintained by TP53 [48].

## 6.9 Inflammation

Injury to skeletal muscle initiates a coordinated and precisely controlled inflammatory response that is localized to the damage site. This is a critical step in the process of muscle repair and if not properly regulated can lead to deterioration and fibrosis [35, 49, 50]. In the early stages of the inflammatory process, pro-inflammatory cytokines such as interleukin 8 (IL8), interferon $\gamma$, (IFNG), and COX-2 (PTGS2) are released at the injury site attracting circulating neutrophils and classically activated macrophages, which then act to clear myofiber debris and promote myoblast proliferation [49, 50] (Fig. 6.7). These monocytes secrete other pro-inflammatory cytokines such as tumor necrosis factor-alpha (TNF) and interleukin-1 beta (IL1B), which stimulate phagocytosis [35, 51].

The primary pathway for inflammation mediated protein degradation is the nuclear factor kappa B (NFKB) dependent pathway. Activation of NFKB is controlled by the I$\kappa\beta$ kinase (IKBKE) complex, which phosphorylates I$\kappa\beta$ targeting it for degradation and enabling the translocation of NFKB to the nucleus [52, 53]. NFKB affects protein turnover by increasing the expression of the ubiquitin ligase MuRF1 (TRIM63) and by binding to and activating interleukin-6 (IL6). IL6 is thought to act in a hormone-like manner to regulate glucose homeostasis possibly via AMPK and can also be produced [53, 54] by the muscle itself [55, 56]. IL6 may also be activated by heat shock factors 1 and 2 and by calcium via its activation of NFKB [50, 56]. NFKB is also activated by reactive oxygen and nitrogen species as well as SOCS3 [57, 58], however, inside the nucleus reactive species act to inhibit NFKB activity [58]. Once activated, NFKB and IL6 act to inhibit muscle regeneration. Evidence suggests that the mitogen-activated protein kinase p38 (MAPK14) is also activated in response to TNF and IL1B. It then acts to upregulate atrogin-1 (FBXO32), a gene involved in muscle atrophy. Additionally, p38 has been shown to activate IL6 [55]. TNF is also shown to increase circulating levels of IFNG, which activates the JAK-STAT pathway and inhibits cell growth and proliferation [59]. TNF and IL1B inhibit the expression of IGF1 a key muscle growth factor [60].

After the initial invasion of neutrophils and classically activated macrophages,
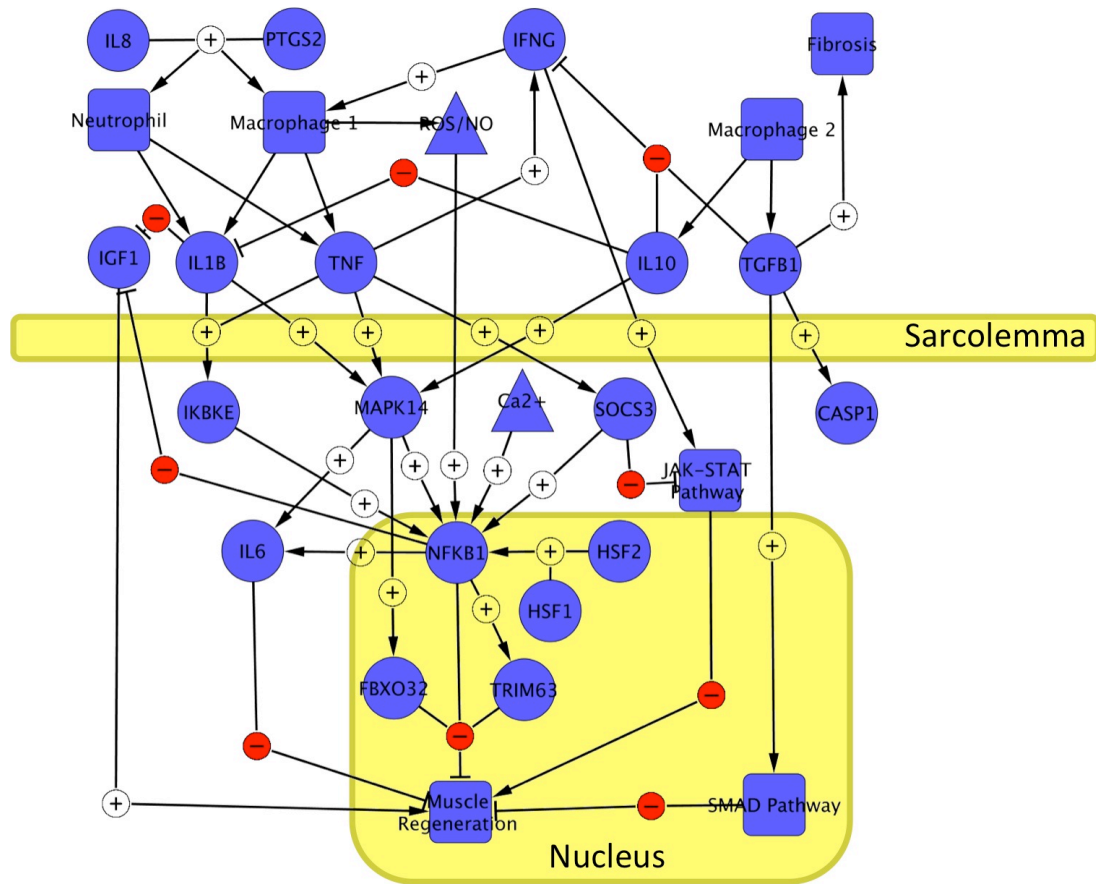
Figure 6.7: Inflammation. Early macrophages and neutrophils enter damaged muscle to clear debris and produce an inflammatory signal. If sustained inflammation can lead to degradation. Secondary macrophages enter to limit the inflammatory signals and repair muscle.

a second population of macrophages secrete cytokines such as interleukin 10 (IL10) and TGFB1 and act to reduce the inflammatory response [35]. IL10 and TGFB1 negatively regulate IFNG production and IL10 inhibits the proteolytic effects of IL1B [50, 59]. TGFB1 plays a role in both the initiation of fibrosis in skeletal muscle by stimulating fibroblast proliferation and inducing myogenic cells to differentiate into myofibroblastic cells. TGFB1 has been shown to inhibit regeneration via activation of Smad proteins [35].

# 6.10   Muscle hypertrophy and atrophy

Skeletal muscle hypertrophy and atrophy are critical processes required to maintain skeletal muscle mass, recover from injury and adapt to exercise (Fig. 6.8). These processes can be triggered at the cellular level by a variety of cues including growth factors, nutritional signals and mechanical stress [53, 54]. Insulin and insulin-like growth factor 1 (IGF1) have been shown to be potent inducers of hypertrophy via IGF1 receptor (IGF1R) and the PI3K/Akt pathway [54]. Activated phosphatidylinositol 3 kinase (PI3KR) creates a lipid binding site on the cell membrane for AKT1, a serine/threonine kinase. AKT1 then results in the activation of the mammalian target of rapamycin (MTOR). Activation of MTOR then in turn activates RPS6KB1, which activates genes responsible for protein synthesis. In addition, PDK1 has also been shown to phosphorylate RPS6KB1 directly [54]. MTOR also participates in the growth process by phosphorylating EIF4EBP1, which results in the dissociation of the EIF4EBP1/EIF4E complex allowing EIF4E to initiate protein translation. A regulatory associated protein of MTOR (RPTOR) facilitates the phosphorylation of RPS6KB1 and 4EBP1 by MTOR and has been shown to bind both proteins. AKT1 may also influence translation by inhibiting the activity of glycogen synthase kinase 3 beta (GSK3B) as GSK3B inhibits EIF2B, thereby blocking its promotion of protein translation [53, 54]. AKT1 also prevents the forkhead box proteins (FOXO) from entering the nucleus via phosphorylation [53, 55]. FOXO transcription factors are known to promote transcription of TRIM63 and FBXO32, which are ubiquitin ligases involved in muscle degradation [61].

Transcriptional regulation also plays a key role in muscle hypertrophy and control is centred around the four muscle regulatory transcription factors: muscle differentiation factor (MYOD1), myogenic factor 5 (MYF5), muscle regulatory factor 4 (MYF6), and myogenin (MYOG). MYOD1 and MYF5 are early myogenic factors important in differentiation [62]. MYOD1 activates p21 (CDKN1A) to arrest the cell cycle and promote differentiation of muscle progenitors [63]. MYOD1 and MYF5 lead to the expression of MYOG and MYF6 that directly to control the transcription of many muscle specific genes [62]. These transcription factors work
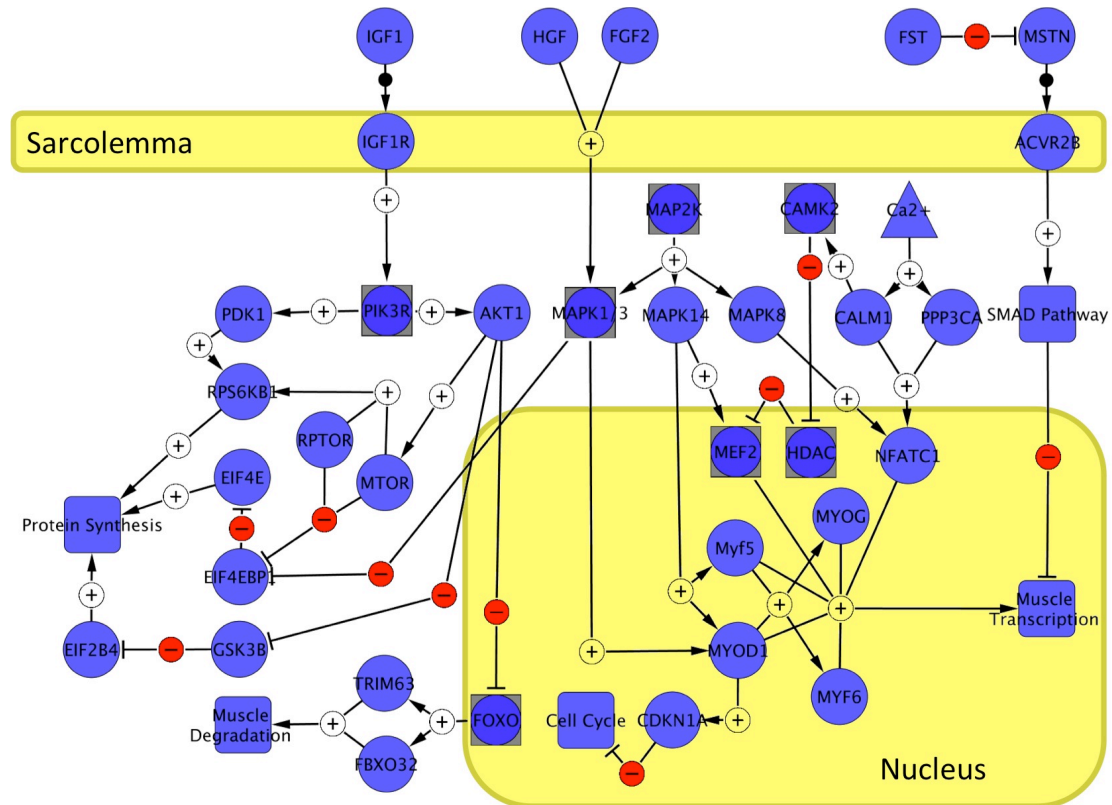
Figure 6.8: Muscle hypertrophy and atrophy. Multiple pathways determine muscle size. IGF1 signals fiber growth and increased protein production. MAPKs can elicit muscle myogenic factors in response to stresses. Autocrine factor MSTN limits muscle growth through the SMAD pathway.

in concert with NFATC1 and muscle enhancement factor 2 (MEF2) for muscle transcription [64].

The family of mitogen-activated protein kinases (MAPK) have also been implicated in growth and hypertrophy in response to exercise [52]. The MAPK family of proteins includes extracellular signal-related kinases 1 and 2 (MAPK1/3), MAPK14 and c-Jun NH2-terminal kinases (MAPK8), which are thought to couple cellular stress with an adaptive transcriptional response and are activated by MAP2K [64]. MAPK1/3 acts to activate downstream target (EIF4E) to initiate protein translation and also to activate MYOD1 [64, 65]. MAPK1/3 can also be activated downstream of growth factors HGF and FGF2 [64]. MAPK14 has also been shown to activate MYOD1 as well as MYF5 and MEF2. The activation of

MAPK8 is correlated with an increase in transcription of the early response genes c-jun and c-fos, which may enhance muscle regeneration [52].

$Ca^{2+}$ can also signal muscle hypertrophy through activation of CALM1 and PPP3CA. These proteins prevent the translocation of NFATC1 to the nucleus where it acts as part of the muscle transcription machinery [47]. Also activated by CALM1 is calcium/calmodulin-dependent protein kinase II (CAMK2) which prevents the binding of histone deacetylase complexes (HDAC). HDAC blocks the binding of important muscle transcription factors such as MEF2 [66].

Skeletal muscle also contains a key autocrine signal to limit muscle growth. Myostatin (MSTN), a member of the transforming growth factor $\beta$ pathway, has been shown to play a significant role in muscle growth as an inhibitor of hypertrophy. MSTN signalling is mediated through its receptor activin IIB (ACVR2B), which conducts a signal to the nucleus through the SMAD pathway. Expression of follistatin (FSTN) has been shown to increase muscle mass through action as a MSTN antagonist [35, 53].

## 6.11  Muscle fiber type

Skeletal muscles have different fiber types that play a role in muscle function. Slow fibers are more oxidative and used for repetitive contractions. Fast fibers are generally larger, more glycolytic, and required for brief high force contractions [67]. Many transcripts related to muscle function may be differentially regulated according to fiber type. Additionally some transcripts have distinct isoforms, which are expressed in different fiber types, delineated in (Fig. 6.9). MYH is the major determine of fiber type in skeletal muscle [67].

*Fixed Muscle Contractures: Skeletal muscle is an extremely adaptable tissue with motor neuron firing being a major determinant of muscle characteristics. Upper motor neuron lesions like those that cause stroke or cerebral palsy are known to create spastic lower motor nerves. This spasticity and altered use often causes muscles to adapt into a pathologic state of fixed muscle contractures [68]. When muscle stiffness, without any active force generation, limits the functional range of*
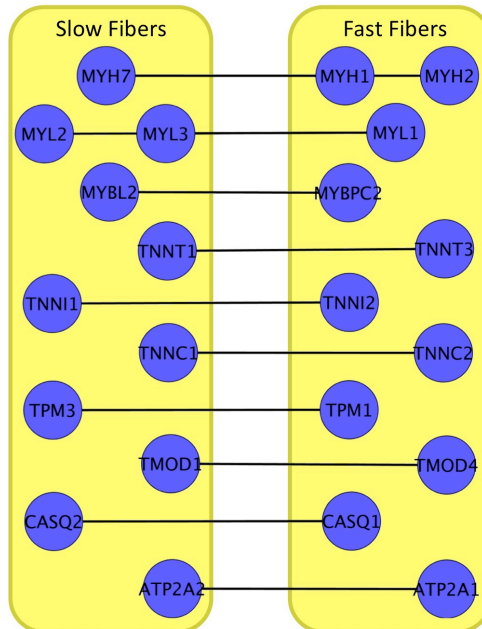
Figure 6.9: Muscle fiber type. Genes that have similar function, but are expressed specifically in either a fast or slow muscle fiber type. MYH is the major determinant of fiber type.

*motion of a joint the muscle has a fixed contracture. This pathologic state of muscle is not the result of any genetic abnormalities of muscle genes themselves, but represents a maladaptive state [69]. The mechanism that leads to restricted muscle in contracture is largely unknown. Recent studies on children with cerebral palsy have suggested that many of the functional muscle networks described here are also altered in cerebral palsy [70]. Many genes related to excitation contraction coupling are up regulated, such as parvalbumin, a protein involved that assists in relaxing the muscle. The extracellular matrix also showed many transcripts that were up regulated including the major component of the basal lamina collagen IV. The muscle from children with cerebral palsy also had conflicting growth signals with both IGF1, a protein that signals hypertrophy, and MSTN, a protein expressed to limit growth, being up regulated [70]. These results demonstrate how the networks described may be used to investigate muscle adaptations and highlight important functional networks altered. It allows for basic understanding of how altered transcripts interact with each other to change muscle function.*

## 6.12 Conclusion

Skeletal muscle requires the synchronization of gene networks in order to conduct its primary function of force generation. Each of these networks has critical genes responsible for the function of that gene network, which have been established within the literature. We have delineated the critical components of these and their relationship to muscle function, however there are additional genes, which may play an important role. These gene networks include: the NMJ signal transduced through ECC to trigger MC, genes critical for the transmission of force through the CYSK out to the ECM, genes involved in MET, gene signals for INF, genes regulating muscle size through MHA, and finally which gene isoforms are present in different FT. This work will allow the use of high throughput technologies with advanced software packages to investigate muscle tissue specifically, enabling objective research onto which networks are altered in a variety of muscle adaptations or pathologies and highlight the primary targets for future therapies.

## 6.13 Acknowledgements

## 6.14 References

[1] Deconinck, N. and Dan, B., 2007. Pathophysiology of duchenne muscular dystrophy: current hypotheses. *Pediatric neurology*, 36:1–7.

[2] Petrof, B.J., Shrager, J.B., Stedman, H.H., Kelly, A.M., and Sweeney, H.L., 1993. Dystrophin protects the sarcolemma from stresses developed during muscle contraction. *Proceedings of the National Academy of Sciences of the United States of America*, 90:3710–3714.

[3] Hopf, F.W., Turner, P.R., Denetclaw, W.F., Reddy, P., and Steinhardt, R.A., 1996. A critical evaluation of resting intracellular free calcium regulation in dystrophic mdx muscle. *The American journal of physiology*, 271:C1325–39.

[4] Spencer, M.J., Montecino-Rodriguez, E., Dorshkind, K., and Tidball, J.G., 2001. Helper (CD4(+)) and cytotoxic (CD8(+)) T cells promote the pathology of dystrophin-deficient muscle. *Clinical immunology (Orlando, Fla)*, 98:235–243.

[5] Haslett, J.N., Sanoudou, D., Kho, A.T., Bennett, R.R., Greenberg, S.A., Kohane, I.S., Beggs, A.H., and Kunkel, L.M., 2002. Gene expression comparison of biopsies from Duchenne muscular dystrophy (DMD) and normal skeletal muscle. *Proceedings of the National Academy of Sciences of the United States of America*, 99:15000–15005.

[6] Schmalbruch, H., 1984. Regenerated muscle fibers in Duchenne muscular dystrophy: a serial section study. *Neurology*, 34:60–65.

[7] Duance, V.C., Stephens, H.R., Dunn, M., Bailey, A.J., and Dubowitz, V., 1980. A role for collagen in the pathogenesis of muscular dystrophy? *Nature*, 284:470–472.

[8] Feltrin, E., Campanaro, S., Diehl, A.D., Ehler, E., Faulkner, G., Fordham, J., Gardin, C., Harris, M., Hill, D., Knoell, R., Laveder, P., Mittempergher, L., Nori, A., Reggiani, C., Sorrentino, V., Volpe, P., Zara, I., Valle, G., and Deegan, J., 2009. Muscle Research and Gene Ontology: New standards for improved data integration. *BMC medical genomics*, 2:6.

[9] Cline, M.S., Smoot, M., Cerami, E., Kuchinsky, A., Landys, N., Workman, C., Christmas, R., Avila-Campilo, I., Creech, M., Gross, B., Hanspers, K., Isserlin, R., Kelley, R., Killcoyne, S., Lotia, S., Maere, S., Morris, J., Ono, K., Pavlovic, V., Pico, A.R., Vailaya, A., Wang, P.L., Adler, A., Conklin, B.R., Hood, L., Kuiper, M., Sander, C., Schmulevich, I., Schwikowski, B., Warner, G.J., Ideker, T., and Bader, G.D., 2007. Integration of biological networks and gene expression data using Cytoscape. *Nature protocols*, 2:2366–2382.

[10] Lockhart, D.J., Dong, H., Byrne, M.C., Follettie, M.T., Gallo, M.V., Chee, M.S., Mittmann, M., Wang, C., Kobayashi, M., Horton, H., and Brown, E.L., 1996. Expression monitoring by hybridization to high-density oligonucleotide arrays. *Nature biotechnology*, 14:1675–1680.

[11] Hu, S., Xie, Z., Qian, J., Blackshaw, S., and Zhu, H., 2011. Functional protein microarray technology. *Wiley interdisciplinary reviews Systems biology and medicine*, 3:255–268.

[12] Wu, H., Xiong, W.C., and Mei, L., 2010. To build a synapse: signaling pathways in neuromuscular junction assembly. *Development (Cambridge, England)*, 137:1017–1033.

[13] Schaeffer, L., de Kerchove d'Exaerde, A., and Changeux, J.P., 2001. Targeting transcription to the neuromuscular synapse. *Neuron*, 31:15–22.

[14] Patton, B.L., 2003. Basal lamina and the organization of neuromuscular synapses. *Journal of neurocytology*, 32:883–903.

[15] Flucher, B.E., Obermair, G.J., Tuluc, P., Schredelseker, J., Kern, G., and Grabner, M., 2005. The role of auxiliary dihydropyridine receptor subunits in muscle. *Journal of muscle research and cell motility*, 26:1–6.

[16] Dulhunty, A.F., 2006. Excitation-contraction coupling from the 1950s into the new millennium. *Clinical and experimental pharmacology & physiology*, 33:763–772.

[17] Treves, S., Vukcevic, M., Maj, M., Thurnheer, R., Mosca, B., and Zorzato, F., 2009. Minor sarcoplasmic reticulum membrane components that modulate excitation-contraction coupling in striated muscles. *The Journal of physiology*, 587:3071–3079.

[18] Völkers, M., Rohde, D., Goodman, C., and Most, P., 2010. S100A1: a regulator of striated muscle sarcoplasmic reticulum Ca2+ handling, sarcomeric, and mitochondrial function. *Journal of biomedicine & biotechnology*, 2010:178614.

[19] Berchtold, M.W., Brinkmeier, H., and Müntener, M., 2000. Calcium ion in skeletal muscle: its crucial role for muscle function, plasticity, and disease. *Physiological reviews*, 80:1215–1265.

[20] Traaseth, N.J., Ha, K.N., Verardi, R., Shi, L., Buffy, J.J., Masterson, L.R., and Veglia, G., 2008. Structural and dynamic basis of phospholamban and sarcolipin inhibition of Ca(2+)-ATPase. *Biochemistry*, 47:3–13.

[21] Beard, N.A., Wei, L., and Dulhunty, A.F., 2009. Ca(2+) signaling in striated muscle: the elusive roles of triadin, junctin, and calsequestrin. *European biophysics journal : EBJ*, 39:27–36.

[22] Huxley, A.F. and NIEDERGERKE, R., 1954. Structural changes in muscle during contraction; interference microscopy of living muscle fibres. *Nature*, 173:971–973.

[23] HUXLEY, H. and HANSON, J., 1954. Changes in the cross-striations of muscle during contraction and stretch and their structural interpretation. *Nature*, 173:973–976.

[24] Clark, K.A., McElhinny, A.S., Beckerle, M.C., and Gregorio, C.C., 2002. Striated muscle cytoarchitecture: an intricate web of form and function. *Annual review of cell and developmental biology*, 18:637–706.

[25] Huxley, H.E., 1985. The crossbridge mechanism of muscular contraction and its implications. *The Journal of experimental biology*, 115:17–30.

[26] Gordon, A.M., Homsher, E., and Regnier, M., 2000. Regulation of contraction in striated muscle. *Physiological reviews*, 80:853–924.

[27] Bessman, S.P. and Geiger, P.J., 1981. Transport of energy in muscle: the phosphorylcreatine shuttle. *Science (New York, NY)*, 211:448–452.

[28] Allikian, M.J. and McNally, E.M., 2007. Processing and assembly of the dystrophin glycoprotein complex. *Traffic (Copenhagen, Denmark)*, 8:177–183.

[29] Han, R. and Campbell, K.P., 2007. Dysferlin and muscle membrane repair. *Current opinion in cell biology*, 19:409–416.

[30] Grounds, M.D., Sorokin, L., and White, J., 2005. Strength at the extracellular matrix-muscle interface. *Scandinavian journal of medicine & science in sports*, 15:381–391.

[31] Jenniskens, G.J., Veerkamp, J.H., and van Kuppevelt, T.H., 2006. Heparan sulfates in skeletal muscle development and physiology. *Journal of cellular physiology*, 206:283–294.

[32] Järvinen, T.A., Kannus, P., Järvinen, T.L., Jozsa, L., Kalimo, H., and Järvinen, M., 2000. Tenascin-C in the pathobiology and healing process of musculoskeletal tissue injury. *Scandinavian journal of medicine & science in sports*, 10:376–382.

[33] Takala, T.E. and Virtanen, P., 2000. Biochemical composition of muscle extracellular matrix: the effect of loading. *Scandinavian journal of medicine & science in sports*, 10:321–325.

[34] Carmeli, E., Moas, M., Reznick, A.Z., and Coleman, R., 2004. Matrix metalloproteinases and skeletal muscle: a brief review. *Muscle & nerve*, 29:191–197.

[35] Serrano, A.L. and Muñoz-Cánoves, P., 2010. Regulation and dysregulation of fibrosis in skeletal muscle. *Experimental cell research*, 316:3050–3058.

[36] Young, M.F., Bi, Y., Ameye, L., and Chen, X.D., 2002. Biglycan knockout mice: new models for musculoskeletal diseases. *Glycoconjugate journal*, 19:257–262.

[37] Goldstein, J.A. and McNally, E.M., 2010. Mechanisms of muscle weakness in muscular dystrophy. *The Journal of general physiology*, 136:29–34.

[38] Ruderman, N.B., Park, H., Kaushik, V.K., Dean, D., Constant, S., Prentki, M., and Saha, A.K., 2003. AMPK as a metabolic switch in rat muscle, liver and adipose tissue after exercise. *Acta physiologica Scandinavica*, 178:435–442.

[39] Westerblad, H., Bruton, J.D., and Katz, A., 2010. Skeletal muscle: energy metabolism, fiber types, fatigue and adaptability. *Experimental cell research*, 316:3093–3099.

[40] Jeukendrup, A.E., 2002. Regulation of fat metabolism in skeletal muscle. *Annals of the New York Academy of Sciences*, 967:217–235.

[41] Holloway, G.P., Luiken, J.J.F.P., Glatz, J.F.C., Spriet, L.L., and Bonen, A., 2008. Contribution of FAT/CD36 to the regulation of skeletal muscle fatty acid oxidation: an overview. *Acta physiologica (Oxford, England)*, 194:293–309.

[42] Hood, D.A., Irrcher, I., Ljubicic, V., and Joseph, A.M., 2006. Coordination of metabolic plasticity in skeletal muscle. *The Journal of experimental biology*, 209:2265–2275.

[43] Holloway, G.P., Bonen, A., and Spriet, L.L., 2009. Regulation of skeletal muscle mitochondrial fatty acid metabolism in lean and obese individuals. *The American journal of clinical nutrition*, 89:455S–62S.

[44] Hudlicka, O. and Brown, M.D., 2009. Adaptation of skeletal muscle microvasculature to increased or decreased blood flow: role of shear stress, nitric oxide and vascular endothelial growth factor. *Journal of vascular research*, 46:504–512.

[45] Kanatous, S.B. and Mammen, P.P.A., 2010. Regulation of myoglobin expression. *The Journal of experimental biology*, 213:2741–2747.

[46] Olesen, J., Kiilerich, K., and Pilegaard, H., 2010. PGC-1alpha-mediated adaptations in skeletal muscle. *Pflügers Archiv : European journal of physiology*, 460:153–162.

[47] Schiaffino, S., 2010. Fibre types in skeletal muscle: a personal account. *Acta physiologica (Oxford, England)*, 199:451–463.

[48] Ljubicic, V., Joseph, A.M., Saleem, A., Uguccioni, G., Collu-Marchese, M., Lai, R.Y.J., Nguyen, L.M.D., and Hood, D.A., 2010. Transcriptional and post-transcriptional regulation of mitochondrial biogenesis in skeletal muscle: effects of exercise and aging. *Biochimica et biophysica acta*, 1800:223–234.

[49] Tidball, J.G., 2005. Inflammatory processes in muscle injury and repair. *American journal of physiology Regulatory, integrative and comparative physiology*, 288:R345–53.

[50] Peake, J., Della Gatta, P., and Cameron-Smith, D., 2010. Aging and its effects on inflammation in skeletal muscle at rest and following exercise-induced muscle injury. *American journal of physiology Regulatory, integrative and comparative physiology*, 298:R1485–95.

[51] Smith, C., Kruger, M.J., Smith, R.M., and Myburgh, K.H., 2008. The inflammatory response to skeletal muscle injury: illuminating complexities. *Sports medicine (Auckland, NZ)*, 38:947–969.

[52] Kramer, H.F. and Goodyear, L.J., 2007. Exercise, MAPK, and NF-kappaB signaling in skeletal muscle. *Journal of applied physiology (Bethesda, Md : 1985)*, 103:388–395.

[53] Zhang, P., Chen, X., and Fan, M., 2007. Signaling mechanisms involved in disuse muscle atrophy. *Medical hypotheses*, 69:310–321.

[54] Glass, D.J., 2005. Skeletal muscle hypertrophy and atrophy signaling pathways. *The international journal of biochemistry & cell biology*, 37:1974–1984.

[55] Febbraio, M.A. and Pedersen, B.K., 2002. Muscle-derived interleukin-6: mechanisms for activation and possible biological roles. *The FASEB journal : official publication of the Federation of American Societies for Experimental Biology*, 16:1335–1347.

[56] Pedersen, B.K. and Fischer, C.P., 2007. Physiological roles of muscle-derived interleukin-6 in response to exercise. *Current opinion in clinical nutrition and metabolic care*, 10:265–271.

[57] Spangenburg, E.E., Brown, D.A., Johnson, M.S., and Moore, R.L., 2006. Exercise increases SOCS-3 expression in rat skeletal muscle: potential relationship to IL-6 expression. *The Journal of physiology*, 572:839–848.

[58] Morgan, M.J. and Liu, Z.g., 2011. Crosstalk of reactive oxygen species and NF-B signaling. *Cell research*, 21:103–115.

[59] Schroder, K., Hertzog, P.J., Ravasi, T., and Hume, D.A., 2004. Interferon-gamma: an overview of signals, mechanisms and functions. *Journal of leukocyte biology*, 75:163–189.

[60] Li, H., Malhotra, S., and Kumar, A., 2008. Nuclear factor-kappa B signaling in skeletal muscle atrophy. *Journal of molecular medicine (Berlin, Germany)*, 86:1113–1126.

[61] Attaix, D., Ventadour, S., Codran, A., Béchet, D., Taillandier, D., and Combaret, L., 2005. The ubiquitin-proteasome system and skeletal muscle wasting. *Essays in biochemistry*, 41:173–186.

[62] Ten Broek, R.W., Grefte, S., and Von den Hoff, J.W., 2010. Regulatory factors and cell populations involved in skeletal muscle regeneration. *Journal of cellular physiology*, 224:7–16.

[63] Kitzmann, M. and Fernandez, A., 2001. Crosstalk between cell cycle regulators and the myogenic factor MyoD in skeletal myoblasts. *Cellular and molecular life sciences : CMLS*, 58:571–579.

[64] Keren, A., Tamir, Y., and Bengal, E., 2006. The p38 MAPK signaling pathway: a major regulator of skeletal muscle development. *Molecular and cellular endocrinology*, 252:224–230.

[65] Williamson, D., Gallagher, P., Harber, M., Hollon, C., and Trappe, S., 2003. Mitogen-activated protein kinase (MAPK) pathway activation: effects of age and acute exercise on human skeletal muscle. *The Journal of physiology*, 547:977–987.

[66] McGee, S.L., 2007. Exercise and MEF2-HDAC interactions. *Applied physiology, nutrition, and metabolism = Physiologie appliquée, nutrition et métabolisme*, 32:852–856.

[67] Zierath, J.R. and Hawley, J.A., 2004. Skeletal muscle fiber type: influence on contractile and metabolic properties. *PLoS biology*, 2:e348.

[68] Farmer, S.E. and James, M., 2001. Contractures in orthopaedic and neurological conditions: a review of causes and treatment. *Disability and rehabilitation*, 23:549–558.

[69] O'Dwyer, N.J. and Ada, L., 1996. Reflex hyperexcitability and muscle contracture in relation to spastic hypertonia. *Current opinion in neurology*, 9:451–455.

[70] Smith, L.R., Pontén, E., Hedström, Y., Ward, S.R., Chambers, H.G., Subramaniam, S., and Lieber, R.L., 2009. Novel transcriptional profile in wrist muscles from cerebral palsy patients. *BMC medical genomics*, 2:44.

# Chapter 7

# Role of the Cytoskeleton in Muscle Mechanical and Transcriptional Responses to Altered Use

## 7.1   Abstract

The intermediate filament protein desmin is the primary component of the skeletal muscle cytoskeleton and is thought to support and organize intracellular structure. In the absence of desmin, myofibrils and cellular organelles are disorganized and mislocalized. In this work we show that not only does desmin play a role in structural organization, it is also involved in the response to altered muscle use. Desmin knockout muscles showed a muted response, both mechanically and transcriptionally, to eccentric contraction induced injury but exhibited elevated expression of many injury response genes in both exercised and control muscles. Additionally, there was a substantially different transcriptional response to aging between muscle with and without desmin. Transcriptional alterations were seen across all categories of muscle physiology from the cytoskeleton to the extracellular matrix to metabolism. Framing these transcriptional changes in the pathways

important to skeletal muscle physiology points to novel areas of influence of this cytoskeletal protein and directs future work to elucidate its function.

## 7.2   Introduction

Cytoskeletal filaments have complex and diverse roles, from providing cellular structure to mechanotransduction, and are critical to cellular function. They are most frequently implicated in sustaining external stresses, and in the absence of components of the cytoskeleton, cells deform, degenerate and rupture [1]. The primary component of the cytoskeleton in muscle is the intermediate filament protein desmin. Desmin has been proposed to function as an integrator of cellular space in muscle, as it surrounds the contractile apparatus and binds to nuclei, mitochondria and costameres at the sarcolemma [2]. Studies in the desmin knockout ($des^{-/-}$) mouse have begun to elucidate the specific roles of desmin in skeletal muscle. In addition to intracellular organization, desmin is also thought to play a role in the response to mechanically induced injury. Immediately following eccentric exercise, desmin immunostaining is lost in fibers that exhibit a concomitant loss of membrane stability, but days following the injury, desmin levels are increased above pre-injury values [3, 4]. Based on these observations, desmin has been hypothesized to play a role in protecting muscle fibers from injury. However, following a bout of eccentric exercise, $des^{-/-}$ muscle was shown to retain more of its stress producing capacity than *wt*, suggesting the opposite - that in the absence of desmin, muscles are protected from injury [5].

These contradictory hypotheses, combined with evidence of increased injury and regeneration in $des^{-/-}$ muscle [6, 7], suggest that the altered mechanical effects of eccentric exercise may only be a part of the differential injury response in $des^{-/-}$ muscle. It is unknown whether, in the absence of desmin, eccentrically exercised muscle is actually sustaining less injury or simply losing less of its force producing capacity. Eccentric contraction (EC) induced injury results in a well-defined pattern of gene expression changes [8–11] and thus we sought to investigate the effects of EC in $des^{-/-}$ muscle at the transcriptional level as well as at the mechanical.

In addition, this study also examined how the transcriptional profile changes with aging, another physiological stressor.

Microarray analysis provides a powerful tool to investigate changes that occur in muscle in the absence of desmin. Though $des^{-/-}$ muscle shows no obvious gross defects and only a modest decrease in function, there are potentially many physiological processes affected at the gene level. For example, decreased stress production in $des^{-/-}$ muscle as noted by Sam et al. [5] could be the result of defects in sarcomere coupling [12], inflammation [13], inefficient metabolic function [14], intracellular calcium dynamics [15] or fiber type switching [16]. These alterations may be subtle during normal activity but have substantial negative effects when muscle is stressed in conditions such as injury and aging. Microarray technology offers the opportunity to investigate each of these possibilities in one experiment and guide further experiments toward promising hypotheses.

The purpose of this work was to determine the effect of desmin deletion on the transcriptional response of skeletal muscle to injury and aging. We hypothesize that microarray analysis will identify genes across many pathways of muscle physiology involved in the differential response of $des^{-/-}$ muscle to EC induced injury and aging and that these responses will be intimately linked. We hope to identify new and promising areas for investigation into the function of desmin in skeletal muscle.

## 7.3 Methods

Experiments were performed on muscles from wildtype (*wt*) 129/Sv (Taconic Farms, Germantown, NY) and desmin knockout ($des^{-/-}$) 129/Sv [17] mice at two ages: adult (7-9 weeks; 29.1±1.2 g; *wt*: n=5, $des^{-/-}$: n=5) and aged (>12 months; 24.9±1.3 g; *wt*: n=5, $des^{-/-}$: n=4). One hindlimb from each mouse was subjected to an exercise protocol of 50 eccentric contractions (EC), while the contralateral limb served as a control. Tibialis anterior (TA) muscles were harvested, flash frozen and processed for microarray analysis 12 hours following EC, a time determined to maximize the expression of muscle-specific injury response genes [10]. The TA

muscle was chosen for analysis as it is the largest of the dorsiflexor muscle group and is known to exhibit signs of injury following EC [10]. All procedures were performed in accordance with the National Institutes of Health Guide for the Use and Care of Laboratory Animals and were approved by the University of California and Department of Veterans Affairs Committees on the Use of Animal Subjects in Research.

### 7.3.1 Eccentric exercise

Animals were continually anesthetized with 2% isoflurane at 2 L/min and secured in a custom designed jig. One foot was secured to a plate attached to a rotational bearing that was able to provide both precise rotational displacements and torque measurements (custom modified model 360B; Aurora Scientific, Ontario, Canada). The animal's knee was positioned and fixed such that the ankle angle ($\alpha$) could be precisely controlled by the rotation of a footplate. Sterile subcutaneous 28-gauge needle electrodes (Grass Instruments, Braintree, MA) were placed in the vicinity of the right peroneal nerve, $\sim$0.5 mm under the skin, just lateral to the midline and distal to the knee joint for stimulation of the dorsiflexor muscle group. Proper placement of electrodes was determined as previously described [10]. Stimulation voltage was set by increasing voltage until peak twitch torque reached a plateau and optimum stimulation frequency was determined by a series of three isometric contractions ranging from 100 to 150 Hz. The frequency resulting in a flat torque record was used for all subsequent contractions.

Once the stimulation parameters were set and the hindlimb secure, initial measurements of isometric torque were taken at $\alpha$=90$^\circ$, which was determined to be the angle of peak isometric dorsiflexion torque [18]. The foot was then dorsiflexed to $\alpha$=52$^\circ$ and isometric torque was recorded again. Eccentric contractions were elicited by stimulating the peroneal nerve for 400 ms while rotating the foot through $\alpha$=76$^\circ$ of plantarflexion ($\alpha$=52$^\circ$-128$^\circ$) once per minute for 50 minutes. The hindlimb dorsiflexor muscle group thus initially contracted isometrically for 150 ms, following which the muscles were stretched at a rate of 520/sec while stimulation continued, resulting in a rapid torque rise (Fig. 7.1A). Following the bout

of eccentric contractions, the ankle was returned to $\alpha=90°$ and isometric torque was again recorded. The contralateral leg was subjected to isometric torque measurements at $\alpha=90°$ only and served as a control for eccentric contraction injury. Mice were then returned to their cages and allowed to recover for 12 hours. Following the recovery period, isometric torque was recorded in both the exercised and contralateral leg at $\alpha=90°$ and the TA muscle from each leg was dissected, flash frozen in liquid nitrogen and stored at $-80°$C. Animals were then euthanized by cervical dislocation.

### 7.3.2 Microarray processing

RNA was extracted from whole TA muscles ($\sim$30 mg tissue) using a combination of standard Trizol (Invitrogen Carlsbad, CA) and RNeasy (Qiagen, Valencia, CA) protocols. Muscles were homogenized for 60 seconds in a rotor-stator homogenizer on ice in 0.5 ml Trizol, 0.1 ml of chloroform was then added and the sample was vigorously vortexed for 15 seconds followed by centrifugation. The supernatant was removed and combined with an equal volume of 70% ethanol and the mixture was filtered through the RNeasy spin column. The column was then washed, incubated with RNAse-free DNAse (Qiagen), washed again and eluted as described in the manufacturers protocol. RNA concentration was determined by the absorbance at 260 nm and the 260 nm to 280 nm absorbance ratio was calculated to define RNA purity. Individual Affymetrix microarrays ("GeneChip" Mouse Genome 430A 2.0 Array; Affymetrix, Santa Clara, CA) were used for each muscle (n=38). RNA processing for the GeneChip, including stringent quality control measures, was performed by the Gene Chip Core at the Department of Veterans Affairs San Diego Health Care System (San Diego, CA).

Genespring software (SiliconGenetics, Redwood City, CA) was used to identify genes that were differentially expressed as a function of genotype, age and treatment. Three independent probe set algorithms were used for background subtraction and normalization (MAS5, RMA and GCRMA) and each feature was normalized per chip and per gene as previously described [19]. Normalized expressions of identified genes, excluding putative genes and expressed sequence tags,

were subjected to three-way ANOVA with a significance level set to 0.05 and a Benjamini and Hochberg False Discovery Rate multiple testing correction for present features. Hierarchical clustering was performed on conditions with a Pearson Centered distance metric and a Centroid linkage rule.

### 7.3.3 Gene classification

To investigate the biological context of transcriptional changes, the role of significant genes in various muscle pathways was investigated. The function of identified genes was investigated using a combination of the NCBI database, gene ontology classification and a broad literature search. Genes were then classified into one of six categories according to their function in muscle: Cytoskeletal, Extracellular Matrix (ECM), Excitation-Contraction (EC) Coupling, Metabolism, Inflammation and Remodeling. The cytoskeletal category included genes involved in cell structure, such as intermediate filaments, and genes encoding contractile proteins, such as myosin isoforms. ECM genes included genes encoding ECM components, such as collagens and proteoglycans, and genes involved in signaling proliferation or breakdown, such as matrix metallopeptidases. The EC Coupling category included genes involved in the function of the neuromuscular junction and genes involved in calcium transport into and out of the sarcoplasmic reticulum. Metabolic genes included those involved in the glycolytic or the fatty acid metabolism pathways as well as genes involved in mitochondrial function and utilization of energy stores such as ATP. Inflammatory genes included genes encoding known inflammatory cell markers, genes involved in response to stress, such as heat shock, and genes promoting or inhibiting portions of the inflammatory pathways. Finally, genes involved in remodeling included those identified as having anabolic or catabolic functions in muscle, such as growth factors and the ubiquitination pathway, genes involved in cell cycle control, genes specific to satellite cells or myoblasts and genes involved in angiogenesis.

The identified categories will inherently have different populations and thus gene ontology (GO) analyses were used to determine if a pathway was over or under represented. GO analyses were performed using a Web-based Gene Set Analysis

Toolkit (WebGestalt; bioinfo.vanderbilt.edu/webgestalt/). In this analysis, a p-value is generated for each pathway based on hypergeometric comparison of the number of genes present in that list to the number of genes expected to be present based on the size of the list.

### 7.3.4   Quantitative real-time PCR

In addition to microarray processing, isolated RNA samples were subjected to quantitative real-time PCR (QPCR) to provide validation of GeneChip expression values and expression levels for genes not on the chip. After RNA was extracted from the muscle and diluted 1:5 with DNase/RNase free water, 1 $\mu$L of each sample was reverse transcribed using standard protocols (Superscript III; Invitrogen). cDNA was amplified with the eppendorf MasterCycler GradientS (Hamburg, Germany) with primers specific to the genes of interest. All primers were tested for cross-reactivity with other transcripts using nBLAST and Oligo (version 6.6; Molecular Biology Insights, Cascade, CO). All samples were run at least in triplicate on a 96 well plate. Each well contained 10 $\mu$L volume made up of the KAPA SYBR FAST Master Mix (2x) Universal (KAPA Biosystems), and forward and reverse primers (Supplementary Table 1).

Amplification conditions were as follows: An initial hold at 95 °C for 2 min was followed by 40 cycles of denaturing at 95 °C for 15 s, followed by annealing/extension at 68 °C for 40 s. The success of each reaction was deduced based on the observation of a single reaction product on an agarose gel and a single peak on the DNA melting temperature curve determined at the end of the reaction. To express QPCR results, the standard curve method was used with the cycles to threshold value representing the PCR cycle number at which the SYBRgreen signal was increased above the threshold. Expression of each gene was normalized to its mean value.

### 7.3.5 Myosin heavy chain isoform determination

Myosin heavy chain (MyHC) isoforms were identified using the gel electrophoresis technique previously described [20]. Briefly, TA muscles ($des^{-/-}$: n=3, $wt$: n=3) were homogenized and centrifuged, and the myofibril-rich pellet was washed and resuspended in buffer supplemented with a protease cocktail (5 $\mu$l of 100 mmol/l PMSF, 10 $\mu$g/$\mu$l leupeptin and 10 $\mu$g/$\mu$l pepstatin A). Protein was then diluted to a concentration of 0.125 mg/ml across all homogenates. Separation of MyHC isoforms was performed with SDS-PAGE on polyacrylamide gels (16 cm x 22 cm, 0.75 mm thickness) for 22 hours at 275 V at 4 °C. Stacking and resolving gels were 4% and 8% polyacrylamide respectively. Following migration, gels were silver stained according to manufacturers instructions (Bio-Rad, Hercules, CA). MyHC isoform (IIa, IIx, and IIb) bands were identified by their relative electrophoretic mobilities. Band intensity was quantified using densitometry (Quantity One, Bio-Rad).

### 7.3.6 Isolated skeletal muscle insulin stimulation

Insulin sensitivity was measured in soleus muscles from adult ($des^{-/-}$: n=8, $wt$: n=7) and aged ($des^{-/-}$: n=6, $wt$: n=5) mice by the 2DOGU technique described previously [21]. Briefly, mice were fasted for four hours, weighed, then anaesthetized via intraperitoneal injection (Nembutal 150 mg/kg). Fasting glucose was measured using the glucose oxidase method with a blood glucose meter (Contour, Bayer) and blood sampled from the tail vein and the epidydimal fat pad was dissected and weighed. The soleus muscle from each hindlimb was dissected for insulin stimulation. Paired soleus muscles were incubated at 35 °C for 30 min in oxygenated (95% O2, 5% CO2) flasks of Krebs-Henseleit buffer (KHB) containing: 0.1% BSA, 2 mM Na-pyruvate, and 6 mM mannitol. One muscle per pair was incubated without insulin and the contralateral muscle with insulin (60 $\mu$U/mL [0.36nM]). After 30 min, muscles were transferred to a second flask and incubated at 35 °C for 20 min in KHB plus 0.1% BSA, 9 mM [14C]-mannitol (0.053 mCi/mmol; PerkinElmer), and 1 mM [3H]-2DG (6 mCi/mmol; PerkinElmer) with the same insulin concentration as in the first incubation. After the second incu-

bation phase, muscles were blotted on ice-cold filter paper, trimmed and freeze-clamped, and then were stored ($-80\,^\circ$C). 2DOGU rate was calculated as previously described [21].

Paired soleus muscles were then homogenized. Equal amounts of protein (30 $\mu$g) were boiled for 5 minutes in 1x laemmli sample buffer and separated on 7% gels by SDS-polyacrylamide gel electrophoresis (PAGE) as previously described [22]. Primary antibodies used for immunoblotting were from Cell Signaling Technology (p-AktSer473, Cat#9271; Akt, Cat#9272). Antibody binding was detected using an enhanced chemiluminescence horse raddish peroxidase substrate detection kit (Bio-Rad). Imaging and band quantification were carried out using a ChemiDoc XRS-plus imaging system (Bio-Rad).

### 7.3.7   Data processing

Torque data was acquired via customized LabView software and analyzed using Matlab. All data was subjected to either a one or two-way ANOVA with repeated measures where appropriate. Significance was set at $\alpha < 0.05$ and all error bars represent mean $\pm$ SEM. Statistical tests used for specific datasets are as listed in the text.

## 7.4   Results

### 7.4.1   Eccentric contraction induced injury

Dorsiflexion torque was measured prior to, immediately following and 12 hours after the eccentric contraction (EC) bout at an ankle angle ($\alpha$) of $90\,^\circ$. Isometric torque was also recorded at $\alpha = 52\,^\circ$ immediately prior to each eccentric contraction (Fig. 7.1A, horizonal line) to evaluate the torque decline during the EC bout. $Des^{-/-}$ dorsiflexors experienced a unique response to the EC bout compared with $wt$ (Fig. 7.1B). Initial isometric torque was significantly lower in $des^{-/-}$ muscles compared to $wt$ at both ages (p<0.05). However, during the EC bout, torque dropped significantly in the $wt$ groups (p<0.001, adult: 32.7$\pm$3.6%, aged:
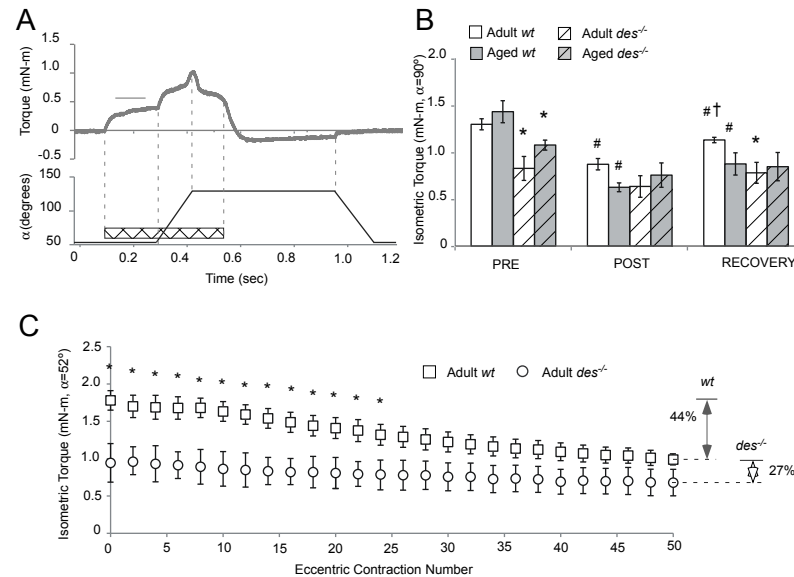
Figure 7.1: $Des^{-/-}$ dorsiflexors exhibit a differential response to an EC bout compared with *wt*. A) A sample EC torque record resulting from stimulation of the hindlimb dorsiflexors (gray). The hatched bar marks the timecourse of stimulation and is superimposed on the ankle angle ($\alpha$). While $\alpha$ remains constant at $\alpha=52\,°$, the contraction is isometric (denoted by a horizontal bar above the torque trace), but as $\alpha$ begins to increase, the contraction becomes eccentric as dorsiflexors are simultaneously stimulated and stretched. B) $Des^{-/-}$ dorsiflexors produce less isometric torque initially (PRE), exhibit a smaller force drop following the EC bout (PRE-POST) and show less recovery 12 hours post bout (POST-RECOVERY). $*p<0.05$ compared to age matched *wt*, # $p<0.05$ compared to PRE, $†p<0.05$ compared to POST, determined by one-way ANOVA with repeated measures. C) Adult $des^{-/-}$ dorsiflexors experience less isometric torque drop than *wt* during the EC bout. Isometric torque prior to every other EC is plotted as a function of EC number for clarity. The torque decrease is quantified by arrows to the right of the plot for each group and the torque drop as a percentage of initial torque is noted. Similar results are seen for aged groups (not shown). $*p<0.05$ as determined by two-way ANOVA with repeated measures and Tukey post-hoc correction.

$55.5\pm6.1\%$) but did not in $des^{-/-}$ (p>0.05, adult: $24.7\pm4.1\%$, aged: $30.3\pm10.9\%$) resulting in no significant torque differences between genotypes post EC. Following 12 hours of recovery, isometric torque production improved significantly in the adult $wt$ group (p<0.01) though it did not fully return to its pre-EC value, consistent with published data [10]. However, torque production did not improve significantly in $des^{-/-}$ groups (p>0.1). Thus, $des^{-/-}$ dorsiflexors produced lower isometric torque, experienced less torque drop following EC and subsequently exhibited reduced recovery. This is also evident in torque measurements during the course of the EC bout where a larger progressive decrease in torque is seen in $wt$ muscles relative to $des^{-/-}$ (Fig. 7.1C). Though $des^{-/-}$ muscles initially produce significantly less isometric torque, there is no longer a significant difference between genotypes by EC number 26.

## 7.4.2   Gene expression as a function of desmin, age and EC

Microarray data was divided according to three descriptors, desmin ($des^{-/-}$, $wt$), age (adult, aged) and EC (EC, control), and subjected to three-way ANOVA (Fig. 7.2). Desmin and age were the most sizeable factors in differential gene expression in muscle. Three-way ANOVA identified 1880 genes with a main effect of desmin and 1384 genes with a main effect of age. Interestingly there were 2011 genes with a significant age-desmin interaction indicating that not only is $des^{-/-}$ muscle inherently different from $wt$, it also ages differently. By comparison, the effect of EC is minor, with only 437 genes with a main effect. However, there are 77 genes with a significant desmin-EC interaction suggesting that $des^{-/-}$ muscle is responding to EC differently than $wt$ at the transcriptional level as well as at the mechanical level. There were no genes with a significant age-EC interaction suggesting that the EC response is similar at both ages, and there were no genes with a significant desmin-age-EC interaction. Expression of a subset of differentially regulated genes was confirmed with QPCR (Fig. D.1).
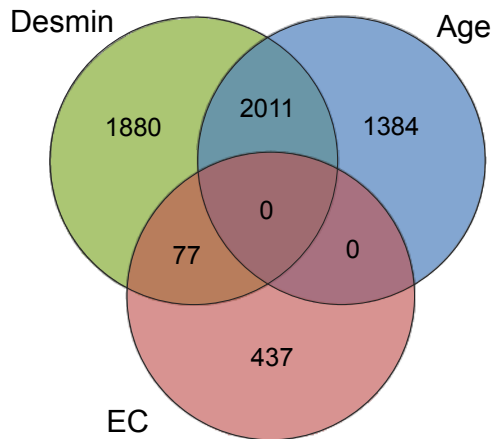
Figure 7.2: Three-way ANOVA identifies differentially expressed genes as a function of desmin, age and EC. The number of genes with a main effect of desmin ($des^{-/-}$, $wt$), age (adult, aged) and EC (EC, control) are noted in colored circles. The number of genes with significant interaction terms are noted in the overlap between appropriate circles. The main effect of desmin, the main effect of age and the interaction between desmin and age accounted for the largest number of genes.

## 7.4.3 The effect of desmin deletion on transcriptional EC response

Of the 77 genes with a significant interaction between desmin and EC, the majority (65) also had a significant main effect of treatment suggesting that the same genes are involved in the $des^{-/-}$ and $wt$ response to EC but regulation of their expression is different between genotypes. 50% of these genes with a known function are classified as being involved in remodeling (Fig. 7.3A) (Table D.2). Several genes known to be primary players in muscle remodeling in response to injury are classified in this category, including myosin binding protein H (Mybph), xin actin-binding repeat containing 1 (Xirp1), BCL2-associated athanogene 3 (Bag3), regulator of calcineurin 1 (Rcan1), musculoskeletal, embryonic nuclear protein 1 (Mustn1) and myogenic transcription factors myogenic differentiation 1 (Myod1) and activating transcription factor 3 (Atf3) [10, 23–25]. The genes classified in the inflammation category are primarily involved in the cellular response to stress and
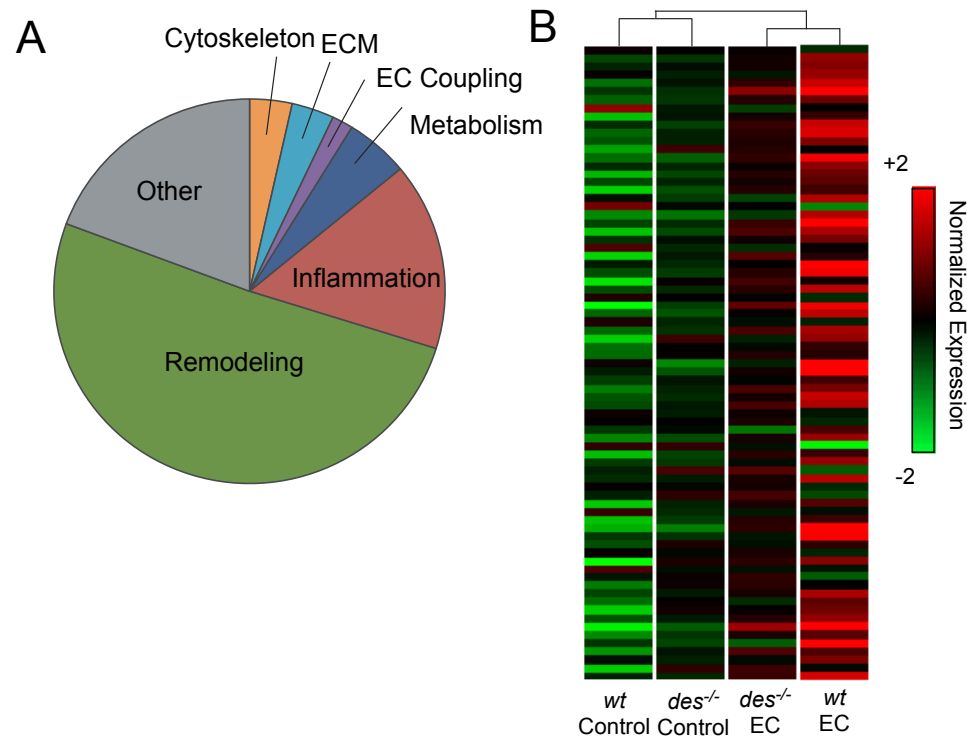
Figure 7.3: Gene expression is differentially regulated in $des^{-/-}$ muscle following EC. A) The function of genes with a significant desmin-EC interaction term as determined by three-way ANOVA was investigated and categorized according to six divisions important to muscle physiology. Remodeling was the most represented category, containing 50% of the genes. B) A heatmap of expression of genes classified in A illustrates patterns of gene expression in control and EC muscle from $des^{-/-}$ and $wt$. A clear difference is apparent between control and EC $wt$ muscle, visualized by the green and red color schemes, respectively. Both control and EC $des^{-/-}$ samples have intermediate expressions of the majority of genes. Hierarchical clustering is indicated at the top of the heat map by horizontal connecting lines. The groups with the most similar expression pattern are $des^{-/-}$ EC and $wt$ EC.

include several heat shock proteins. The one exception was Il1r1, the receptor for interleukin-1$\beta$, a primary upstream driver of the inflammatory pathway in muscle [26]. Representation of the other categories was low in comparison to remodeling and inflammation. Consistent with gene classification results, GO pathway analysis identified the genes with a significant desmin-EC interaction as being primarily involved in MAP kinase signaling (GO:0033549, $p<0.05$ and GO:0017017, $p<0.05$). MAP kinase signaling pathways are activated by a variety of environmental stressors, including exercise, and are involved in the regulation of cellular growth, differentiation and survival [27, 28].

A hierarchical clustering algorithm based on the 77 genes with a significant desmin-EC interaction, separates $des^{-/-}$ and $wt$ controls in one cluster and $des^{-/-}$ and $wt$ EC groups in another cluster based on similarities in expression patterns (Fig. 7.3B). If the expression of each gene in each group is compared in a heatmap, the $wt$ EC group clearly differentiates itself from $wt$ control by its primarily red rather than green color scheme, indicating that the majority of genes are upregulated with EC. By comparison, the $des^{-/-}$ EC shows a more muted increase in expression relative to control, indicating a damped response to EC. However, inspection of the heat map shows that the expression of these genes in $des^{-/-}$ control samples is intermediate between $wt$ control and $wt$ EC suggesting a low level of injury response in control $des^{-/-}$ muscle.

## 7.4.4 The effect of desmin deletion on the transcriptional response to aging

Three-way ANOVA identified 2011 genes with a significant age-desmin interaction, more genes than had a significant main effect of age or desmin, indicating that $des^{-/-}$ muscle ages differently than $wt$. Genes with a significant age-desmin interaction and greater than a 2-fold change between genotypes at either age were classified according to function (Table D.3). The majority of these genes fell into the categories of remodeling (23%), inflammation (17%) and metabolism (17%), though ECM (12%), cytoskeleton (7%) and EC coupling (7%) categories were also well represented (Fig. 7.4A). This suggests that differential aging in $des^{-/-}$ muscle
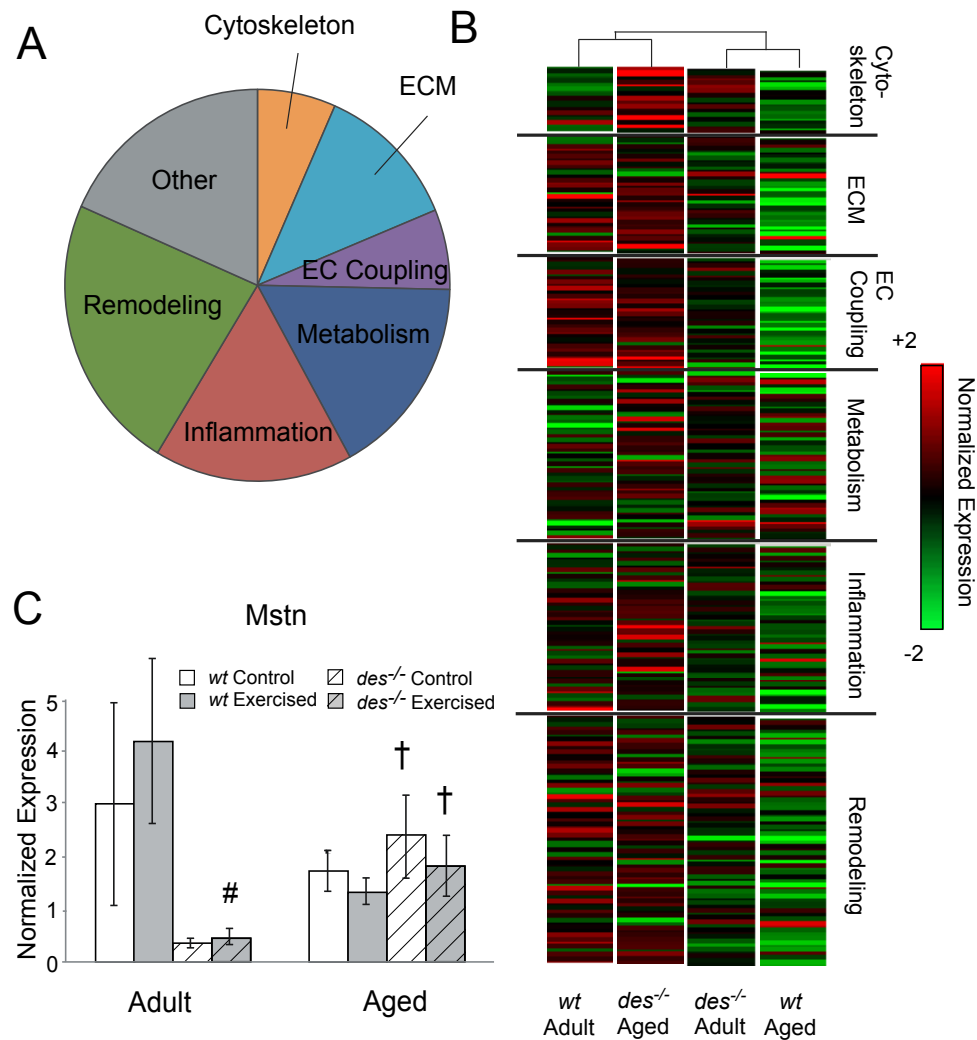
Figure 7.4: Gene expression is differentially regulated in $des^{-/-}$ muscle with age. A) The function of genes with a significant desmin-age interaction term as determined by three-way ANOVA was investigated and categorized according to six divisions important to muscle physiology. B) A heatmap of expression of genes classified in A illustrates patterns of gene expression in control muscle from adult and aged $des^{-/-}$ and $wt$. Expression values for genes are categorized according to the divisions defined in A. Surprisingly, hierarchical clustering, as indicated by horizontal lines at the top of the heat map, groups adult $des^{-/-}$ with aged $wt$ and aged $des^{-/-}$ with adult $wt$. C) Expression of the myostatin gene (Mstn) as determined by QPCR. Expression increases with age in the $des^{-/-}$ samples but remains unchanged in $wt$ resulting in a significant desmin-age interaction. # $p<0.05$ compared to age and treatment matched $wt$, †$p<0.05$ compared to genotype and treatment matched adult.

occurs across the spectrum of physiology from fuel consumption to structure. Hierarchical clustering on these genes identifies adult $des^{-/-}$ and aged $wt$ as having similar expression patterns, suggesting $des^{-/-}$ muscle may be experiencing some signs of early senescence (Fig. 7.4B). However, if the heat map of gene expression is subdivided into the physiological categories, clear differences in expression patterns can be seen between aged $des^{-/-}$ and $wt$, especially in the categories of cytoskeleton and EC coupling, indicating more changes are occurring in $des^{-/-}$ muscle than simply an accelerated aging process.

## 7.4.5 Remodeling, inflammation and fibrosis in $des^{-/-}$ muscle

Many genes identified as major players in the muscle hypertrophy and atrophy pathways are differentially regulated with age in $des^{-/-}$ muscle, including downstream targets of insulin-like growth factor 1: thymoma viral proto-oncogene 1 (Akt1), phosphatidylinositol 3-kinase, regulatory subunit, polypeptide 2 (Pik3r2, p85 $\beta$), tuberous sclerosis 1/2 (Tsc1 and Tsc2) and forkhead box O3 (Foxo3) [26, 29]. Additionally, several genes were differentially regulated that have been implicated in mechanotransduction, linking external mechanical stresses to muscle turnover: Jun-B oncogene (Junb), FBJ osteosarcoma oncogene (Fos), mitogen-activated protein kinase kinase 1 (Map2k1) and mitogen-activated protein kinase 14 (Mapk14) [26, 30, 31]. Additionally, myogenic transcription factors, myogenin (Myog) and myogenic transcription factor 5 (Myf5), and more than 20 genes involved in ubiquitin-mediated protein degradation were differentially regulated with aging. Myostatin, a protein involved in the negative regulation of skeletal muscle growth, was not included in the mouse GeneChip, and thus expression values of the myostatin gene (Mstn) were determined by QPCR. Mstn expression values increase significantly in both control and EC $des^{-/-}$ muscle with age, but remain the same in $wt$ groups, resulting in a significant desmin-age interaction as determined by three-way ANOVA.

Several fundamental components of the inflammatory pathway are also differentially regulated with age, including interleukin 6 (Il6) and its receptor

(Il6ra), interferon gamma receptor 1 (Ifngr1) and suppressor of cytokine signaling 3 (Socs3), which is a known activator of nuclear factor $\kappa\beta$ [26, 32]. Also in this category are genes involved in the inflammatory response to stress, including heat shock factors 1 and 2 (Hsf1, Hsf2), nitric oxide synthase 1 (Nos1) and over 15 other heat shock related proteins. Additionally, genes involved in the fibrotic pathway were differentially regulated with age, including transforming growth factor $\beta$ (Tgfb1), and its receptor (Tgfbr3) and CCAAT/enhancer binding protein (C/EBP), beta (Cebpb), which is involved in the regulation of fibrotic inflammatory signals [33, 34]. Consistent with differential regulation of the fibrotic pathway, genes involved in the structure of the ECM are also differentially regulated with age including the genes for collagens I, III, IV, V, VI and XV (Col1a1, Col3a1, Col4a1, Col4a2, Col5a1, Col5a2, Col5a3, Col6a1, Col6a2, Col15a1) and laminins $\beta$1 and $\gamma$1 (Lamb2, Lamc1). These results are consistent with recent studies that have identified signs of increased inflammation and regeneration in $des^{-/-}$ muscle as well a progressive accumulation of ECM with age [6, 7].

## 7.4.6 Fiber type specific expression in $des^{-/-}$ muscle

The majority of genes with a significant desmin-age interaction that were categorized as being part of the muscle cytoskeleton were components of the contractile apparatus associated with the slow (type I) fiber type (Fig. 7.5A). These included the slow muscle isoforms of myosin heavy chain (Myh7), myosin light chain (Myl3), the T, I and C components of the troponin complex (Tnnt1, Tnni1, Tnnc1), tropomyosin (Tpm3) and the Z-disk associated protein myozenin (Myoz2) [26, 35]. Additionally, several genes classified as being part of EC coupling are also part of the slow fiber pathway including ATPase (Atp2a2), calsequestrin (Casq2) and calcium/calmodulin-dependent protein kinase II, alpha (Camk2a) [36]Smith:0xPw2hjc. The expression of all of these genes is more than 2-fold increased in $des^{-/-}$ muscle compared to $wt$ in aged samples, but not in adult (Fig. 7.5A). Interestingly, one of the primary genes involved in the control of fiber type switching from fast to slow, peroxisome proliferative activated receptor, gamma, coactivator $1\alpha$ (Ppargc1a a.k.a PGC-$1\alpha$) is 2-fold downregulated in
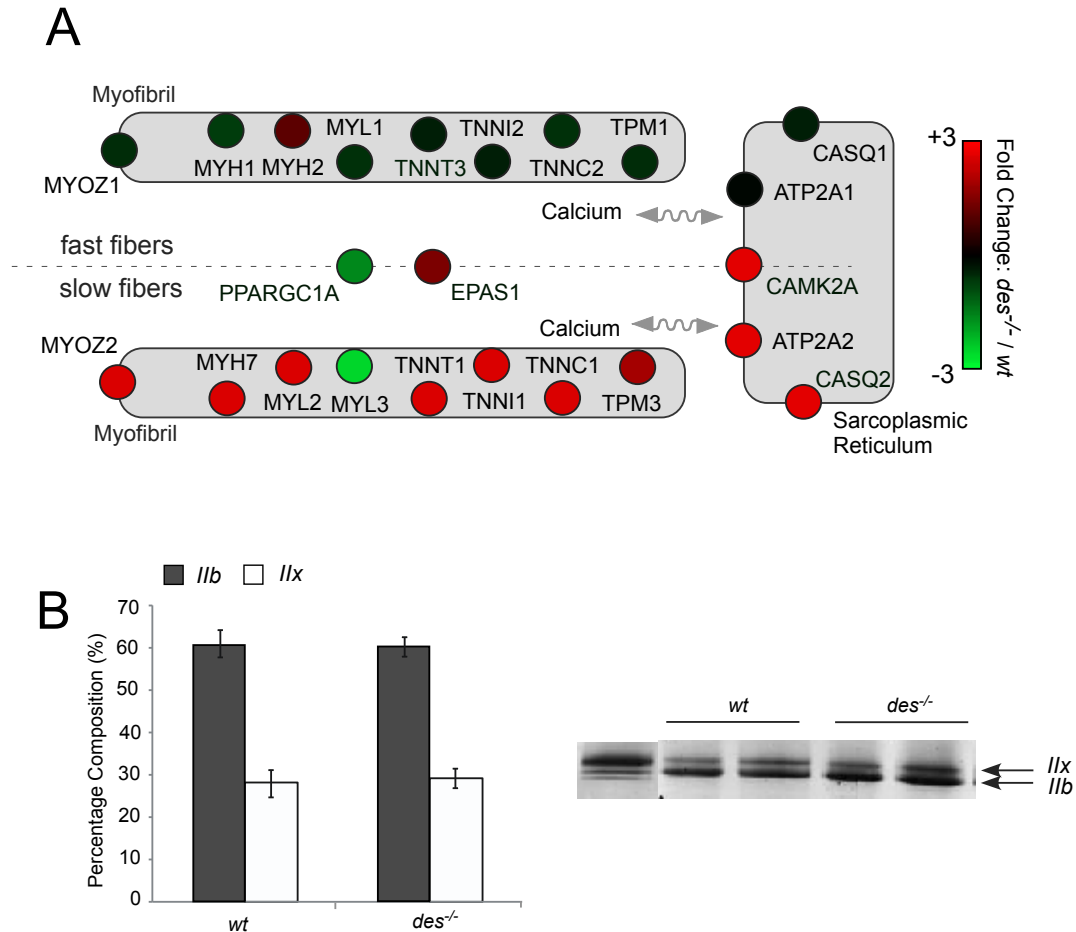
Figure 7.5: $Des^{-/-}$ muscle experiences fiber type specific expression changes with age. A) A schematic of genes involved in the slow fiber program including fold changes in expression in aged $des^{-/-}$ muscle over aged $wt$. Slow isoforms of genes are shown below the dotted division and fast isoforms are shown above. The majority of slow isoform genes have high fold changes, indicating increased expression of the slow fiber program in aged $des^{-/-}$ muscle. Three genes that are not specific to fast or slow fibers but are involved in the fiber type switch are depicted on the dotted division. B) Relative expression of myosin heavy chain isoforms IIb and IIx is not significantly different between genotypes.

aged $des^{-/-}$ muscle compared to *wt*, which might suggest a preferentially fast fiber type in aged $des^{-/-}$ muscle. However, endothelial PAS domain protein 1 (Epas1 a.k.a. HIF-2$\alpha$), a mediator of the PGC-1$\alpha$ fiber type switch was elevated 2 fold in aged $des^{-/-}$ muscle [36, 37]. Surprisingly, however, no significant increase in the slower type myosin heavy chain type IIb was detected between aged $des^{-/-}$ and *wt* (Fig. 7.5B).

## 7.4.7 Peripheral fat accumulation and insulin resistance in $des^{-/-}$ muscle

Several genes with a significant desmin-age interaction that were categorized as being involved in metabolism have been shown to regulate the insulin signaling pathway (Fig. 7.6A). Specifically, three negative regulators of insulin signaling were substantially increased in aged $des^{-/-}$ muscle compared with aged *wt*, including fetuin beta (Fetub), a putative inhibitor of insulin receptor tyrosine kinase activity, and toll-like receptor 4 (Tlr4) and inhibitor of kappaB kinase beta (Ikbkb), which when activated are known to lead to inhibition of IR substrate 1 (IRS1) signaling (Olivier et al., 2000; Mathews et al., 2006; Tsukumo et al., 2007). Additionally, an inhibitor of thymoma viral proto-oncogene 1 (Akt1), tribbles homolog 3 (Trib3) was increased in aged $des^{-/-}$ muscle [38]. Consistent with a negative regulation of the insulin signaling pathway, serum/glucocorticoid regulated kinase 1 (Sgk1), a downstream target of PI3K that is also involved in glucose transporter type 4 (Slc2a4 a.k.a. GLUT-4) translocation was 2.5-fold lower in aged $des^{-/-}$ muscle [39]. This combined with an increase in Trib3 expression suggests that insulin-stimulated glucose uptake by $des^{-/-}$ muscle may be impaired. Additionally, three isoforms of pyruvate dehydrogenase kinase (Pdk2, Pdk3, Pdk4), which inhibit pyruvate dehydrogenase activity, were differentially regulated with age in $des^{-/-}$ muscle suggesting further potential alterations in glucose metabolism [40].

In addition to genes involved in muscle insulin signaling, two genes involved in singlaing related to leptin, which controls appetite and feeding behavior, were upregulated in aged $des^{-/-}$ muscle compared with *wt*. The leptin gene was not included on the GeneChip, but CCAAT/enhancer binding protein (C/EBP), alpha
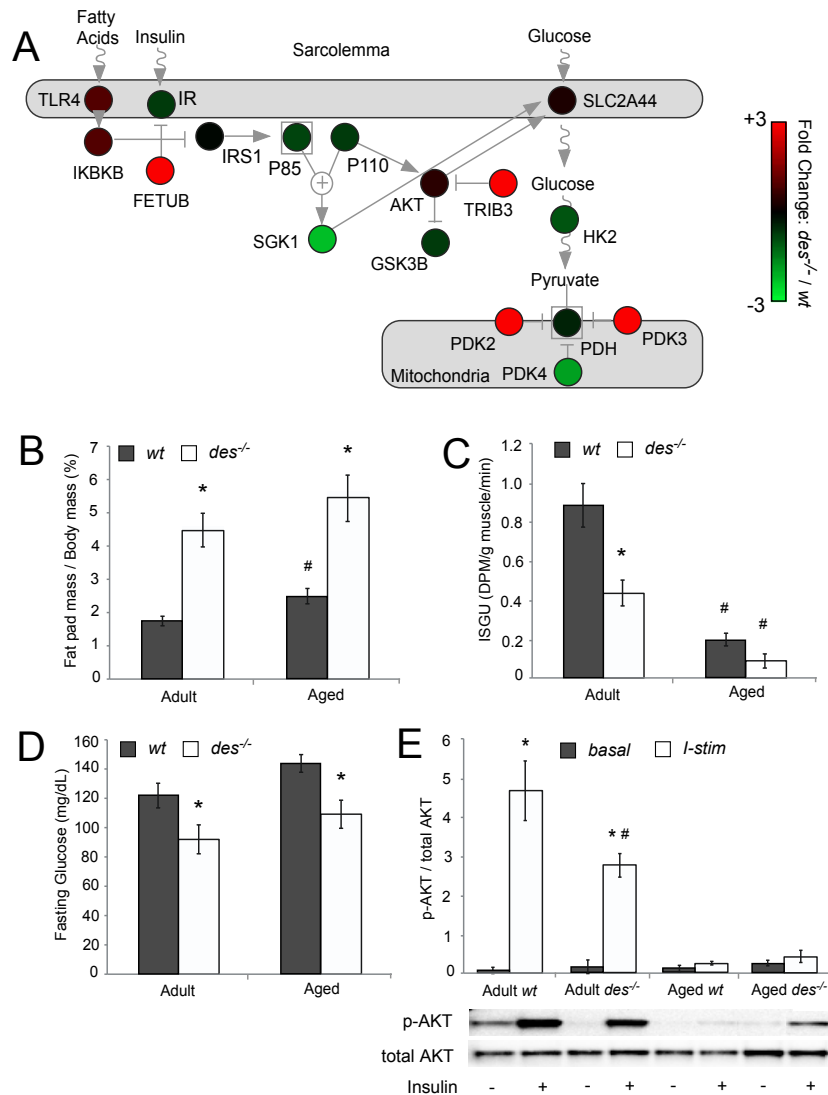
Figure 7.6: $Des^{-/-}$ mice have increased fat mass and decreased muscular insulin sensitivity. A) A schematic of genes involved in insulin stimulated glucose uptake in muscle including fold changes in expression in aged $des^{-/-}$ muscle over aged $wt$. B) $Des^{-/-}$ mice have a significantly increased fat pad to body mass ratio over $wt$ mice. C) Insulin stimulated glucose uptake (ISGU) in the soleus muscle is significantly impaired in the adult $des^{-/-}$ group compared with $wt$. D) $Des^{-/-}$ mice have significantly decreased blood glucose levels following four hours of fasting. *p<0.05 compared to age matched $wt$, # p<0.05 compared adult, same genotype. E) Insulin stimulated Akt phosphorylation is significantly reduced in isolated adult $des^{-/-}$ soleus muscle compared to $wt$, though basal levels are unchanged. Images of phosphorylated Akt and total Akt western blots are shown below the graph. *p<0.05 compared to basal, # p<0.05 compared $wt$, same age.

(Cebpa), an inhibitor of leptin was 3-fold increased and agouti related protein (Agrp), a downstream target of leptin was more than 30-fold increased. Expression increases in both of these genes have been shown to promote appetite and weight gain [41]. Adult and aged $des^{-/-}$ mice have increased accumulation of peripheral fat compared with $wt$ (p<0.05) as determined by the epidydimal fat pad mass as a percentage of body mass (Fig. 7.6B). This increase was due only to an increase in fat mass as body masses were not significantly different between genotypes.

Consistent with gene changes that suggest lower insulin sensitivity in $des^{-/-}$ muscle, insulin-stimulated glucose uptake in isolated soleus muscles was significantly reduced in adult $des^{-/-}$ muscle compared with $wt$ (p<0.01) and was reduced in aged $des^{-/-}$ muscle compared with aged $wt$, although this did not reach significance (p>0.05) (Fig. 7.6C). Despite the aforementioned changes in gene expression and skeletal muscle insulin action, fasting blood glucose levels were significantly lower in adult and aged $des^{-/-}$ mice compared with $wt$ (p<0.05) (Fig. 7.6D). Insulin stimulated Akt1 phosphorylation levels in the adult $des^{-/-}$ soleus were significantly reduced compared with adult $wt$ (p<0.05) despite no significant difference in basal values (p>0.1) (Fig. 7.6E). In aged muscles, however, there was not a significant increase in Akt1 phosphorylation following insulin stimulation over basal values, and no difference in the response between genotypes (p>0.05).

## 7.5  Discussion

An exercise bout of 50 eccentric contractions, though minimally invasive, is still a substantial insult to muscle. Tetanic isometric torque drops as much as 50% following the bout and takes a full 7 days to recover to its pre-EC value [10]. Additionally, eccentrically exercised muscle shows significant histological signs of injury including localized myofibrillar disruption, loss of membrane integrity and infiltration of inflammatory cells [3, 42]. It is surprising then that the effect of desmin is the primary driver of differential gene expression in this study (Fig. 7.2). From a transcriptional standpoint, this data suggests that a muscle lacking desmin is less similar to a $wt$ muscle than an injured muscle is to a noninjured muscle or

than an aged muscle is to a young muscle. This data also indicates that not only are $des^{-/-}$ muscles different transcriptionally than $wt$, they respond differently to both injury and aging. This suggests that desmin plays a role in the cellular response to these "stressors."

Desmin has long been hypothesized to play a role in muscular response to EC induced injury, but the nature of that role remains unclear [3–5]. Desmin filaments distribute externally applied strain among sarcomeres, which could prevent excessive sarcomere lengthening by coupling sarcomeres to a stiffer "anchor" or could act to promote excessive lengthening by coupling sarcomeres to sites of high strain. Either explanation is possible. Expression data in $des^{-/-}$ muscle indicates a muted response to EC injury. EC response genes identified in injured $wt$ muscle were similarly regulated in $des^{-/-}$ with EC but with smaller changes (Fig. 7.3B). This effect paralleled the muted mechanical response to EC in $des^{-/-}$ dorsiflexors (Fig. 7.1). However, expression of EC response genes was elevated in the $des^{-/-}$ control group compared with $wt$ suggesting that $des^{-/-}$ muscle is already involved in an injury response before the imposed bout. If sites of prior injury in $des^{-/-}$ muscle are more susceptible to damage induced by EC, then further cytoskeletal disruption may not be incurred. It is also possible that the isometric force drop in $wt$ muscle is due in part to dissociation of the desmin network at the injury site, since loss of desmin immunostaining in injured fibers is seen as soon as 5 minutes following EC injury and the EC bout lasted for 50 minutes in this study. More studies are required to test these hypotheses.

A substantial number of genes involved in remodeling and inflammation are differentially regulated in $des^{-/-}$ muscle with age, supporting the hypothesis that control $des^{-/-}$ muscle is injury-responsive. Increased expression of genes involved in inflammation and remodeling in $des^{-/-}$ muscle has been noted previously [7]. Additionally, $des^{-/-}$ muscle has been shown to exhibit signs of increased regeneration, inflammation and fibrosis that increase as a function of age [6, 7]. These results suggest that the differential transcriptional response in aging $des^{-/-}$ muscle may be the result of cycles of injury that result in inflammation and eventual fibrosis and support the hypothesis that desmin acts to protect muscle from injury.

However, many genes classified as being involved in the cytoskeleton, EC coupling and metabolism were also differentially regulated with age in $des^{-/-}$ muscle and do not appear to be related to muscle injury. Based on the expression pattern of these genes, this study identified two additional pathways altered in $des^{-/-}$ muscle: the slow fiber pathway and insulin signaling. A transition to a slower fiber type was noted previously in the $des^{-/-}$ soleus, but no change was seen in fast-twitch muscle such as the gastrocnemius [6]. Similarly, we saw no significant increase in the slower myosin heavy chain type IIb in $des^{-/-}$ TA muscles. It is possible that there is a small increase in slower fiber types that myosin heavy chain electrophoresis was unable to detect.

The mechanism behind a potential transition to a slower fiber type is unclear. Fiber type transitions from fast to slow are seen in endurance trained muscles [43] and in muscles with alterations in calcium handling or calcineurin [44]. It is possible that without desmin to keep sarcomeres laterally aligned, the sarcoplasmic reticulum is being damaged by contraction or stretch, resulting in a transition to slower fiber types. Additionally, in the absence of desmin, mitochondria accumulate in the subsarcolemmal space and may have altered function which could also influence fiber typing [45]. Though progressive inflammation, regeneration and fibrosis are characteristic of dystrophic muscle, the switch to a slower fiber type would be unique to $des^{-/-}$ muscle as dystrophic muscle has been shown to exhibit a switch to a faster fiber type [46].

Many of the metabolic genes differentially regulated with age in $des^{-/-}$ muscle are involved in insulin signaling and glucose metabolism. Specifically, the gene expression of Tlr4, Ikbkb and Trib3, were increased in $des^{-/-}$ muscle. Tlr4 is a receptor that is activated by saturated fatty acids, which leads to activation of Ikbkb, and serine phosphorylation of IRS-1, and subsequent impairment of insulin-stimulated glucose uptake and Trib3 inhibits insulin-stimulated activation of Akt, which is an integral insulin signaling protein. These results suggest that $des^{-/-}$ muscle may be more insulin resistant, which was supported by evidence of reduced insulin-stimulated glucose uptake (Fig. 7.6C) and Akt phosphorylation in isolated $des^{-/-}$ soleus (Fig. 7.6E). Chronic inflammation has been linked to insulin resis-

tance especially as mediated through Ikbkb signaling [47]. This microarray study identified many genes differentially regulated with age in $des^{-/-}$ muscle which are involved in the inflammatory pathway and thus insulin resistance in $des^{-/-}$ muscle may be the result of chronic inflammation.

It should be noted that muscle insulin sensitivity is closely tied to obesity and $des^{-/-}$ mice have significantly increased fat mass, so it is possible that increased fat was a causative mechanism for the differential gene regulation in insulin signaling. However, insulin mediated glucose uptake values are not correlated with percentage fat or fat pad mass ($r^2$ <0.3). $Des^{-/-}$ mice have been shown to participate less in voluntary exercise than $wt$ mice so it is also possible that their increased adiposity is a result of inactivity [48]. Interestingly, Agrp, a protein that is primarily involved in appetite regulation was one of the most highly upregulated genes in aged $des^{-/-}$ muscle (>30 fold), It is tempting to speculate that increases in Agrp are leading to increased feeding, adiposity and subsequent insulin resistance in $des^{-/-}$ mice, but the mechanism for alterations in a cytoskeletal protein resulting in changes in a neuropeptide are completely unknown.

In conclusion, this study identified pathways involved in the alterations in muscle physiology due to desmin loss, injury and aging. The differential response to injury and aging in muscle lacking desmin suggests that this protein plays a role in physiological adaptation to these muscle "stressors." Though more studies are required to define this role, this study has pointed to new and promising areas of desmin research

## 7.6  Acknowledgements

Chapter 7 in part is currently being prepared for submission for publication of the material "Transcriptional Alterations in Aging and Injured Skeletal Muscle

due to Desmin Deletion." Meyer G.M., Schenk S. and Lieber R.L. The dissertation author was the primary investigator and author of this material.

## 7.7 References

[1] Galou, M., Gao, J., Humbert, J., Mericskay, M., Li, Z., Paulin, D., and Vicart, P., 1997. The importance of intermediate filaments in the adaptation of tissues to mechanical stress: evidence from gene knockout studies. *Biology of the cell / under the auspices of the European Cell Biology Organization*, 89:85–97.

[2] Lazarides, E., 1980. Intermediate filaments as mechanical integrators of cellular space. *Nature*, 283:249–256.

[3] Lieber, R.L., Thornell, L.E., and Fridén, J., 1996. Muscle cytoskeletal disruption occurs within the first 15 min of cyclic eccentric contraction. *Journal of applied physiology (Bethesda, Md : 1985)*, 80:278–284.

[4] Barash, I.A., Peters, D., Fridén, J., Lutz, G.J., and Lieber, R.L., 2002. Desmin cytoskeletal modifications after a bout of eccentric exercise in the rat. *American journal of physiology Regulatory, integrative and comparative physiology*, 283:R958–63.

[5] Sam, M., Shah, S., Fridén, J., Milner, D.J., Capetanaki, Y., and Lieber, R.L., 2000. Desmin knockout muscles generate lower stress and are less vulnerable to injury compared with wild-type muscles. *American journal of physiology Cell physiology*, 279:C1116–22.

[6] Li, Z., Mericskay, M., Agbulut, O., Butler-Browne, G., Carlsson, L., Thornell, L.E., Babinet, C., and Paulin, D., 1997. Desmin is essential for the tensile strength and integrity of myofibrils but not for myogenic commitment, differentiation, and fusion of skeletal muscle. *The Journal of cell biology*, 139:129–144.

[7] Meyer, G. and Lieber, R.. Skeletal muscle fibrosis develops in response to compliant fibers. *The Journal of Physiology, London (In Review)*.

[8] Booth, F.W. and Kirby, C.R., 1992. Changes in skeletal muscle gene expression consequent to altered weight bearing. *The American journal of physiology*, 262:R329–32.

[9] Zambon, A.C., McDearmon, E.L., Salomonis, N., Vranizan, K.M., Johansen, K.L., Adey, D., Takahashi, J.S., Schambelan, M., and Conklin, B.R., 2003. Time- and exercise-dependent gene regulation in human skeletal muscle. *Genome biology*, 4:R61.

[10] Barash, I.A., Mathew, L., Ryan, A.F., Chen, J., and Lieber, R.L., 2004. Rapid muscle-specific gene expression changes after a single bout of eccentric contractions in the mouse. *American journal of physiology Cell physiology*, 286:C355–64.

[11] Yang, Y., Creer, A., Jemiolo, B., and Trappe, S., 2005. Time course of myogenic and metabolic gene expression in response to acute exercise in human skeletal muscle. *Journal of applied physiology (Bethesda, Md : 1985)*, 98:1745–1752.

[12] Meyer, G.A., Kiss, B., Ward, S.R., Morgan, D.L., Kellermayer, M.S.Z., and Lieber, R.L., 2010. Theoretical predictions of the effects of force transmission by desmin on intersarcomere dynamics. *Biophysical journal*, 98:258–266.

[13] Hardin, B.J., Campbell, K.S., Smith, J.D., Arbogast, S., Smith, J., Moylan, J.S., and Reid, M.B., 2008. TNF-alpha acts via TNFR1 and muscle-derived oxidants to depress myofibrillar force in murine skeletal muscle. *Journal of applied physiology (Bethesda, Md : 1985)*, 104:694–699.

[14] Cady, E.B., Jones, D.A., Lynn, J., and Newham, D.J., 1989. Changes in force and intracellular metabolites during fatigue of human skeletal muscle. *The Journal of physiology*, 418:311–325.

[15] Ito, K., Komazaki, S., Sasamoto, K., Yoshida, M., Nishi, M., Kitamura, K., and Takeshima, H., 2001. Deficiency of triad junction and contraction in mutant skeletal muscle lacking junctophilin type 1. *The Journal of cell biology*, 154:1059–1067.

[16] Bottinelli, R., Schiaffino, S., and Reggiani, C., 1991. Force-velocity relations and myosin heavy chain isoform compositions of skinned fibres from rat skeletal muscle. *The Journal of physiology*, 437:655–672.

[17] Milner, D.J., Weitzer, G., Tran, D., Bradley, A., and Capetanaki, Y., 1996. Disruption of muscle architecture and myocardial degeneration in mice lacking desmin. *The Journal of cell biology*, 134:1255–1270.

[18] Lieber, R.L., 1997. Muscle fiber length and moment arm coordination during dorsi- and plantarflexion in the mouse hindlimb. *Acta anatomica*, 159:84–89.

[19] Smith, L.R., Pontén, E., Hedström, Y., Ward, S.R., Chambers, H.G., Subramaniam, S., and Lieber, R.L., 2009. Novel transcriptional profile in wrist muscles from cerebral palsy patients. *BMC medical genomics*, 2:44.

[20] Talmadge, R.J. and Roy, R.R., 1993. Electrophoretic separation of rat skeletal muscle myosin heavy-chain isoforms. *Journal of applied physiology (Bethesda, Md : 1985)*, 75:2337–2340.

[21] Cartee, G.D. and Bohn, E.E., 1995. Growth hormone reduces glucose transport but not GLUT-1 or GLUT-4 in adult and old rats. *The American journal of physiology*, 268:E902–9.

[22] McCurdy, C.E. and Cartee, G.D., 2005. Akt2 is essential for the full effect of calorie restriction on insulin-stimulated glucose uptake in skeletal muscle. *Diabetes*, 54:1349–1356.

[23] Bassel-Duby, R. and Olson, E.N., 2006. Signaling pathways in skeletal muscle remodeling. *Annual review of biochemistry*, 75:19–37.

[24] Kostek, M.C., Chen, Y.W., Cuthbertson, D.J., Shi, R., Fedele, M.J., Esser, K.A., and Rennie, M.J., 2007. Gene expression responses over 24 h to lengthening and shortening contractions in human muscle: major changes in CSRP3, MUSTN1, SIX1, and FBXO32. *Physiological genomics*, 31:42–52.

[25] Warren, G.L., Summan, M., Gao, X., Chapman, R., Hulderman, T., and Simeonova, P.P., 2007. Mechanisms of skeletal muscle injury and repair revealed by gene expression studies in mouse models. *The Journal of physiology*, 582:825–841.

[26] Smith, L., Meyer, G., and Lieber, R.L. Systems analysis of genes related to skeletal muscle function. *Wiley interdisciplinary reviews Systems biology and medicine (In Review)*.

[27] Goodyear, L.J., Chang, P.Y., Sherwood, D.J., Dufresne, S.D., and Moller, D.E., 1996. Effects of exercise and insulin on mitogen-activated protein kinase signaling pathways in rat skeletal muscle. *The American journal of physiology*, 271:E403–8.

[28] Widegren, U., Jiang, X.J., Krook, A., Chibalin, A.V., Björnholm, M., Tally, M., Roth, R.A., Henriksson, J., Wallberg-henriksson, H., and Zierath, J.R., 1998. Divergent effects of exercise on metabolic and mitogenic signaling pathways in human skeletal muscle. *The FASEB journal : official publication of the Federation of American Societies for Experimental Biology*, 12:1379–1389.

[29] Glass, D.J., 2005. Skeletal muscle hypertrophy and atrophy signaling pathways. *The international journal of biochemistry & cell biology*, 37:1974–1984.

[30] Burkholder, T.J., 2007. Mechanotransduction in skeletal muscle. *Frontiers in bioscience : a journal and virtual library*, 12:174–191.

[31] Kramer, H.F. and Goodyear, L.J., 2007. Exercise, MAPK, and NF-kappaB signaling in skeletal muscle. *Journal of applied physiology (Bethesda, Md : 1985)*, 103:388–395.

[32] Tidball, J.G., 2005. Inflammatory processes in muscle injury and repair. *American journal of physiology Regulatory, integrative and comparative physiology*, 288:R345–53.

[33] Ruffell, D., Mourkioti, F., Gambardella, A., Kirstetter, P., Lopez, R.G., Rosenthal, N., and Nerlov, C., 2009. A CREB-C/EBPbeta cascade induces M2 macrophage-specific gene expression and promotes muscle injury repair. *Proceedings of the National Academy of Sciences of the United States of America*, 106:17475–17480.

[34] Serrano, A.L. and Muñoz-Cánoves, P., 2010. Regulation and dysregulation of fibrosis in skeletal muscle. *Experimental cell research*, 316:3050–3058.

[35] Chemello, F., Bean, C., Cancellara, P., Laveder, P., Reggiani, C., and Lanfranchi, G., 2011. Microgenomic analysis in skeletal muscle: expression signatures of individual fast and slow myofibers. *PloS one*, 6:e16807.

[36] Yan, Z., Okutsu, M., Akhtar, Y.N., and Lira, V.A., 2011. Regulation of exercise-induced fiber type transformation, mitochondrial biogenesis, and angiogenesis in skeletal muscle. *Journal of applied physiology (Bethesda, Md : 1985)*, 110:264–274.

[37] Rasbach, K.A., Gupta, R.K., Ruas, J.L., Wu, J., Naseri, E., Estall, J.L., and Spiegelman, B.M., 2010. PGC-1alpha regulates a HIF2alpha-dependent switch in skeletal muscle fiber types. *Proceedings of the National Academy of Sciences of the United States of America*, 107:21866–21871.

[38] Liu, J., Wu, X., Franklin, J.L., Messina, J.L., Hill, H.S., Moellering, D.R., Walton, R.G., Martin, M., and Garvey, W.T., 2010. Mammalian Tribbles homolog 3 impairs insulin action in skeletal muscle: role in glucose-induced insulin resistance. *American journal of physiology Endocrinology and metabolism*, 298:E565–76.

[39] Jeyaraj, S., Boehmer, C., Lang, F., and Palmada, M., 2007. Role of SGK1 kinase in regulating glucose transport via glucose transporter GLUT4. *Biochemical and biophysical research communications*, 356:629–635.

[40] Wu, P., Inskeep, K., Bowker-Kinley, M.M., Popov, K.M., and Harris, R.A., 1999. Mechanism responsible for inactivation of skeletal muscle pyruvate dehydrogenase complex in starvation and diabetes. *Diabetes*, 48:1593–1599.

[41] Mantzoros, C.S. and Moschos, S.J., 1998. Leptin: in search of role(s) in human physiology and pathophysiology. *Clinical endocrinology*, 49:551–567.

[42] Armstrong, R.B., Ogilvie, R.W., and Schwane, J.A., 1983. Eccentric exercise-induced injury to rat skeletal muscle. *Journal of applied physiology (Bethesda, Md : 1985)*, 54:80–93.

[43] Green, H.J., Klug, G.A., Reichmann, H., Seedorf, U., Wiehrer, W., and Pette, D., 1984. Exercise-induced fibre type transitions with regard to myosin, parvalbumin, and sarcoplasmic reticulum in muscles of the rat. *Pflügers Archiv : European journal of physiology*, 400:432–438.

[44] Jordan, T., Jiang, H., Li, H., and DiMario, J.X., 2004. Inhibition of ryanodine receptor 1 in fast skeletal muscle fibers induces a fast-to-slow muscle fiber type transition. *Journal of cell science*, 117:6175–6183.

[45] Milner, D.J., Mavroidis, M., Weisleder, N., and Capetanaki, Y., 2000. Desmin cytoskeleton linked to muscle mitochondrial distribution and respiratory function. *The Journal of cell biology*, 150:1283–1298.

[46] Marshall, P.A., Williams, P.E., and Goldspink, G., 1989. Accumulation of collagen and altered fiber-type ratios as indicators of abnormal muscle gene expression in the mdx dystrophic mouse. *Muscle & nerve*, 12:528–537.

[47] Arkan, M.C., Hevener, A.L., Greten, F.R., Maeda, S., Li, Z.W., Long, J.M., Wynshaw-Boris, A., Poli, G., Olefsky, J., and Karin, M., 2005. IKK-beta links inflammation to obesity-induced insulin resistance. *Nature medicine*, 11:191–198.

[48] Haubold, K.W., Allen, D.L., Capetanaki, Y., and Leinwand, L.A., 2003. Loss of desmin leads to impaired voluntary wheel running and treadmill exercise performance. *Journal of applied physiology (Bethesda, Md : 1985)*, 95:1617–1622.

# Chapter 8

# Conclusions

It is increasingly evident that not only is the performance of skeletal muscle not limited to the force-producing sarcomere, where the majority of research has focused, but that these sarcomeres cannot function properly in isolation from the other structures that compose muscle. Examples abound of how alterations to seemingly minor or remote components of muscle have drastic effects on active and passive properties, including muscular dystrophies (disruption of the sarcomere-cell membrane connection), cerebral palsy (aberrant signals at the neuromuscular junction) and rotator cuff tears (loss of connection between muscle and bone) [1–3]. The wide-ranging effects of these disorders highlight the importance of the interactions between muscle components in adaptation and physiology. Muscle is a highly dynamic system, not only in the sense that it experiences continually changing stress and strains, but also in its ability to adapt to environmental cues, adding or reducing mass or length in response to functional demands [4, 5]. To understand the physiology of muscle, to diagnose a myopathy, to target a therapy, it is not sufficient to take a static view where the function of each component is described in isolation, consideration must be made of the dynamic composite.

Deletion of the intermediate filament protein desmin provides an excellent opportunity to study the integrative link between the contractile apparatus in the cell and the extracellular matrix (ECM). The work presented in this dissertation supports a role for desmin in the maintenance of sarcomere integrity and injury prevention.

## 8.1 Sarcomere length heterogeneity is restricted by desmin

The structural arrangement of desmin filaments in the muscle fiber suggests a role in maintaining the lateral integrity of the sarcomere lattice [6]. In support of this hypothesis, $des^{-/-}$ muscle has been shown to have increased Z-disk misalignment and sarcomere disorganization [7, 8]. However, these were static studies on fixed tissue and since high-resolution, real-time sarcomere studies in intact muscle are not technically feasible, the effect of desmin on intersarcomere dynamics was an ideal problem to investigate using modeling. Chapter 2 described the development of a finite element model of a muscle fiber incorporating desmin that simulated intersarcomere dynamics during passive stretch and fixed-end contraction. In the absence of desmin, the model predicted increasing sarcomere length heterogeneity with increasing fiber length and with increasing contraction duration. In simulations incorporating desmin, the mechanical links between sarcomeres distributed strain between neighboring sarcomeres, restricting length discrepancies. In this way, desmin could act to restrict overextension of a weaker sarcomere by linking it to a stronger neighbor (illustrated in Fig. 1.5). The model also predicted that the link desmin provides to the ECM is critical. The ECM is a stabilizing force when linked to the contractile apparatus and acts as much, much "stronger neighbor." Desmin thus provides lines of mechanical "communication" not only within the cell (intersarcomere) but also to the extracellular environment and both are important.

## 8.2 The mechanical properties of both fibers and ECM are altered in the absence of desmin

To investigate alterations in the integrity of muscle fibers and ECM in the absence of desmin, the material properties of both components were defined. Toward this aim, two new methods were developed; the first, described in Chapter 3, extracted the material properties of the ECM from mechanical tests on fibers and

fiber bundles and the second, described in Chapter 4, developed a new model to more comprehensively describe the passive viscoelasticity of muscle fibers. These techniques were implemented in Chapter 5 where fibers from adult $des^{-/-}$ muscle were shown to be significantly more compliant than $wt$ (Fig. 5.1), while fiber bundles were stiffer (Fig. 5.2). Using the technique described in Chapter 3 combined with fiber data, bundle data and immunohistochemistry, ECM in $des^{-/-}$ muscle was shown to first proliferate and then stiffen with age resulting in a fibrotic state. It is tempting to speculate that changes to the ECM are a compensatory response to the increase in fiber compliance, that the muscle is trying to "stiffen up" to protect fibers from damage, but more studies are required to test this hypothesis.

## 8.3 In the absence of desmin, muscle shows signs of chronic injury

Sarcomere overextension is thought to be the primary cause of muscle injury and soreness resulting from eccentric contractions, common in exercise [9–11]. These injuries are highly localized and individual overextended sarcomeres are difficult to indentify, but injured muscle shows characteristic signs of regeneration such as centralized nuclei and small diameter fibers. Results from the finite element model developed in Chapter 2 hypothesize that $des^{-/-}$ muscle should show increased signs of injury and regeneration and indeed it does have a higher percentage of centralized nuclei and small diameter fibers (Fig. 5.7). Additionally, $des^{-/-}$ muscle shows increased expression of many inflammatory genes and genes known to be upregulated in muscle injury and regeneration (Fig. 5.6).

## 8.4 Desmin deletion alters the muscular response to injury and aging

Microarray technology is a powerful tool to investigate potential alterations in many areas of muscle function in one experiment, but it is only useful if gene

expression changes can be interpreted in the context of muscle physiology. In order to provide a framework in which to analyze muscle microarray data, Chapter 6 outlines nine pathways involved in muscle physiology and their constituent genes. Within this framework, areas of muscle physiology differentially affected by altered use in $des^{-/-}$ muscle were identified. In response to eccentric contraction induced injury, $des^{-/-}$ muscle showed both a muted transcriptional response (Fig. 7.2) consistent with its muted mechanical response (Fig. 7.1). However, expression of the genes involved in injury response was increased in $des^{-/-}$ muscle suggesting a low level of injury response. In addition to the remodeling, inflammation and fibrosis discussed previously, the slow fiber and insulin signaling pathways were differentially affected by age in $des^{-/-}$ muscle illustrating again how a defect in one protein with a seemingly simple structural role can have far-reaching effects on the physiology of muscle.

## 8.5   Summary

By providing a mechanical link between sarcomeres and to the ECM, the desmin network can uniformly distribute externally imposed strains, restricting sarcomere overextension. In the absence of desmin, muscle shows signs of increased injury, inflammation and regeneration, which worsen with age. Concurrent with this response is muscle fibrosis, where the ECM adapts by proliferating and stiffening. These results suggest a mechanism where, in the absence of desmin, sarcomeres are overextended during everyday activity because they are not well connected to a stabilizing network. The resulting fibrotic response stiffens the muscle, perhaps as a protective mechanism to compensate for the lack of support inside the fiber. This model of muscle injury, and its subsequent adaptations, is extremely interesting because it is mild, progressive and physiological and provides insight into what is arguably the most common form of muscle damage.

# 8.6 References

[1] Smith, L.R., Lee, K.S., Ward, S.R., Chambers, H.G., and Lieber, R.L., 2011. Hamstring contractures in children with spastic cerebral palsy result from a stiffer extracellular matrix and increased in vivo sarcomere length. *The Journal of physiology*, 589:2625–2639.

[2] BOURNE, G.H. and GOLARZ, M.N., 1959. Human muscular dystrophy as an aberration of the connective tissue. *Nature*, 183:1741–1743.

[3] Nakagaki, K., Ozaki, J., Tomita, Y., and Tamai, S., 1996. Fatty degeneration in the supraspinatus muscle after rotator cuff tear. *Journal of shoulder and elbow surgery / American Shoulder and Elbow Surgeons [et al]*, 5:194–200.

[4] Glass, D.J., 2003. Signalling pathways that mediate skeletal muscle hypertrophy and atrophy. *Nature cell biology*, 5:87–90.

[5] Adams, G.R., 2002. Invited Review: Autocrine/paracrine IGF-I and skeletal muscle adaptation. *Journal of applied physiology (Bethesda, Md : 1985)*, 93:1159–1167.

[6] Lazarides, E., 1980. Intermediate filaments as mechanical integrators of cellular space. *Nature*, 283:249–256.

[7] Shah, S.B., Su, F.C., Jordan, K., Milner, D.J., Fridén, J., Capetanaki, Y., and Lieber, R.L., 2002. Evidence for increased myofibrillar mobility in desmin-null mouse skeletal muscle. *The Journal of experimental biology*, 205:321–325.

[8] Li, Z., Mericskay, M., Agbulut, O., Butler-Browne, G., Carlsson, L., Thornell, L.E., Babinet, C., and Paulin, D., 1997. Desmin is essential for the tensile strength and integrity of myofibrils but not for myogenic commitment, differentiation, and fusion of skeletal muscle. *The Journal of cell biology*, 139:129–144.

[9] Proske, U. and Morgan, D.L., 2001. Muscle damage from eccentric exercise: mechanism, mechanical signs, adaptation and clinical applications. *The Journal of physiology*, 537:333–345.

[10] Fridén, J. and Lieber, R.L., 2001. Eccentric exercise-induced injuries to contractile and cytoskeletal muscle fibre components. *Acta physiologica Scandinavica*, 171:321–326.

[11] Morgan, D.L. and Allen, D.G., 1999. Early events in stretch-induced muscle damage. *Journal of applied physiology (Bethesda, Md : 1985)*, 87:2007–2015.

# Appendix A

# Desmin Stiffness Measurement

Desmin was purified from chicken gizzard under denaturing conditions, following tissue extraction with KI [1]. Samples were stored on ice in 6 M urea for up to six months without noticeable loss of polymerization ability. Prior to testing, desmin filaments were reconstituted by removal of the denaturant and the addition of salt. Briefly, small aliquots were dialyzed against 10 mM TrisHCl (pH 8, 4 °C, 32 h), then against 1 mM NaHCO$_3$ (pH 8, 4 °C, 32 h). Protein aggregates were removed by ultracentrifugation (100,000g, 30 min, 4 °C) and filtration (0.22 $\mu$m membrane filter, Millipore, Bedford, MA). Filament reconstitution was initiated by the addition of imidazole (pH 7, 5 mM final concentration) and MgCl$_2$ (2 mM final concentration). Desmin polymerization was monitored by measuring absorbance due to light scatter (OD at 320 nm) as a function of time.

For AFM measurements, desmin filaments were attached to freshly cleaved mica. A 20 $\mu$l sample of desmin filaments was pipetted onto the mica surface and incubated at room temperature for 25 min. Unbound fibrils were washed away by rinsing with polymerization buffer. Then, non-contact (AC) mode AFM images of the adsorbed filaments were acquired with an MFP3D (Asylum Research, Santa Barbara, CA) AFM instrument. Silicon-nitride cantilevers (Olympus) were used for scanning either in air (AC160TS, resonance frequency 300 kHz) or in liquid (BioLever, lever B, resonance frequency 35 kHz). 512 x 512-pixel images were collected at a typical scanning frequency of 1 Hz.

The elastic properties of desmin were assessed from the fluctuation in the
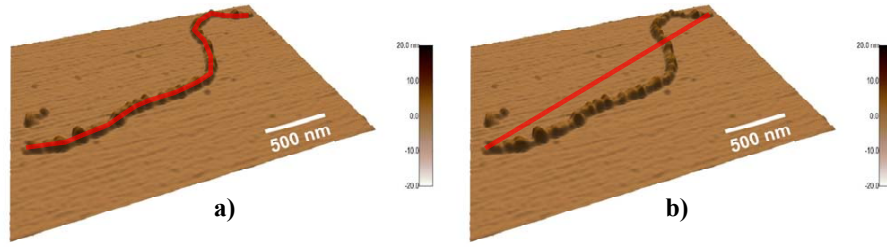
Figure A.1: Atomic Force Microscopy (AFM) images of desmin filaments adsorbed to a mica surface were analyzed for contour length a) and end-to-end distance b).

shape of the filaments adsorbed to mica surface, assuming that desmin filament behavior is similar to that of semi-flexible polymers. Atomic force microscopy (AFM) images of 128 desmin filaments were analyzed for contour length ($L$) and end-to-end distance ($R$) (Fig. A.1). Persistence length ($P$) of the desmin filament was obtained by fitting the mean-square end-to-end distance versus contour length data with the following equation under the assumption that the filaments were equilibrated to the surface [2].

$$R^2 = 4PL \left( 1 - \frac{2P}{L} \left( 1 - e^{\frac{-L}{2P}} \right) \right) \tag{A.1}$$

The elastic modulus (E) was calculated from the persistence length as shown below where I is the area moment of inertia.

$$E = \frac{k_B T P}{I} \tag{A.2}$$

The area moment of inertia for desmin, with a filament diameter (d) of 10 nm is given by the equation below.

$$I = \frac{\pi d^4}{64} \tag{A.3}$$

Persistence and contour length data fit well to the worm-like chain model ($r^2 = 0.97$) and the elastic modulus of a single desmin filament was thus calculated to be 3.7 MPa (Fig. A.2).
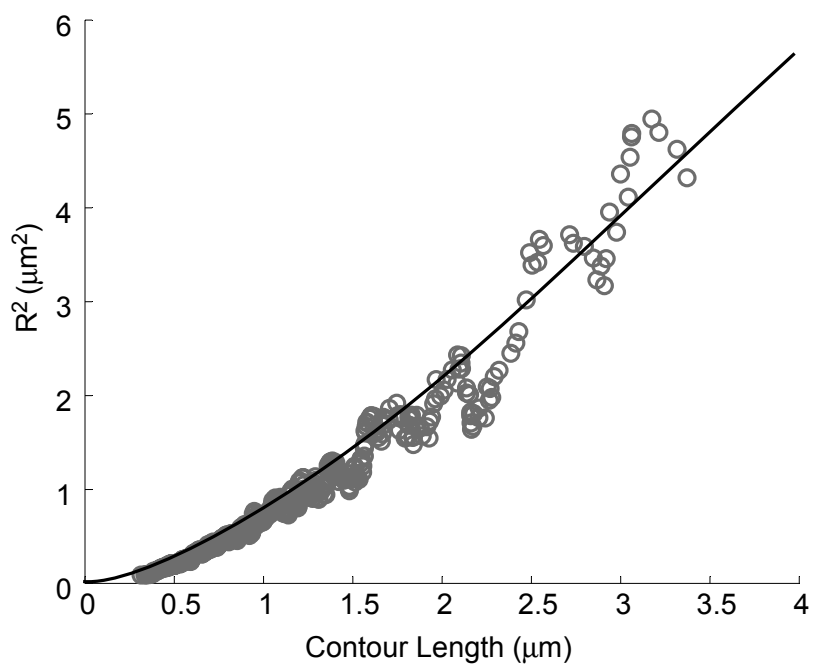
Figure A.2: Mean-square end-to-end distance versus contour length for desmin filaments adsorbed to a mica surface. Data are fit according to Eq. A.1.

# A.1 References

[1] Geisler, N. and Weber, K., 1980. Purification of smooth-muscle desmin and a protein-chemical comparison of desmins from chicken gizzard and hog stomach. *European journal of biochemistry / FEBS*, 111:425–433.

[2] Bustamante, C., Marko, J.F., Siggia, E.D., and Smith, S., 1994. Entropic elasticity of lambda-phage DNA. *Science (New York, NY)*, 265:1599–1600.

# Appendix B

# Details of Comparative Models of Linear Viscosity

## B.1  Hill models of viscoelasticity

The first and most basic model of muscle viscoelasticity was proposed by A. V. Hill [1] in 1938 as a contractile element which provides structural damping under passive conditions in series with a spring which provides transient stiffness to the system under conditions of fast stretch. These two elements are placed in parallel with another spring which provides a time-invariant material stiffness (Fig. B.1A). In the case of passive muscle, this model is equivalent to a standard linear solid model of viscoelasticity, since the contractile element can be represented by a linear dashpot. The Hill model reproduces the basic form of muscle stress relaxation, but fails to accurately reproduce the fast phases of stress decay since it is limited by a single decay rate [2]. Raw data from a mouse muscle fiber during a stress relaxation test to 30% FL at 20 FL/sec (Fig. B.2, black) reveal that the Hill model (Fig. B.2, blue) underestimates the decay rate in short time (inset) and overestimates it in long time as it attempts to describe multiple decay rates with one time constant.

To overcome this limitation, the classic Hill model is frequently modified to include additional branches of a dashpot and a series spring [3–5]. These models
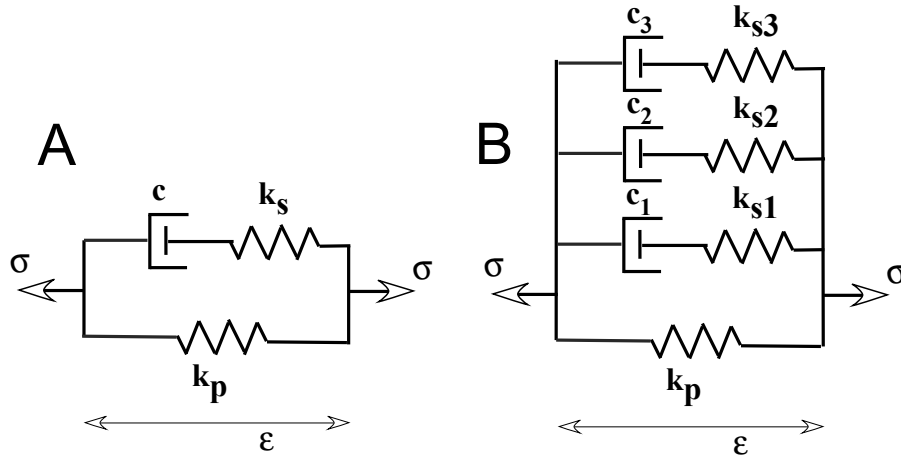
Figure B.1: Schematics of the classic Hill model of muscle viscoelasticity (A) and the 3rd order Hill model (generalized Maxwell model) (B). The contractile element is represented by a dashpot with damping constant c since only passive muscle mechanics are considered here. The series and parallel springs are represented by linear spring constants of modulus $k_s$ and $k_p$ respectively. The 3rd order Hill model includes two additional branches of dashpot and series spring in parallel, which add two additional time constants to the stress decay during relaxation.

can include $n$ number of branches, which provide $n$ number of exponential stress decay rates. The stress response of the $n^{th}$ order Hill model to a strain profile ($\varepsilon$) can be determined by solving the following system of coupled linear differential equations (Eq. B.1).

$$
\begin{aligned}
\dot{\sigma} &= k_p \dot{\varepsilon} + \sum_{i=1}^{n} k_{si} \dot{\varepsilon}_i \\
\dot{\varepsilon}_i &= \dot{\varepsilon} - \frac{k_{si}}{c_i} \varepsilon_i
\end{aligned}
\tag{B.1}
$$

As additional branches are added to the classic Hill model, it is better able to represent the shape of the stress decay. However, each additional branch adds an equation to the system increasing the complexity and the number of parameters. If too many branches are added, some of the parameters become redundant and thus difficult to interpret. Ideally, the minimum number of branches would be added in order to improve the fit to some predetermined tolerance. For the data considered here, the 3rd order Hill model best meets this goal, yielding an $r^2$ value
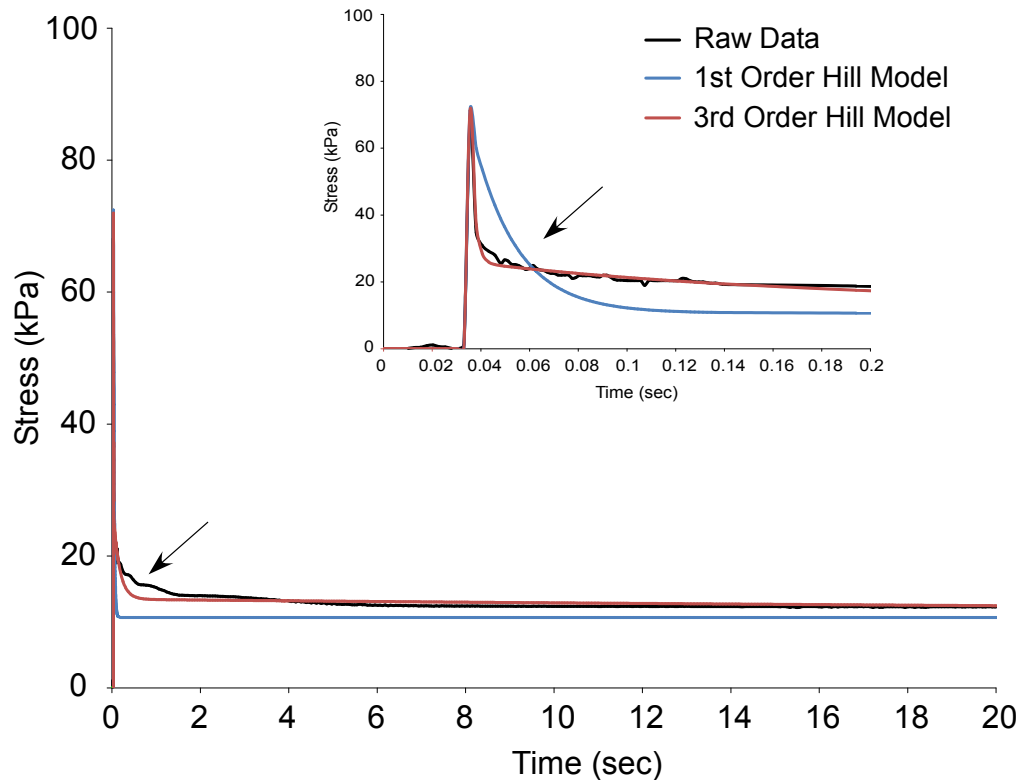
Figure B.2: The 3rd order Hill model better represents stress relaxation data from a mouse muscle fiber than the 1st order Hill structural model. The fiber was stretched to 30% FL at 20 FL/sec to approximate an instantaneous length change. The 3rd order Hill model (red) provides a better fit to the raw data (black) than the 1st order Hill model (blue) during the phase of fast relaxation. Inset shows the data magnified over the first 0.2 seconds of stress relaxation.

of 0.98 with only two additional branches. The 3rd order Hill model fit to the raw data (Fig. B.2, red) provides a much better representation of the stress decay than the classic $1^{st}$ order Hill model though still misestimating the decay rates at some points (arrow).

# B.2   The quasi-linear viscoelastic theory

Quasi-linear viscoelasticity (QLV) was developed to provide a more general formulation of viscoelasticity, which would be more flexible in its ability to describe nonlinear elastic materials. The basic tenet of this model is that viscoelastic

behavior of soft tissues is composed of a nonlinear elasticity superimposed on a linear relaxation. This property is stated mathematically in Equation B.2 where $K(\varepsilon,t)$ is the relaxation function describing the response of the tissue to a infinite rate step elongation from 0 to $\varepsilon$. $G(t)$ is the reduced relaxation function which describes the normalized stress decay and $T^{(e)}(\varepsilon)$ is the elastic response and is a function of strain alone.

$$K(\varepsilon, t) = G(t)T^{(e)}(\varepsilon) \tag{B.2}$$

The elastic function is typically either a polynomial or an exponential similar to the springs in nonlinear versions of structural models. The reduced relaxation function can take many forms, but the two most common use a sum of exponentials [? ] or an exponential integral formulation [2]. The relaxation function that uses $G(t)$ as a sum of exponentials reduces to the solution of the generalized Hill model for infinite rate step strains and thus wont be considered separately. The other commonly used form of the reduced relaxation function is given by Equation B.3, where $E_1(t)$ is the exponential integral [? ].

$$G(t) = \frac{1 + c\left[E_1\left(\frac{t}{\tau_2}\right) - E_1\left(\frac{t}{\tau_1}\right)\right]}{1 + c\ln\left(\frac{\tau_2}{\tau_1}\right)} \tag{B.3}$$

The derivation of the exponential integral formulation of stress relaxation is based on the assumption of a continuous spectrum of relaxation. Essentially, instead of having a discrete number of individual decay rates $(\tau_i)$, $\tau$ is allowed to be a continuous variable changing in time from $\tau_1$ to $\tau_2$.

Equation B.2 applies only to stress responses to instantaneous step changes in strain or approximations thereof, i.e. the infinite rate assumption. It is a specific case of a more general formulation given by Equation B.4.

$$T(t) = \int_{-\infty}^{t} G(t - \tau)\frac{\partial T^{(e)}[\varepsilon(\tau)]}{\partial \varepsilon}\frac{\partial \varepsilon(\tau)}{\partial \tau}d\tau \tag{B.4}$$

To describe the response of a tissue to a generic elongation history, this equation makes use of the superposition principle. It represents a generic response as an infinite sum of relaxation responses to infinitesimally small step-changes in strain. Thus, this model requires that relaxation be a function of time only and that the sample obey superposition.

## B.3   References

[1] Hill, A., 1938. The heat of shortening and the dynamic constants of muscle. In Proceedings of the Royal Society of London Series B.

[2] Best, T.M., McElhaney, J., Garrett, W.E., and Myers, B.S., 1994. Characterization of the passive responses of live skeletal muscle using the quasi-linear theory of viscoelasticity. *Journal of biomechanics*, 27:413–419.

[3] Ito, D., Tanaka, E., and Yamamoto, S., 2010. A novel constitutive model of skeletal muscle taking into account anisotropic damage. *Journal of the mechanical behavior of biomedical materials*, 3:85–93.

[4] Zhang, W., Chen, H.Y., and Kassab, G.S., 2007. A rate-insensitive linear viscoelastic model for soft tissues. *Biomaterials*, 28:3579–3586.

[5] Quaia, C., Ying, H.S., Nichols, A.M., and Optican, L.M., 2009. The viscoelastic properties of passive eye muscle in primates. I: static forces and step responses. *PloS one*, 4:e4850.

# Appendix C

# Supplemental Figures Supporting Fibrosis and Inflammation in $Des^{-/-}$ Muscle

This appendix contains additional information regarding work presented in Chapter 5.

## C.1  References

[1] Joe, A.W.B., Yi, L., Natarajan, A., Le Grand, F., So, L., Wang, J., Rudnicki, M.A., and Rossi, F.M.V., 2010. Muscle injury activates resident fibro/adipogenic progenitors that facilitate myogenesis. *Nature cell biology*, 12:153–163.

[2] Arnold, L., Henry, A., Poron, F., Baba-Amer, Y., van Rooijen, N., Plonquet, A., Gherardi, R.K., and Chazaud, B., 2007. Inflammatory monocytes recruited after skeletal muscle injury switch into antiinflammatory macrophages to support myogenesis. *The Journal of experimental medicine*, 204:1057–1069.

[3] Arora, P.D. and McCulloch, C.A., 1994. Dependence of collagen remodelling on alpha-smooth muscle actin expression by fibroblasts. *Journal of cellular physiology*, 159:161–175.

Table C.1: Forward and reverse primers used for quantitative real-time PCR. Genes are: collagen type I (Col1a1), collagen type III (Col3a1), transforming growth factor $\beta$ (Tgfb1), interleukin-6 (Il6), muscle LIM protein (Csrp3), and insulin-like growth factor (Igf1).

| Gene: | | |
|-------|---------|--------------------------|
| Col1a1 | Foward: | GGCAACAGCCGCTTCACCTAC |
| Col1a1 | Reverse: | GCGGGAGGACTTGGTGGTTTT |
| Col3a1 | Foward: | CACGGAAACACTGGTGGACAGATT |
| Col3a1 | Reverse: | ATGCCAGCTGCACATCAAGGAC |
| Tgfb1 | Foward: | GACTCTCCACCTGCAAGACCAT |
| Tgfb1 | Reverse: | GGGACTGGCGAGCCTTAGTT |
| Il6 | Foward: | CCTTCTTGGGACTGATFigGCTGG |
| Il6 | Reverse: | GCCTCCGACTTGTGAAGTGGT |
| Csrp3 | Foward: | ATCAGAGAAGTGCCCACGATG |
| Csrp3 | Reverse: | GTAAGCCCTCCAAACCCAAT |
| Igf1 | Foward: | AGCAGTCTTCCAACCCAATTA |
| Igf1 | Reverse: | CACGGACAGAGCGAGCTG |

Table C.2: Antibody list used to identify cell populations using flow cytometry. Each antibody is listed along with its conjugated fluorophore, its source and catalog number and a reference indicating what the antibody identifies.

| Antibody: | Conjugated Fluor: | Source: | Reference: |
|-----------|-------------------|---------|------------|
| Sca-1 | FITC | BD Pharmingen #553335 | [1] |
| $\alpha$7-integrin | PE | Ablab | [1] |
| CD34 | AlexaFluor700 | eBiosciences #56-0341-82 | [1] |
| CD31 | EFluor450 | eBiosciences #48-0311-82 | [1] |
| CD45 | EFluor450 | eBiosciences #48-0451-82 | [1] |
| CD11b | FITC | BD Pharmingen #553310 | [2] |
| F4/80 | APC | AB Serotec MCA497AP | [2] |
| Ly-6c | PerCP | eBioscience #45-5932-80 | [2] |
| ER-TR7 | PE | Santa Cruz Biotechnology | [1] |
| $\alpha$SMA | FITC | Abcam (ab8211) | [3] |
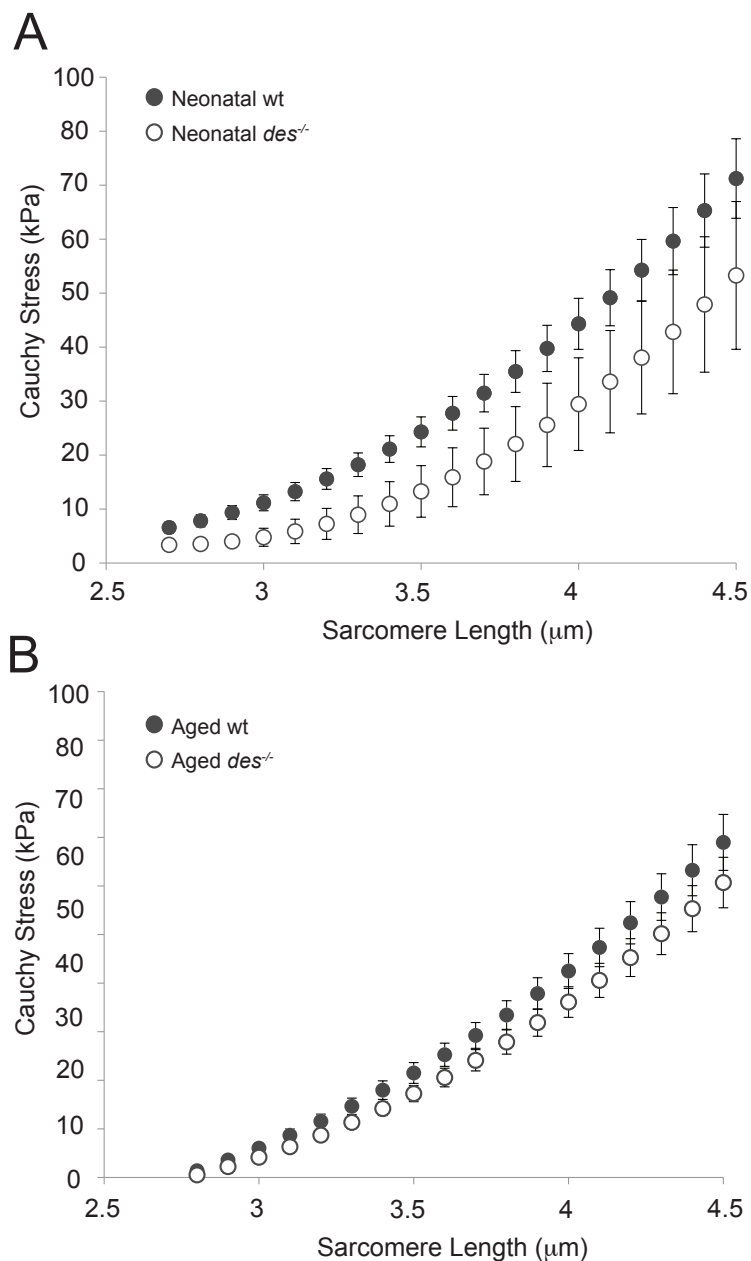
Figure C.1: $Des^{-/-}$ fibers from neonatal and aged muscle showed no significant passive stress difference compared to *wt*. (A) Passive Cauchy stress-sarcomere length quadratic curve-fits for neonatal wt (n=21) and $des^{-/-}$ (n=7) fibers. (B) Passive Cauchy stress-sarcomere length quadratic curve-fits for aged wt (n=16) and $des^{-/-}$ (n=17) fibers.
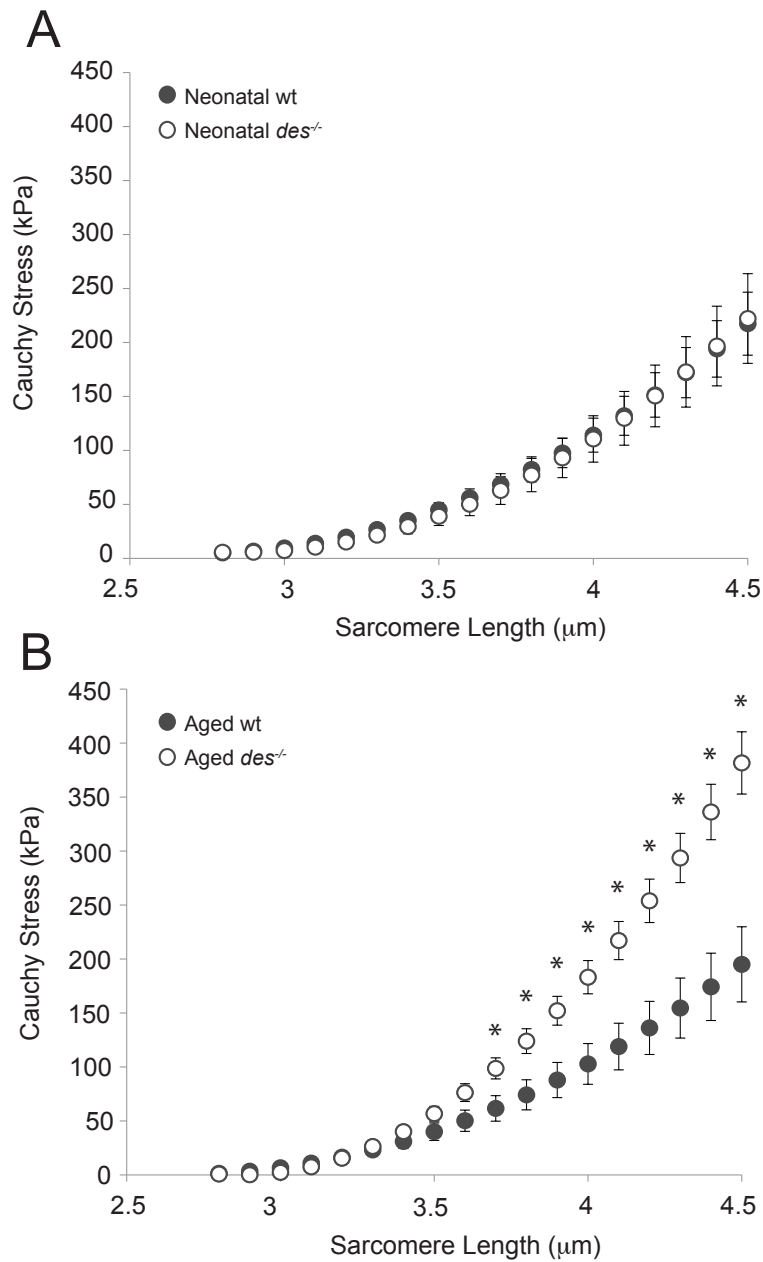
Figure C.2: [$Des^{-/-}$ bundles from aged, but not neonatal, muscle were stiffer compared to *wt*. (A) Passive Cauchy stress-sarcomere length quadratic curve-fits for neonatal *wt* (n=38) and $des^{-/-}$ (n=15) bundles. (B) Passive Cauchy stress-sarcomere length quadratic curve-fits for aged *wt* (n=9) and $des^{-/-}$ (n=15) bundles. Aged $des^{-/-}$ bundles had significantly higher stress compared to *wt* at sarcomere lengths greater than 3.7 $\mu$m as determined by ANOVA with repeated measures.
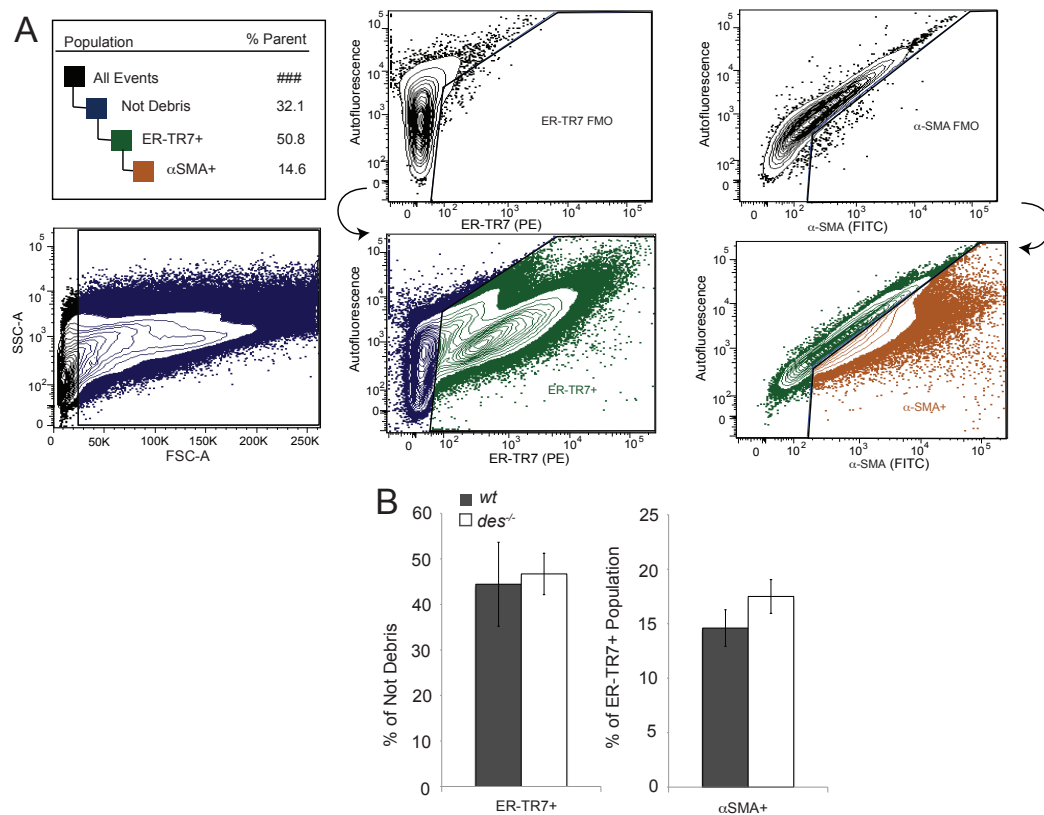
Figure C.3: Identification of fibroblast and myofibroblast populations using flow cytometry. (A) Schematic of the gating tree to identify ER-TR7 and ? smooth muscle actin ($\alpha$SMA) positive populations. All events were first gated to eliminate debris (FSC-A voltage less than 25,000). Further gating was performed on each colors fluorescence-minus-one (FMO) control where the positive/negative gate is drawn with a 1% error rate (shown in black and white with arrows pointing to the implementation of the gates on the sample). The ER-TR7+ gate identified cells positive for ER-TR7 (a reticular fibroblast marker). The $\alpha$SMA+ gate then identified which of the ER-TR7 positive cells are also positive for ?SMA (a marker for the myofibroblast phenotype). Each population is shown color-coded with a legend in the top left indicating the cell number as a fraction of parent. (B) Quantification of flow cytometry results showed no significant differences between $des^{-/-}$ and $wt$ ER-TR7+ or $\alpha$SMA+ populations.
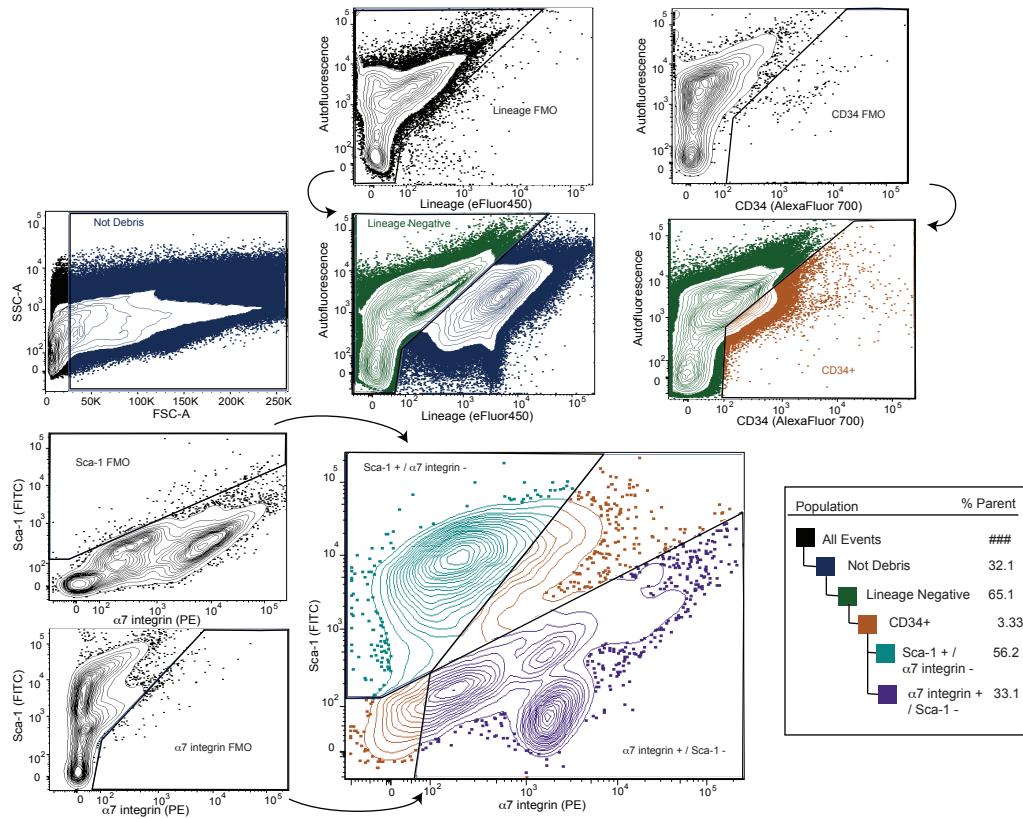
Figure C.4: Schematic of the gating tree to identify $\alpha$7-integrin+ / Sca-1- and Sca-1+ / $\alpha$7-integrin- populations. All events were first gated to eliminate debris (FSC-A voltage less than 25,000). Further gating was performed on each colors fluorescence-minus-one (FMO) control where the positive/negative gate was drawn with a 1% error rate (shown in black and white with arrows pointing to the implementation of the gates on the sample). The Lineage Negative gate eliminated cells positive for CD45 (an immune cell marker) and CD31 (an endothelial cell marker). Next the Lineage Negative population was gated for cells positive for CD34 (a general stem cell marker). The CD34 population was then divided into $\alpha$7-integrin (a muscle progenitor marker) positive and Sca-1 (a fibroadipogenic progenitor marker) negative and Sca-1 positive / $\alpha$7-integrin negative subsets based on the overlap of FMO gates. Each population is shown color-coded with a legend in the bottom right indicating the cell number as a fraction of parent.
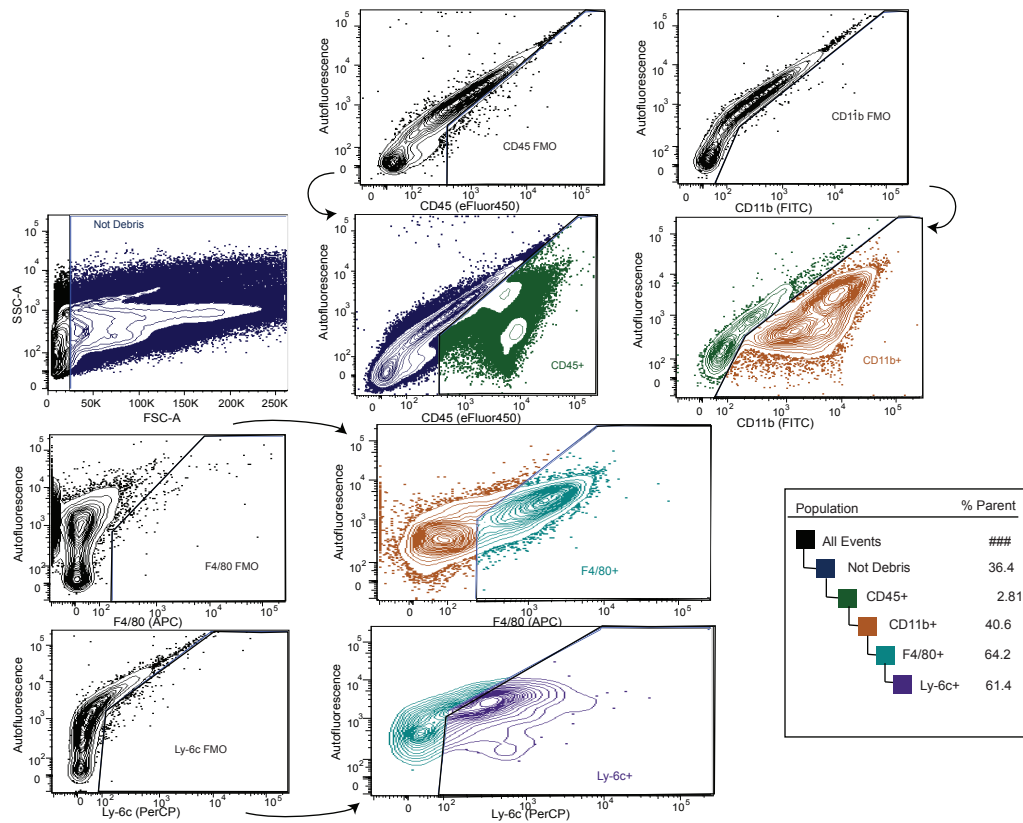
Figure C.5: Schematic of the gating tree to identify CD11b+ / F4/80+ populations. All events were first gated to eliminate debris (FSC-A voltage less than 25,000). Further gating was performed on each colors fluorescence-minus-one (FMO) control where the positive/negative gate is drawn with a 1% error rate (shown in black and white with arrows pointing to the implementation of the gates on the sample). These cells were then gated for positive CD45 signal (an immune cell marker). Next the CD45+ population was gated for cells positive for CD11b (a more specific immune cell marker known to be expressed by macrophages) and that population was gated for positive F4/80 signal (a macrophage specific marker). This population was then divided into Ly-6c positive and Ly-6c negative subsets, which is thought to divide classically activated macrophages (M1) from alternatively activated macrophages (M2) [2]. Each population is shown color-coded with a legend in the bottom right indicating the cell number as a fraction of parent.

# Appendix D

# Supplemental Figures and Tables Supporting Gene Expression Changes in Des$^{-/-}$ Skeletal Muscle

This appendix contains additional information regarding work presented in Chapter 7.
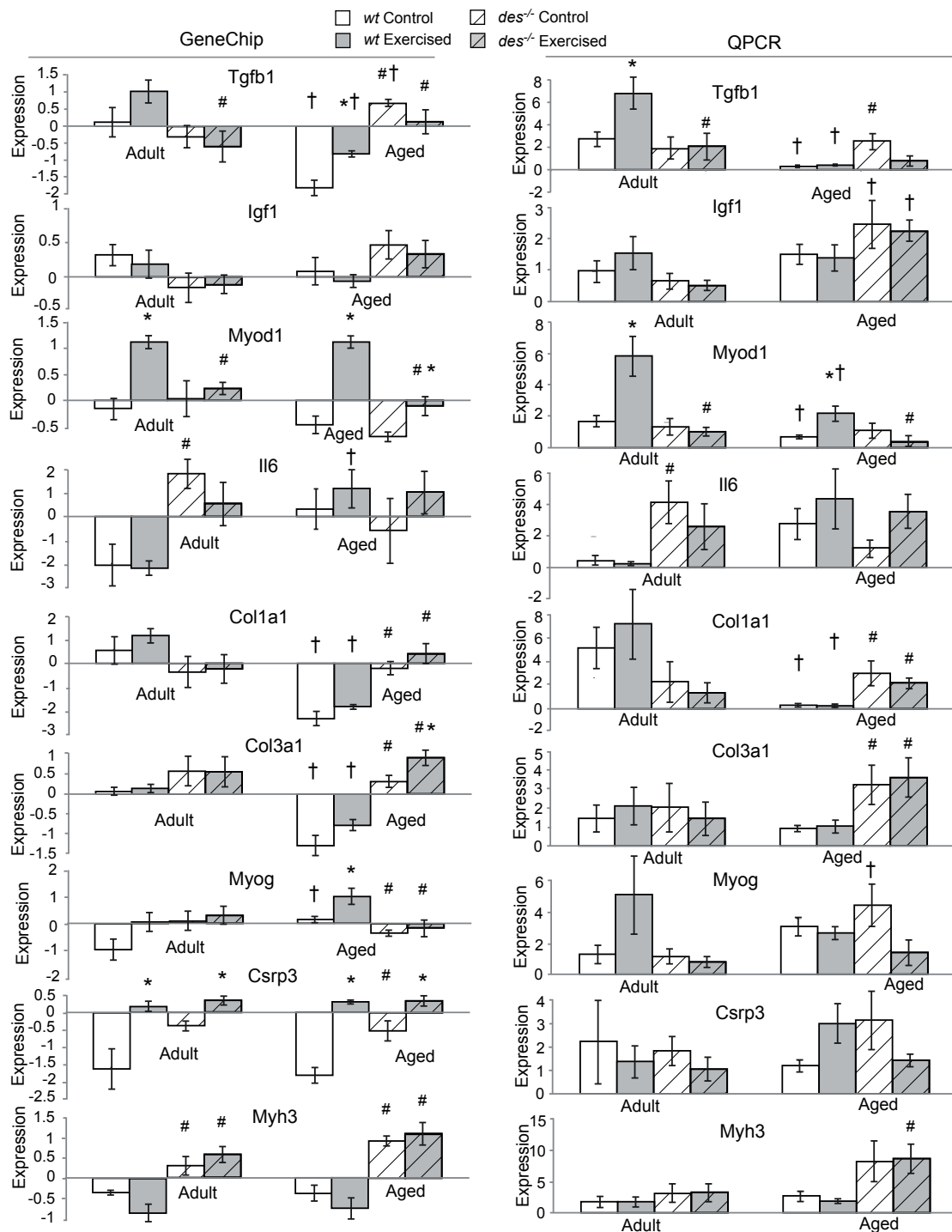
Figure D.1: Expression of 9 select genes confirmed by QPCR. ∗p<0.05 compared to age matched control, same genotype, # p<0.05 compared to age and treatment matched wt, †p<0.05 compared to genotype and treatment matched adult.

Table D.1: Forward and reverse primers used for quantitative real-time PCR. Genes are: collagen type I (Col1a1), collagen type III (Col3a1), transforming growth factor $\beta$ (Tgfb1), interleukin-6 (Il6), muscle LIM protein (Csrp3), insulin-like growth factor (Igf1), myosin heavy chain 3 (Myh3), myogenic differentiation 1 (Myod1), myogenin (Myog) and myostatin (Mstn).

| Gene: | | |
| --- | --- | --- |
| Col1a1 | Foward: | GGCAACAGCCGCTTCACCTAC |
| Col1a1 | Reverse: | GCGGGAGGACTTGGTGGTTTT |
| Col3a1 | Foward: | CACGGAAACACTGGTGGACAGATT |
| Col3a1 | Reverse: | ATGCCAGCTGCACATCAAGGAC |
| Tgfb1 | Foward: | GACTCTCCACCTGCAAGACCAT |
| Tgfb1 | Reverse: | GGGACTGGCGAGCCTTAGTT |
| Il6 | Foward: | CCTTCTTGGGACTGATGCTGG |
| Il6 | Reverse: | GCCTCCGACTTGTGAAGTGGT |
| Csrp3 | Foward: | ATCAGAGAAGTGCCCACGATG |
| Csrp3 | Reverse: | GTAAGCCCTCCAAACCCAAT |
| Igf1 | Foward: | AGCAGTCTTCCAACCCAATTA |
| Igf1 | Reverse: | CACGGACAGAGCGAGCTG |
| Myh3 | Foward: | AGTATGAGCGGCGTGTTAAG |
| Myh3 | Reverse: | CTTGCTCACTCCTCGCTTTCA |
| Myod1 | Foward: | ACCCAGGAACTGGGATATGGA |
| Myod1 | Reverse: | AAGTCGTCTGCTGTCTCAAA |
| Myog | Foward: | TCCCAACCCAGGAGATCAT |
| Myog | Reverse: | TGCAGGCAGCTCATAGTAGG |
| Mstn | Foward: | CAGCCTGAATCCAACTTAGG |
| Mstn | Reverse: | TCGCAGTCAAGCCCAAAGTC |

Table D.2: Genes with a significant desmin-EC interaction. Genes are listed by symbol, title and Entrez gene ID.

| Gene | Gene Title | Entrez ID |
|------|-----------|-----------|
| Wdr1 | WD repeat domain 1 | 22388 |
| Flnc | filamin C, gamma | 68794 |
| Lamc2 | laminin, gamma 2 | 16782 |
| Itgb6 | integrin beta 6 | 16420 |
| Cdk5r1 | cyclin-dependent kinase 5, regulatory subunit 1 (p35) | 12569 |
| Il1r1 | interleukin 1 receptor, type I | 16177 |
| Dnajb1 | DnaJ (Hsp40) homolog, subfamily B, member 1 | 81489 |
| Hspb8 | heat shock protein 8 | 80888 |
| Dnaja4 | DnaJ (Hsp40) homolog, subfamily A, member 4 | 58233 |
| Cxcl10 | chemokine (C-X-C motif) ligand 10 | 15945 |
| Stk39 | serine/threonine kinase 39, STE20/SPS1 homolog | 53416 |
| Srxn1 | sulfiredoxin 1 homolog (S. cerevisiae) | 76650 |
| Hspb3 | heat shock protein 3 | 56534 |
| Klf5 | Kruppel-like factor 5 | 12224 |
| Slc40a1 | solute carrier family 40, member 1 | 53945 |
| Pex11a | peroxisomal biogenesis factor 11 alpha | 18631 |
| Nr1d1 | nuclear receptor subfamily 1, group D, member 1 | 217166 |
| Rcan1 | regulator of calcineurin 1 | 54720 |
| Dusp10 | dual specificity phosphatase 10 | 63953 |
| Rras2 | related RAS viral (r-ras) oncogene homolog 2 | 66922 |
| Ier5 | immediate early response 5 | 15939 |
| Tnfrsf12a | tumor necrosis factor receptor superfamily, mem. 12a | 27279 |
| Sox4 | SRY-box containing gene 4 | 20677 |
| Xirp1 | xin actin-binding repeat containing 1 | 22437 |
| Mybph | myosin binding protein H | 53311 |
| Ptpn14 | protein tyrosine phosphatase, non-receptor type 14 | 19250 |
| Bag3 | BCL2-associated athanogene 3 | 29810 |
| Pitx2 | paired-like homeodomain transcription factor 2 | 18741 |
| Plscr1 | phospholipid scramblase 1 | 22038 |
| Atf3 | activating transcription factor 3 | 11910 |
| Hbegf | heparin-binding EGF-like growth factor | 15200 |
| Nab2 | Ngfi-A binding protein 2 | 17937 |
| Figf | c-fos induced growth factor | 14205 |
| Cgref1 | cell growth regulator with EF hand domain 1 | 68567 |
| Mnat1 | menage a trois 1 | 17420 |
| E2f8 | E2F transcription factor 8 | 108961 |
| Myd116 | myeloid differentiation primary response gene 116 | 17872 |
| Clu | clusterin | 100046120 |

Table D.2, Genes with a significant desmin-EC interaction, Continued. Genes are listed by symbol, title and Entrez gene ID.

| Gene | Gene Title | Entrez ID |
|------|-----------|-----------|
| Rnf115 | ring finger protein 115 | 67845 |
| Siah2 | seven in absentia 2 | 20439 |
| Myod1 | myogenic differentiation 1 | 17927 |
| Fgf1 | fibroblast growth factor 1 | 14164 |
| Lmcd1 | LIM and cysteine-rich domains 1 | 30937 |
| Mustn1 | musculoskeletal, embryonic nuclear protein 1 | 66175 |
| P2rx5 | purinergic receptor P2X, ligand-gated ion channel, 5 | 94045 |
| Angel2 | angel homolog 2 (Drosophila) | 52477 |
| Hmga1 | high mobility group AT-hook 1 | 15361 |
| Reps1 | RalBP1 associated Eps domain containing protein | 19707 |
| Glrx | glutaredoxin | 93692 |
| Sap30 | sin3 associated polypeptide | 60406 |
| Yipf5 | Yip1 domain family, member 5 | 67180 |
| Inmt | indolethylamine N-methyltransferase | 21743 |
| Mettl6 | methyltransferase like 6 | 67011 |
| Tiam2 | T-cell lymphoma invasion and metastasis 2 | 24001 |
| Tmpo | thymopoietin | 21917 |
| Slc22a5 | solute carrier family 22, member 5 | 20520 |
| Rrad | Ras-related associated with diabetes | 56437 |
| Mansc1 | MANSC domain containing 1 | 67729 |
| Pdia3 | protein disulfide isomerase associated 3 | 14827 |
| Pvr | poliovirus receptor | 52118 |
| Dlg5 | discs, large homolog 5 (Drosophila) | 71228 |
| Zfp639 | zinc finger protein 639 | 67778 |
| Fam114a2 | family with sequence similarity 114, member A2 | 67726 |
| Ubtd1 | ubiquitin domain containing 1 | 226122 |
| Hhatl | hedgehog acyltransferase-like | 74770 |
| Nle1 | notchless homolog 1 (Drosophila) | 217011 |
| Zfp295 | zinc finger protein 295 | 114565 |
| Tmem135 | transmembrane protein 135 | 72759 |
| Spg11 | spastic paraplegia 11 | 214585 |
| Herc2 | hect domain and RCC1 (CHC1)-like domain 2 | 15204 |
| Pacrg | PARK2 co-regulated | 69310 |
| Dusp14 | dual specificity phosphatase 14 | 56405 |
| Rilpl1 | Rab interacting lysosomal protein-like 1 | 75695 |
| Sh3bp2 | SH3-domain binding protein 2 | 24055 |
| Lpin3 | lipin 3 | 64899 |
| Amfr | autocrine motility factor receptor | 100046262 |
| Ankrd13a | ankyrin repeat domain 13a | 68420 |

Table D.3: Genes with a significant desmin-age interaction that are more than 2-fold changed between genotypes at either age. Genes are listed by symbol, title and Entrez gene ID.

| Gene | Gene Title | Entrez ID |
| --- | --- | --- |
| Ntn4 | netrin 4 | 57764 |
| Tgfbr3 | transforming growth factor, beta receptor III | 21814 |
| Camk2a | calcium/calmodulin-dependent protein kinase II alpha | 12322 |
| Fv1 | Friend virus susceptibility 1 | 14349 |
| Met | met proto-oncogene | 17295 |
| Ankrd33b | ankyrin repeat domain 33B | 67434 |
| Myl2 | myosin, light polypeptide 2, regulatory, cardiac, slow | 17906 |
| Sod3 | superoxide dismutase 3, extracellular | 20657 |
| Tnnt1 | troponin T1, skeletal, slow | 21955 |
| Trim35 | tripartite motif-containing 35 | 66854 |
| Tnni1 | troponin I, skeletal, slow 1 | 21952 |
| Gdf15 | growth differentiation factor 15 | 23886 |
| Entpd6 | ectonucleoside triphosphate diphosphohydrolase 6 | 12497 |
| Col15a1 | collagen, type XV, alpha 1 | 12819 |
| Ass1 | argininosuccinate synthetase 1 | 11898 |
| Myh7 | myosin, heavy polypeptide 7, cardiac muscle, beta | 140781 |
| Trim12 | tripartite motif-containing 12 | 76681 |
| Atn1 | atrophin 1 | 13498 |
| Smn1 | survival motor neuron 1 | 20595 |
| Zfp395 | zinc finger protein 395 | 380912 |
| Tnnc1 | troponin C, cardiac/slow skeletal | 21924 |
| Tmem98 | transmembrane protein 98 | 103743 |
| Chst12 | carbohydrate sulfotransferase 12 | 59031 |
| Fam129a | family with sequence similarity 129, member A | 63913 |
| Asb18 | ankyrin repeat and SOCS box-containing 18 | 208372 |
| Pcgf1 | polycomb group ring finger 1 | 69837 |
| Prkar2a | protein kinase, cAMP dep. regulatory, type II alpha | 19087 |
| Snai1 | snail homolog 1 (Drosophila) | 20613 |
| Nr1d1 | nuclear receptor subfamily 1, group D, member 1 | 217166 |
| Bcam | basal cell adhesion molecule | 57278 |
| Gna12 | guanine nucleotide binding protein, alpha 12 | 14673 |
| Zfp385a | zinc finger protein 385A | 29813 |
| Zbtb45 | zinc finger and BTB domain containing 45 | 232879 |
| Npnt | nephronectin | 114249 |
| Slc1a1 | solute carrier family 1 | 20510 |
| Myo7a | myosin VIIA | 17921 |
| Vat1 | vesicle amine transport protein 1 homolog | 26949 |

Table D.3, Genes with a significant desmin-age interaction that are more than 2-fold changed between genotypes at either age, Continued.

| Gene | Gene Title | Entrez ID |
|------|-----------|-----------|
| Nog | noggin | 18121 |
| Slc29a1 | solute carrier family 29, member 1 | 63959 |
| Arhgap10 | Rho GTPase activating protein 10 | 78514 |
| Anpep | alanyl (membrane) aminopeptidase | 16790 |
| Tgfb1 | transforming growth factor, beta 1 | 21803 |
| Prune | prune homolog (Drosophila) | 229589 |
| Pitpnb | phosphatidylinositol transfer protein, beta | 56305 |
| Osr2 | odd-skipped related 2 (Drosophila) | 107587 |
| Ate1 | arginyltransferase 1 | 11907 |
| Tmcc3 | transmembrane and coiled coil domains 3 | 319880 |
| Itga5 | integrin alpha 5 (fibronectin receptor alpha) | 16402 |
| Trib3 | tribbles homolog 3 (Drosophila) | 228775 |
| Btrc | beta-transducin repeat containing protein | 12234 |
| Slc25a24 | solute carrier family 25, member 24 | 229731 |
| Mr1 | major histocompatibility complex, class I-related | 15064 |
| Usp13 | Sr513 protein | 72607 |
| Phospho1 | phosphatase, orphan 1 | 237928 |
| Uchl1 | ubiquitin carboxy-terminal hydrolase L1 | 22223 |
| Plekhj1 | pleckstrin homology domain containing, fam.J mem.1 | 78670 |
| Col1a1 | collagen, type I, alpha 1 | 12842 |
| Synpo2 | synaptopodin 2 | 118449 |
| Sulf2 | sulfatase 2 | 72043 |
| Pdk2 | pyruvate dehydrogenase kinase, isoenzyme 2 | 18604 |
| Srgap3 | SLIT-ROBO Rho GTPase activating protein 3 | 259302 |
| Dnaja4 | DnaJ (Hsp40) homolog, subfamily A, member 4 | 58233 |
| Krt25 | keratin 25 | 70810 |
| Galc | galactosylceramidase | 14420 |
| Etv5 | ets variant gene 5 | 104156 |
| Asns | asparagine synthetase | 27053 |
| Obfc2b | oligosaccharide-binding fold containing 2B | 69917 |
| Ruvbl2 | RuvB-like protein 2 | 20174 |
| Ccdc91 | coiled-coil domain containing 91 | 67015 |
| Trp53 | transformation related protein 53 | 22059 |
| Ccnt1 | cyclin T1 | 100047121 |
| Garnl1 | GTPase activating RANGAP domain-like 1 | 56784 |
| Anxa6 | annexin A6 | 11749 |
| Mapk6 | mitogen-activated protein kinase 6 | 50772 |
| G6pdx | glucose-6-phosphate dehydrogenase X-linked | 14380 |

Table D.3, Genes with a significant desmin-age interaction that are more than 2-fold changed between genotypes at either age, Continued.

| Gene | Gene Title | Entrez ID |
|------|-----------|-----------|
| Casq2 | calsequestrin 2 | 12373 |
| Eif2s3x | eukaryotic translation initiation factor 2, subunit 3 | 100048746 |
| Spock2 | sparc/osteonectin | 94214 |
| E2f4 | E2F transcription factor 4 | 104394 |
| Myoz2 | myozenin 2 | 59006 |
| Dyrk1b | dual-specificity tyrosine-(Y)-phosphorylation kinase 1b | 13549 |
| Mthfd2 | methylenetetrahydrofolate dehydrogenase | 17768 |
| Isyna1 | myo-inositol 1-phosphate synthase A1 | 71780 |
| Pknox2 | Pbx/knotted 1 homeobox 2 | 208076 |
| Ccl21a | chemokine (C-C motif) ligand 21A | 18829 |
| Cebpa | CCAAT/enhancer binding protein (C/EBP), alpha | 12606 |
| S100a4 | S100 calcium binding protein A4 | 20198 |
| Pck2 | phosphoenolpyruvate carboxykinase 2 (mitochondrial) | 74551 |
| Usp22 | ubiquitin specific peptidase 22 | 216825 |
| Il6ra | interleukin 6 receptor, alpha | 16194 |
| Smtnl1 | smoothelin-like 1 | 68678 |
| Mapre3 | microtubule-associated, RP/EB family, member 3 | 100732 |
| Psmb7 | proteasome (prosome, macropain) subunit, beta type 7 | 19177 |
| Ppm1b | protein phosphatase 1B, magnesium dependent, beta | 666025 |
| Asb15 | ankyrin repeat and SOCS box-containing 15 | 78910 |
| Fez1 | fasciculation and elongation protein zeta 1 (zygin I) | 235180 |
| Abcb8 | ATP-binding cassette, sub-family B, member 8 | 74610 |
| Scn4a | sodium channel, voltage-gated, type IV, alpha | 110880 |
| Cbr3 | carbonyl reductase 3 | 109857 |
| Klc2 | kinesin light chain 2 | 16594 |
| Ube2n | ubiquitin-conjugating enzyme E2N | 93765 |
| Prkaca | protein kinase, cAMP dependent, catalytic, alpha | 18747 |
| Manba | mannosidase, beta A, lysosomal | 110173 |
| Col3a1 | collagen, type III, alpha 1 | 12825 |
| Eya1 | eyes absent 1 homolog (Drosophila) | 14048 |
| Lgals9 | lectin, galactose binding, soluble 9 | 16859 |
| Slc16a3 | solute carrier family 16, member 3 | 80879 |
| Shc1 | src homology 2 domain-containing trans. protein C1 | 20416 |
| Ltbp4 | latent transforming growth factor beta binding protein 4 | 108075 |
| Atp2a2 | ATPase, Ca++ transporting, slow twitch 2 | 11938 |
| Crlf1 | cytokine receptor-like factor 1 | 12931 |
| Atp8a1 | ATPase, class I, type 8A, member 1 | 11980 |

Table D.3, Genes with a significant desmin-age interaction that are more than 2-fold changed between genotypes at either age, Continued.

| Gene | Gene Title | Entrez ID |
|------|-----------|-----------|
| Csdc2 | cold shock domain containing C2, RNA binding | 105859 |
| Atp6v0b | ATPase, H+ transporting, lysosomal V0 subunit B | 114143 |
| Chrne | cholinergic receptor, nicotinic, epsilon polypeptide | 11448 |
| Cxx1b | CAAX box 1 homolog B (human) | 553127 |
| Nacc1 | nucleus accumbens associated 1 | 66830 |
| Adamtsl5 | ADAMTS-like 5 | 66548 |
| Usp20 | ubiquitin specific peptidase 20 | 74270 |
| Sema3c | semaphorin 3C | 20348 |
| Akt2 | thymoma viral proto-oncogene 2 | 100048123 |
| Alg2 | asparagine-linked glycosylation 2 homolog | 56737 |
| Zfp142 | zinc finger protein 142 | 77264 |
| Ednra | endothelin receptor type A | 13617 |
| Anxa5 | annexin A5 | 11747 |
| Cyb5r3 | cytochrome b5 reductase 3 | 109754 |
| Atp9a | ATPase, class II, type 9A | 11981 |
| Fbxw5 | F-box and WD-40 domain protein 5 | 30839 |
| Mlf2 | myeloid leukemia factor 2 | 100048413 |
| Lgals3bp | lectin, galactoside-binding, soluble, 3 binding protein | 19039 |
| Eif2ak1 | eukaryotic translation initiation factor 2 alpha kinase | 15467 |
| Actr1b | ARP1 actin-related 1 homolog B, centractin beta | 226977 |
| Mmp15 | matrix metallopeptidase 15 | 17388 |
| Ctnnd1 | catenin (cadherin associated protein), delta 1 | 12388 |
| Sel1l | sel-1 suppressor of lin-12-like (C. elegans) | 20338 |
| Lman2 | lectin, mannose-binding 2 | 66890 |
| Aldh4a1 | aldehyde dehydrogenase 4 family, member A1 | 212647 |
| Pdgfb | platelet derived growth factor, B polypeptide | 18591 |
| Ube2r2 | ubiquitin-conjugating enzyme E2R 2 | 67615 |
| Sema6d | semaphorin 6D | 214968 |
| Sigmar1 | sigma non-opioid intracellular receptor 1 | 18391 |
| Lamc1 | laminin, gamma 1 | 226519 |
| Nudcd1 | NudC domain containing 1 | 67429 |
| Ndrg4 | N-myc downstream regulated gene 4 | 234593 |
| Nt5c2 | 5'-nucleotidase, cytosolic II | 76952 |
| Cbara1 | calcium binding atopy-related autoantigen 1 | 216001 |
| Fadd | Fas (TNFRSF6)-associated via death domain | 14082 |
| Apobec3 | apolipoprotein B, catalytic polypeptide 3 | 80287 |
| Nos1 | nitric oxide synthase 1, neuronal | 18125 |

Table D.3, Genes with a significant desmin-age interaction that are more than 2-fold changed between genotypes at either age, Continued.

| Gene | Gene Title | Entrez ID |
|------|-----------|-----------|
| Nr1h2 | nuclear receptor subfamily 1, group H, member 2 | 22260 |
| Kcnk2 | potassium channel, subfamily K, member 2 | 16526 |
| Stom | stomatin | 13830 |
| Pycr1 | pyrroline-5-carboxylate reductase 1 | 209027 |
| Ap2a1 | adaptor protein complex AP-2, alpha 1 subunit | 11771 |
| Hlcs | holocarboxylase synthetase | 110948 |
| Bcl2l13 | BCL2-like 13 (apoptosis facilitator) | 94044 |
| Slc35c1 | solute carrier family 35, member C1 | 228368 |
| Smad3 | MAD homolog 3 (Drosophila) | 17127 |
| Serpinh1 | serine peptidase inhibitor, clade H, member 1 | 12406 |
| Mmab | methylmalonic aciduria type B homolog | 77697 |
| Unc93b1 | unc-93 homolog B1 (C. elegans) | 54445 |
| Rhob | ras homolog gene family, member B | 11852 |
| Dcakd | dephospho-CoA kinase domain containing | 68087 |
| Cdh13 | cadherin 13 | 12554 |
| Cd74 | CD74 antigen | 16149 |
| Mcpt4 | mast cell protease 4 | 17227 |
| Mid2 | midline 2 | 23947 |
| Aplnr | apelin receptor | 23796 |
| Igfbp4 | insulin-like growth factor binding protein 4 | 16010 |
| Zbtb7b | zinc finger and BTB domain containing 7B | 100046682 |
| Arfip2 | ADP-ribosylation factor interacting protein 2 | 76932 |
| Add1 | adducin 1 (alpha) | 11518 |
| Iffo1 | intermediate filament family orphan 1 | 320678 |
| Arnt | aryl hydrocarbon receptor nuclear translocator | 11863 |
| Ano10 | anoctamin 10 | 102566 |
| Rab11fip5 | RAB11 family interacting protein 5 (class I) | 52055 |
| Mlec | malectin | 109154 |
| Reep6 | receptor accessory protein 6 | 70335 |
| Stat6 | signal transducer and activator of transcription 6 | 20852 |
| Jph1 | junctophilin 1 | 57339 |
| Cxcl14 | chemokine (C-X-C motif) ligand 14 | 57266 |
| Anapc11 | anaphase promoting complex subunit 11 | 66156 |
| Elmod3 | ELMO/CED-12 domain containing 3 | 100047355 |
| Pfkl | phosphofructokinase, liver, B-type | 18641 |
| Nucb1 | nucleobindin 1 | 18220 |
| Igsf8 | immunoglobulin superfamily, member 8 | 140559 |
| Scamp4 | secretory carrier membrane protein 4 | 100113398 |

Table D.3, Genes with a significant desmin-age interaction that are more than 2-fold changed between genotypes at either age, Continued.

| Gene | Gene Title | Entrez ID |
|---|---|---|
| Tnfrsf19 | tumor necrosis factor receptor superfamily, mem. 19 | 29820 |
| Padi2 | peptidyl arginine deiminase, type II | 18600 |
| Atf7 | activating transcription factor 7 | 223922 |
| Ache | acetylcholinesterase | 11423 |
| Ube2m | ubiquitin-conjugating enzyme E2M | 22192 |
| Dhrs7 | dehydrogenase/reductase (SDR family) member 7 | 66375 |
| Raver1 | ribonucleoprotein, PTB-binding 1 | 71766 |
| Col6a1 | collagen, type VI, alpha 1 | 12833 |
| Usp25 | ubiquitin specific peptidase 25 | 30940 |
| Cdkn1b | cyclin-dependent kinase inhibitor 1B | 12576 |
| Cap1 | CAP, adenylate cyclase-associated protein 1 | 12331 |
| Pltp | phospholipid transfer protein | 18830 |
| Ptprg | protein tyrosine phosphatase, receptor type, G | 19270 |
| Fntb | farnesyltransferase, CAAX box, beta | 110606 |
| Smyd1 | SET and MYND domain containing 1 | 12180 |
| Sema6c | semaphorin 6C | 20360 |
| Col6a2 | collagen, type VI, alpha 2 | 12834 |
| Tpsb2 | tryptase beta 2 | 17229 |
| Ogg1 | 8-oxoguanine DNA-glycosylase 1 | 18294 |
| P2ry2 | purinergic receptor P2Y, G-protein coupled 2 | 18442 |
| Tpm3 | tropomyosin 3, gamma | 59069 |
| Ralgds | ral guanine nucleotide dissociation stimulator | 19730 |
| Mtmr3 | myotubularin related protein 3 | 74302 |
| Hsf4 | heat shock transcription factor 4 | 26386 |
| Ddx19b | DEAD box polypeptide 19b | 13680 |
| Olfml2b | olfactomedin-like 2B | 320078 |
| Ehmt2 | euchromatic histone lysine N-methyltransferase 2 | 110147 |
| Dbn1 | drebrin 1 | 56320 |
| Nrbp1 | nuclear receptor binding protein 1 | 192292 |
| Urm1 | ubiquitin related modifier 1 homolog | 68205 |
| Ncor2 | nuclear receptor co-repressor 2 | 20602 |
| Wars | similar to Wars protein | 22375 |
| Ncstn | nicastrin | 59287 |
| Pygb | brain glycogen phosphorylase | 110078 |
| Aldh18a1 | aldehyde dehydrogenase 18 family, member A1 | 56454 |
| Atp6v0a1 | ATPase, H+ transporting, lysosomal V0 subunit A1 | 11975 |
| Tradd | TNFRSF1A-associated via death domain | 71609 |
| Wwp2 | WW domain containing E3 ubiquitin protein ligase 2 | 66894 |

Table D.3, Genes with a significant desmin-age interaction that are more than 2-fold changed between genotypes at either age, Continued.

| Gene | Gene Title | Entrez ID |
| --- | --- | --- |
| Alg12 | asparagine-linked glycosylation 12 homolog | 223774 |
| Stat5a | signal transducer and activator of transcription 5A | 20850 |
| Sepx1 | selenoprotein X 1 | 27361 |
| Fcrls | Fc receptor-like S, scavenger receptor | 80891 |
| Neurl1a | neuralized homolog 1A (Drosophila) | 18011 |
| Mbc2 | membrane bound C2 domain containing protein | 23943 |
| Wfs1 | Wolfram syndrome 1 homolog (human) | 22393 |
| Fzr1 | fizzy/cell division cycle 20 related 1 (Drosophila) | 56371 |
| Cfp | complement factor properdin | 18636 |
| Copg2 | coatomer protein complex, subunit gamma 2 | 54160 |
| Trf | transferrin | 22041 |
| P4ha1 | procollagen-proline, alpha 1 polypeptide | 18451 |
| Nosip | nitric oxide synthase interacting protein | 66394 |
| Smtn | smoothelin | 29856 |
| Sirt1 | sirtuin 1 | 93759 |
| Agpat6 | 1-acylglycerol-3-phosphate O-acyltransferase 6 | 102247 |
| Elmo2 | engulfment and cell motility 2, ced-12 homolog | 140579 |
| Mpz | myelin protein zero | 17528 |
| Rnf167 | ring finger protein 167 | 70510 |
| Ccnd3 | cyclin D3 | 12445 |
| Arhgef10l | Rho guanine nucleotide exchange factor (GEF) 10-like | 72754 |
| Hmbox1 | homeobox containing 1 | 219150 |
| S100a13 | S100 calcium binding protein A13 | 20196 |
| Maged1 | melanoma antigen, family D, 1 | 94275 |
| Vamp1 | vesicle-associated membrane protein 1 | 22317 |
| Cacng6 | calcium channel, voltage-dependent, gamma subunit 6 | 54378 |
| Crym | crystallin, mu | 12971 |
| Zfp358 | zinc finger protein 358 | 140482 |
| Arf4 | ADP-ribosylation factor 4 | 11843 |
| Spen | SPEN homolog, transcriptional regulator | 56381 |
| Pex19 | peroxisomal biogenesis factor 19 | 19298 |
| Git1 | G protein-coupled receptor kinase-interactor 1 | 216963 |
| Clcn1 | chloride channel 1 | 12723 |
| Fgfbp1 | fibroblast growth factor binding protein 1 | 14181 |
| Pknox1 | Pbx/knotted 1 homeobox | 18771 |

Table D.3, Genes with a significant desmin-age interaction that are more than 2-fold changed between genotypes at either age, Continued.

| Gene | Gene Title | Entrez ID |
|------|-----------|-----------|
| Plekha3 | pleckstrin homology domain-containing, A mem. 3 | 83435 |
| Ybx2 | Y box protein 2 | 100045903 |
| Uba1 | ubiquitin-like modifier activating enzyme 1 | 22201 |
| Eef1a2 | eukaryotic translation elongation factor 1 alpha 2 | 13628 |
| Col19a1 | collagen, type XIX, alpha 1 | 12823 |
| Slc6a9 | solute carrier family 6, member 9 | 14664 |
| Fads1 | fatty acid desaturase 1 | 76267 |
| Fbxo17 | F-box protein 17 | 50760 |
| Mccc2 | methylcrotonoyl-Coenzyme A carboxylase 2 (beta) | 78038 |
| Klc4 | kinesin light chain 4 | 74764 |
| Epas1 | endothelial PAS domain protein 1 | 100048537 |
| Vamp2 | vesicle-associated membrane protein 2 | 22318 |
| Med24 | mediator complex subunit 24 | 23989 |
| Ube2v1 | ubiquitin-conjugating enzyme E2 variant 1 | 66589 |
| Smad7 | MAD homolog 7 (Drosophila) | 17131 |
| Tie1 | tyrosine kinase 1 | 21846 |
| Ilk | integrin linked kinase | 16202 |
| Ccdc123 | coiled-coil domain containing 123 | 72140 |
| Apbb1 | amyloid beta precursor protein-binding, B, mem. 1 | 11785 |
| Epn1 | epsin 1 | 13854 |
| Tnfrsf22 | tumor necrosis factor receptor superfamily, member 22 | 79202 |
| D2hgdh | D-2-hydroxyglutarate dehydrogenase | 98314 |
| Loxl1 | lysyl oxidase-like 1 | 16949 |
| Glt25d1 | glycosyltransferase 25 domain containing 1 | 234407 |
| Clptm1 | cleft lip associated transmembrane protein 1 | 56457 |
| Bmp5 | bone morphogenetic protein 5 | 12160 |
| Tfpt | TCF3 (E2A) fusion partner | 69714 |
| Tiam2 | T-cell lymphoma invasion and metastasis 2 | 24001 |
| Col5a2 | collagen, type V, alpha 2 | 12832 |
| Ncdn | neurochondrin | 26562 |
| Shmt2 | serine hydroxymethyltransferase 2 (mitochondrial) | 108037 |
| Fbn1 | fibrillin 1 | 14118 |
| Palm | paralemmin | 18483 |
| Rab11b | RAB11B, member RAS oncogene family | 19326 |
| Mapt | microtubule-associated protein tau | 17762 |
| Prcp | prolylcarboxypeptidase (angiotensinase C) | 100048391 |
| Rbpj | recomb. signal binding protein for kappa J | 19664 |
| Dullard | Dullard homolog (Xenopus laevis) | 100048221 |

Table D.3, Genes with a significant desmin-age interaction that are more than 2-fold changed between genotypes at either age, Continued.

| Gene | Gene Title | Entrez ID |
|------|-----------|-----------|
| Rps6kb2 | ribosomal protein S6 kinase, polypeptide 2 | 58988 |
| Pcid2 | PCI domain containing 2 | 234069 |
| Cth | cystathionase (cystathionine gamma-lyase) | 107869 |
| Col5a1 | collagen, type V, alpha 1 | 12831 |
| Wdr22 | WD repeat domain 22 | 320808 |
| Ttc7b | tetratricopeptide repeat domain 7B | 104718 |
| Ace | angiotensin I converting enzyme 1 | 11421 |
| Mall | mal, T-cell differentiation protein-like | 228576 |
| Pitpnm2 | phosphatidylinositol transfer protein, membrane 2 | 19679 |
| Phf12 | PHD finger protein 12 | 268448 |
| Serpinb6a | serine peptidase inhibitor, B, mem. 6a | 20719 |
| Ppif | peptidylprolyl isomerase F (cyclophilin F) | 105675 |
| Evi2b | ecotropic viral integration site 2b | 14017 |
| Coro6 | coronin 6 | 216961 |
| Acot9 | acyl-CoA thioesterase 9 | 64833 |
| Alpl | alkaline phosphatase, liver/bone/kidney | 11647 |
| Vsig2 | V-set and immunoglobulin domain containing 2 | 57276 |
| Maz | MYC-associated zinc finger protein | 17188 |
| Tec | tec protein tyrosine kinase | 21682 |
| Anxa4 | annexin A4 | 11746 |
| Itpkb | inositol 1,4,5-trisphosphate 3-kinase B | 320404 |
| Jam2 | junction adhesion molecule 2 | 67374 |
| Lfng | O-fucosylpeptide 3-beta-N-acetylaminyltransferase | 16848 |
| Pctp | phosphatidylcholine transfer protein | 18559 |
| Rab40b | Rab40b, member RAS oncogene family | 217371 |
| Slc25a25 | solute carrier family 25, member 25 | 227731 |
| Egr2 | early growth response 2 | 13654 |
| Prkch | protein kinase C, eta | 18755 |
| Eln | elastin | 13717 |
| Junb | Jun-B oncogene | 16477 |
| Pde4a | phosphodiesterase 4A, cAMP specific | 18577 |
| Ccnk | cyclin K | 100046615 |
| Arid5b | AT rich interactive domain 5B (MRF1-like) | 71371 |
| Atp1b4 | ATPase, (Na+)/K+ transporting, beta 4 polypeptide | 67821 |
| Grb14 | growth factor receptor bound protein 14 | 50915 |
| Cav3 | caveolin 3 | 12391 |
| Shank3 | SH3/ankyrin domain gene 3 | 58234 |
| Magix | MAGI family member, X-linked | 54634 |

Table D.3, Genes with a significant desmin-age interaction that are more than 2-fold changed between genotypes at either age, Continued.

| Gene | Gene Title | Entrez ID |
|------|-----------|-----------|
| Tmbim1 | transmembrane BAX inhibitor motif containing 1 | 69660 |
| Tpbg | trophoblast glycoprotein | 21983 |
| Rbpms | RNA binding protein gene with multiple splicing | 100044395 |
| Pctk3 | PCTAIRE-motif protein kinase 3 | 18557 |
| Gpx3 | glutathione peroxidase 3 | 14778 |
| Cttn | cortactin | 13043 |
| Cpox | coproporphyrinogen oxidase | 12892 |
| Rasip1 | Ras interacting protein 1 | 69903 |
| Ptx3 | pentraxin related gene | 19288 |
| Cstb | cystatin B | 13014 |
| Ccrn4l | CCR4 carbon catabolite repression 4-like | 100047134 |
| Sat1 | spermidine/spermine N1-acetyl transferase 1 | 20229 |
| Tinagl1 | tubulointerstitial nephritis antigen-like 1 | 94242 |
| Ramp1 | receptor (calcitonin) activity modifying protein 1 | 51801 |
| Slc2a1 | solute carrier family 2, member 1 | 20525 |
| Ctgf | connective tissue growth factor | 14219 |
| Sertad1 | SERTA domain containing 1 | 55942 |
| Myct1 | myc target 1 | 68632 |
| Epb4.1 | erythrocyte protein band 4.1 | 269587 |
| Adfp | adipose differentiation related protein | 11520 |
| Tnfaip6 | tumor necrosis factor alpha induced protein 6 | 21930 |
| Vtn | vitronectin | 22370 |
| Serpina1a | serine peptidase inhibitor, A, mem. 1A | 20700 |
| Rgs4 | regulator of G-protein signaling 4 | 19736 |
| Irf5 | interferon regulatory factor 5 | 27056 |
| S100a16 | S100 calcium binding protein A16 | 67860 |
| Hspa2 | heat shock protein 2 | 15512 |
| Klf15 | Kruppel-like factor 15 | 66277 |
| Pkp2 | plakophilin 2 | 67451 |
| Icam1 | intercellular adhesion molecule 1 | 15894 |
| Vwf | Von Willebrand factor homolog | 22371 |
| F2r | coagulation factor II (thrombin) receptor | 14062 |
| Notch3 | Notch gene homolog 3 (Drosophila) | 18131 |
| Ankrd10 | ankyrin repeat domain 10 | 102334 |
| Tmem128 | transmembrane protein 128 | 66309 |
| Emp1 | epithelial membrane protein 1 | 13730 |
| Tspan8 | tetraspanin 8 | 216350 |
| Lmo7 | LIM domain only 7 | 380928 |

Table D.3, Genes with a significant desmin-age interaction that are more than 2-fold changed between genotypes at either age, Continued.

| Gene | Gene Title | Entrez ID |
| --- | --- | --- |
| Ccl12 | chemokine (C-C motif) ligand 12 | 20293 |
| Rbm3 | RNA binding motif protein 3 | 19652 |
| Id2 | inhibitor of DNA binding 2 | 15902 |
| Pnmt | phenylethanolamine-N-methyltransferase | 18948 |
| Fgl2 | fibrinogen-like protein 2 | 14190 |
| Ptprc | protein tyrosine phosphatase, receptor type, C | 19264 |
| Prss23 | protease, serine, 23 | 76453 |
| Tceal3 | transcription elongation factor A (SII)-like 3 | 331532 |
| Map2k6 | mitogen-activated protein kinase kinase 6 | 26399 |
| Bdh1 | 3-hydroxybutyrate dehydrogenase, type 1 | 71911 |
| Dusp2 | dual specificity phosphatase 2 | 13537 |
| Arl6ip5 | ADP-ribosylation factor-like 6 interacting protein 5 | 65106 |
| Myo5a | myosin VA | 17918 |
| Plaur | plasminogen activator, urokinase receptor | 18793 |
| Ramp2 | receptor (calcitonin) activity modifying protein 2 | 54409 |
| Midn | midnolin | 59090 |
| Vegfb | vascular endothelial growth factor B | 22340 |
| Ptpn2 | protein tyrosine phosphatase, non-receptor type 2 | 19255 |
| Socs3 | suppressor of cytokine signaling 3 | 12702 |
| Selp | selectin, platelet | 20344 |
| Efcab4a | EF-hand calcium binding domain 4A | 213573 |
| Aldh1l1 | aldehyde dehydrogenase 1 family, member L1 | 107747 |
| Slc22a4 | solute carrier family 22, member 4 | 30805 |
| Sdc4 | syndecan 4 | 20971 |
| Prkg1 | protein kinase, cGMP-dependent, type I | 19091 |
| Il6 | interleukin 6 | 16193 |
| Mlf1 | myeloid leukemia factor 1 | 17349 |
| Dynll2 | dynein light chain LC8-type 2 | 68097 |
| Cntf | ciliary neurotrophic factor | 12803 |
| Spin1 | spindlin 1 | 20729 |
| C1d | C1D nuclear receptor co-repressor | 57316 |
| Ppp1r10 | protein phosphatase 1, regulatory subunit 10 | 52040 |
| Ccdc52 | coiled-coil domain containing 52 | 212514 |
| Gnl2 | guanine nucleotide binding protein-like 2 (nucleolar) | 633966 |
| Usp53 | ubiquitin specific peptidase 53 | 99526 |
| Cebpz | CCAAT/enhancer binding protein zeta | 12607 |

Table D.3, Genes with a significant desmin-age interaction that are more than 2-fold changed between genotypes at either age, Continued.

| Gene | Gene Title | Entrez ID |
|------|------------|-----------|
| Phf21a | PHD finger protein 21A | 192285 |
| Il18 | interleukin 18 | 16173 |
| Cnot4 | CCR4-NOT transcription complex, subunit 4 | 53621 |
| Myef2 | myelin basic protein expression factor 2, repressor | 17876 |
| Topors | topoisomerase I binding, arginine/serine-rich | 106021 |
| Tbk1 | TANK-binding kinase 1 | 56480 |
| Wsb1 | WD repeat and SOCS box-containing 1 | 78889 |
| Cramp1l | Crm, cramped-like (Drosophila) | 57354 |
| Timm9 | translocase of inner mitochondrial membrane 9 | 30056 |
| Hbegf | heparin-binding EGF-like growth factor | 15200 |
| Dusp6 | dual specificity phosphatase 6 | 67603 |
| Oxsr1 | oxidative-stress responsive 1 | 108737 |
| Pdgfa | platelet derived growth factor, alpha | 18590 |
| Aff1 | AF4/FMR2 family, member 1 | 17355 |
| Taf1d | TATA box binding protein (Tbp)-associated factor D | 75316 |
| Atp13a3 | ATPase type 13A3 | 224088 |
| Ets1 | E26 avian leukemia oncogene 1, 5' domain | 23871 |
| Gm561 | gene model 561, (NCBI) | 228715 |
| Mrpl32 | mitochondrial ribosomal protein L32 | 75398 |
| Otub1 | OTU domain, ubiquitin aldehyde binding 1 | 107260 |
| Aifm1 | apoptosis-inducing factor, 1 | 26926 |
| Glul | glutamate-ammonia ligase (glutamine synthetase) | 14645 |
| Agpat1 | 1-acylglycerol-3-phosphate O-acyltransferase 1 | 55979 |
| Dnajc19 | DnaJ (Hsp40) homolog, subfamily C, member 19 | 67713 |
| Mrpl54 | mitochondrial ribosomal protein L54 | 66047 |
| Picalm | phosphatidylinositol binding clathrin assembly protein | 233489 |
| Tgfb2 | transforming growth factor, beta 2 | 21808 |
| Foxn2 | forkhead box N2 | 14236 |
| Bmp6 | bone morphogenetic protein 6 | 12161 |
| Rab9 | RAB9, member RAS oncogene family | 56382 |
| Ankrd49 | ankyrin repeat domain 49 | 56503 |
| Nucks1 | nuclear casein kinase and cyclin-dependent kinase 1 | 98415 |
| Pdcd10 | programmed cell death 10 | 56426 |
| Fam13c | family with sequence similarity 13, member C | 71721 |
| Peli1 | pellino 1 | 67245 |
| Siah1a | seven in absentia 1A | 20437 |
| Yme1l1 | YME1-like 1 (S. cerevisiae) | 27377 |
| Rps20 | ribosomal protein S20 | 623568 |

Table D.3, Genes with a significant desmin-age interaction that are more than 2-fold changed between genotypes at either age, Continued.

| Gene | Gene Title | Entrez ID |
|---|---|---|
| Spp1 | secreted phosphoprotein 1 | 20750 |
| Cebpb | CCAAT/enhancer binding protein, beta | 12608 |
| Btg2 | B-cell translocation gene 2, anti-proliferative | 12227 |
| Snrpd3 | small nuclear ribonucleoprotein D3 | 67332 |
| Socs2 | suppressor of cytokine signaling 2 | 216233 |
| Sephs2 | selenophosphate synthetase 2 | 20768 |
| Gadd45a | growth arrest and DNA-damage-ind. 45 alpha | 13197 |
| Acyp2 | acylphosphatase 2, muscle type | 75572 |
| Sox17 | SRY-box containing gene 17 | 20671 |
| Tmem42 | transmembrane protein 42 | 66079 |
| Kdelr2 | KDEL ER protein retention receptor 2 | 66913 |
| Arf5 | ADP-ribosylation factor 5 | 100046958 |
| Pigu | phosphatidylinositol anchor biosynthesis, U | 228812 |
| Nup54 | nucleoporin 54 | 269113 |
| Rbbp6 | retinoblastoma binding protein 6 | 19647 |
| Cyfip2 | cytoplasmic FMR1 interacting protein 2 | 76884 |
| Myf5 | myogenic factor 5 | 17877 |
| Zfp52 | zinc finger protein 52 | 22710 |
| Klf4 | Kruppel-like factor 4 (gut) | 16600 |
| Rnpc3 | RNA-binding region containing 3 | 67225 |
| Pdlim5 | PDZ and LIM domain 5 | 56376 |
| Cspp1 | centrosome and spindle associated protein 1 | 211660 |
| Dnajc3 | DnaJ homolog, subfamily C, member 3 | 100037258 |
| Dnajc13 | DnaJ homolog, subfamily C, member 13 | 235567 |
| Dmtf1 | cyclin D binding myb-like transcription factor 1 | 23857 |
| Dpyd | dihydropyrimidine dehydrogenase | 99586 |
| Pdk4 | pyruvate dehydrogenase kinase, isoenzyme 4 | 27273 |
| Sfrs15 | splicing factor, arginine/serine-rich 15 | 224432 |
| Foxo3 | forkhead box O3 | 56484 |
| Ptplb | protein tyrosine phosphatase-like, member b | 70757 |
| Kifap3 | kinesin-associated protein 3 | 16579 |
| Klhl9 | kelch-like 9 (Drosophila) | 242521 |
| Skil | SKI-like | 20482 |
| Id1 | inhibitor of DNA binding 1 | 15901 |
| Cdc42ep3 | CDC42 effector protein 3 | 260409 |
| Fbp2 | fructose bisphosphatase 2 | 14120 |
| Tle1 | transducin-like enhancer of split 1 | 21885 |
| Utp18 | UTP18, processome component | 217109 |

Table D.3, Genes with a significant desmin-age interaction that are more than 2-fold changed between genotypes at either age, Continued.

| Gene | Gene Title | Entrez ID |
|------|------------|-----------|
| Siva1 | SIVA1, apoptosis-inducing factor | 668686 |
| Usf1 | upstream transcription factor 1 | 22278 |
| Tgfa | transforming growth factor alpha | 21802 |
| Aurka | aurora kinase A | 20878 |
| Plk2 | polo-like kinase 2 (Drosophila) | 20620 |
| Fbxl20 | F-box and leucine-rich repeat protein 20 | 72194 |
| Pdrg1 | p53 and DNA damage regulated 1 | 68559 |
| Plau | plasminogen activator, urokinase | 18792 |
| Taf7 | TAF7 RNA polymerase II | 24074 |
| Clec3b | C-type lectin domain family 3, member b | 21922 |
| Nfxl1 | nuclear transcription factor, X-box binding-like 1 | 100978 |
| Phf17 | PHD finger protein 17 | 269424 |
| Golt1b | golgi transport 1 homolog B | 66964 |
| Ccnl1 | cyclin L1 | 56706 |
| Sesn1 | sestrin 1 | 100047324 |
| Mospd2 | motile sperm domain containing 2 | 76763 |
| Bnip3l | BCL2/adenovirus E1B interacting protein 3-like | 12177 |
| Dmxl1 | Dmx-like 1 | 240283 |
| Slc38a2 | solute carrier family 38, member 2 | 67760 |
| Chchd3 | coiled-coil-helix-coiled-coil-helix domain containing 3 | 100046321 |
| Mdm4 | transformed mouse 3T3 cell double minute 4 | 17248 |
| Sphk1 | sphingosine kinase 1 | 20698 |
| Lsm5 | LSM5, U6 small nuclear RNA associated | 66373 |
| Kin | antigenic determinant of rec-A protein | 16588 |
| Skp1a | S-phase kinase-associated protein 1A | 21402 |
| Mrps36 | mitochondrial ribosomal protein S36 | 66128 |
| Snhg6 | small nucleolar RNA host gene 6 | 73824 |
| Gda | guanine deaminase | 14544 |
| Lnx1 | ligand of numb-protein X 1 | 16924 |
| Ccnl1 | cyclin L1 | 56706 |
| Tgfa | transforming growth factor alpha | 21802 |
| Adamts1 | a disintegrin-like and metallopeptidase | 11504 |
| Smc2 | structural maintenance of chromosomes 2 | 14211 |
| Fbp2 | fructose bisphosphatase 2 | 14120 |
| Procr | protein C receptor, endothelial | 19124 |
| Angptl7 | angiopoietin-like 7 | 654812 |
| Gda | guanine deaminase | 14544 |
| Hsf2 | heat shock factor 2 | 15500 |